Non-Destructive Evaluation of Railway Trackbed Ballast

Robert De Bold

Doctor of Philosophy

The University of Edinburgh

2011

PhD Thesis: Non-Destructive Evaluation of Railway Trackbed Ballast

Robert De Bold, 2011

Supervisors: Prof Michael Forde and Dr Antonis Giannopoulos, University of Edinburgh.

Institute for Infrastructure and Environment
School of Engineering
University of Edinburgh
Alexander Graham Bell Building
The Kings Buildings
Edinburgh EH9 3JL
SCOTLAND

DECLARATION

This thesis, the work discussed, and results reported were carried out solely by myself unless otherwise stated within the text.

Robert De Bold,
Edinburgh, 2011.

ABSTRACT

The “green agenda” combined with highway congestion has accelerated the demand for increased freight and passenger travel on the world’s railways. These increases have driven demand for more efficient and rapid investigation of trackbed ballast.

Network Rail and other rail infrastructure operators spend significant financial sums on inspecting, tamping, adjusting, cleaning, and replacing trackbed ballast. Such maintenance is often to the detriment of normal network operation.

Industry requires a method of ballast evaluation that is non-intrusive, cheap, can appraise long stretches of track in a short period of time, and give a fingerprinting result from which time-to-maintenance can be calculated and planned. Thus, the aim was to develop evaluation methods using non-destructive testing techniques.

A 10-year old full-scale trackbed composed of variously fouled ballast was re-visited and used for experimentation. The condition of the ballast was calculated using the Ionescu Fouling Index.

Earlier research at the University of Edinburgh enabled researchers worldwide to characterise ballast using ground penetrating radar (GPR). This research was repeated, validated and taken forward in a series of GPR experiments on the trackbed using a range of antennas from 500MHz to 2.6GHz. New "scatter" metrics were developed to determine ballast condition from the GPR waveforms. These metrics were then used to predict the Ionescu Fouling Index with a correlation coefficient greater than 0.9.

One of the current approaches to evaluating the stiffness of railway ballast is to use a Falling Weight Deflectometer (FWD). The viability of using a Prima 100 mini-FWD on railways to measure stiffness was determined and deemed to be ineffective on ballast.

The applicability of the impulse response technique on railways was determined. An instrumented hammer was used to excite the ballast, with a geophone measuring the response. The Frequency Response Function of this was successfully correlated with the Ionescu Fouling Index with a correlation coefficient also greater than 0.9.

Finally, using GPR data and measured stiffness data collected by Banverket, Sweden, a numerical model to successfully relate radar responses to stiffness was developed.

ACKNOWLEDGMENTS

I gratefully acknowledge the financial support of EPSRC and the University of Edinburgh; and Germann Instruments for the loan of instrumentation.

I would like to thank Professor Mike Forde and Dr Antonis Giannopoulos for their support throughout the research.

I would like to thank the undergraduate MEng students, David Connolly, Scott Patience, Gerry O'Connor, and JP Morrissey, for their work on collecting data on the University of Edinburgh track.

I would also like to thank my office colleagues, Francis Drossaert, Ria Diamanti, Craig Warren, and David Connolly, for their friendship over the years.

Particularly, I owe sincere thanks to Rui Wang for her love and encouragement; and to my mother, Pat McVeigh, for her encouragement and love.

CONTENTS

FIGURES

TABLES

CHAPTER 1 INTRODUCTION

1.1 Railway Industry Background

The "green agenda" combined with highway congestion has accelerated the demand for increased freight and passenger travel on the world's railways.

According to a recent UK Department of Transport publication (UK National Statistics, 2010), the distance travelled by UK national rail passengers has increased significantly and continuously since 1994/5 to 2008/9, from 28.7 to 50.7 billion passenger kilometres (Figure 1.1).

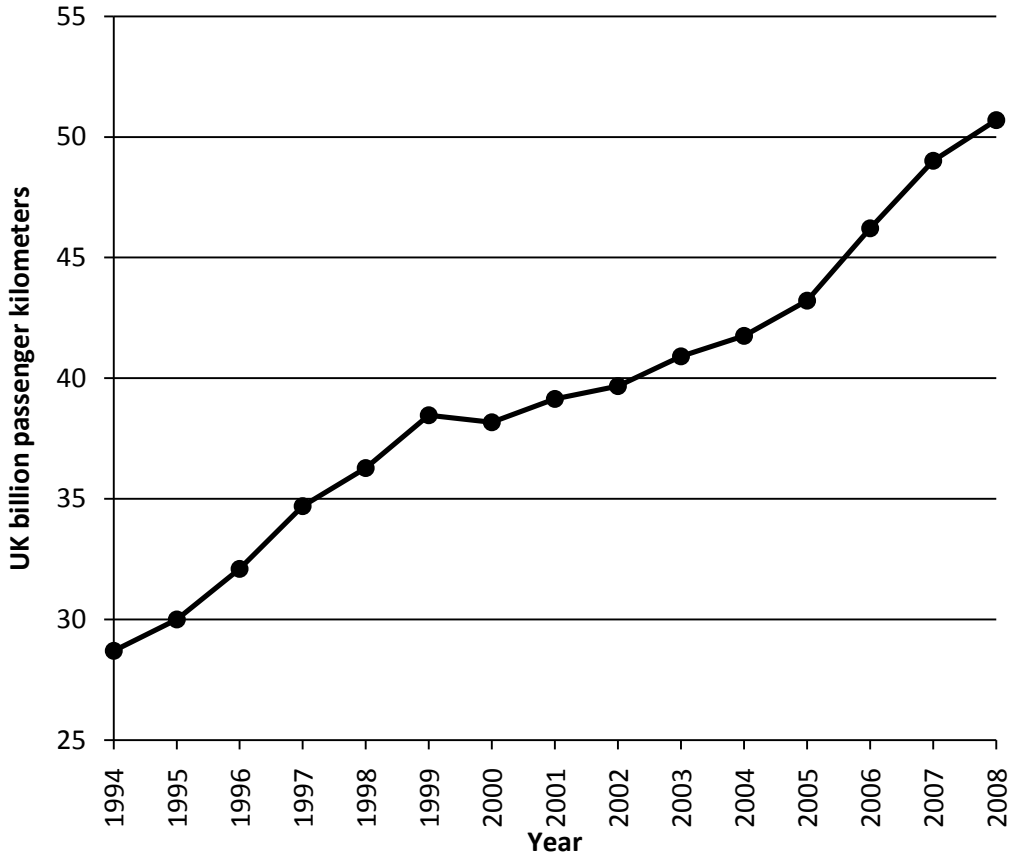

Figure 1.1 Distance travelled by UK rail passengers (UK National Statistics, 2010)

This amount of traffic is greater than the "high forecast" predicted by Railtrack PLC in 1997 of approximately 42 billion passenger miles by 2007 (Gallagher, 1999).

This growth has been promoted and supported by the policies of the Labour Government elected in 1997, which, effectively, stopped all new major road constructions.

This policy has also had a major effect on civil engineering contracting companies; many of which now derive much of their revenues from railway related works, including track renewals.

As part of the privatisation of British Rail, the owner of the national rail network from 1996 was Railtrack PLC. However, Railtrack was placed in administration on 7 October 2001. Consequently, in October 2002 the Government undertook the transfer of the responsibilities and assets of Railtrack PLC to the newly formed Network Rail, a "Company Limited by Guarantee", which has no shareholders, pays no dividends, and finances its own activities from surplus revenue and borrowing. In place of shareholders, Network Rail has 114 members that represent different interest groups.

It was widely perceived that Railtrack's demise was brought about by its "lack of attention to its core business leading to underinvestment in the infrastructure, loss of engineering skills and poor asset knowledge" (Network Rail, 2004).

Network Rail has around 32,000 employees, 20,000 miles of track, 40,000 bridges and tunnels, 1,000 signal boxes, 9,000 level crossings, 2,500 stations, 17 major stations, and, 8,200 commercial properties (Network Rail, 2006).

According to the Network Rail website (Network Rail, 2008), the mission statement of Network Rail has been to "transport more passengers, move more freight, improve safety and reduce delays – all at a reduced cost; improve train punctuality, year-on-year; reduce broken rails to 280 per year by March 2008 (from 444 in 2002/3); and reduce the annual running cost of the railway infrastructure to £4.3 billion by 2008/09." These cost savings are composed of annual 8% reduction targets in maintenance costs for 2007/8 and 2008/9 (Network Rail, 2006).

Proponents of privatisation argue that private companies focus on passengers; train-operating companies (TOCs) were created alongside a focussed infrastructure company, Railtrack (now Network Rail). Although controversial, the privatisation of the UK railways has encouraged train-operating companies to maximise passenger numbers beyond the Railtrack's optimistic projections. Consequently, there is great

pressure to find innovative methods to reduce maintenance costs, especially on the 20,000 miles of track.

A similar growth trend in the use of railways can be seen in the United States; however, in this case the growth is in the freight haulage sector (Figure 1.2).

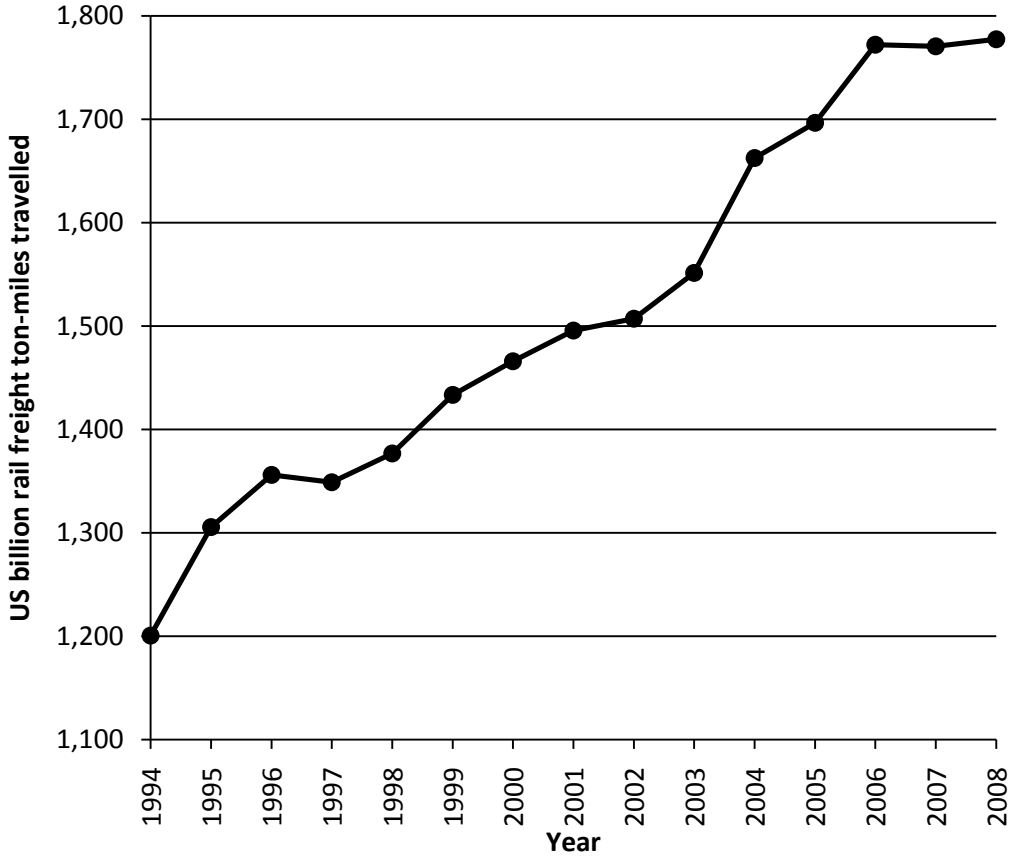

Figure 1.2 US rail freight ton-miles per year (Association of American Railroads, 2010)

International statistics showing freight usage and passenger usage of railways around the world is available from the International Union of Railways (UIC, 2010). From these figures, a ratio between freight usage and passenger usage can be calculated (Table 1.1).

In general, apart from some passenger usage concentrated on the east coast of the United States, most US railway use is for "heavy haul freight" (Association of American Railroads, 2010); British and European railway use tends to be passenger dominant (Eurostat, 2007).

Country	Railway Length (km)	Year	Billion tonne-km	Year	Billion passenger-km	Year	Ratio: $\frac{\text{tonne-km}}{\text{passenger-km}}$
United States	226,427	2007	2820.0	2007	22.5	2006	125.33
Kazakhstan	14,205	2008	191.2	2006	13.6	2006	14.05
Russia	128,000	2006	2090.0	2007	173.0	2007	12.08
Belarus	5,491	2008	45.7	2006	10.0	2006	4.59
Ukraine	21,676	2008	240.8	2006	53.2	2006	4.52
China	86,000	2009	2523.9	2009	787.9	2009	3.20
Poland	19,627	2008	42.7	2006	17.0	2006	2.51
Czech Republic	9,487	2008	16.3	2006	6.9	2006	2.37
Austria	5,755	2008	19.5	2006	8.9	2006	2.20
Sweden	9,830	2008	11.5	2006	5.7	2006	2.02
Romania	10,784	2008	14.7	2006	8.1	2006	1.83
Argentina	35,897	2007	12.6	2006	7.0	2003	1.81
Iran	8,160	2008	20.5	2006	12.6	2006	1.63
Germany	41,896	2008	89.7	2006	74.7	2006	1.20
European Union	*241,034*	*2006*	*382.7*	*2006*	*371.3*	*2006*	*1.03*
India	63,327	2007	481.0	2007	696.0	2007	0.69
Switzerland	3,619	2007	12.5	2008	18.0	2008	0.69
France	29,901	2008	42.1	2006	78.5	2006	0.54
Spain	15,064	2008	11.1	2006	21.3	2006	0.52
Italy	16,862	2008	21.9	2006	46.4	2006	0.47
United Kingdom	16,321	2008	22.2	2006	50.7	2008	0.44
South Korea	3,381	2008	10.6	2006	31.4	2006	0.34
Japan	23,474	2007	23.0	2006	254.0	2007	0.09

Table 1.1 International rail usage statistics (UIC, 2010)

1.2 Permanent Way Structure

The permanent way structure (a "railway track") in the UK is traditionally composed of a superstructure and substructure. The superstructure consists of rails, fastenings, and sleepers (referred to as ties in many parts of the world); under which there is the substructure ("trackbed") composed of a ballast layer of crushed granular material generally sized 25-50mm on top of the formation layer.

The rails effectively act as beams transmitting the train load onto the sleepers, which in turn transfer and distribute the load to the ballast and formation layer (Figure 1.3).

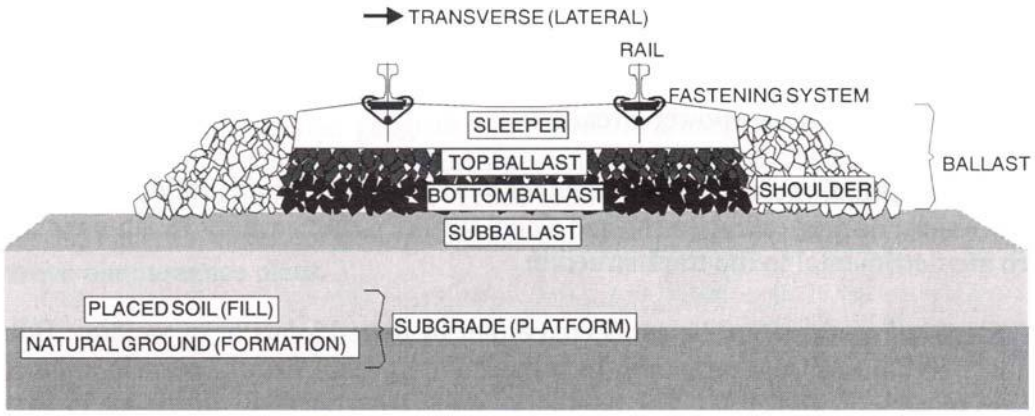

Figure 1.3 Conventional permanent way structure (Selig & Waters, 1994)

1.2.1 Rails

Rails are two parallel longitudinal steel elements laid on top of, and perpendicular to, the sleepers. They are typically of the form of an asymmetrical I-section (Figure 1.4).

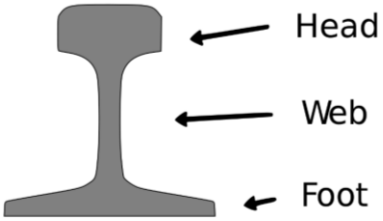

Figure 1.4 Typical rail cross-section (Wikipedia, 2010)

They are affixed to the sleepers by means of fastenings. The rails guide the train's wheels without the need for steering and transfer the train's lateral and vertical loading onto the sleepers and thence the sub-structure and formation. The rails can also serve the secondary function of completing a low voltage circuit that operates the networks signals (Selig & Waters, 1994).

There are two methods by which rail sections may be connected, either by bolting the joints together by means of a fishplate (Figure 1.5), or, through continuous welded rails (CWR) (Figure 1.6).

Figure 1.5 Fishplate (Wikipedia, 2010)

Figure 1.6 Continuous welded rail (Wikipedia, 2010)

With fishplate connections, the joint interface can separate vertically creating a depression that results in an impact load when trafficked by a train. This creates vibration and a poorer ride for passengers. This impact loading can accelerate sleeper wear, ballast deterioration, and even induce rail failure resulting in derailment (Selig & Waters, 1994). In the UK, about 35% of track is still jointed, although this is continuously falling as new rail is installed (Railway Technical, 2010).

Most modern railways use continuously welded rail (CWR) where the rails are welded together to form a long continuous rail that is very strong, requires less maintenance, and provides a smooth ride with less friction (Esveld, 2001).

Due to their continuous nature, continuously welded rail can suffer from distortion due to environmental conditions, and, if not restrained with clips or anchors, rails would lengthen in hot weather and shrink in cold weather (Esveld, 2001). Where CWR separates due to cold contraction, this can be detected due to the break in the track circuit; whereas, a buckle created due to heat expansion, cannot be detected, and is, therefore, more dangerous (Esveld, 2001).

Rail grinding is a common maintenance activity to correct irregularities in the rail longitudinal plane and is often considered a rail maintenance activity independent of other track work (Schoech, 2004).

Rail surface irregularities influence track quality, and conversely track quality can affect the development of rail surface fatigue; it has, therefore, been suggested that such track maintenance work should be integrated with other activities, and, in particular, that track tamping and rail grinding should be linked (Schoech, 2004).

It has also been found that the grinding of adapted rail profiles can be used to reduce the occurrence of specific faults or problems, such as, reducing lateral wear, reducing gauge corner fatigue, and improving running behaviour of vehicles (Schoech, 2005).

1.2.2 Fastenings

A rail fastening system is used to connect the rail to the sleeper in order to resist the various forces that may cause the rail to move, deform, deviate, or fail due to trafficking or environmental conditions.

The type of fastening system chosen is dependent on the type of sleeper material.

Wooden sleepers feature steel plates between the rail and the sleeper in order to distribute imposed forces over a greater surface area; this protects the wood from mechanical wear (Figure 1.7).

Figure 1.7 Chair fastening (Wikipedia, 2010)

Typically, concrete sleepers use spring fasteners (a common variety being the "Pandrol clip").

Pads are located between the rail and the sleeper to provide electrical insulation for the track signal circuits and reduce wheel-induced vibration through a more resilient contact interface (Figure 1.8).

Figure 1.8 Pandrol clip (Wikipedia, 2010)

1.2.3 Sleepers

The function of railway sleepers (or "ties" in the USA) is to distribute traffic loading from the rail evenly onto the ballast and sub-grade, and to maintain the alignment of the rail under trafficking and changing environmental conditions.

Sleepers are generally laid perpendicular to the rail and provide the structure to which the rails are affixed. They also ensure that the rails are a uniform distance apart.

Other sleeper arrangements exist, such as Y-shaped sleepers, which give a high resistance to track movement but also higher noise levels (Ogilvie & Quante, 2001).

Traditionally, sleepers have been made of a hardwood (Hay, 1982). Softwoods have also been used when hardwoods were unavailable, but they are susceptible to wear, although they accept treatment (usually creosote) more readily (Hay, 1982). Wooden ties are also susceptible to rotting, splitting, insect infestation, damage due to movement of the rail connection, and the rail connection working loose.

Concrete sleepers are heavier than their wooden counterparts and can offer a more secure fastening system and more effectively resist movement; although, under heavy loading they can be less flexible and crack where a wooden equivalent might not (Railway Technical, 2010).

Steel sleepers have been used for over 50 years but are less common than other types of sleeper. Steel sleepers can be lightweight, more precisely manufactured, faster to install with less site preparation, offering greater stability, and requiring reduced maintenance than wooden or concrete alternatives (Corus, 2010). Being made from steel, they also have the advantage of being 100% recyclable.

Even less commonly used are sleepers made from composite materials, plastics, resins, and rubber. Such sleepers can have the advantage of being impervious to rot and insect attack and giving improved lateral stability (Grant, 2005). They also have the advantage of being able to replace wooden sleepers piecemeal – tracks with concrete sleepers require all the sleepers to be concrete or none and use different equipment (Schut, 2004).

1.2.4 Ballast

Track ballast forms the material into which sleepers are embedded; it is packed between, below, and around the sleepers. The area of ballast between two sleepers is referred to as a crib. Ballast, composed of crushed granular material featuring continuous voids, serves several functions as part of a railway (Hay, 1982): -

- To provide a medium to distribute loads transmitted via the sleepers from dynamic rail loading due to trafficking into the subgrade.
- To anchor the sleepers, and, consequently rails, in place, and prevent lateral, vertical and longitudinal movements.
- To provide immediate drainage to prevent ponding of water around rails and sleepers.
- To provide continuous voids in the material around the sleepers to prevent capillary action, which also reduces the effects from frost heave.
- To facilitate maintenance operations where surface irregularities can be corrected through mechanical manipulation of the ballast ("tamping") or adjustment of the position of the sleeper to re-align the track.
- To prevent the growth of vegetation.
- To provide a medium to dampen the dynamic forces of rail trafficking.

Additional ballast functions have also been noted (Selig & Waters, 1994): -

- Absorb airborne noise.
- Provide adequate electrical resistance between the rails.

In all situations, a good ballast should be strong, hard-wearing, stable, drainable, easy to clean, workable, resistant to deformation, easily available, and reasonably cheap to purchase (Hay, 1982).

In general, the ballast should be between 28mm and 50mm in diameter as the inclusion of particles finer than this will reduce drainage efficiency, and the inclusion of larger particles will result in improper distribution of the dynamic loading from the sleeper (Bonnett, 2005).

Historically, other materials have been used as ballast, including, ashes, chalk, clay, earth, cinders from train fireboxes; however, it became clear that good-quality ballast

made of crushed stone was necessary for good drainage and a suitable foundation (Solomon, 2001).

Angular stones are preferable as these interlock with each other, reducing track movement (Bonnett, 2005).

Soft materials, such as limestone, are not particularly suitable, as they can degrade under load when wet; granite, is one of the better materials, although more expensive (Bonnett, 2005).

1.2.5 Ballast Grading

There is no universal code for ballast specification; in the UK, the former British Rail specification (BR1203, 1988) has been predominantly used. This was superseded in 2002, by a British and European standard (BS EN 13450, 2002) which specifies the physical and geometrical parameters for various grades of ballast.

The British and European standard (BS EN 13450, 2002) features numerous particle size distribution grading categories of ballast for various uses and locations (Table 1.2).

Sieve size mm	Railway ballast size 31.5mm to 50mm			Railway ballast size 31.5mm to 63mm		
	Percentage passing by mass					
	Grading category					
	A	B	C	D	E	F
80	100	100	100	100	100	100
63	100	97 to 100	95 to 100	97 to 99	95 to 99	93 to 99
50	70 to 99	70 to 99	70 to 99	65 to 99	55 to 99	45 to 70
40	30 to 65	30 to 70	25 to 75	30 to 65	25 to 75	15 to 40
31.5	1 to 25	1 to 25	1 to 25	1 to 25	1 to 25	0 to 7
22.4	0 to 3	0 to 3	0 to 3	0 to 3	0 to 3	0 to 7
31.5 to 50	≥50	≥50	≥50	-	-	-
31.5 to 63	-	-	-	≥50	≥50	≥85
NOTE 1 The requirement for passing the 22.4 mm sieve applies to railway ballast sampled at the place of production. NOTE 2 In certain circumstances a 25 mm sieve may be used as an alternative to the 22.4 mm sieve when a tolerance of 0 to 5 would apply (0 to 7 for category F).						

Table 1.2 Categories for grading (BS EN 13450, 2002)

The different placement of these grading categories is dependent on climatic conditions (BS EN 13450, 2002). As can be seen from the freeze-thaw table (Table 1.3), the more inhospitable the environmental conditions (i.e., a "Continental" climate featuring seawater, as opposed to a "Mediterranean" climate featuring frost-free dry conditions), the smaller the grading of ballast required.

Environmental conditions	Climate		
	Mediterranean	Atlantic	Continental [a]
	Category		
Frost free or dry situation	D	D	D
Partial saturation, no salt	D	C	B
Saturated, no salt	D	B	A
Salt (seawater)	C	B	A
[a] *The Continental category could also apply to Iceland, parts of Scandinavia and to mountainous regions where severe winter weather conditions are experienced.*			

Table 1.3 Ballast freeze-thaw severity categories (BS EN 13450, 2002)

However, despite category "A" ballast being generally smaller in size than the other categories, there is also less permitted fines content (Table 1.4) as it is likely that it is the fines content that retains water through capillary action, and, thus, creates conditions suitable for freeze-thaw damage.

Sieve size mm	Maximum percentage passing by mass				
	Fines content category				
	A	B	C	Declared	D
0.063	0.5	1.0	1.5	>1.5	No requirement
NOTE The requirement applies to railway ballast sampled at the place of production.					

Table 1.4 Categories for fines content (BS EN 13450, 2002)

However, much of the ballast material on the current British network will still be as per British Rail standard (BR1203, 1988) (Table 1.5).

Square Mesh Sieve Size		% To Pass
mm	Inches	
63	2.48	100
50	1.97	97-100
28	1.10	0-20
14	0.55	0-2
1.18	0.05	0-0.8

Table 1.5 BR1203 ballast grading curve (BR1203, 1988)

It can be seen that the bulk of the material (77% to 80%) is between 28mm and 50mm (or, 1.10" and 1.97") in size.

The American Railway Engineering and Maintenance-of-Way Association recommend "size 4" ballast for general use (AREMA, 2003), this is identical to the American ASTM standard "C33 gradation 4" (ASTM C33, 2008) (Table 1.6).

Square Mesh Sieve Size		% To Pass
mm	Inches	
51	2.0	100
38	1.5	90-100
25	1.0	20-55
19	0.75	0-15
9.5	0.375	0-5

Table 1.6 ASTM C33 gradation 4 (ASTM C33, 2008)

It can be seen that the bulk of the material (75% to 90%) is between 19mm and 38mm (or, 0.75" and 1.50") in size.

Therefore, in comparing ballast standards, North American ballast is a finer grade than UK ballast, and that there is a broad range of acceptable European ballast sizes.

1.2.6 Sub-Ballast

A railway track may feature a sub-ballast layer. This is generally composed of sand or gravel and functions to prevent the migration of soil from the sub-grade into the ballast and to reduce stresses transferred to the sub-grade; commonly, these functions are not

achieved (AREMA, 2003). The use of modern geotextiles at the interface between ballast and sub-ballast has been found to be more effective and also contributes to the stiffening of the ballast, thus, spreading the vertical loads across the sleepers more effectively.

1.2.7 Sub-Grade

The sub-grade is the foundation layer of the railway track; it provides a suitable and stable base on which all other layers can be built. The dynamic loading from rail traffic can penetrate five metres (Selig & Waters, 1994) and this would be some way into the sub-grade layer; therefore, it is important that the strength and durability of the sub-grade is sufficient.

Sub-grade has been traditionally made of locally-sourced soil as other alternatives were not economical (Selig & Waters, 1994).

Increased sub-grade stiffness can reduce ballast, rail, and sleeper deterioration. Commonly, sub-grade can be improved through compaction, grouting, or preloading, improving the drainage, and introducing additive materials (Selig & Waters, 1994). However, this can be prohibitively expensive and not practicable to retrofit given the ongoing usage of a track. In modern high-speed lines, materials such as sand and gravel have been used in combination with the natural soil and engineered fill.

1.3 Stress Bulb

According to Lamb and Whitman (Lambe & Whitman, 1979), the principal stresses under a strip load can be visualised as a "bulb" (Figure 1.9).

The diagram depicts the various forces within a cross-section of a strip load where the strip load, in this case a railway track, is normal to the paper. At greater depths and distances horizontally from the strip load, the resultant stresses in the ground from the strip load would decrease, thus giving the pressure bulb shape.

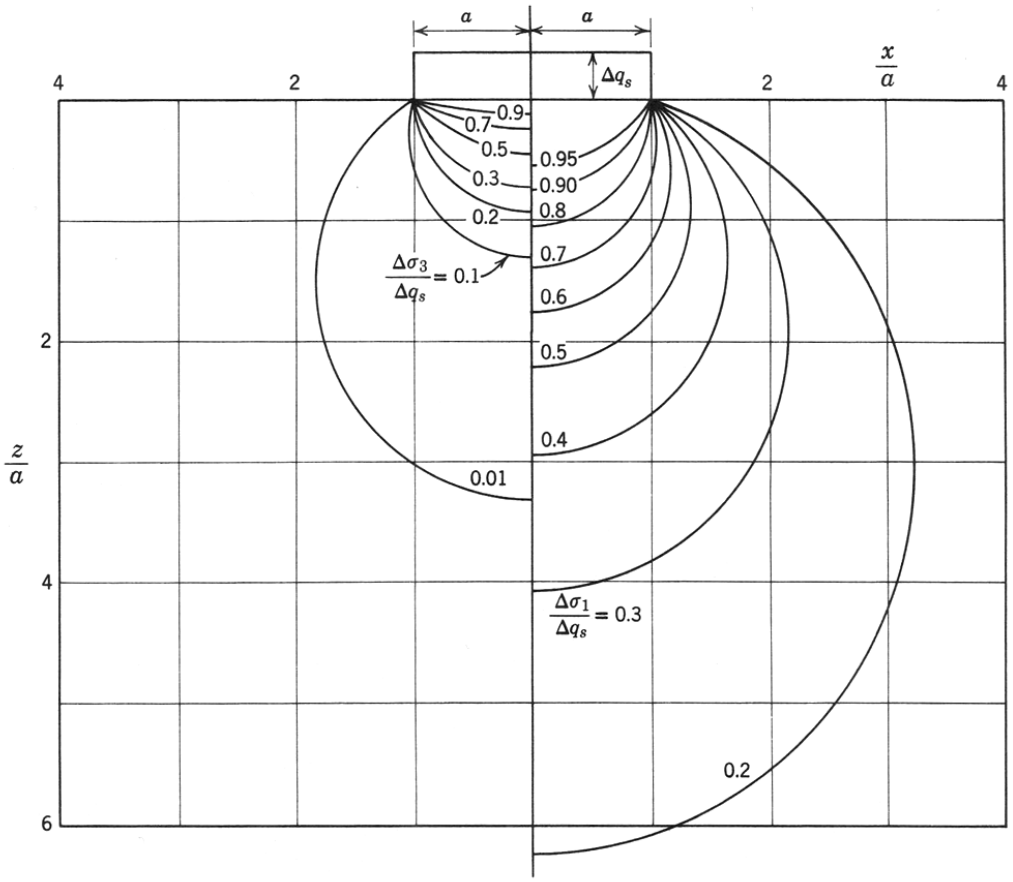

Figure 1.9 Principal stresses under strip load (Lambe & Whitman, 1979)

Where: z is the soil depth;
x is the lateral distance from the strip load (the track);
a is the distance from the centre to the edge of the strip load;
Δq_s is the normal stress due to the strip load;
Δq_3 is the horizontal stress resultant within the soil (or ballast); and,
Δq_1 is the vertical stress resultant within the soil (or ballast).

The left of the diagram depicts the ratio of the resultant horizontal stress to that of the applied stress and the right of the diagram depicts the ratio of the resultant vertical stress to that of the applied stress.

If the broad assumption is made that a railway track is a 2m wide strip load, i.e., the length of a sleeper across the track that transmits the dynamic loading into the ballast, then some example calculations can be made (Table 1.7).

Position	a	x	z	x/a	z/a	$\Delta\sigma_3/\Delta q_s$	$\Delta\sigma_1/\Delta q_s$
2m below middle of track	1	0	2	0	2	0.07	0.54
2m below edge of track	1	1	2	1	2	0.04	0.47
5m below middle of track	1	0	5	0	5	$\ll$0.01	0.26
5m below edge of track	1	1	5	1	5	$\ll$0.01	0.24

Table 1.7 Example strip load calculations

Therefore, it can be seen that there is only a marginal difference between the forces experienced under the centre or edge of a railway track, and that horizontal stresses are much less significant.

The main points to note from these calculations are that at 2m depth, the vertical stress is approximately half the applied stress, and at 5m depth, the vertical stress is approximately a quarter of the applied stress.

This can be compared to the assertion in *1.2.7 Sub-Grade* that dynamic loading from rail traffic can penetrate five metres (Selig & Waters, 1994).

1.4 Ballast Deterioration

Ballast deteriorates over time through a process of degradation, where the particles mechanically interact (generally due to dynamic train loading), or otherwise weather, and change shape; or, through fouling, where fine particles accumulate in the void structure.

A number of mechanisms for ballast deterioration and sources of fouling have been determined (Table 1.8).

Particulate infiltration from below is a major source of fouling, producing 16% of fouling material, as are sources deposited from above, producing 7% of fouling material; however, overall, some 76% of ballast fouling material is due to breakdown of the ballast itself, primarily due to mechanical interaction.

Category	Sources of ballast fouling	Amount
Ballast breakdown	Mechanical interaction from handling (at quarry, from dumping, compaction, tamping, transportation) Mechanical interaction due to traffic (repeated loading, vibration, slurry hydraulic action) Chemical weathering, including acid rain Freezing of water in particles	76%
Ballast surface infiltration	Delivered with ballast Dropped from trains Wind blown Water borne Splashing from adjacent wet spots	7%
Sleeper wear	Vertical axial loading/movement Horizontal/lateral loading movement Mechanical abrasion between sleeper / ballast	1%
Underlying granular layer infiltration	Old track bed breakdown Sub-ballast particle migration from inadequate gradation	13%
Subgrade infiltration	Infiltration from subgrade into ballast	3%

Table 1.8 Sources of ballast fouling (Selig & Waters, 1994)

Such deteriorated ballast is defined as "spent" and fails to provide the drainage and mechanical functions required (Figure 1.10).

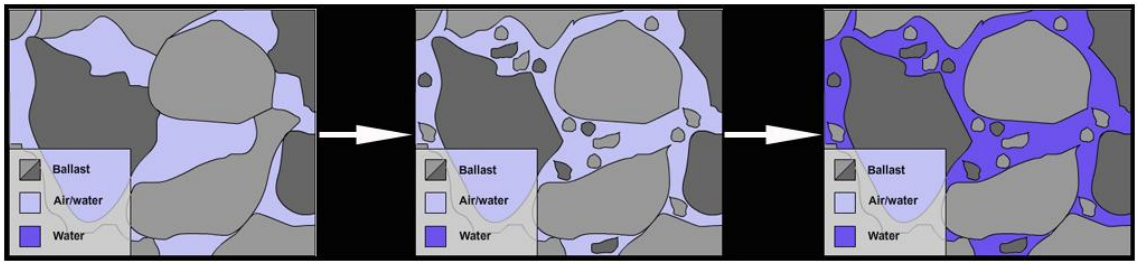

Figure 1.10 Deterioration of ballast

Identification of spent ballast is often undertaken visually, but this can be unreliable. One of the most reliable ways to determine ballast condition is to take a sample and to undertake a particle size distribution analysis as per American ASTM standards (ASTM D6913-04, 2009) or British Standards (BS 1377-2, 1990). This is time consuming, laborious, requires track possession, and, therefore, is seldom used. If one waits for ballast symptoms to become obvious, then the maintenance regime to deal with deterioration is a reactive one, and, consequently, cost-inefficient.

1.5 Current Maintenance Equipment

1.5.1 Network Rail

In dealing with ballast and track maintenance in the UK, Network Rail deploy several pieces of on-track plant to maintain their network (Network Rail, 2008).

1.5.2 New Measurement Train

The "New Measurement Train" (NMT) provides engineering information on asset condition (Figure 1.11).

Figure 1.11 New Measurement Train (Network Rail, 2008)

The NMT is able to travel at up to 125mph allowing it to be scheduled in between timetabled trains and is part of the company's objective to replace manual inspection with mechanised measurement. The train produces video footage of track infrastructure and wheel-rail interface, six foot gauging data, and information on track geometry. It can check the condition of all main lines in Great Britain in a fortnight. It is intended for the NMT to adapt to take advantage of new technologies as they are developed.

1.5.3 Eurailscout Train

Network Rail also utilise a number of Eurailscout trains (Eurailscout, 2009); specifically the UFM 160 – Universal Rail Measurement Vehicle (Figure 1.12).

This is able to travel up to 160kph (100mph) and measures rail geometry, overhead wires, rail cross section, rail surface, takes video recordings of track and surroundings, and positioning data.

Figure 1.12 UFM 160 – Universal Rail Measurement Vehicle (Eurailscout, 2009)

1.5.4 High Output Ballast Cleaner

The "High Output Ballast Cleaner" (Figure 1.13), is an 800 metre, 3,200 tonne track vehicle that can clean ballast foundation.

Around 600 metres of track ballast can be cleaned in a typical midweek eight-hour night shift, and around 1,400 metres in 16-hour weekend shift.

Figure 1.13 High Output Ballast Cleaner(Network Rail, 2008)

The High Output Ballast Cleaner works at around a quarter of a mile per hour and continuously: -

- Excavates ballast from beneath the track, while holding the track in position;
- Passes the excavated material through large vibrating sieves;
- Removes "fines" to specialist wagons in the train;
- Returns the larger pieces of ballast back to the track; and,
- Adds new ballast from wagons within the train to make up for the "fines" removed.

1.5.5 Tamping and Lining Machines

Tamping and lining machines are the bulk of on-track plant and are used to pack the ballast to make the tracks more durable, and ensure the track is in the correct position by correcting the level and alignment of the track (Figure 1.14).

Figure 1.14 Tamping and lining machine (Network Rail, 2008)

The open structure of the ballast can also facilitate maintenance of track geometry through rearrangement of ballast particles by "tamping".

Note that "tamping" of dense ballast will actually result in dilation of the ballast. Under traffic this dilated material may well recompact and return to its previous density resulting in track settling – known as "ballast memory" (Bell, 2008).

1.5.6 Stoneblower

One alternative to tamping is the "Stoneblower" machine developed by Harsco Track Technologies (Harsco Track Technologies, 2009) in cooperation with Network Rail (Figure 1.15).

Figure 1.15 Stoneblower (Hondawanderer, 2010)

It was developed specifically as an alternative to traditional tamping methods for the restoration of track vertical and lateral alignment (McMichael & McNaughton, 2003). The machine pneumatically injects smaller-sized ballast under sleepers to achieve track positioning to a stated accuracy of 1mm without disturbing the pre-existing compacted foundation. The method has been demonstrated to extend the time required between track maintenance cycles (Zarembski & Newman, 2008). However, additional material may restrict future tamping operations.

1.5.7 Ballast Improvement

Another way to improve the mechanical performance of a track is through ballast reinforcement. Techniques include placing geogrids, application of resins (such as XiTrack), containment of ballast in fabric wraps or bags ("ballast bags"), or addition of randomly-orientated reinforcing fibres. However, there is a significant lack of scientific investigation or understanding of the performance of these techniques (Zervos, 2011).

XiTrack is of particular interest; it is a fast-setting visco-elastic polymer that can be added to the ballast after construction of the track. It penetrates into the ballast to form a three-dimensional reinforcing cage. The depth of penetration can be pre-determined by altering the polymer rheology. Research has shown it to be effective in reducing the need for regular re-alignment of track in problem areas (Woodward et al., 2004).

1.6 Problem Statement

It is clear from the variety of equipment described above that track maintenance is an ongoing issue and that much track maintenance relates directly to the ballast. Network Rail and other rail infrastructure operators spend significant financial sums on inspecting ballast, tamping or adjusting ballast, and cleaning or replacing ballast (Network Rail, 2008). Such maintenance is often to the detriment of normal network operation.

Therefore, it can be concluded that industry requires a method of trackbed ballast evaluation that is non-intrusive, cheap, can appraise long stretches of track in a short period of time, and give a fingerprinting result from which time-to-maintenance can be calculated and planned. Therefore, the overall aim of this research is to develop

evaluation methods using non-destructive testing techniques. Detailed objectives indicating how this aim is to be achieved are outlined in 1.9 Research Objectives.

1.7 Potential Non-Destructive Testing Methods for Trackbed Ballast

1.7.1 NDT Sources

In considering various potential forms of non-destructive testing (NDT) methods to evaluate trackbed ballast, the following methods were considered. The focus of the research is on the ballast rather than the whole of the trackbed, i.e., ballast and subgrade, etc. Most method descriptions are summarised from ACI publications (ACI 228.2R S2.2, 2011) (ACI 228.2R S2.3, 2011) (ACI 228.2R S2.8, 2011).

The majority of the methods are intended for testing solid structural elements or piles, rather than a loose unbound material such as ballast. However, it is intended for the development of any new testing technique to investigate the applicability of testing the ballast through or in conjunction with measurements taken from the railway track structural elements (rails and sleepers); therefore, the structural or pile testing techniques will be investigated.

It has been suggested that the most effective monitoring should be vehicle mounted and aim to give a continuous track stiffness profile, identifying sites for consideration for remedial treatment (Berggren, 2009). In fact, this was one of the objectives of the EU-financed Eurobalt project (EUropean Research for an Optimised BALlasted Track), which was a joint research project with several rail administrations, rail industries, and universities from France, Germany, UK, and Sweden (Huille, 1997).

1.7.2 Falling Weight Deflectometer

A Falling Weight Deflectometer (FWD) is a static stiffness measurement device originally developed for highways. It has been adapted for the railway industry to evaluate railway trackbeds. For this task, the FWD is a large and heavy piece of equipment.

Use of an FWD involves dropping a known mass onto a pavement surface to simulate traffic loading. This imparts an impulsive load into the ground, which is measured

along with the velocity response of the ground to the impulsive loading. The loading impulse and response are used to determine the pavement properties (Sharpe, 2000).

An example schematic can be seen in Figure 1.16.

In the railway context, the testing procedure requires disconnection of clips from sleepers over sections of track and, thus, track possession. This makes the testing procedure very time-consuming and expensive. Currently, the FWD is suggested as being the only satisfactory way to assess trackbed stiffness (Sharpe, 2000).

The advantages of this method are that it is a tried and tested technique with available testing equipment. However, it is time-consuming and expensive.

In terms of trackbed evaluation, this method not only evaluates the properties of the ballast, but, due to its size, the whole of the trackbed including the subgrade.

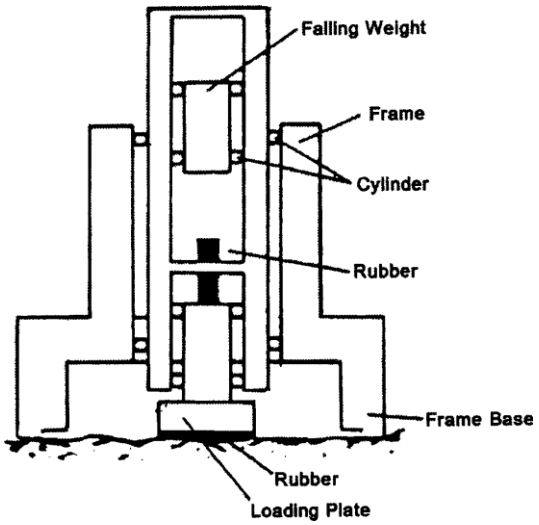

Figure 1.16 Schematic of FWD test (Loizos et al., 2003)

1.7.3 Sonic Echo

Sonic Echo was one of the first NDT techniques to be made commercially available for pile length evaluation or integrity testing (Paquet, 1968) (Steinbach & Vey, 1975).

The method typically uses a small hammer (1kg) to impact the test element. Measurement is made of the transit time for the stress wave to travel along the element and be reflected back to a transducer (usually an accelerometer), which is coupled to

the element at the point of impact. Only a relatively small amount of energy is required to be generated by the hammer impact

An example can be seen in Figure 1.17 (where the signal is amplified by the function at the bottom of the graph).

If the length of the test element or the wave velocity is known, then the other can be calculated. The calculated velocity can provide information on the material quality. Where the length is known, a premature reflection arrival can infer a break, defect, significant change in cross section, or a change in density of surrounding material. In certain cases, changes in polarity of the reflected wave can indicate whether the anomaly is due to an increase or decrease of stiffness at the reflective point.

The advantages of this method are that it is quick, and portable. However, it reveals little information about nature of defects other than their presence.

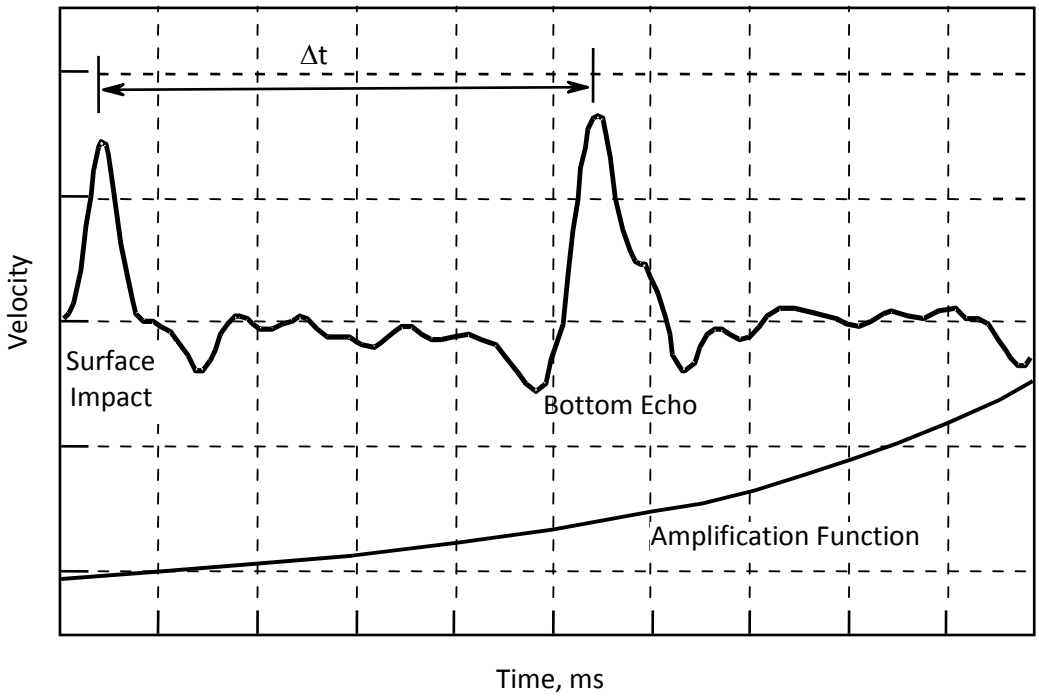

Figure 1.17 Example of sonic-echo test result (ACI 228.2R S2.3, 2011)

In terms of trackbed evaluation, this method seems more suited to solid structural elements only. The information obtained from the method is limited to a time-of-reflection waveform; therefore, it not likely to provide much useful information about ballast condition given that its unbound nature is likely to cause innumerable hard-to-analyse reflections.

1.7.4 Impulse Response

The Impulse Response testing method was originally developed from steady-state vibration testing of piles (Davis & Dunn, 1974), where a controlled force was applied to the shaft head by a frequency generator.

Using a new generation of faster computers undertaking a Fast Fourier Transform (FFT), it was combined with a modally tuned hammer that permitted the method to be applied to other structures (Davis & Hertlein, 1990). The hammer impact force is recorded by a load cell, and the element response by a transducer.

The impact and transducer response are both converted into the frequency domain. At each frequency value, the transducer value is divided by the force value to provide a normalised response, or a Frequency Response Function (FRF) (Ewins, 1984).

The FRF contains information on the condition and integrity of the tested element, including stiffness, and can reveal such characteristics as honeycombing in concrete. A relatively small amount of energy is required to be generated by the hammer impact.

An example can be seen in Figure 1.18.

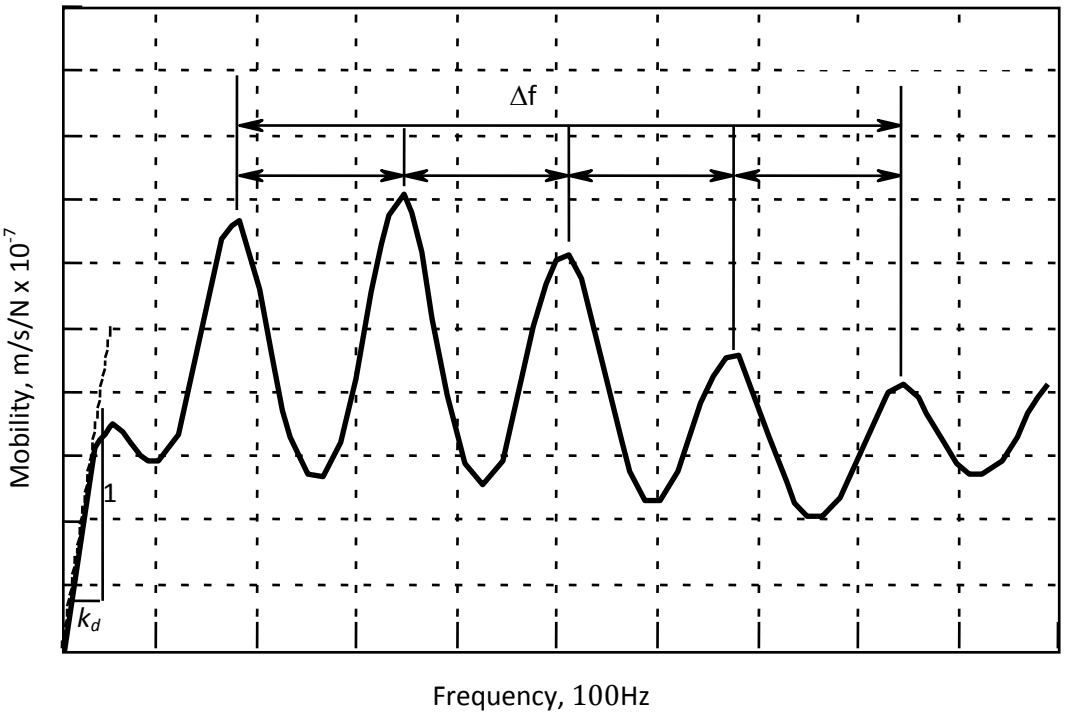

Figure 1.18 Example of impulse-response plot of a pile (ACI 228.2R S2.3, 2011)

The advantages of this method are that it is quick, portable, and measures stiffness. However, there is the requirement for complex interpretations of results.

In terms of trackbed evaluation, this method has particular potential. The ability of the method to differentiate between different concrete density conditions indicates that it may be able to distinguish between ballast conditions, e.g., clean or spent. In addition, since FRF normalises the response suggest that it may be suitable to be implemented as a hand-held device where it could permit unavoidably inconsistent testing to produce consistent results.

1.7.5 Impedance Logging

Impedance Logging creates an image of the variation in test element impedance (usually a pile) by combining the sonic echo time-domain response with the characteristic impedance measured by impulse response (Paquet, 1991).

The hammer impact generates a propagating wave that reflects back to the origin and produces a "reflectogram". Analysis of the mobility plot from the impulse response confirms the test element length and establishes its characteristic impedance.

These combine to produce the impedance log. This can be analysed to determine presence, location, and relative sizes of defects: a defect extending across the entire test element cross-section (zero impedance) is equivalent to 100% reflection.

An example can be seen in Figure 1.19.

The advantages of this method are that it is quick, portable, and measures stiffness; However, it requires very good test data for accurate analysis. Full analysis requires experience, and cannot yet be completed on site at time of test.

In terms of trackbed evaluation, this method again seems more suited to solid structural elements only. Again, given that the information obtained from the method is derived from time-of-reflection waveform, it not likely to give much useful information about ballast condition due to its unbound nature.

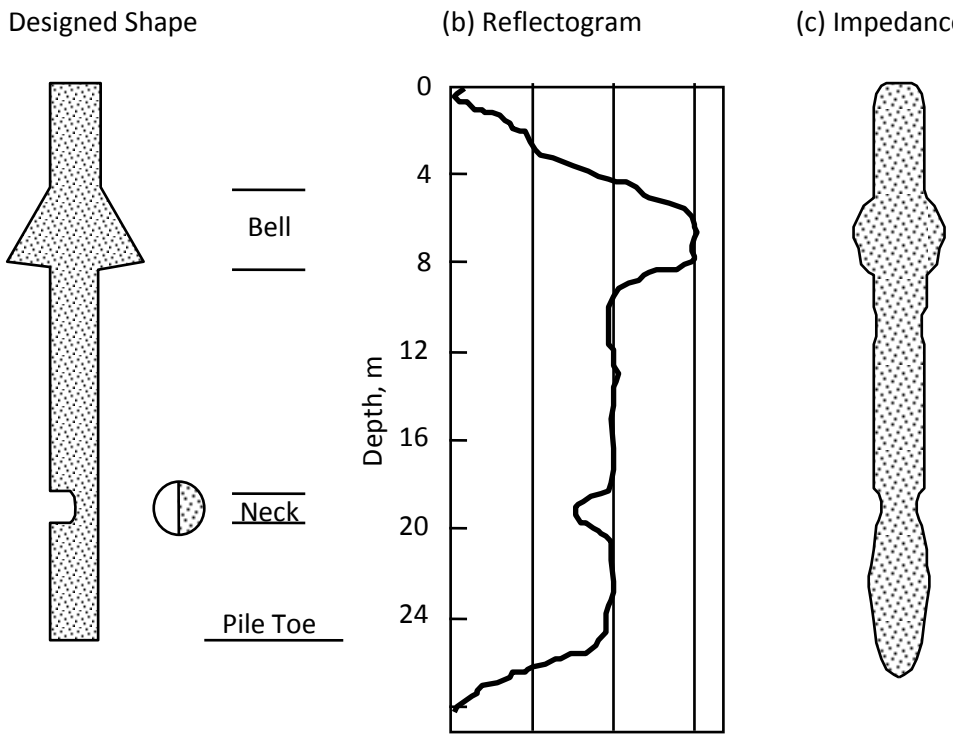

Figure 1.19 Impedance logging example (ACI 228.2R S2.3, 2011)

Where: -

a. Planned defects in experimental pile;
b. Reflectogram obtained by signal processing of sonic-echo data; and,
c. Impedance log.

1.7.6 Crosshole Sonic Logging

The Crosshole Sonic Logging method requires the presence of pre-placed tubes or drilled boreholes down the length of the test element (Levy, 1970).

During testing, two transducers are placed in separate tubes at the same depth. A transmitting transducer emits an ultrasonic pulse that is detected by the receiving transducer. The tubes are filled with water for better coupling. Both transducers are raised, with their positions logged against the ultrasonic pulse travel time. The presence of an anomaly is indicated by an increase in the time of flight of the signal, or the complete absence of a received signal.

An example log can be seen in Figure 1.20.

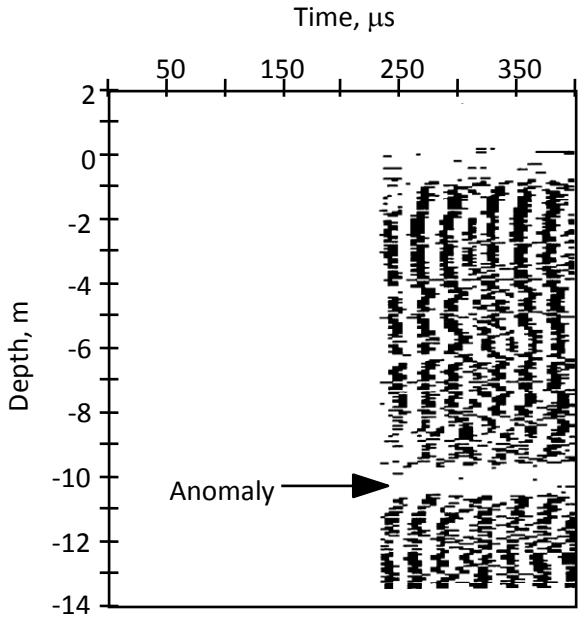

Figure 1.20 Example of crosshole sonic log (ACI 228.2R S2.3, 2011)

The advantages of this method are that it is quick in operation, detection of irregularities between tubes is more accurate than in surface reflection tests, and performance is not limited by depth. However, it requires pre-placed tubes, may not detect irregularities at the edge of the test element, and information obtained is limited to the material immediately between pairs of tubes.

In terms of trackbed evaluation, this method would presumably require two boreholes to be placed through the ballast for any section of ballast to be tested. This immediately highlights numerous practical limitations with this method, such as the effort required for drilling numerous boreholes, the inability of the boreholes to be water-filled, and, again, the suitability of the method for a loosely bound material. Again, the information obtained from the method is derived from time-of-reflection waveform, which is not likely to give any useful information about ballast condition given its unbound nature. It is clear that any such invasive technique would be wholly inappropriate for evaluating long stretches of railway trackbed.

1.7.7 Parallel Seismic

The Parallel Seismic method was developed in order to test piles where direct access to the shaft head was no longer possible without removal of material, structural alterations, or demolition (Davis, 1995).

The method utilises a small diameter borehole that is bored parallel to and as close to the test element as possible. The tube is filled with water (as an acoustic couplant) and an acoustic receiving transducer is used to take measurements at various depths.

The test element structure is struck as close to the shaft head as possible with a hammer equipped with an electronic trigger. Some of the energy imparted into the pile is transmitted into the soil, and the time of this is detected by the transducer.

The time difference between the impact and being received by the transducer at various depths is recorded. The transit time will increase proportionally with the depth of the transducer. However, any significant discontinuity or inclusion in the pile will result in a disproportionately longer transit time. This can be detected through simple analysis of the transit times.

An example result can be seen in Figure 1.21 where the depth of a pile shaft is indicated by change in slope of the line representing the arrival time of the stress pulse.

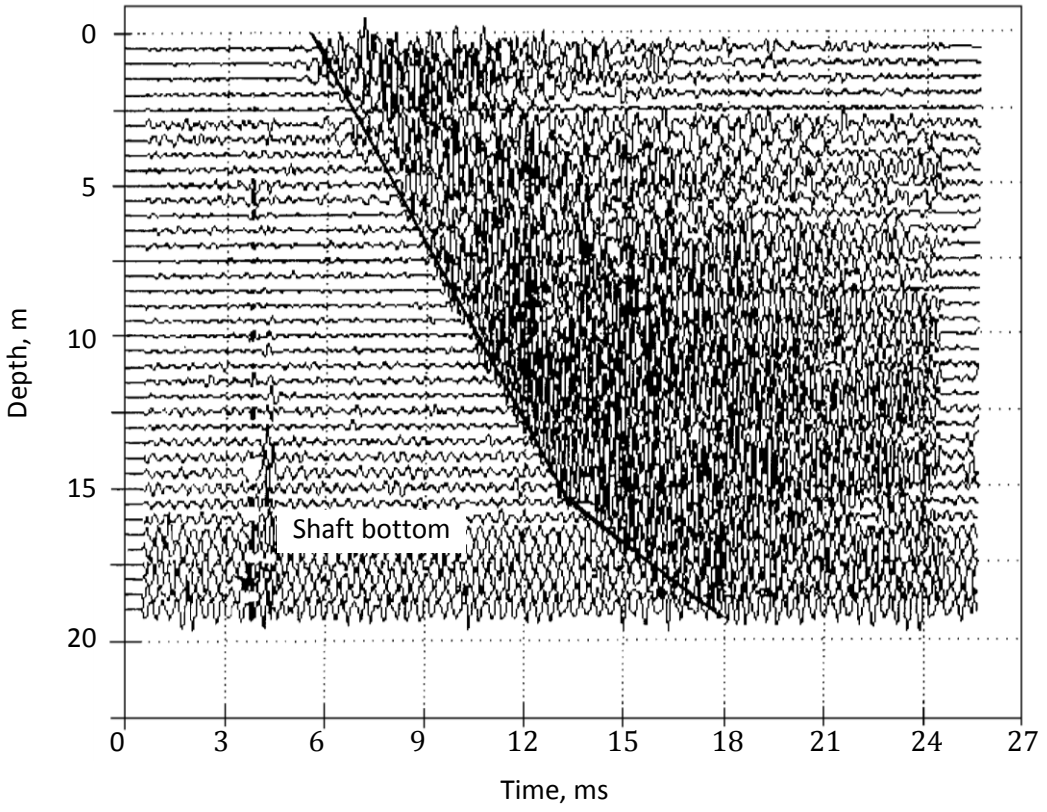

Figure 1.21 Example of results from parallel-seismic test (ACI 228.2R S2.3, 2011)

The advantages of this method are that it is quick in operation, foundations under existing structures can be tested, and it is not affected by soil damping as much as surface reflection methods. However, it requires testing holes to be bored adjacent to the foundation that is to be inspected, and may not detect defects that are not complete discontinuities.

In terms of trackbed evaluation, this method would be an improvement on the Crosshole Sonic Logging method due to only requiring one smaller borehole. However, all the other limitations of Crosshole Sonic Logging would still be present, which would make it unsuitable for testing ballast.

1.7.8 Ultrasonic Pulse Velocity

Ultrasonic Pulse Velocity is one of the oldest non-destructive methods for testing concrete. The method determines the travel time of compressional waves over a known distance.

The method was originally pioneered in Canada to measure the extent of cracking in dams (Leslie & Cheesman, 1949), and in England to measure the quality of concrete (Jones, 1949).

The method requires a transmitting transducer to be coupled to one face of the structure and a receiving transducer coupled on the opposite face. The transmitter produces a stress pulse and the transit time for it to be received is measured.

The speed of propagation of stress waves depends on the density and the elastic constants of the solid. In concrete, variations in these properties are often from structural or material abnormalities. Therefore, a survey of wave speeds through the structure can reveal the location of such abnormalities. Travel times through inferior concrete would be greater. Propagation through a crack or discontinuity would result in wave reflection and no arrival of signal at the receiving side. Such a survey can take the form of a two-dimensional tomographic image. The degree of signal attenuation can also be an indicator of material quality.

An example schematic can be seen in Figure 1.22.

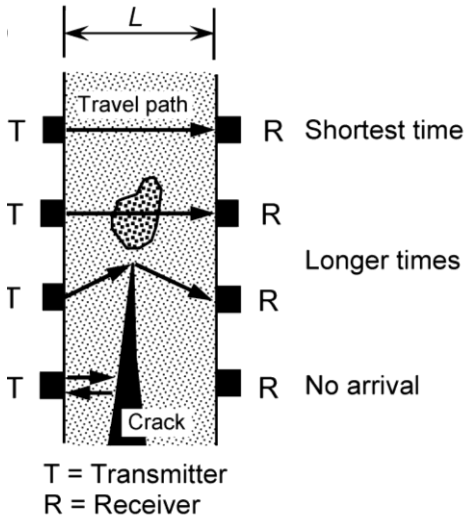

Figure 1.22 Ultrasonic pulse velocity (ACI 228.2R S2.2, 2011)

The advantages of this method are that it is portable, and relatively easy to use; however, it requires access to two sides of the test element, and does not provide information on depth of defect.

In terms of trackbed evaluation, this method could be used to couple two transducers to the ballast surface to investigate the potential of deriving density information. However, the loose bound nature of the ballast and the low power, high frequency nature of the ultrasonic pulse would likely mean that any signal would be highly attenuated. If applied to ballast, this method would be similar to using the impulse response technique, in that they both feature a location on the ballast surface for signal transmission and a location to receive the signal. However, the impulse response technique would provide more data for analysis than the ultrasonic pulse time-of-travel waveform.

1.7.9 Ultrasonic Echo

The Ultrasonic Echo method is very similar to, yet overcomes the requirement of the Ultrasonic Pulse Velocity method to have access to the rear side of the test element by utilising the effect of signal reflection. This also gives the benefit of being able to determine the depth of any defect.

In the 1960s, such methods used P-waves to determine concrete thickness (Bradfield & Gatfield, 1964) and detect flaws (Alexander & Thornton, 1989). In the 1990s, an

Ultrasonic Echo system utilising S-waves and multiple sensors was developed (Kozlov et al., 1997).

In Ultrasonic Echo methods, a pulse is transmitted into an accessible surface on one side of the test element and the arrival time of stress waves reflected back from defects or interfaces is measured. The transmitting transducer also acts as the receiving transducer. Tomographic cross-sectional images of a test element can be composited by placing signal traces from progressive locations beside each other.

An example schematic can be seen in Figure 1.23.

The advantages of this method are that it requires access to only one face, provides information on depth of defect, and tomographic cross-sectional images can be produced. However, it is only applicable to limited member thicknesses, and experienced operators are required.

In terms of trackbed evaluation, this method shares the anticipated disadvantages of the Ultrasonic Pulse Velocity due to the use of an ultrasonic pulse, with the anticipated disadvantages of other methods featuring analysis from the time-of-reflection waveform. This method, therefore, it not likely to be suitable for ballast evaluation.

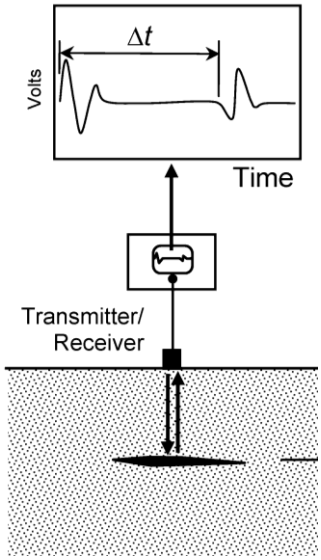

Figure 1.23 Ultrasonic echo schematic (ACI 228.2R S2.2, 2011)

1.7.10 Impact Echo

Impact Echo utilises an impact to generate a stress pulse into the test element and eliminates the requirement for a transmitting transducer. Internal anomalies and external surfaces reflect the stress waves. However, the stress pulse is not focused like a pulse from an ultrasonic transducer, but rather propagates into the test element in all directions, with reflections arriving back from many directions.

The impact is produced by tapping a small steel sphere against the test element. The stress waves that propagate into the test element are of a lower frequency (1 to 60 kHz) than those from traditional ultrasonic methods.

The stress waves propagate through the test element and surface displacements caused by the arrival of reflected waves are recorded by a transducer located near the impact point. The received test data is analysed as amplitude versus frequency, where dominant frequencies can be associated with multiple reflections of stress waves within the structure. This can provide information about the thickness of the structure, its integrity, and the location of flaws.

The method can determine concrete slab or masonry structure thickness, and the location and extent of cracks, delaminations, voids, honeycombing, and debonding. It can also locate voids in subgrade beneath slabs and pavements. The method is not adversely affected by the presence of steel reinforcing bars.

An example schematic can be seen in Figure 1.24.

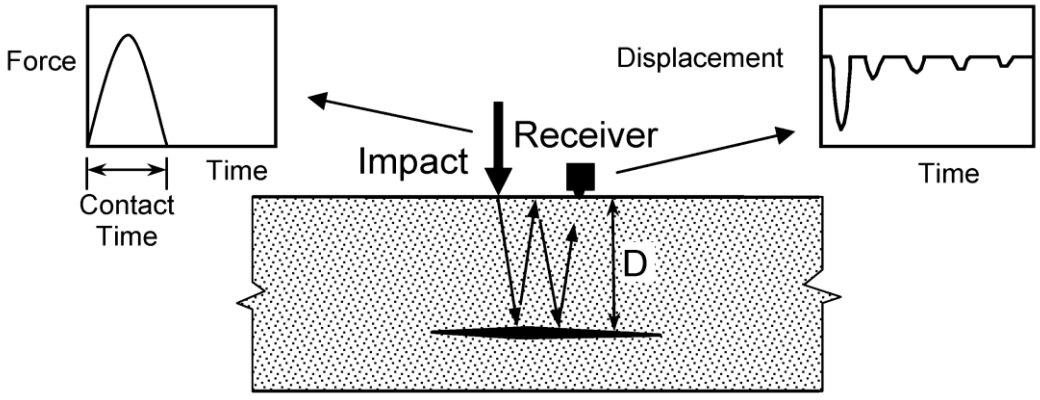

Figure 1.24 Impact echo schematic (ACI 228.2R S2.2, 2011)

The advantages of this method are that it requires access to only one face, there is commercially available equipment, it is capable of locating a variety of defects, and does not require coupling materials. However, an experienced operator is required, and current instrumentation limited to testing members 1m thick.

In terms of trackbed evaluation, this method is, in many ways, quite similar to the Impulse Response technique except that the waveform of the impact is not recorded, and thus, the received signal cannot be normalised. Furthermore, the impact signal is low energy, high frequency, and, consequently, highly dispersive. Therefore, impulse response would seem to offer more potential.

1.7.11 Spectral analysis of surface waves

In the 1980s, at University of Texas at Austin researchers undertook development of a testing technique called Spectral Analysis of Surface Waves (SASW) that involved a range of surface waves, or R-waves. Frequencies were generated by an impactor or vibrator. (Heisey et al., 1982).

The generated surface waves propagate along the surface of the test element. Two transducers monitor the motion of the surface waves as they travel along the test element surface and record the journey time of the various frequency components. The received signals are processed and used to infer the stiffness of the underlying layers.

An example schematic can be seen in Figure 1.25.

The impact pulse contains a range of frequencies (depending on the impactor). Low frequency components penetrate more deeply than high frequency components.

In a layered system, different frequency components of the surface waves propagate with different speeds; these are termed "phase velocities".

Using a process called "inversion", these phase velocities are matched against, and iteratively used to refine a layer model of the test site (consisting of density and elastic constraints), which results in the calculation of stiffness parameters.

The SASW technique can successfully determine the elastic modulus profiles of areas of soil, asphalt and concrete pavement systems, and concrete structural elements.

The advantages of this method are that it is capable of determining the elastic properties of layered or inter-layered systems, such as pavements, inter-layered good and poor-quality concrete. However, an experienced operator is required, and it involves complex signal processing.

In terms of trackbed evaluation, this method would likely be more suited to evaluating ballast properties in the absence of the railway track structure (sleepers and rails), otherwise it would be anticipated to be overly complex and likely infeasible.

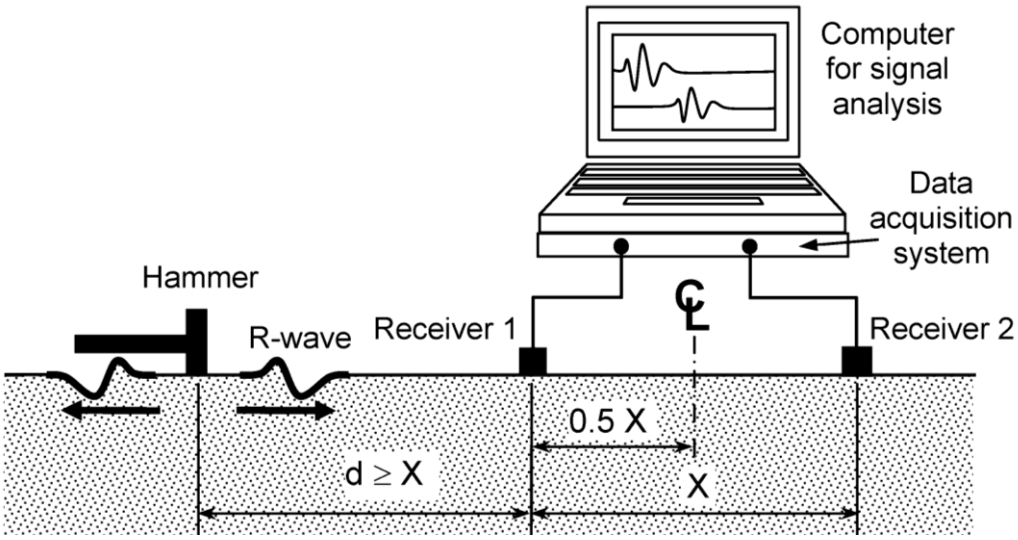

Figure 1.25 Spectral analysis of surface waves schematic (ACI 228.2R S2.3, 2011)

1.7.12 Ground Penetrating Radar

Instead of a physical wave, a ground penetrating radar (GPR) transmitting antenna radiates short pulses of electromagnetic radiation into the ground. Given the properties of electromagnetic radiation, the ground structure needs to be an insulator. This wave travels through the ground material and is reflected back when changes in dielectric properties are encountered at material interfaces. A receiving antenna measures variations in the reflected signal time profile and the amplitude.

Variations in the condition and configuration of the material will cause changes in the received signal. Therefore, the return time, amplitude, shape, and polarity of the received signal contains information on the medium, distance of the reflector, speed of the pulse through the medium, and how much of the pulse was attenuated. From these factors, inferences about the test element's material properties and make-up can be made.

Where several scans from a moving pass, or several passes, of the radar antenna are pieced together, an inferred image of the subsurface structure of an area can be made.

An example result can be seen in Figure 1.26 where three underground responses from pipes have been detected (appearing as parabolas).

The advantages of this method are that it is potentially non-contact, could permit high speed scanning, and has the ability to penetrate across material-air interfaces. However, it is sensitive to the presence of moisture, chlorides, and metal, and the region irradiated by the antenna is limited to a cone-shaped volume directly below the antenna. Congested reinforcement can prevent penetration beyond the reinforcement, cracks and delaminations in concrete are not easy to detect unless moisture is also present, and depth penetration can be limited where high frequency antennas are used. Furthermore, the behaviour of electromagnetic pulses propagating through structures is not completely known, and an experienced operator is required to operate the equipment and interpret the large amounts of data obtained.

In terms of trackbed evaluation, this method comes with many limitations but has the significant benefit of not requiring physical interaction, or potentially actual contact, with the ballast.

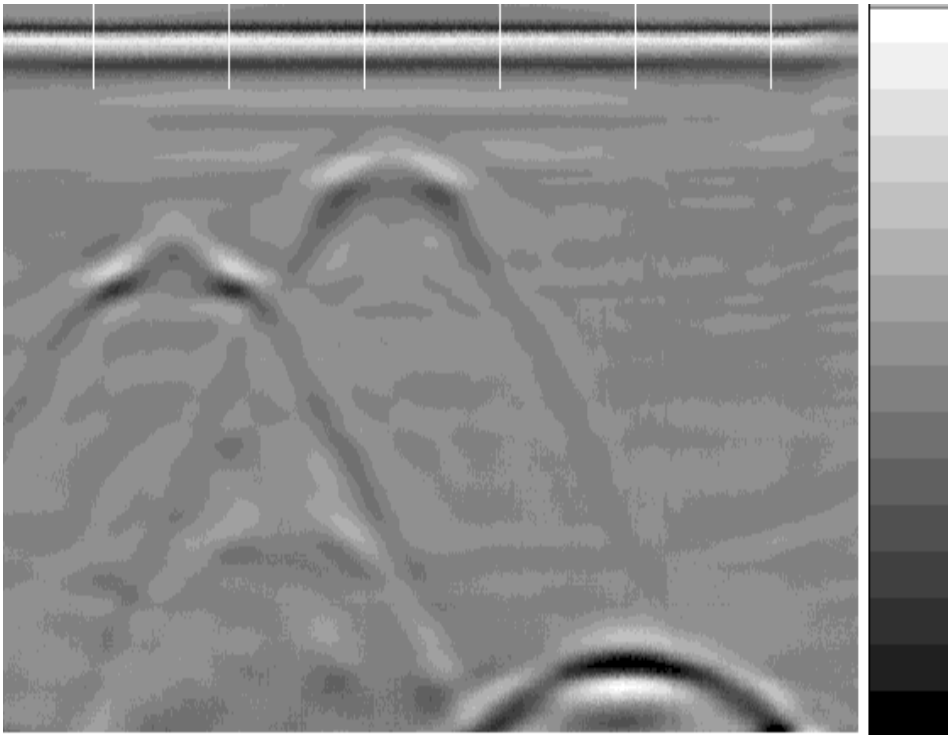

Figure 1.26 Example of a GPR plot

1.8 Selection of Methods to Further Investigate

Many of the above noted methods rely on a test signal traversing a solid, linear, uniform, isotropic element, such as a pile or a beam, and deviations from the solid, linear, uniform, isotropic nature are detected. These conditions are not comparable to railway track ballast, which is, essentially, a voided, irregular, loose, unbound, non-linear, non-uniform, non-isotropic material.

It is the features associated with ground penetrating radar that offer the most interest regarding this technique for research regarding railway ballast. It is known that the reflected signal contains information on the medium in the form of return time, amplitude, shape, and polarity of the received signal, and this offers the opportunity to research new ways of data analysis with regard to ballast condition.

Given that there is some enthusiasm for GPR within the international railway industry and that there has been previous research at the University of Edinburgh into the use of GPR in railways on the University's 10m-long full-scale railway track, it is intended to verify and extend this area of work (Clark et al., 1998)(Gallagher, 1999) (Gallagher et al., 2000) (Clark et al., 2001) (Clark et al., 2004).

Falling weight deflectometry is an accepted method for determining the whole trackbed condition, i.e., ballast and lower layers, and it is intended that some aspects of this method should be further investigated to determine whether a less intrusive alternative can be developed. Therefore, experimentation with a mini-falling weight deflectometer (Prima-100 6050) was undertaken (with potential for the results to be correlated with the radar data).

Work was also undertaken to gather and analyse the raw impact and response data from a physical impulse applied onto the railway track structure, i.e., impulse response testing. For this, the frequency response function (FRF) was determined from an instrumented hammer (PCB) blow and the response recorded by a low frequency geophone, both connected to a laptop running LabView software via a National Instruments 9233 analogue to digital converter.

Furthermore, a large amount of railway track radar data is available from collaborative partners. Roadscanners of Tampere, Finland, gathered large amounts of radar data of the Banverket track at Borlänge, Sweden; and full-scale track data collected under

funding from the Federal Railroad Administration is available from Volpe Centre, Cambridge, MA, and Amtrak. This data is to be numerically analysed in an attempt to measure track bed and subgrade stiffness.

Similarly, of the "impact" techniques, impulse response offers the prospect of a technique that can assess to the depths of a loosely bound medium such as railway ballast and generate a broad enough spectrum of data to assess.

1.9 Research Objectives

The detailed objectives can be summarised as: -

1. Investigate the University of Edinburgh 10m-long full-scale railway track with the objective of evaluating the condition of the ballast – see Chapter 2 University of Edinburgh Railway.
2. Investigate the history, theory and application of GPR, including previous University of Edinburgh research, with the objective of determining how to take the research forward – see Chapter 3 Ground Penetrating Radar.
3. Investigate GPR analysis techniques with the objective of validating previous research using GPR to fingerprint ballast condition – see Chapter 4 GPR Testing.
4. Investigate methods of analysing GPR data with the objective of developing new metrics to determine ballast condition – see Chapter 5 GPR Analysis.
5. Investigate the use of the Prima 100 mini-FWD on railways with the objective of determining its viability for measuring stiffness – see Chapter 6 Mini Falling Weight Deflectometer.
6. Investigate the history, and theory of impulse response, including previous research at other universities, with the objective determining its applicability on railways – see Chapter 7 Impulse Response.
7. Investigate the impulse response measurement system using an instrumented hammer and geophone with the objective of developing a method to evaluate ballast condition – see Chapter 8 Impulse Response Analysis.
8. Analyse Roadscanners data of the Banverket track with the objective of developing techniques to relate the radar responses to the stiffness measurements – see Chapter 9 Dynamic Track Modulus From GPR.

The original research work plan from the first year report can be seen in Appendix 1.

CHAPTER 2 UNIVERSITY OF EDINBURGH RAILWAY

2.1 Railway Track History

A 10m-long full-scale railway track was constructed at the University of Edinburgh in 1999 (Figure 2.1) as part of a previous research project (Gallagher, 1999) investigating the deterioration of railway ballast using ground penetrating radar (GPR).

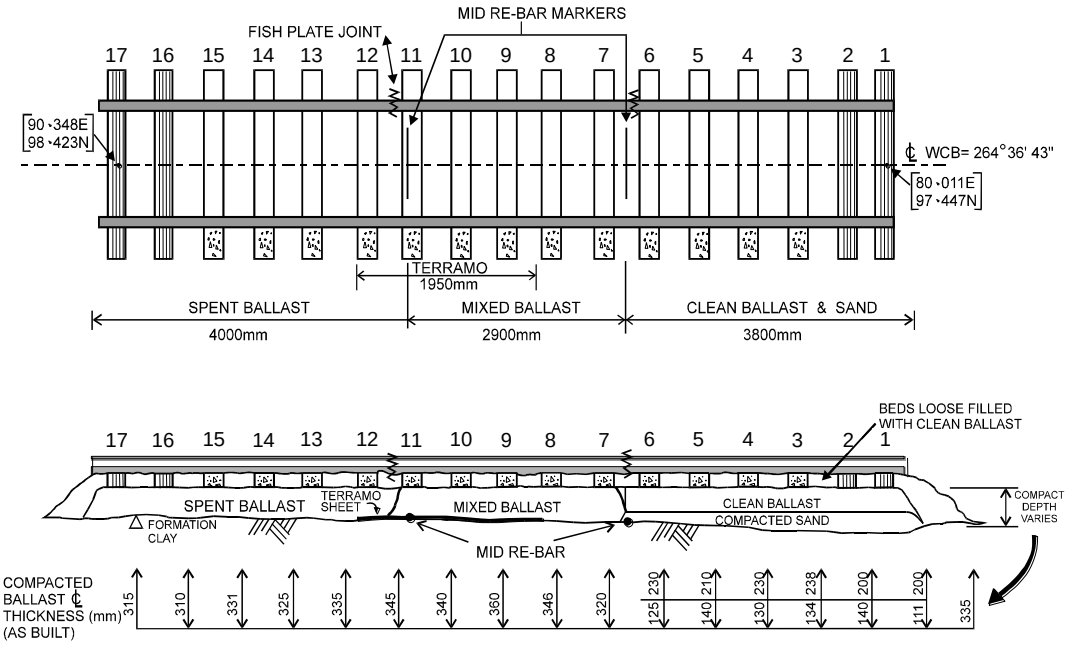

Figure 2.1 Full-scale railway track facility (Gallagher, 1999)

The purpose of the railway track was to create a full-scale test facility without the boundary effects of a laboratory experiment.

The construction deliberately featured three areas where differing quality of ballast was used: “clean”, “mixed”, and “spent”; in order to represent different levels of deterioration.

The track was built to British Rail Standard (BR1203, 1988) (Figure 2.2).

Figure 2.2 University of Edinburgh railway track construction

The "spent" ballast, representing deteriorated ballast, was also in accordance with British Rail standards and featured the addition of "30% fines" where 30% of the ballast material passed through a 14mm sieve; whereas, "clean" ballast would feature a maximum of 2% passing through the 14mm sieve.

Both timber and concrete sleepers were used as they are both in active service; two sleepers at either end of the track were wooden. A geotextile, sand blanket, and rebar markers were also originally incorporated to determine the effect, if any, they would have on the GPR plot.

2.2 Railway Track Modifications

Further research (Drossaert et al., 2005) was carried out using the University of Edinburgh railway track in 2005. The objective was to determine whether subsurface voids could be detected on railways using GPR. For this, the area of Crib 11 was excavated, the spoils piled either side on Crib 9 and Crib 13, and a plastic container inserted, and then the ballast replaced (Figure 2.3).

Figure 2.3 University of Edinburgh railway track excavation

The container could be filled and drained of liquids with ease given that it was connected to the surface via a downpipe. The tank was installed to a depth of 113cm from the top of the sleepers with dimensions of 25cm by 30cm by 55cm and a capacity of 40 litres.

Numerous other, less invasive, experiments were also conducted on the railway track since its construction.

However, since construction in 1999, although never trafficked, the railway track has been subjected to alteration, experimentation, and exposure to the weather and surrounding environment since its construction. It was presumed that this will have changed the as-built specification of the ballast, which, in fact, was never precisely known even when being built.

Consequently, a full investigation of the ballast condition by means of a basic visual inspection and then a particle size distribution (PSD) analysis was undertaken to quantify the status of the ballast.

2.3 Ballast Visual Inspection

In order to be able to take a representative sample of ballast for each crib, the upper layer of ballast present in each crib was removed to a depth of 120mm to the underside of the sleeper.

The removed layer of ballast for each crib was carefully placed and stored on individual polythene sheeting to avoid cross contamination of adjacent cribs and to retain the integrity of the condition of each crib for future testing. At this point, a visual inspection of the individual cribs was undertaken and recorded.

The following table of pictures represents the visual inspection of the ballast prior to sampling (Figure 2.4 to Figure 2.19).

Figure 2.4 Crib 1: Few fines; built clean

Figure 2.5 Crib 2: Few fines; built clean

Figure 2.6 Crib 3: Few fines; built clean

Figure 2.7 Crib 4: Few fines; built clean

Figure 2.8 Crib 5: Few fines; built clean

Figure 2.9 Crib 6: Few fines; built clean

Figure 2.10 Crib 7: Some fines; built mixed

Figure 2.11 Crib 8: Many fines; built mixed

Figure 2.12 Crib 9: Many fines; built mixed

Figure 2.13 Crib 10: Many fines; built mixed

Figure 2.14 Crib 11: Few fines; built spent

Figure 2.15 Crib 12: Many fines; built spent

Figure 2.16 Crib 13: Many fines; built spent

Figure 2.17 Crib 14: Many fines; built spent

Figure 2.18 Crib 15: Many fines; built spent

Figure 2.19 Crib 16: Many fines; built spent

2.4 Particle Size Distribution Sampling and Fouling Index

Particle size distribution (PSD) tests, conducted as per the appropriate British standard (BS 812-103.1, 1985) were undertaken for each crib. From each crib, a sample in excess of 10kg (a bucket-full) was removed using a metal scoop (Figure 2.20). The samples were then bagged, numbered, and taken to the laboratory.

Figure 2.20 PSD sampling

Sieve analysis was carried out in accordance with BS 812: Part 103.1: 1985 Clause 3.2. The method of dry sieving was appropriate given that the ballast particles did not show signs of agglomeration, having a significant presence of silt or clay; if agglomeration was present, "wet sieving" (Clause 7.2) would have had to been undertaken.

British Standard, "Soils for civil engineering purposes - Part 2: Classification tests" (BS 1377-2, 1990) recommends the use of 19 different sieves with progressively smaller sieve aperture sizes: -

> *75mm, 63mm, 50mm, 37.5mm, 28mm, 20mm, 14mm, 10mm, 6.3mm, 5mm, 3.35mm, 2mm, 1.18mm, 600µm, 425µm, 300µm, 212µm, 150µm, 63µm.*

However, only 13 sieve sizes were available: -

> *75mm, 63mm, 50mm, 37.5mm, 28mm, 20mm, 14mm, 10mm, 6.3mm, 3.35mm, 2mm, 600µm, 63µm.*

Given the size ranges that were of interest in the ballast (14mm and 75μm – see 2.5 Particle Size Distribution Analysis below), the missing sieves were not a problem.

The sieves were placed within a "shaker" in order of decreasing aperture size from top to bottom. The ballast sample was placed on top of the coarsest sieve and covered with a lid (Figure 2.21).

Figure 2.21 PSD shaker

The mechanical shaker vibrated and caused the ballast sample particles to descend through the upper (larger) sieve meshes to be retained by lower (smaller) sieve meshes. Each sieve was then removed and contained the sample of ballast material that was larger in size than the mesh size of the sieve yet smaller than the mesh size of the sieve located directly above in the shaker.

As per the British Standard (BS 812-103.1, 1985) the separation was checked by hand-sieving once removed from the shaker. The sieve with the largest mesh size was shaken first, followed progressively by the other sieves with smaller mesh sizes. Each was hand-sieved for no less than two minutes with a "varied motion, backwards and forwards, left to right, circular, clockwise and anti-clockwise, and with frequent jarring so that the material is kept moving over the sieve surface in frequently changing directions" without forcing ballast through the sieve.

The material retained on, and later cleaned from, each sieve was weighed, and recorded as a cumulative percentage weight of the original crib sample. Results for the missing sieve sizes were interpolated from the existing data. The information was charted on standard Edinburgh University PSD charts. The charts also featured grading curves as per (BS EN 13450, 2002) showing spent and clean ballast.

Results can be seen in Appendix 2.

2.5 Particle Size Distribution Analysis

The PSD results were analysed to determine the fouling index for each crib. There are two common methods for calculating a "fouling index" for ballast deterioration: Selig & Waters (Selig & Waters, 1994) and Ionescu (Ionescu, 2004).

A limitation of such a fouling index is that although the degree of fouling is related to the spentness of the ballast, it is not a full measurement of spentness. This is because fouling index is solely a description of the fines content of a particular ballast sample but spentness is a description of a collection of various other variables such as fines content, drainage efficiency, and surface texture (Parker, 1997). However, "fouling index" is a commonly accepted numerical assessment of ballast condition and strong indicator as to whether it is "spent" or not.

The Selig & Waters method passes the ballast material through two sieve sizes, 0.075mm and 4.75mm, and sums the percentage passing each sieve to determine the Fouling Index: -

$$F_I = P_{0.075} + P_{4.75}$$ **Equation 2.1**

Where, F_I = Fouling Index
$P_{0.075}$ = % passing 0.075mm sieve
$P_{4.75}$ = % passing the 4.75mm sieve

The Ionescu method is much the same, except the 4.75mm sieve is replaced with a 14mm sieve: -

$$F_I = P_{0.075} + P_{14}$$ **Equation 2.2**

Where, F_I = Fouling Index
$P_{0.075}$ = % passing 0.075mm sieve
P_{14} = % passing the 14mm sieve

The Ionescu method adheres to Australian standards that are similar to the material parameters used in British trackbed construction; whereas, the Selig & Waters method is suited to finer graded US ballast (cf. *Table 1.5 BR1203 ballast grading curve* and *Table 1.6 ASTM C33 gradation 4* under *1.2.5 Ballast Grading*). Since the trackbed was constructed to BR1203 specifications, the Ionescu method was used.

The categories of fouling developed by Selig & Waters were used in conjunction with the derived fouling index formula to determine the test track condition. However, the threshold for "clean" was slightly changed to 1.5% (from 1%) so that for the purposes of analysis in this thesis, Cribs 1 to 6, including Crib 11, shall be considered "Clean"; Cribs 7 to 10 shall be "Mixed"; and, Cribs 12 to 16, shall be "Spent" (Table 2.1).

Category	Fouling Index (F_I)
Clean	<1.5
Moderately Clean	1.5 - 10
Moderately Fouled	10 - 20
Fouled	20 - 40
Highly Fouled	>40

Table 2.1 Categories of fouling (modified Selig & Waters, 1994)

Applying Ionescu's formula to the PSD results gave Table 2.2 and Figure 2.22.

It can be seen from Table 2.2 that Crib 11, which was excavated in order to place a plastic tank, is "clean" when according to the as-built records it should be "fouled". Similarly, it can be seen that Cribs 9, 10, 12, and 13, where the spoil from Crib 11 was stored during the excavation process, have a higher fouling index than their immediate neighbours. Therefore, it can be construed that the excavation and ballast replacement process removed many of the fines from the ballast of Crib 11 and that some of these fines were deposited on the ballast of Cribs 9, 10, 12, and 13, thus increasing their fouling indexes.

Crib No.	F_I	Category
1	0.90%	Clean
2	1.05%	Clean
3	0.77%	Clean
4	0.84%	Clean
5	1.37%	Clean
6	0.79%	Clean
7	3.00%	Moderately Clean
8	4.80%	Moderately Clean
9	7.12%	Moderately Clean
10	7.20%	Moderately Clean
11	0.99%	Clean
12	13.79%	Moderately Fouled
13	17.45%	Moderately Fouled
14	10.79%	Moderately Fouled
15	11.70%	Moderately Fouled
16	20.47%	Fouled

Table 2.2 Ballast fouling index

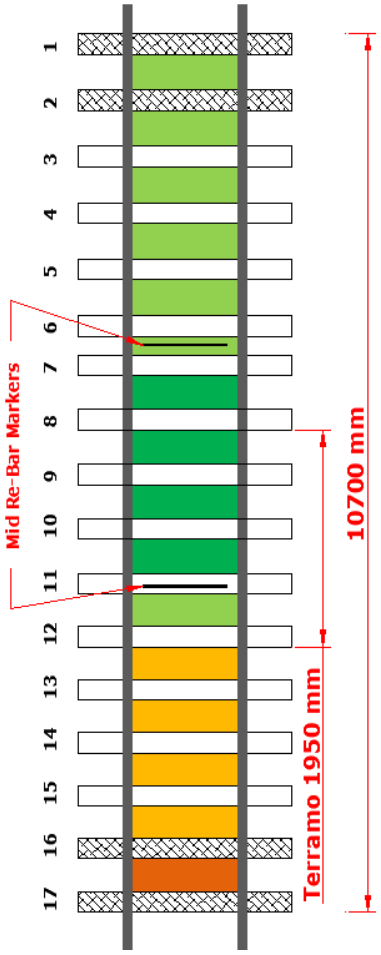

Figure 2.22 Ballast condition schematic

2.6 Conclusions

Inspection and analysis of the University of Edinburgh railway track has shown: -

1. If used for experimentation, the University of Edinburgh railway track has an advantage over laboratory setups in that it is full-scale and would not suffer from potential edge effects of attempting to replicate part of a railway track in a constrained cut-down model.
2. The Ionescu method of determining Fouling Index was used in preference to the Selig & Waters method because the Ionescu method adheres to Australian standards that are similar to the material parameters used in British trackbed construction.
3. In order to group together Cribs 1 to 6 (including Crib 11) as "Clean", the Fouling Index threshold for "clean" was slightly changed to 1.5% (from 1%).

CHAPTER 3 GROUND PENETRATING RADAR

3.1 GPR History and Application

Ground penetrating radar (GPR), sometimes called "georadar", "ground probing radar", or "subsurface radar", is a geophysical imaging method based on measuring reflected electromagnetic (EM) waves transmitted into the ground in the form of radar pulses in the microwave band of the radio spectrum (UHF/VHF frequencies).

The existence of electromagnetic waves was first postulated by James Clerk Maxwell (Maxwell, 1861), and it was Heinrich Hertz in 1887 who successfully developed a simple transmitter and receiver in order to prove Maxwell's theory (Hertz, 1887). He found that these waves could be transmitted through different types of materials, and were reflected by others, such as conductors and dielectrics (Hertz, 1888a)(Hertz, 1888b).

In 1896, Guglielmo Marconi registered a patent, the first of many, relating to the "Improvement of Transmitting Electrical Impulses and Signals" (Marconi, 1896). This patent is often credited as the invention of radio; although it is much debated as to whether his work was more advanced than that of Hertz or Tesla or the many other pioneers researching wireless telegraphy at that time.

The first use of electromagnetic radiation to detect remote objects was in 1904 (Ender, 2002), when Christian Hülsmeyer gave public demonstrations of his “anti-ship-colliding" system (Hülsmeyer, 1904) in Germany and the Netherlands. In 1910, Löwy and Leimbach buried dipole antennas in an array of vertical boreholes and compared the magnitude of signals when successive dipole pairs were used to transmit and receive (Löwy & Leimbach, 1910). This permitted a crude shadow image to be formed of an ore body within the array, which preferentially absorbed radiation (Daniels, 2004).

It was in 1917 that Nikola Tesla first established principles regarding frequency and power levels for the first primitive radar units (Page, 1962).

Progress in radar development continued throughout the pre-World War II years, with the United Kingdom and Germany leading in the advances of the use of radio for

detection and tracking of aircraft; however, there were also developments in the United States, the Soviet Union, and Japan; the war itself gave a great surge to further radar developments (Page, 1962). The acronym RADAR (for RAdio Detection And Ranging) was coined by the US Navy in 1940, and the subsequent name "radar" was soon widely used (Page, 1962).

The first reported use of radar to penetrate the ground surface directly was for conducting surveys of glaciers in Austria in order to determine their depth (Stern, 1929) (Stern, 1930). However, the technology was largely forgotten about until the 1950s (Olhoeft, 1996), when up until then most radar research had been into wave propagation above and along the surface of the Earth (Annan, 2002).

The next reported attempt at GPR was to use the interference between direct air transmitted signals and signals reflected from a water table to determine its depth (El Said, 1956).

Further research in the field was undertaken to investigate the phenomenon of US Air Force aircraft using radar altimeters crashing when attempting to land on glaciers in Greenland; the radar was seeing through the ice and misreporting the aircraft's height above the ice (Waite & Schmidt, 1961).

Much of the research in the early 1960s was similarly involved in research into radio echo sounding in ice (Annan, 2002). Studies in polar regions and on glaciers was undertaken by groups such as the Scott Polar Research Institute at Cambridge (Bailey et al., 1964) and the Geophysical and Polar Research Center at the University of Wisconsin (Bently, 1964) (Walford, 1964).

Into the 1970s, GPR research continued into the ability of radar to map subsoil properties and the water table (Olhoeft, 1996) and find applications in other favourable geological materials, such as salt in salt domes (Holser et al., 1972), salt deposits (Thierbach, 1973), and coal in coal mines (Cook, 1973).

Also during this period, there was research into the application of GPR for the Apollo 17 moon exploration programme in order to determine lunar surface electrical properties (Simmons et al., 1973) and to be used as a lunar surface sounder (Ward et al., 1973).

It was only in the early 1970s that GPR devices became commercially available when Rex Morey and Art Drake founded Geophysical Survey Systems Inc. (GSSI) for the manufacturing and selling of such systems (Morey, 1974). This lead to an explosion of applications, publications, and research related to GPR, with over 300 patents related to the field being registered in the subsequent 20 years (Olhoeft, 1996).

Consequently, this resulted in a much better understanding of the electrical character of natural occurring geological materials and the relationship between electrical conductivity and dielectric polarization of these materials (Olhoeft, 1975) (Olhoeft, 1987).

Into the 1980s, further advances were made in the fields of using GPR to survey frozen environments (Annan & Davis, 1976), archaeology to search for caves (Dolphin et al., 1978), or mining coal (Coon et al., 1981), and surveying hard rock for potential suitability for nuclear waste storage (Davis & Annan, 1986). Other companies were also formed that commercially produced GPR units, such as Xadar, OYO Corporation, A-Cubed Inc (later Sensors & Software Inc), and Mala in the early 1990s (Annan, 2002).

Into the 1990s and beyond, GPR also began to find roles in other fields such as concrete inspection, road and rail inspection, utilities detection, as well as being firmly accepted and established in the previously listed fields of geology, civil engineering, surveying, and archaeology.

3.2 GPR Principles

To generate a GPR profile, a transmitting antenna radiates electromagnetic pulses within the radio range into the ground and a receiving antenna measures variations in the reflected signal time profile and the amplitude. For pulsed GPR systems, the transmitted pulse is a single bipolar pulse. The most commonly used pulses for concrete evaluation range from 1 to 3 nanoseconds (ns) in duration, consisting of a few peaks, with a nominal centre frequency value, commonly, between 400MHz and 2.6GHz for structural surveys (ACI 228.2R S2.8, 2011).

Materials can be characterised as *dielectrics*, *conductors*, or *magnetics* depending on whether *polarisation*, *conduction*, or *magnetisation, respectively,* are the predominant phenomenon (Balanis, 1989). Dielectric materials (insulators) contain bound positive and negative charges that are not free to travel; whereas, conductors are materials

where the predominant characteristic is the motion of electrical charges and the creation of current flow; as such, GPR electromagnetic waves cannot penetrate through conducting materials. Most materials encountered with GPR are non-magnetic.

However, for dielectric materials, as each pulse travels through the material, a portion of the energy is reflected back to the antenna as the signal moves through material interfaces between two media of differing dielectric properties.

Electromagnetic wave propagation is affected by changes in dielectric properties, and, therefore, variations in the condition and configuration of the material will cause changes in the received signal. The return time, amplitude, shape, and polarity of the received signal thus contains information on the transmitted medium, distance of the reflector, speed of the pulse through the medium, and how much of the pulse was attenuated (ACI 228.2R S2.8, 2011).

The time profile of the interface reflections can be used to infer an underground structural profile, which in materials such as concrete, the presence of voids, honeycombing, and high moisture and chloride content can also be inferred. Therefore, this reflected time domain signal can be construed to translate to an underground material profile.

This can be seen in Figure 3.1, where a diagram of a railway profile (left of diagram) is matched against a typical scan response profile (middle), and the combination of several scans produce an underground radar image profile (right).

A railway trackbed is a multi-layered structure, with each layer having different dielectric properties. Between each layer, an interface is formed, such as the ballast-subballast interface, or ill-defined interfaces, such as inclusion anomalies and heterogeneities within a layer. Due to its layered nature, GPR is ideally suited for railway applications; with data potentially being collected at high speeds (Clark et al., 2004).

There are two types of GPR antenna: a bowtie antenna and a horn antenna. Bowtie antennas feature two internal bowtie dipoles and require to be coupled directly with the ground; horn antennas can be suspended a greater distance above the ground.

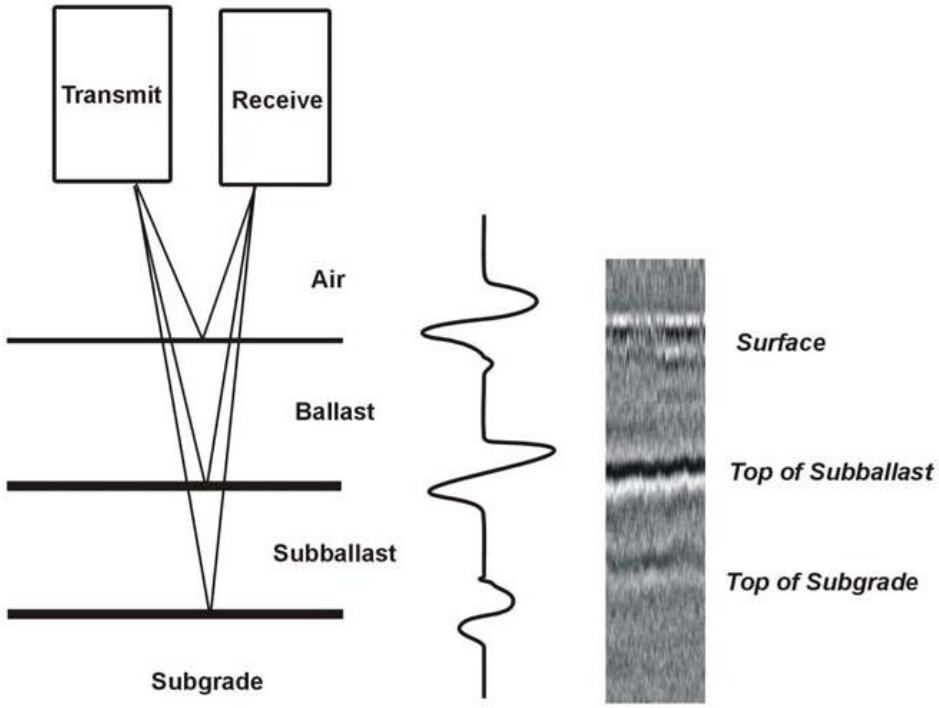

Figure 3.1 Generation of a GPR profile (unknown source)

GPR is non-invasive and non-destructive and has numerous applications in imaging subsurface features in a variety of media. For example, the features can be objects, changes in material, voids, and cracks; and the media can be rock, soil, ice, fresh water, pavements, and structures. The depth penetration of GPR is determined by the electrical conductivity of the ground materials and the transmitted frequency.

In materials of greater conductivity, electromagnetic energy is more quickly dissipated into heat, causing a loss in signal strength; thus, a lesser depth penetration is achieved in materials of greater conductivity.

Similarly, partly because higher frequencies correspond to increased current flow, and, therefore, electromagnetic energy loss, higher frequencies cannot penetrate as far as lower frequencies. They do, however, give better resolution of the upper layers due to the shorter wavelengths being able to resolve correspondingly smaller objects. For work investigating a layered underground structure, the frequency should be chosen so that the thickness of the thinnest layer of interest can be seen. In addition, a range of antenna may be required.

Due to the high electrical permittivity of water, depth penetration in moist soils is also significantly reduced. Generally, greatest depth penetration, e.g., up to 15m, is achieved

in dry granular soils or massive dry materials such as granite or concrete. The amount of energy reflected from and transmitted through an interface depends on the differences in the dielectric values of the two layers.

3.3 GPR Theory

The dielectric constant or electrical permittivity and the conductivity of a material are the primary material properties that affect the transmission and reflection of electromagnetic energy.

A material's dielectric constant, also known as dielectric permittivity, is the amount of electrostatic energy stored per unit volume for a unit potential gradient. Electrical conductivity, the reciprocal of electrical resistivity, is a measure of the ease with which an electrical current can flow through a material.

The ratio of a material's dielectric constant to that of free space is defined as the relative dielectric constant, ε_r: -

$$\varepsilon_r = \frac{\varepsilon}{\varepsilon_0}$$

Where, ε = dielectric constant (F/m); **Equation 3.1**

ε_0 = dielectric constant of free space (air), which is 8.85×10^{-12} F/m.

By definition, the relative dielectric constant of air is 1, and typical values for other materials are shown in Table 3.1.

Material	Range of ε_r
Air	1
Portland cement concrete	6 to 11
Bituminous concrete	3 to 5
Gravel	5 to 9
Sand	2 to 6
Rock	6 to 12
Water	80

Table 3.1 Material ranges of ε_r (ACI 228.2R S2.8, 2011)

The dielectric constant of water is much greater than the other listed materials; therefore, water is generally the most significant dielectric contributor to construction

materials and explains why radar is highly sensitive to moisture. As a construction material's moisture content increases, the overall dielectric constant of the material also increases (Padaratz & Forde, 1995).

The relative dielectric constant governs the speed of the electromagnetic wave in a particular material and various calculations are used to convert GPR time signal responses into depth profiles.

The simplified velocity equation of electromagnetic waves in a dielectric medium for low-loss materials (materials having a small dissipation of electric or electromagnetic power) is (Daniels et al., 1988): -

$$v = \frac{c}{\sqrt{\varepsilon_r}}$$

Where, v = velocity of propagation;
c = speed of light (3×10^8m/s); and,
ε_r = dielectric constant of medium.

Equation 3.2

This velocity of propagation will vary with the composition and water content of the medium, and for the ballast and subballast layers will generally fall within the range [1.2-2.0] $\times 10^8$m/s. For comparison, v in pure water is 3.33×10^7m/s. The simplified equation above is only valid for low conductivity materials – at higher conductivies, the velocity is frequency dependent.

The depth of the reflecting interface is calculated from the measured round trip travel time, i.e., the time there and back, and the speed of the electromagnetic wave: -

$$t_r = \frac{2d}{v} = \frac{2d\sqrt{\varepsilon_r}}{c}$$

Where, t_r = two-way travel time; and,
d = depth to interface.

Equation 3.3

Given that the two-way travel time for each layer can be determined from the GPR time-domain waveform responses; then, assuming the relative dielectric constant of the material into which the pulse is transmitted is known, the depths can be calculated. The pulse width of a GPR system is the reciprocal of the operating frequency; thus, at 400MHz the pulse width is 2.5ns.

The resolution that a GPR system can achieve is an important consideration. Resolution refers to the minimum size that a pulse of duration τ can determine. In a medium of dielectric constant ε_r, this is approximately (Skolnik, 1980): -

$$\Delta R = \frac{c\tau}{2\sqrt{\varepsilon_r}} \qquad \text{Equation 3.4}$$

Where, τ = transmitted pulse width; and,
ΔR = "range resolution".

The minimum discernable layer thickness can be calculated by using Equation 3.3 with the pulse being a known finite duration and t being equal to one-third the pulse duration, where, in this case, the resolution is assumed to be one-third of the wavelength, λ, (McCann and Forde 2001).

Therefore, for example, for a material with a dielectric constant of 6 ($v = 123$mm/s) and a pulse duration of 6ns (equivalent to 1GHz central frequency), the minimum discernable thickness would be approximately 45mm. Similarly, when surveying layered material, the material layers have to be thick enough in order for the reflections from successive layers to be discernable.

From further research into this subject (Padaratz et al., 1997) calculated a table that summarized the resolution and minimum depth (Z_{min}) that can be detected for different centre frequencies and concrete conditions (Table 3.2).

Material	ε_r	Frequency in air (MHz)	Frequency in material (MHz)	Velocity (mm/ns)	Wave-length (mm)	Resolution (mm)	Z_{min} (mm)
Dry Concrete	6	1,500	1,050	123	117	59	39
Damp Concrete	10	1,500	1,050	95	90	45	30
Dry Concrete	6	900	630	123	195	98	65
Damp Concrete	10	900	630	95	151	76	50
Dry Concrete	6	500	350	123	351	176	117
Damp Concrete	10	500	350	95	271	136	90
Dry Concrete	6	100	70	123	1757	879	586
Damp Concrete	10	100	70	95	1357	679	452
Where ε_r = relative dielectric constant							

Table 3.2 Characteristics of radar propagation in concrete (Padaratz et al., 1997)

These numbers are based upon the assumptions that resolution is based upon $\lambda/2$ and the minimum detectable depth is $\lambda/3$, and that the centre frequency in air of a dipole radar antenna signal reduces by approximately 30% when brought into contact with concrete.

The contrast in dielectric constant determines the amount of reflected energy at the interface between two dissimilar materials. For low-loss dielectrics, the ratio of the reflected to incident amplitudes of the electromagnetic field (reflection coefficient) is (Bungey & Millard, 1993): -

$$\rho_{1,2} = \frac{\sqrt{\varepsilon_{r1}} - \sqrt{\varepsilon_{r2}}}{\sqrt{\varepsilon_{r1}} + \sqrt{\varepsilon_{r2}}}$$ **Equation 3.5**

Where, $\rho_{1,2}$ = reflection coefficient;
ε_{r1} = relative dielectric constant of Material 1(incident wave); and,
ε_{r2} = relative dielectric constant of Material 2.

Equation 3.5 shows that where the dielectric constant of Material 2 is greater than Material 1, the reflection coefficient is a negative number. A negative reflection coefficient would indicate a change in polarity, or phase reversal, of the reflected wave, which means that the positive part of the wave is reflected as a negative part.

Where a conductor such as metal is encountered, there is complete reflection and phase reversal. Consequently, ground penetrating radar is very effective at detecting conducting objects within a non-conducting material. However, the strength of such reflections can obscure other weaker reflections, and multiple reflections from numerous or repeating metallic objects, such as a reinforcement mesh in concrete, can mask reflections from beyond the metal objects (Bungey et al., 1994). Plastic ducts are now used in many new post-tensioned concrete bridge beams to enable post-construction inspection by GPR (Bungey et al., 1997).

Unlike testing methods that use a physical stress wave, such as impact-echo or impulse-response, radar waves can penetrate beyond material-air interfaces. In air, the acoustic impedance (analogous in this case to dielectric constant) is very low and virtually negligible in comparison to the acoustic impedance of most solid materials; this results in almost complete reflection from the material-air interface. Whereas the relative values of dielectric constants for air and materials such as concrete can result in much

of the electromagnetic wave energy continuing past the material air boundary to be later reflected back from other interfaces and detected by the GPR unit.

Conductivity, and, to a lesser extent, the dielectric constant of a material determines the energy loss; this signal attenuation can be approximated (Bungey & Millard, 1993): -

$$\alpha = 1.69 \times 10^3 \frac{\sigma}{\sqrt{\varepsilon_r}}$$ Where, α = signal attenuation (dB/m); and, σ = conductivity ($\Omega^{-1}m^{-1}$). **Equation 3.6**

It should be noted that conductivity can be frequency dependant; for concrete, the conductivity at 1GHz is about 1.5 times the conductivity at 0Hz (direct current) (Halabe et al., 1993).

3.4 GPR Radar Scatter

Scattering losses are frequency dependant – they increase as the frequency increases. GPR signals are sent through many kinds of materials and encounter many heterogeneous electrical and magnetic properties.

Small-scale heterogeneities generate weak or undetectable responses but attenuate energy as the EM field passes due to scattering (Annan, 2008) (Figure 3.2).

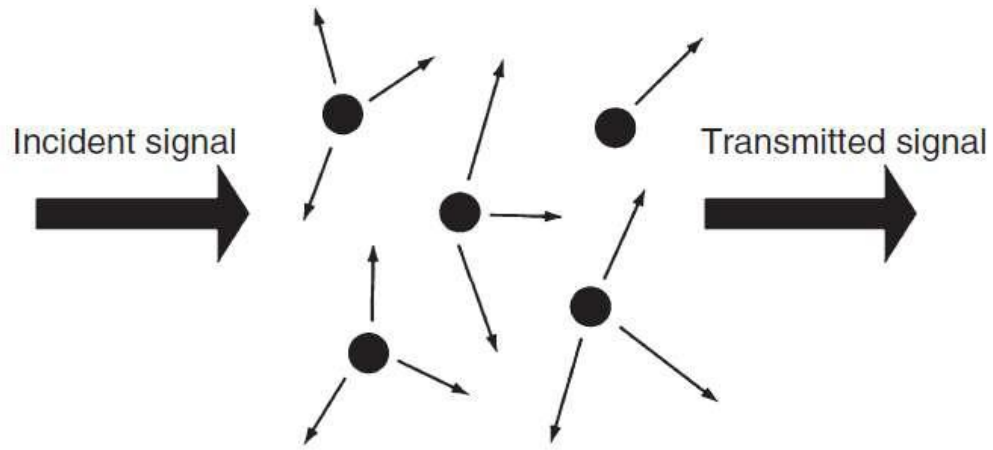

Figure 3.2 Signal scattered by small heterogeneities (Annan, 2008)

3.5 GPR on Concrete

There has been much research into the field of using of GPR in concrete.

The influence of the size and shape of voids within a concrete structure on the GPR response have been investigated (Bungey & Millard, 1995), as well as the influence of the void size below a concrete pavement (Steinway et al., 1981) (Halabe et al., 1993). Similarly, the effects on the response signal of different levels of concrete moisture content (Shaw et al., 1993), or different levels of moisture and chloride content under asphalt overlays (Maser & Roddis, 1990), have been investigated.

Theoretical models for predicting the dielectric properties of concrete as a function of temperature, porosity, moisture and salt contents, and radar frequency have also been developed (Padaratz & Forde, 1995), which also showed that the electromagnetic wave velocity is frequency dependent at higher frequencies.

In addition, models that determined radar waveform synthesis and inversion (Halabe et al., 1995) (Giannopoulos, 1997) were developed. Such modelling can be used to generate theoretical radar waveforms and undertake simulated testing of layered media, such as overlaid bridge decks and pavements, with features such as reinforcing bars and delaminations; or, to estimate the physical properties of concrete bridge decks from radar waveforms (Halabe et al., 1995). The finite element analysis method has also been used to simulate the propagation of electromagnetic pulses through concrete (Millard et al., 1993).

3.6 GPR on Railways

Much of the work in the field of using GPR on railways has concentrated on monitoring the subsurface; there has been little work in attempting to determine track modulus or stiffness. It is still being researched and is now partially deployed commercially (Hugenschmidt, 2000)(Eriksen et al., 2004) (Kathage et al., 2005) (Roberts et al., 2006a)(Roberts et al., 2006b) (Xie et al., 2008).

GPR has been found to be useful in determining the layering profile of track substructure and areas of high moisture content within it; such areas produce stronger reflections (Dolphin et al., 1978) and water pockets can also be detected (Zarembski, 1987).

One field study found that by making the broad assumption that the velocity of signal propagation in ballast is 1.4×10^8m/s, that the thickness of the ballast layer could be calculated to an accuracy of 3cm. Some determination of the extent of subsoil penetration into the ballast layer could also be identified (Hugenschmidt, 2000). The limitation of this work is that the accuracy is not related to antenna wavelength.

The University of Edinburgh research into ground penetrating radar (GPR) testing of a railway trackbed (Clark et al., 1998)(Gallagher, 1999) (Gallagher et al., 2000) (Clark et al., 2001) (Clark et al., 2004) was the first to relate antenna centre frequency to resolution. Similar work by others (Sharpe & Collop, 1998) (Jack & Jackson, 1998) (Hugenschmidt, 1999) also showed that spent ballast could be identified visually at the same time as track failure. Previously, the maintenance regime of visually identifying failure as a means to deal with ballast deterioration was a reactive one, and, consequently, cost-inefficient.

Therefore, the GPR method of assessment can be used for a qualitative first indication of ballast condition and potential fines migration at poor formation sites, and also facilitates the better targeting of intrusive and disruptive site investigations (Brough et al., 2003). It has also been proposed that GPR can be used as a method for trackbed quality control by providing continuous ballast depth data (Sharpe, 2000).

3.7 GPR Field Experiments at the University of Edinburgh

The University of Edinburgh research (Gallagher, 1999) found that on studying the time-amplitude plot of a single radar pulse reflection from the test track, it could be seen that where the ballast was "spent" the signal plot featured "scattering" between the surface reflection response and the ballast-formation layer interface reflection. Where the ballast was not spent, there was no "scattering" (Figure 3.3 and Figure 3.4).

Two antennas were used, a 900MHz and a 500MHz. The 500MHz antenna demonstrated increased power and the lower centre frequency resulted in a greater depth penetration over the 900MHz. The resolution was significantly lower (approximately halved, consequent with the reduction in frequency). However, the reflection times through the same media were similar. None of the antennas managed to produce reflections through the sleepers.

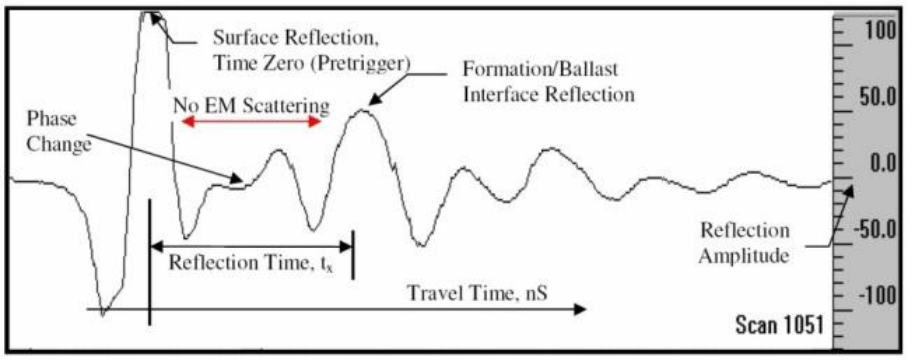

Figure 3.3 Typical 500MHz antenna signal plot in clean ballast (Gallagher, 1999)

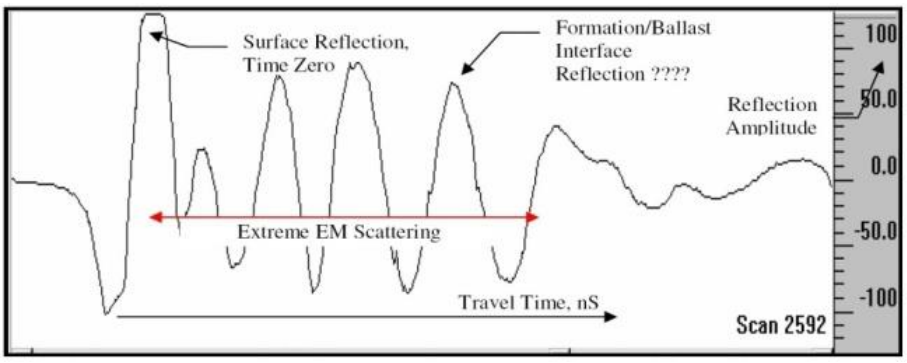

Figure 3.4 Typical 500MHz antenna signal plot in spent ballast (Gallagher, 1999)

The 500MHz and 900MHz signals through the clean ballast gave no EM scattering, and a clear formation reflection. Through the mixed ballast, there was increased EM scattering, a less clear formation reflection, and a reduced propagation velocity consequent with a greater dielectric constant. Through the spent ballast there was extreme EM scattering making the formation reflection indistinguishable, and a further reduced propagation velocity. The 900MHz signals demonstrated greater scattering than the 500MHz signals through the same material.

The different results were attributed to the spent ballast having a greater fines content with fewer air voids, and poorer drainage efficiency and, consequently, greater moisture content due to moisture retention from soil suction. Loss of voids (with a very low dielectric value), and replacement with moist fines (with a significantly higher dielectric value), resulted in the increased scattering and attenuation.

The experiments were repeated several times over one year in different weather conditions. It was found that the clean ballast results varied by 5% to 7%; the spent ballast results varied by up to 25%. Ballast-saturation tests carried out in the lab (Clark

et al., 2001) determined that the greater variability of the spent ballast was due to its ability to hold water due to soil suction, or capillarity, and become saturated due to rain; the clean ballast is more free-draining and less affected by rain.

A further set of similar experiments were carried out using "bistatic" antennas. This permitted the transmitter location to be fixed and multiple readings taken as the receiver was incrementally moved further away, along the track. It was possible to observe the reflection from the ballast-formation interface. Given identification of the time of reflection to the ballast-formation interface from two, or more, known receiver distances, basic trigonometry could be used to determine the depth to formation without reference to calculated propagation velocity and the inaccuracy influences of weather conditions.

The maximum separation achievable where meaningful readings could be taken and the depth calculated reduced with increased levels of ballast deterioration. The 500MHz antenna could be separated twice the distance of the 900MHz antenna. This earlier research at the University of Edinburgh demonstrated that railway ballast could be fingerprinted using GPR.

GPR research on void detection on the track undertaken in 2005 (Drossaert, 2008) found that a 40 litre plastic container buried between 58cm and 113cm deep could not be identified using a 900MHz or a 500MHz GSSI antenna. Furthermore, Drossaert concluded that it is difficult to detect small voids in railway ballast due to the presence of sleepers plus strong attenuation of the signal caused by highly conductive materials around the tank. Drossaert stated that detection of voids in railway ballast is of crucial importance for the safety of railway traffic and, thus, further investigation is needed.

3.8 GPR Laboratory Experiments at the University of Edinburgh

Other GPR research work on ballast undertaken at the University of Edinburgh (Clark, 2001) sought to characterise the condition of ballast related to relative permittivity or dielectric constant in laboratory tests.

The objectives of the laboratory work were to determine if ballast condition, i.e., clean or spent, could be determined from the calculated relative permittivity or dielectric constant, ε_r; and to assess the influence of antenna frequency using 500MHz and 900MHz antennas.

For the laboratory experiments, a large brick tank structure was constructed in which the ballast could easily be placed to a suitable depth (Figure 3.5).

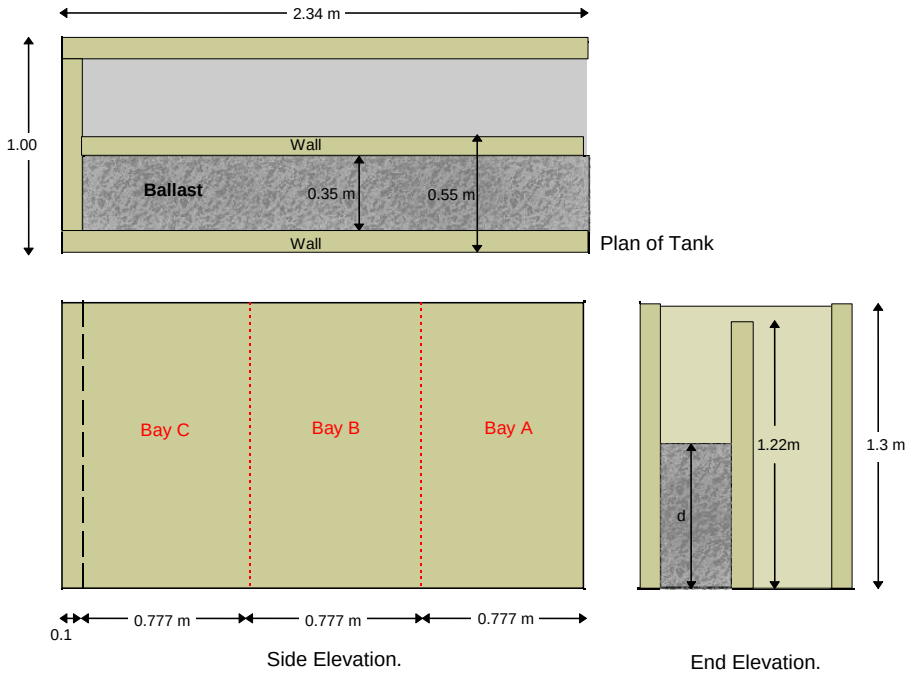

Figure 3.5 Tank dimensions (Clark, 2001)

The experiment was undertaken twice: once with unused clean ballast and once with spent ballast at the end of its life span recovered from a railway trackbed. The placing and compaction of the ballast was intended to mimic real track conditions (Figure 3.6)

Figure 3.6 Tank containing 0.75m of spent ballast (Clark, 2001)

The experiment was undertaken by dragging each radar antenna along the surface of each ballast type, as can be seen in Figure 3.7.

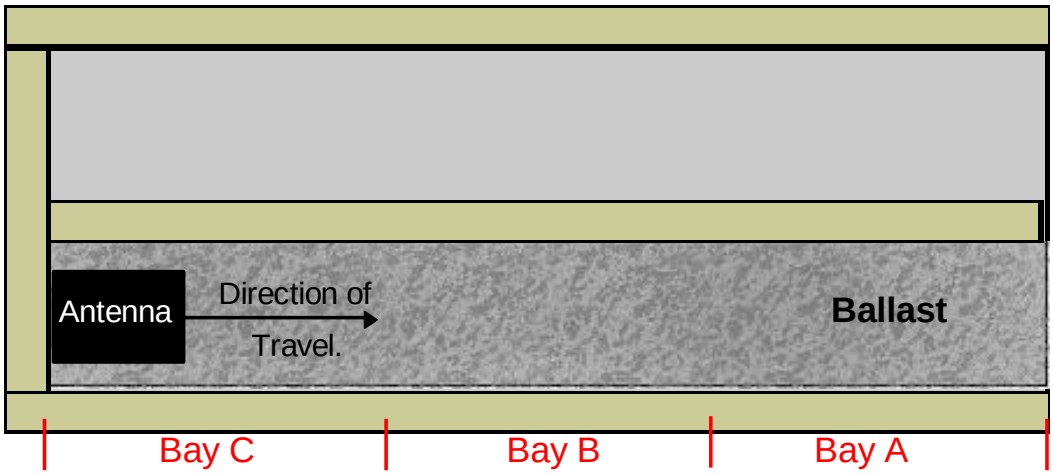

Figure 3.7 Plan view of test rig (Clark, 2001)

The ballast was assumed to be a low loss (and low conductivity) material, and, therefore, Equation 3.3 was suitable to be used to determine the dielectric constant and velocity of wave propagation for the different types of ballast tested (Table 3.3).

Material (* by volume)	ε_r	velocity (m/s)	Density (Mg/m^3)
Air	1	3.00x10^8	
Water	81	0.33x10^8	1
Dry Clean Ballast	3.0	1.73 x10^8	1.6
Wet Clean Ballast (5% water*)	3.5	1.60 x10^8	
Saturated Clean Ballast	26.9	0.48 x10^8	
Dry Spent Ballast	4.3	1.45 x10^8	1.8
Wet Spent Ballast (5% water*)	7.8	1.07 x10^8	
Saturated Spent Ballast	38.5	0.58 x10^8	

Table 3.3 List of electromagnetic properties for various materials (Clark, 2001)

These variations in dielectric constant values were attributed to: -

- Clean ballast having a greater volume of air voids, which lowers the average dielectric constant of the medium;
- Water increasing the average dielectric constant of the medium; and,
- Spent ballast, with greater fines, can hold more water than clean ballast; thus "wet spent" ballast has a higher dielectric constant than "wet clean" ballast.

It was found that the dielectric constant for the spent ballast under dry or wet conditions was greater than that for the clean ballast. These results for the dielectric constant were also comparable with other results for ballast (Sussmann, 1999), as can be seen in Table 3.4: -

Ballast Material	ε_r (Sussmann, 1999)
Dry Clean	3.6
Moist Clean	4
Dry Spent	3.7
Moist Spent	5.1
Wet Spent	7.2

Table 3.4 Comparable published dielectric constants of ballast (Sussmann, 1999)

The correlation between Sussmann (1999) and Clark (2001) is encouraging given the slight difference between UK and US ballast gradings.

The radar plots of the ballast using the 900MHz and 500MHz antennas can be seen in Figure 3.8 and Figure 3.9.

Analysis of the plots show where the: -

i. Electromagnetic wave enters the ballast surface;
ii. Wave reflects from base of tank; and,
iii. Diagonal "swipe signatures" are caused by reflections from the tank walls.

The 500MHz antenna had a greater depth penetration and showed the ground reflection from the laboratory concrete floor more clearly than the 900MHz antenna. The 500MHz antenna also had a lesser resolution than the 900MHz antenna resulting in less reflection, and less clutter, from the individual ballast particles, which also resulted in more pronounced swipe signatures.

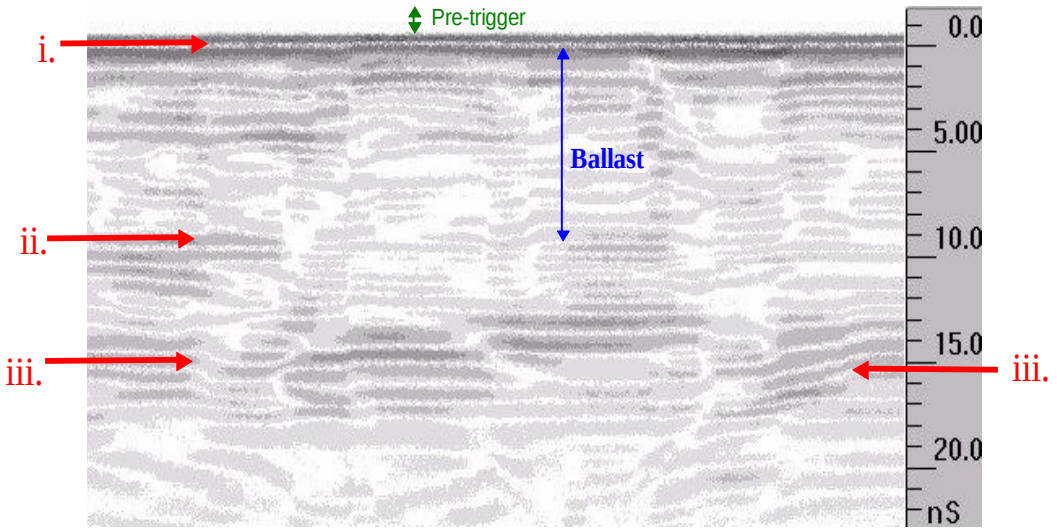

Figure 3.8 Subsurface profile of 1m of spent ballast – 900MHz antenna (Clark, 2001)

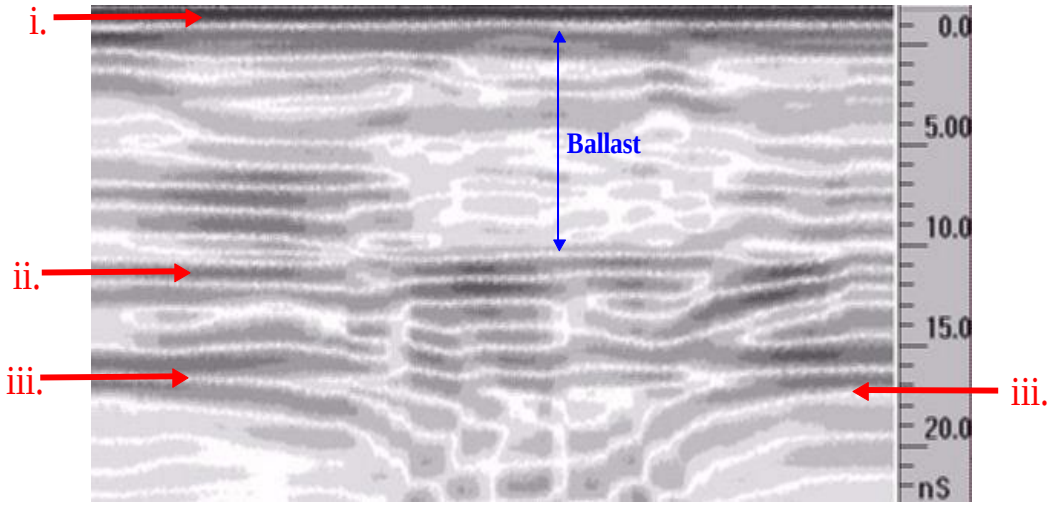

Figure 3.9 Subsurface profile of 1m of spent ballast – 500MHz antenna (Clark, 2001)

3.9 Conclusions

The previous research at the University of Edinburgh used GPR to undertake field and laboratory testing of ballast.

The field experiments results could be used to differentiate between clean and spent ballast through a visual inspection of the radar waveform.

With the laboratory experiments, there was no attempt to analyse the waveform of the reflected signals, only its velocity; however, the presence of the edge effects would make waveform analysis unreliable. Such edge effects are unavoidable in a contained laboratory experiment; therefore, laboratory experimentation is suitable for

determining the dielectric constant value, but not waveform analysis. Field experimentation free from boundary effects would be required where analysis of the waveform was desired.

It is, therefore, the intention of this research to undertake controlled GPR field experiments on the University of Edinburgh track where edge or boundary effects would not be an issue in order to develop a numerical method of waveform analysis to calibrate the results with the particle size distribution results.

CHAPTER 4 GPR TESTING

4.1 Ballast Waveform Analysis

The concept of analysing the GPR waveform to determine the quality of ballast has been undertaken before. At the Transportation Technology Center, Inc. (TTCI) in Pueblo, Colorado, analyses of the waveform taken from horn antennas (Roberts et al., 2006a) were used to detect ballast fouling. GPR research at Edinburgh used bowtie antennas. It should be noted that relatively closely coupled, but airborne, bow tie antennas emit more power into the ballast than horn antennas. Airborne bow tie antennas are particularly effective when coupled at $\lambda/_{10}$ or less (Davidson & Forde, 1996).

At TTCI, they found that with the use of 2GHz horn antennas that clean ballast gave a more scattered response than fouled ballast (Al-Qadi et al., 2008) (cf. *3.7 GPR Field Experiments at the University of Edinburgh*).

In contrast to traditional GPR data analysis, in which individual reflections are charted, the 2GHz horn antenna data from the ballast was processed to generate a representative scattering amplitude envelope, i.e., a running average between peak signal responses, that showed the average scattering amplitude versus depth.

A change in the size of the envelope was determined to indicate a change in ballast condition. A "gain restoration curve", which was empirically derived from the amplitude correction required to achieve constant amplitude versus arrival time from data obtained over a section of thick, clean ballast, was, presumably, applied to discount the effects of attenuation (Figure 4.1).

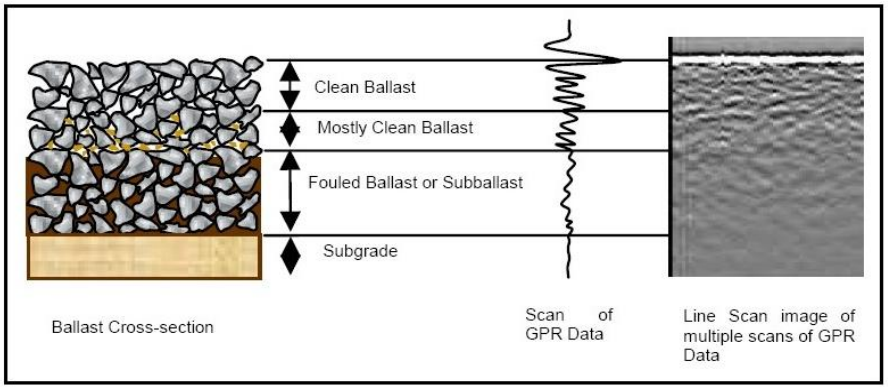

Figure 4.1 Interpretation 2GHz horn antenna data (Roberts et al., 2006a)

Radar signals through the clean ballast scattered due to the void spaces present in clean ballast – but not in spent ballast where they had been in-filled with fouling material. The fouled ballast was more homogenous; hence, the signal scattered less.

This rationale was presented in subsequent research (Roberts et al., 2006b), which stated that because spent ballast has a "finer, well-graded particle size with fewer air voids" that "The clean ballast near the surface generates a significant scattering pattern, while the scattering pattern generated by the fouled ballast at the bottom is insignificant because the air voids in fouled ballast are much smaller than the signal wavelength" (Figure 4.2 and Figure 4.3).

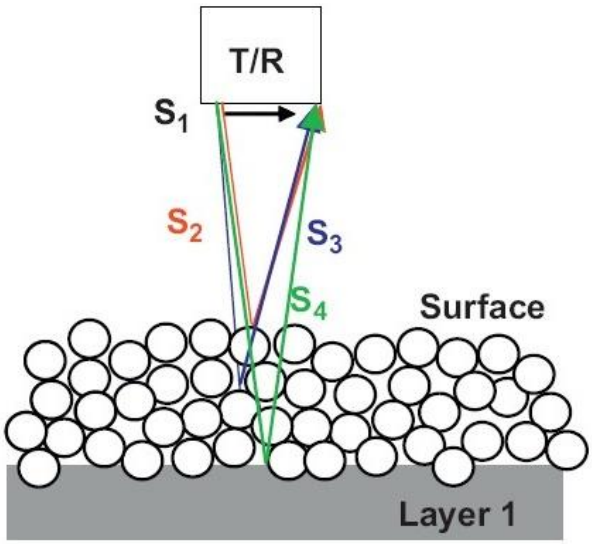

Figure 4.2 Paths of EM waves (Al-Qadi et al., 2008)

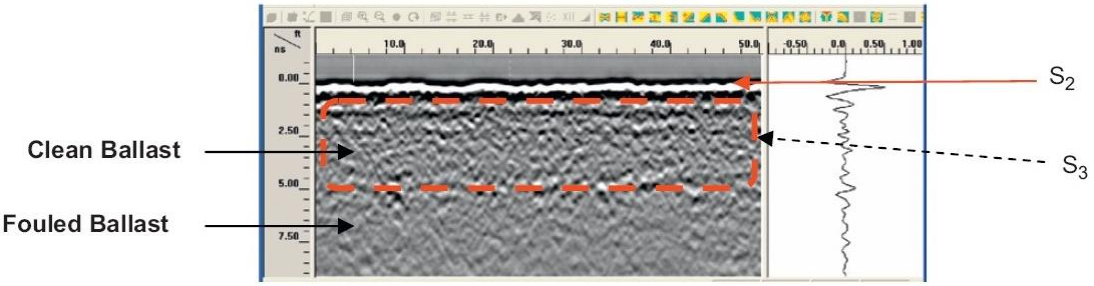

Figure 4.3 GPR data from railroad (Al-Qadi et al., 2008)

The results of this analysis can be seen in Figure 4.4.

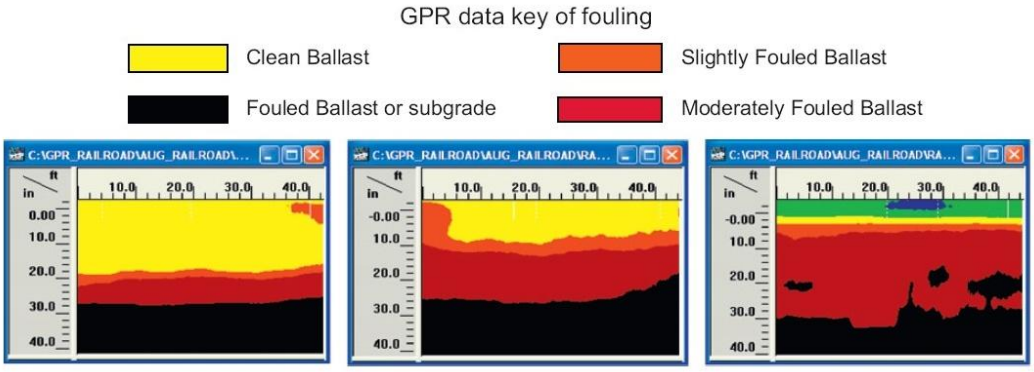

Figure 4.4 Scattering amplitude envelope analysis (Roberts et al., 2006b)

The sample on the left of Figure 4.4 is typical of clean ballast, with mixed ballast displayed in the middle and finally spent ballast on the right. Thus, "From the image analysis, ballast thickness, ballast fouling condition, and trapped water can be assessed" (Roberts et al., 2006b).

The above research at TTCI was conducted on ballast composed of a clean layer of ballast, over a mixed layer of ballast, over a spent layer of ballast, all of varying thicknesses. This is in contrast to the Edinburgh experiments.

4.2 Experimentation with 500MHz GSSI Antenna

To replicate previous work at the University of Edinburgh and investigate further the idea of analysing GPR waveforms, a 500MHz GSSI antenna was used on the University of Edinburgh track. Numerous radar scans were taken of the track ballast at the University of Edinburgh track.

The ballast was seen to be in an apparently dry condition. Each crib was scanned with a stationary antenna placed between the sleepers (Figure 4.5).

The orientation of the antenna was parallel with the sleepers with the transmitter end nearer one rail and the receiver end nearer the other rail (cf. *Figure 5.1 Simplified GSSI antenna layout* and *Figure 5.2 Data collection method* under *5.3 Data Collection*). The actual surface features at 7ns on the above radar scans; therefore, the time scale should be rebased with the subtraction of 7ns. The data was imported into Excel as a series of scans composed of 512 samples (each sample is a "voltage value" descriptive of the strength of reflection).

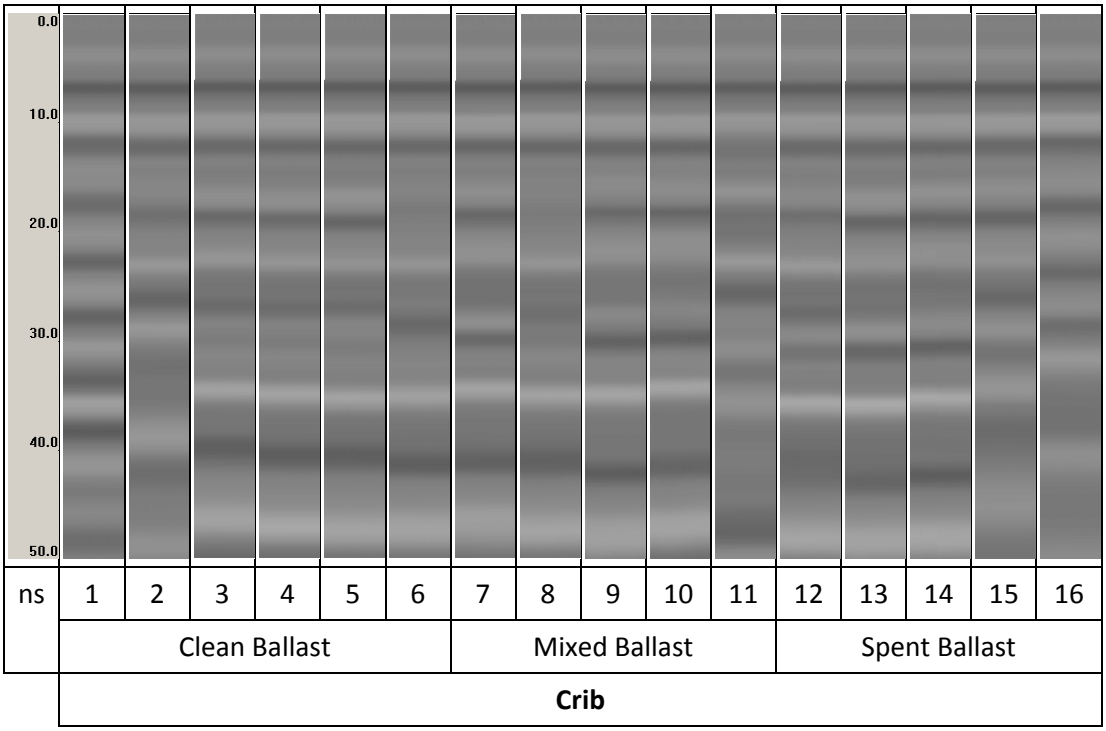

Figure 4.5 Crib radar scans

For each crib between 75 and 159 scans were taken. The number of scans recorded for each crib varied because the transmission period for the antenna was manually controlled, i.e., very briefly turned on then off. In any case, the scan result within each crib were virtually identical. Furthermore, the voltage value at each sample number was averaged with the others at the same sample number to smooth out any anomalies. The number of scans recorded for each crib is noted in Table 4.1.

Crib	1	2	3	4	5	6	7	8	9	10	11	12	13	14	15	16
Scans	75	111	131	143	155	151	147	151	155	151	128	159	155	151	175	139

Table 4.1 Radar scans extracted for analysis

These averaged responses for each crib Space were plotted.

Figure 4.6 shows the traces for the clean ballast (Crib 1, 2, 3, 4, 5, 6), Figure 4.7 shows the traces for the mixed ballast (Crib 7, 8, 9, 10, 11), Figure 4.8 shows the traces for the spent ballast (Crib 12, 13, 14, 15, 16).

In all figures, the surface interface can be seen around sample 100, and the formation interface can be seen around radar sample 150.

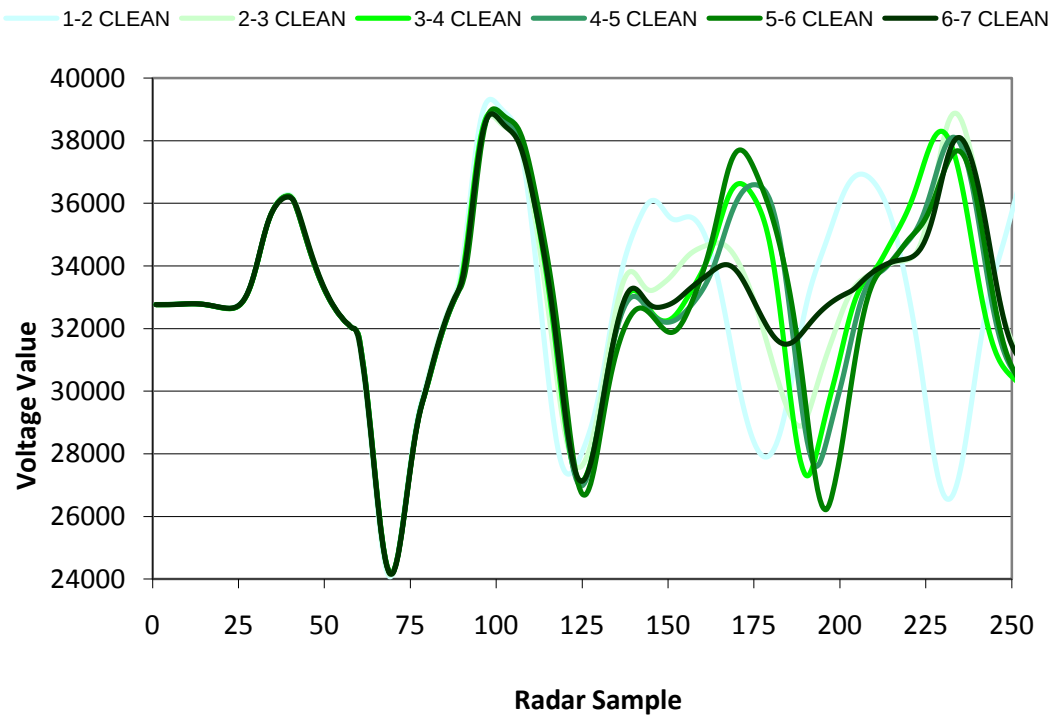

Figure 4.6 Clean ballast radar responses

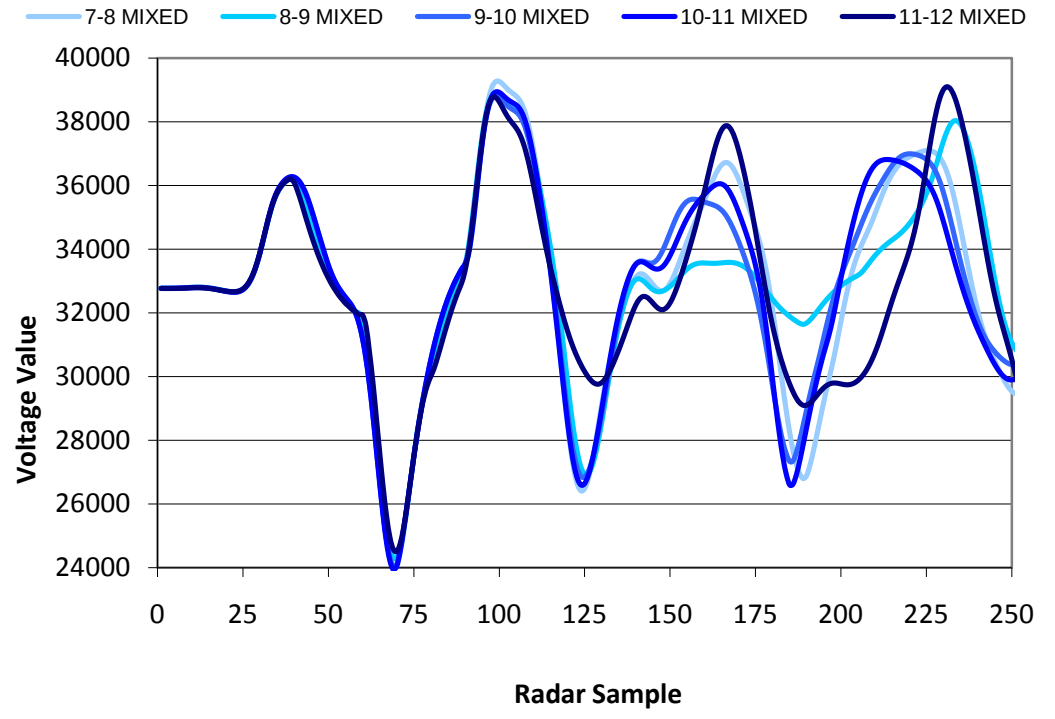

Figure 4.7 Mixed ballast radar responses

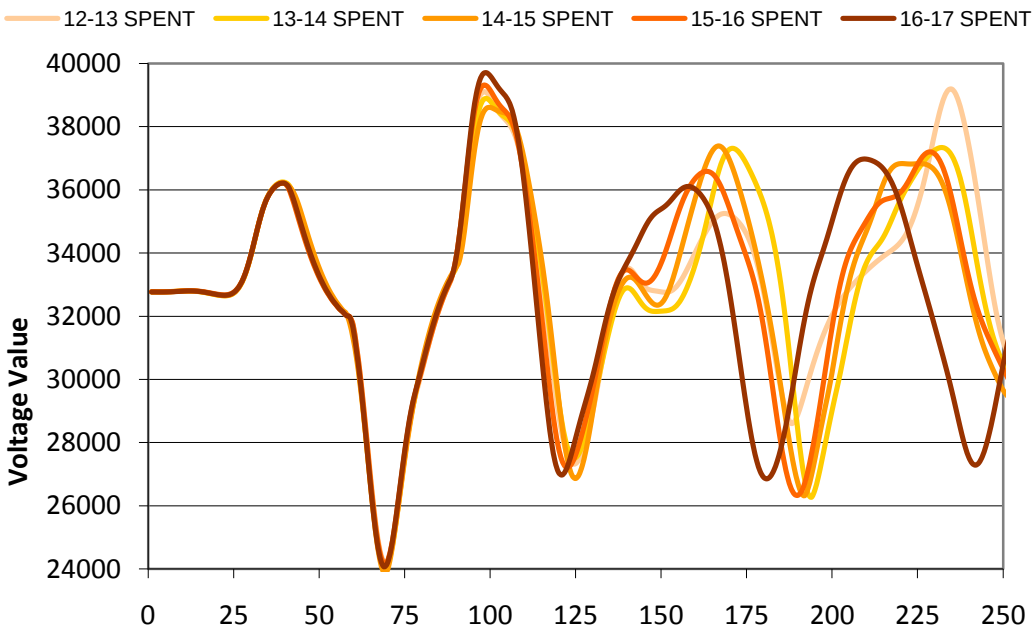

Figure 4.8 Spent ballast radar responses

However, the depth to the formation interface varies for each crib. These depths were taken from the as-built drawings (Figure 2.1), and put into Table 4.2.

The number of the radar sample at which the formation interface was noted for each crib. This was then rebased through the subtraction of 98 to 100 sample positions so that the start of the ground wave is considered as time zero (this can be seen on the four radar response figures above – around the 99th scan is the peak of the first reflection response – the ground).

Given that the range of the scans was set at 50ns and composed of 512 samples, therefore the time step of each sample is 50ns/512, or 0.098ns. This produced the two-way travel time to the formation interface; and the velocity of the signal could be deduced.

Finally, using Equation 3.3, the dielectric constant could be calculated from the equation of the velocity of electromagnetic waves in a dielectric medium, and the average values for the clean, mixed, and spent ballast are noted.

It can be clearly seen that the more "spent" the ballast the greater the dielectric constant.

Ballast	Crib	Formation depth (mm)	Formation at scan (512=50ns)	Base at scan	Reflection time (ns)	Velocity (m/s)	ε_v	Ave ε_v
Clean	1	0.311	145	98	4.6	135516596	4.9	3.327
	2	0.340	140	99	4.0	169834146	3.1	
	3	0.372	140	99	4.0	185818537	2.6	
	4	0.360	140	99	4.0	179824390	2.8	
	5	0.350	144	99	4.4	159288889	3.5	
	6	0.355	140	98	4.1	173104762	3.0	
Mixed	7	0.320	161	100	6.0	107436066	7.8	7.313
	8	0.346	160	99	6.0	116165246	6.7	
	9	0.360	160	99	6.0	120865574	6.2	
	10	0.340	165	99	6.4	105503030	8.1	
	11	0.345	166	100	6.4	107054545	7.9	
Spent	12	0.335	169	98	6.9	96630986	9.6	9.236
	13	0.325	170	98	7.0	92444444	10.5	
	14	0.331	166	99	6.5	101177313	8.8	
	15	0.310	163	98	6.3	97673846	9.4	
	16	0.315	158	98	5.9	107520000	7.8	

Table 4.2 Crib ballast dielectric constant calculations

It can be noted that there is quite a range of values between the clean and spent ballast and that the results for the spent ballast are greater than may have been expected in Table 3.4 from experiments carried out on the track in 1999. However, this could be accounted for by the fact that the testing was undertaken on a dry day in March when it had been raining the day before. Thus, the free-draining clean ballast had completely dried out, but the spent ballast was still quite moist accounting for the high dielectric values.

4.3 Conclusions

Earlier research at the University of Edinburgh (Gallagher et al., 1999) showed that GPR can determine the depth of a railway ballast layer and gain an indication of whether the ballast is clean, mixed, or spent. Recent work by practitioners has relied

on the Edinburgh research and has focused on developing high-speed data collection systems – using later Edinburgh research (Clark et al., 2004).

Given that the metric used in the TTCI research is the "scattering amplitude envelope" and that this would be expected to diminish with depth due to attenuation, the "scattering amplitude envelope" method, relies on discerning changes in the amplitude and relating that to changes in the ballast condition through empirically derived calibrations. It is not a true numerical analysis of the GPR waveform.

However, the simple waveform analysis undertaken with the 500MHz antenna on the University of Edinburgh track to calculate the dielectric constant by isolating scans from each crib and determining precisely the time of surface and formation interface reflections, repeated and confirmed previous findings and showed that the application of such methods can reveal useful findings.

Therefore, from this, an alternative measurement of "scattering" that is not attenuation related could be further investigated and developed.

CHAPTER 5 GPR ANALYSIS

5.1 Objectives

The objectives of this experimental work are to develop a numerical method of analysing the incidents of scatter, rather than the amplitude of the scatter, using a range of different frequency antennas.

5.2 Experimental Procedure

Gallagher, Figure 3.4, defined the increased scattering through a visual inspection of a signal plot, where the increased numbers of large peaks were a result of the EM wave being scattered by the smaller particles of the spent ballast. It has been stated that the signal from ballast can be assumed to be a random signal and that statistical analysis would be a more suitable method of analysis (Roberts et al., 2006b).

5.3 Data Collection

The track was scanned with a range of GSSI antennas of different frequencies: 500MHz, 900MHz, 1.0GHz, 1.6GHz, and 2.6GHz.

The higher frequency bowtie antennas may not be suitable for detecting faults or anomalies in ballast and may be more suited to tasks such as locating objects in concrete. Their inclusion was intended to reveal trends in the analysis across the range of frequencies.

All data was collected using either a trolley or with a survey wheel designed to hold the antennas and measure distances travelled.

The data was recorded without any gain settings distorting the collected data.

The scanning procedure started with the antennas moving from Sleeper 1 to Sleeper 17. Given that bowtie antennas transmit from one side of their casing and receive at the other (Figure 5.1), this was undertaken twice with the antenna in perpendicular then parallel orientation (Figure 5.2).

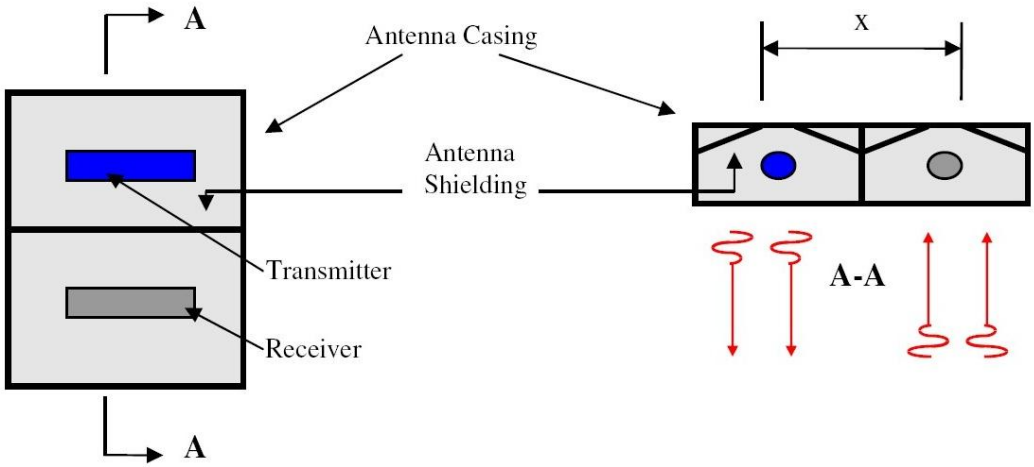

Figure 5.1 Simplified GSSI antenna layout (Gallagher, 1999)

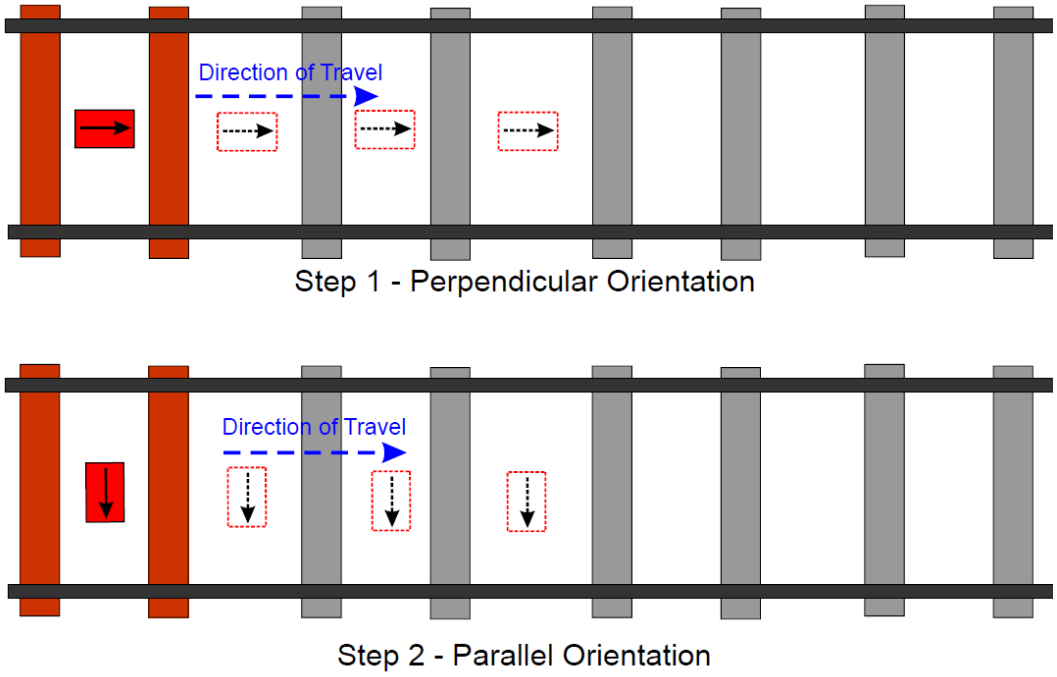

Figure 5.2 Data collection method (Gallagher, 1999)

A scan rate of 200scans/m was used, resulting in over 2000 scans for each run of the test track; although, 100scans/m was used for the 500MHz and 900MHz. Each scan was composed of 512 samples, giving over one million data values per run.

5.4 Data Analysis

The raw numerical data for each run was imported into an individual spreadsheet and contour plots of the radar data were produced and these were used to visually isolate

the “cribs” (Figure 5.3) – those areas between the sleepers where the ballast is on the surface creating Crib 1 to Crib 16.

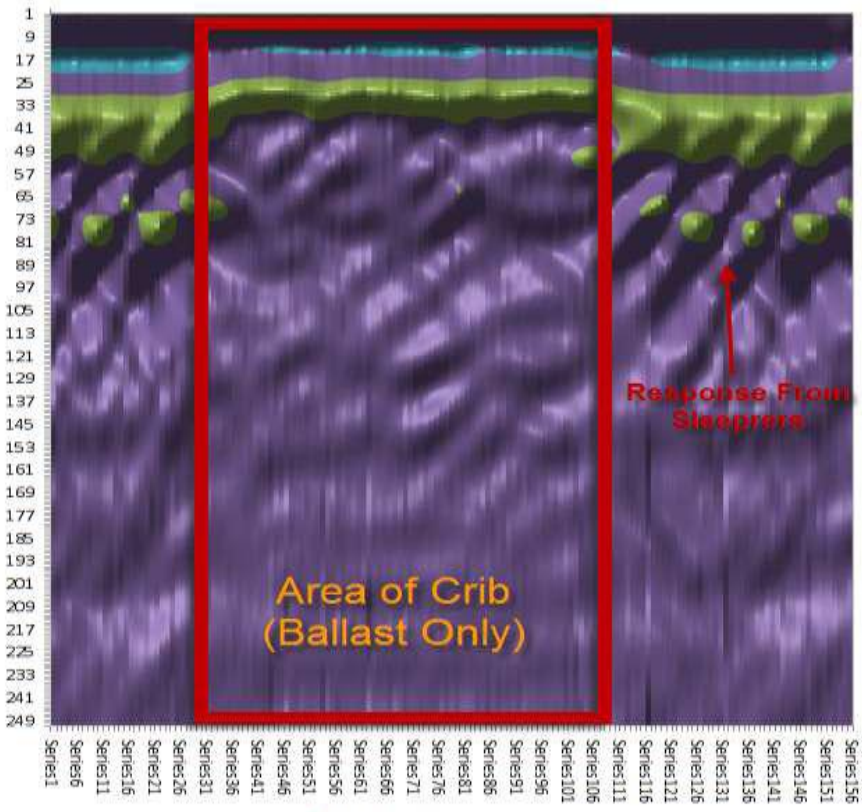

Figure 5.3 Example of 3D contour plot used for crib isolation for 2.6GHz data

In order to calculate the incidents of scatter for each crib, three metrics were devised: -

Scan area A numerical integration of a scan response to determine its “area” – the greater the magnitude of the responses, the greater the area.

Axis crossings The number of times the scan response crosses the zero amplitude axis – the more interfaces encountered by the signal, the more axis crossings.

Inflection points The number of times the gradient of the scan response changes through zero – the more interfaces, the more inflection points.

5.4.1 Scan Area Analysis

For each scan, the average signal value was calculated. This value was taken as the zero amplitude axis for that scan and a simple trapezoidal rule was utilised to integrate

some or all the 512 sample values of each scan (Figure 5.4) to determine the "area" of the scan as highlighted in yellow.

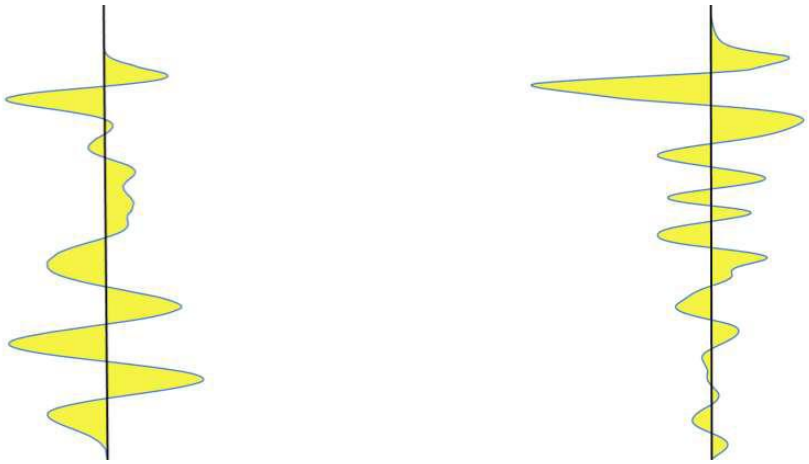

Figure 5.4 Scan area for typical clean (left) and spent (right) responses

5.4.2 Axis Crossings Analysis

For each scan, the average signal value was calculated; this was taken as the zero amplitude axis for that scan. The number of times that the signal crossed the average value was counted. Extrapolating from Gallagher's findings from signal responses through spent ballast (Gallagher, 1999), it was anticipated that the more a signal is scattered, the more it should cross the axis.

A simple algorithm counted the number of crossing points. For any sample value that was between a sample value greater than the average scan value and a sample value lower than the average scan value, an axis-crossing was counted (Figure 5.5).

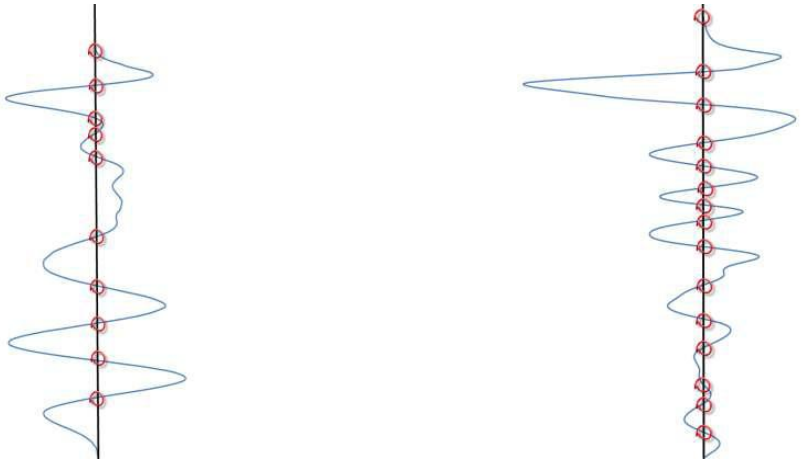

Figure 5.5 Axis crossings for typical clean (left) and spent (right) responses

5.4.3 Inflection Points Analysis

For each scan, the number of inflection points was counted. It was anticipated that the more scattered a response, the more inflection points it should have.

The number of inflection points was calculated by using a variation of the algorithm used to count the crossing points. For any sample value that was between two greater value samples or between two lower value samples, an inflection point was counted (Figure 5.6). This method did not require the location of the zero amplitude axis.

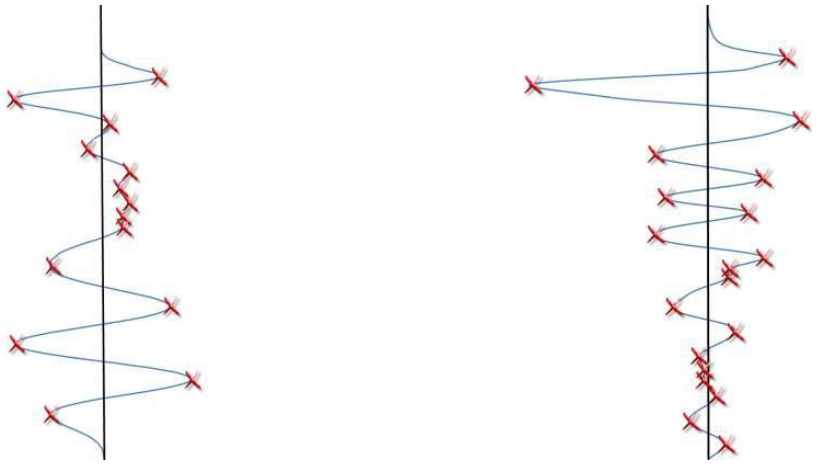

Figure 5.6 Inflection points for typical clean (left) and spent (right) responses

5.5 Time Range

Given the different frequencies of each antenna, different depths of penetration were achieved and recorded. It was noted at which of the 512 samples that the ground surface occurred and where the response was visually considered to have become noise dominant. Therefore, for the analysis three different time ranges were used: -

Full time range	All 512 samples collected were analysed.
Common time range	Only 5ns of data below the initial ground reflection was analysed in order to limit analysis to ballast responses.
Proportional time range	By evaluating the skin depth of each antenna and the original range it was set to detect, a ratio of the relative penetration of each antenna was calculated.

5.6 Results & Discussion

By using the Scan Area Analysis, the Axis Crossings Analysis, and the Inflection Points Analysis metrics, the amount of signal scattering was identified. The data was analysed using three different approaches to determining which sample time ranges to use: the full 512 samples, a reduced common range (5ns), and a time range proportional to penetration.

5.7 Full Time Range

The average results of the scattering analysis for each type of ballast using the full time range of the scan are listed in Table 5.1. The highest values for each section of analysis (area, crossings, and inflections) are highlighted in red and the lowest in green.

Antenna	Orien.	Range (ns)	Area Of Scan			Axis Crossings			Inflection Points		
			Clean	Mod. Clean	Mod. Fouled, Fouled	Clean	Mod. Clean	Mod. Fouled, Fouled	Clean	Mod. Clean	Mod. Fouled, Fouled
500 MHz	Perp.	23	1269272	1820730	2088340	15.57	16.02	16.99	17.50	18.12	19.31
	Parallel	23	1179536	1568375	2059104	15.31	16.02	16.70	17.81	17.28	18.62
900 MHz	Perp.	20	696421	987018	1235757	27.69	23.48	24.05	45.92	37.05	36.17
	Parallel	20	817121	1077727	1555518	26.25	23.67	23.91	46.10	38.22	35.31
1.0 GHz	Perp.	20	703692	952372	974882	29.58	29.06	28.55	33.59	32.20	31.07
	Parallel	20	972730	1210584	1204123	26.67	25.77	26.97	32.79	31.68	31.89
1.6 GHz	Perp.	20	430589	416034	407551	21.86	19.86	19.41	56.49	52.07	54.22
	Parallel	20	383307	426471	423533	19.63	15.95	16.79	54.81	51.50	53.42
2.6 GHz	Perp.	10	333581	339728	338602	20.59	20.30	20.23	16.44	15.16	14.98
	Parallel	10	376546	394878	385945	20.27	19.98	19.56	23.48	22.48	22.04

Table 5.1 Results of scattering analysis for full time range

5.7.1 Full Time Range Scan Area Analysis

It can be seen that the clean ballast has the smallest area in most cases with the spent or mixed ballast having the largest areas. This trend is very strong at the lower frequencies under 1GHz; this appears to correlate with Gallagher et al. 1999 (Gallagher et al., 1999).

5.7.2 Full Time Range Axis Crossings Analysis

Similar to the area analysis, there is a difference in behaviour between high and low frequency antennas. With antennas of 900MHz or over, the clean ballast features more axis crossings than the spent ballast. Below 900MHz, the behaviour is the reverse with the spent ballast having more axis crossings than the clean.

5.7.3 Full Time Range Inflection Points Analysis

The results are very similar to the axis crossing points analysis with the same behaviour occurring. Again, the 900MHz antenna appears to be the point at which the behaviour changes, with almost 20% more inflection points.

5.8 Common Time Range

The average results of the scattering analysis for each type of ballast using the common time range of the scan are listed in Table 5.2. The highest values for each section of analysis (area, crossings, and inflections) are highlighted in red and the lowest in green.

Antenna	Orien.	Range (ns)	Scan Area			Axis Crossings			Inflection Points		
			Clean	Mod. Clean	Mod. Fouled, Fouled	Clean	Mod. Clean	Mod. Fouled, Fouled	Clean	Mod. Clean	Mod. Fouled, Fouled
500 MHz	Perp.	5	519361	649110	493665	3.95	3.87	3.78	4.47	4.47	5.32
	Parallel	5	495875	585394	531113	3.38	3.96	4.26	4.77	4.40	5.25
900 MHz	Perp.	5	222113	242224	258231	6.91	5.58	6.72	9.14	7.91	8.44
	Parallel	5	201378	242690	253223	6.45	5.40	6.74	8.89	7.51	8.36
1.0 GHz	Perp.	5	149771	187753	190682	7.85	8.08	7.74	9.22	8.97	8.55
	Parallel	5	179378	218713	201614	6.84	7.24	7.21	8.81	8.75	8.76
1.6 GHz	Perp.	5	382593	362212	352233	9.89	9.73	9.50	11.04	11.30	10.86
	Parallel	5	353525	412695	403925	8.47	8.29	8.05	10.28	9.23	9.59
2.6 GHz	Perp.	5	299528	302294	300923	10.63	10.65	10.75	14.42	13.22	12.96
	Parallel	5	331064	347733	339890	10.55	10.50	10.36	14.32	13.55	13.05

Table 5.2 Results of scattering analysis for common range

5.8.1 Common Time Range Scan Area Analysis

The trend in results of the area analysis are similar in trend to those of the full time range; the clean ballast generally has the smaller area, although, the clear difference

between clean ballast and fouled ballast at frequencies below 900MHz is no longer present.

5.8.2 Common Time Range Axis Crossings Analysis

Unlike the full range analysis, the trend in the results is of a more random nature.

5.8.3 Common Time Range Inflection Points Analysis

The trend in the results is also similar to those of the full time range. The 900MHz antenna contains significantly more inflection points for clean ballast while the 500MHz antenna has more inflection points in spent ballast. All of the high frequency antennas, with the exception of the 1.6GHz perpendicular antenna, have more inflection points in clean ballast than in spent ballast.

5.9 Proportional Time Range

The average results of the scattering analysis for each type of ballast using the proportional time range of the scans are listed in Table 5.3. Each antenna was analysed in a time range proportional to its penetration. The highest values for each section of analysis (area, crossings, and inflections) are highlighted in red and the lowest in green.

Antenna	Orien.	Range (ns)	Scan Area			Axis Crossings			Inflection Points		
			Clean	Mod. Clean	Mod. Fouled, Fouled	Clean	Mod. Clean	Mod. Fouled, Fouled	Clean	Mod. Clean	Mod. Fouled, Fouled
500 MHz	Perp.	10	809911	1019195	1073568	7.89	8.13	8.50	9.06	9.20	10.34
	Paral.	10	738316	916886	1461600	7.28	8.17	8.83	9.55	9.20	10.49
900 MHz	Perp.	5	249568	263324	274524	6.80	5.81	6.86	9.07	7.91	8.62
	Paral.	5	223292	258191	269580	6.40	5.60	6.52	8.96	7.37	8.28
1.0 GHz	Perp.	5	226772	249176	252872	7.03	7.04	7.13	8.45	8.06	7.87
	Paral.	5	939912	1178165	1172130	6.34	6.29	6.58	7.82	7.68	7.77
1.6 GHz	Perp.	3	386661	361702	353061	5.34	5.61	5.57	5.14	5.44	5.53
	Paral.	3	355258	412466	406161	4.91	4.59	4.52	4.89	4.94	4.92
2.6 GHz	Perp.	2	73915	80889	80193	1.00	1.00	1.00	0.49	0.39	0.39
	Paral.	2	93239	94230	95571	1.00	1.00	1.00	0.51	0.47	0.52

Table 5.3 Results of scattering analysis for proportional range

5.9.1 Proportional Range Scan Area Analysis

Akin to all the previously analysed time ranges, the clean ballast has a smaller area for the lower frequency antennas, but, yet again, this trend is not as clear as with the full time range results.

5.9.2 Proportional Range Axis Crossings Analysis

Although it appears that for most antennas the fouled ballast has a greater number of axis crossings, the numerical difference is not significant enough to demonstrate a clear trend.

5.9.3 Proportional Inflection Points Analysis

The trend in the results appears to be of a more random nature; although, the change in behaviour at 900MHz does still seem to be present.

5.10 Metric Evaluation

To evaluate the effectiveness of this method of measuring the scattering, the correlation between the scattering analysis for each crib and the fouling index for each crib was investigated using the Pearson correlation co-efficient. This describes the quality of the correlation between the impulse response test results and fouling index. The strength of the correlation is represented by a number between -1 and 1 where "1" indicates a strong positive linear relationship, "0" indicates zero linear relationship and -1 indicates a strong negative linear relationship. The equation is noted below: -

$$\rho_{x,y} = \frac{n\sum x_i y_i - \sum x_i \sum y_i}{\sqrt{n\sum x_i^2 - (\sum x_i)^2}\sqrt{n\sum y_i^2 - (\sum y_i)^2}}$$

Where, n = number of samples
x_i = x-axis sample value
y_i = y-axis sample value

Equation 5.1

Each area scan value for each crib was plotted against the measured fouling index for that crib and the trend line correlation value calculated. The best correlation was achieved with the 500MHz antenna using the full time range giving a correlation coefficient of 0.8 in the perpendicular orientation and 0.9 in the parallel orientation (Figure 5.7).

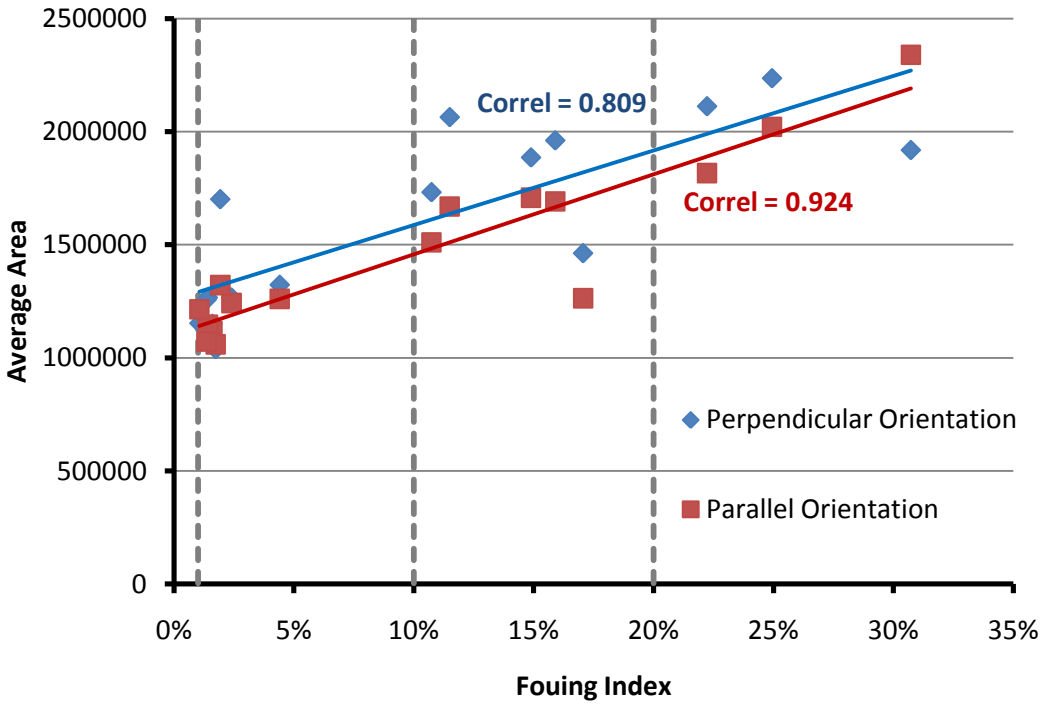

Figure 5.7 500MHz full time range correlation analysis

The numerical correlation values for all experiments were also calculated (Table 5.4). Where the results correlated with a coefficient greater than 0.6, the cell is light green; greater than 0.8, the cell is dark green; less than -0.6, yellow; less than -0.8, orange.

Antenna	Orien.	Scan Area			Axis Crossings			Inflection Points		
		Full Range	Com. Range	Prop. Range	Full Range	Com. Range	Prop. Range	Full Range	Com. Range	Prop. Range
500 MHz	Perp.	0.809	0.019	0.499	0.286	-0.356	0.378	0.462	0.616	0.619
	Paral.	0.924	0.566	0.816	0.295	0.674	0.613	0.034	0.133	0.213
900 MHz	Perp.	0.740	0.569	0.502	-0.599	-0.157	-0.074	-0.719	-0.488	-0.392
	Paral.	0.756	0.634	0.648	-0.439	0.076	0.041	-0.802	-0.289	-0.340
1.0 GHz	Perp.	0.436	0.519	0.519	-0.336	0.072	0.149	-0.481	-0.296	-0.423
	Paral.	0.678	0.641	0.679	-0.061	0.504	0.234	-0.340	-0.006	-0.057
1.6 GHz	Perp.	-0.185	-0.228	-0.257	-0.327	-0.388	0.180	-0.251	-0.079	0.448
	Paral.	0.545	0.672	0.676	-0.274	-0.466	-0.551	-0.221	-0.306	0.136
2.6 GHz	Perp.	0.282	0.111	0.722	-0.120	0.065	0.000	-0.647	-0.683	-0.563
	Paral.	0.326	0.342	0.301	-0.306	-0.140	0.000	-0.687	-0.721	0.035

Table 5.4 Fouling index correlation factors for full-time range scattering analysis

5.10.1 Scan Area Metric Evaluation

There was a strong correlation between the scan area metric and the fouling index for the full-time range. Yet, one would expect the common time range of 5ns to be as effective if not more so, because, by design, this time range only includes radar responses from the ballast layer and not the subgrade and formation. However, signal reflections that occur at depth below the ballast layer still travel through the ballast layer twice. The scan area metric is effectively measuring returned energy and by restricting the analysis only to the energy that reaches the base of the ballast layer and back, does not allow the assessment to include the effects of the ballast layer on the energy that goes beyond the ballast layer and comes back.

For low frequency antennas scattering occurs more in spent ballast, correlating with Gallagher (Gallagher et al., 1999). With higher frequency antennas, it is almost impossible to distinguish between clean and spent ballast in terms of scattering. This contradicts Al-Qadi (Al-Qadi et al., 2008) who stated that with high frequency antennas more scattering occurs in clean ballast – however they used horn antennas.

The noticeably improved results in lower frequency antennas may be due to the increased power of the antenna itself, with the lower frequency antennas less likely to interpret minor changes in particle size and constituency as a change in material layer, which ultimately results in a better indication of ballast depth and layer interfaces.

5.10.2 Axis Crossings & Inflection Point Metric Evaluation

These results are less promising with a large number of negative correlations for both metrics and very few strong correlations. The large negative values are mainly for the full-time range data and suggest that there is a possible link between the scattering analysis and fouling index. The axis crossings metric does not demonstrate any correlation. Both these approaches are inappropriate for determining ballast.

It had been expected that when the range of data analysed was shortened to the depth of the ballast, i.e., 5ns, the correlation with the fouling index would improve. However, the opposite was true. It may be that the sub-ballast material gives a different response when under clean or spent ballast, and this may be due to drainage differences between clean and spent ballast.

5.11 Conclusions

The results for this method are summarised below: -

Scan area Clean ballast had the smallest area with most antennas; the spent or mixed ballast had the largest areas. The 500MHz antenna in the parallel orientation using the full time range gave the best correlation (0.92) between fouling index and scan area.

Axis crossings With antennas of 900MHz or over, clean ballast featured more axis crossings than spent ballast. Below 900MHz, the behaviour reversed with the spent ballast having more axis crossings than the clean. There were no particularly strong correlations between fouling index and axis crossings.

Inflection points With antennas of 900MHz or over, clean ballast featured more inflection points than the spent ballast. Below 900MHz, the behaviour reversed with the spent ballast having more inflection points than the clean. The 900MHz antenna in the parallel orientation using the full time range gave the best correlation (-0.80) between fouling index and inflection points.

Therefore, the 500MHz antenna in the parallel orientation using the full time range and scan area method gives the best results.

A peer-reviewed paper of this research can be seen in Appendix 11 (De Bold et al., 2010a).

CHAPTER 6 MINI FALLING WEIGHT DEFLECTOMETER

6.1 Falling Weight Deflectometry

Use of a Falling Weight Deflectometer (FWD) is a static stiffness measurement technique used in the pavement industry. Similar special equipment has been developed for the railway industry.

An FWD operates by dropping a known weight onto a circular plate resting on the surface of interest. This imparts a physical impulse into the ground, which is measured by one or more geophones. The geophones are located at the point of impact and, often, at 300mm intervals from the point of impact in order to measure the velocity profile of the surface response to the load.

The measured impulsive load and velocity response of the ground are used to determine the structural properties of the pavement (Sharpe, 2000). This is done by integrating the velocity response time histories, and the peak displacements are used to give a "static" deflection bowl that characterises the quasi-static deflection response of the pavement (Brough et al., 2003).

When modified for use in the rail industry, the load is applied close to the rail seat area of a sleeper, and the transient deflections of the sleeper and ballast are measured (Sharpe & Collop, 1998).

The deflections of the loaded sleeper, the ballast in the adjacent crib and the ballast in the next crib, are interpreted as corresponding to the sleeper deflection, the deflection of the loaded ballast, and the deflection of the formation, respectively (Brough et al., 2003).

It has been noted that a simple mass-spring-dashpot model can assess the characteristics of the forces transmitted to the ground by the falling weight so as to be able to rationally decide on its size, mass, and dropping height (Roesset et al., 1994)(Thilakasiri et al., 1996)(Roesset et al., 1996).

A simplified FWD is shown in Figure 6.1.

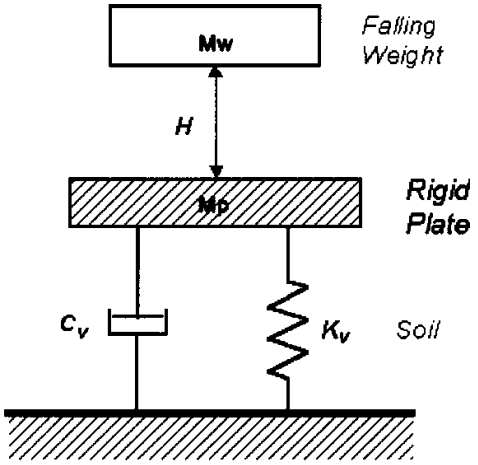

Where, c = damping co-efficient
m = impinging mass
k = stiffness of the spring

Figure 6.1 Principles of FWD (Loizos et al., 2003)

The equation that describes the motion of a rigid mass impinging vertically on a spring-dashpot system, and remaining in contact with it thereafter, is the well known linear equation for a single degree of freedom system (Loizos et al., 2003): -

$$m\ddot{x} + c\dot{x} + kx = f(t) \qquad \textbf{Equation 6.1}$$

Where, x = displacement
$\dot{x}$ = velocity
$\ddot{x}$ = acceleration

The FWD is suggested as being the only satisfactory way of obtaining sufficient data to assess trackbed stiffness magnitude and variation for an individual site (Sharpe, 2000). However, due to the FWD impact penetrating beyond the ballast into the lower layers and subgrade, the FWD it is more suited to evaluating the whole trackbed stiffness rather than just the condition of the ballast.

It should be noted that the FWD is a large and heavy piece of equipment that is difficult to operate on virgin ground, particularly ground that is unbound such as railway tracks. The testing procedure requires disconnection of clips from sleepers over sections of track and, thus, track possession. This makes the testing procedure very time consuming and expensive.

6.2 Experimentation with Mini-FWD

6.2.1 Prima100 6050

Initial investigative work on the University of Edinburgh track, involved the use of a mini-FWD; a Prima100 6050 – a commercially available piece of equipment that automatically interprets stiffness from measured responses. The geophone of the Prima100 is located in the centre of the underside of the load plate, and is approximately 1cm^2. The device can be seen in Figure 6.2.

Figure 6.2 Prima100 6050

As noted previously, the track was constructed, as part of an earlier project (Gallagher, 1999), so that approximately one third is composed of "clean" ballast, one third of "mixed" ballast, and one third of "spent" ballast. It was anticipated that there would be differences in stiffness measurements of these three types of ballast (the layout of the track can be seen in Figure 2.1).

6.2.2 Mini-FWD Test Setup

All the sleepers and cribs (the areas of ballast exposed between the sleepers) were tested with the Prima100 6050. Each time the mini-FWD was used on a specific location, numerous uses (drops) of the device were required. This was necessary because only in analysis of the results could it be seen if the drop was successful or if it had generated spurious results. The source of spurious results could come from the weight not being dropped correctly, if the device was not held firmly in position (letting

it "jump" on impact), or if the ballast beneath gave way significantly (i.e., stones settling abruptly). Such spurious results were disregarded.

The results for each drop feature a stiffness value for the surface tested (measured in MPa) and a maximum deflection value of the surface tested (measured in μm). It should be noted that where several tests were conducted that the tables below feature results labelled "max peak deflection" – the greatest of all the max deflection values for that set of drops, "average peak deflection" – the average of all the max deflection values for that set of drops, and "min peak deflection" – the lowest of all the max deflection values for that set of drops.

Figure 6.3 shows the measured load impulses and recorded deflections on an area of the Edinburgh track at Crib 5. The impact force curves are shown in blue and the ballast response curves are shown in red.

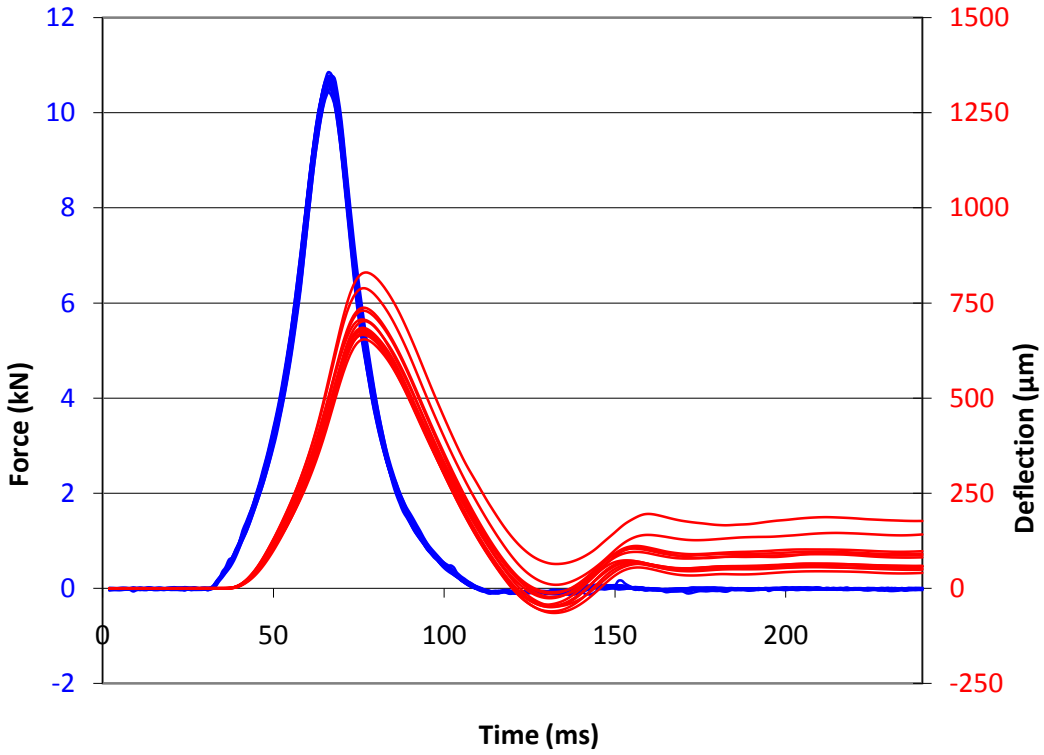

Figure 6.3 Prima100 6050 multiple test results on Crib 5

6.2.3 Sleeper Mini-FWD Tests

Each sleeper was tested with multiple drops (between 4 and 11 successful drops were carried out on each sleeper). The mini-FWD was kept in a fixed position for all drops on each sleeper.

Each set of results for a sleeper gave fairly consistent results, but there was some variation between sets of results for different sleepers. The results can be seen in Table 6.1 (the full results can be seen in Appendix 3).

Sleeper	1w	2w	3	4	5	6	7	8	9	10	11	12	13	14	15	16w	17w
Max Stiffness (MPa)	31	50	164	285	322	281	152	141	196	366	266	188	173	255	298	53	31
Ave Stiffness (MPa)	30	41	157	258	277	257	144	140	160	353	238	168	159	218	280	50	20
Min Stiffness (MPa)	29	34	122	232	239	227	137	138	152	344	206	157	142	202	271	48	17
Max Peak Defl (μm)	1206	989	330	179	176	188	306	307	274	124	203	276	300	214	158	842	2238
Ave Peak Defl (μm)	1165	916	266	161	155	165	290	297	261	121	177	257	255	197	154	804	1912
Min Peak Defl (μm)	1130	752	250	149	131	154	268	281	209	116	156	221	224	163	147	757	1161

Table 6.1 Results of all tests on each sleeper (w=wood)

There is a clear difference in behaviour between the wooden sleepers and the concrete sleepers, as can seen in Table 6.2 which averages the results in Table 6.1 on the basis of the construction material.

Sleeper Material	Wood	Concrete
Max Stiffness (MPa)	53	366
Ave Stiffness (MPa)	35	216
Min Stiffness (MPa)	17	122
Max Peak Defl (μm)	2238	330
Ave Peak Defl (μm)	1199	212
Min Peak Defl (μm)	752	116

Table 6.2 Wood vs concrete sleeper results

There was some degree of consistency between the results for the wooden and concrete sleepers; the wooden sleepers gave markedly lower stiffness results with a stiffness range of 17-53MPa and markedly higher peak deflection results with a range of 752-2238mm; whereas, the concrete sleeper stiffness results gave a range of 122-366MPa and peak deflection results with a range of 116-330mm.

6.2.4 Crib Mini-FWD Tests

The same tests were carried out on each of the cribs (between 4 and 14 successful drops were carried at each position). The FWD was kept in the same fixed position for all tests. It should be noted that the results for the first few drops on a crib were

usually spurious, and only after a few further drops for the mini-FWD to "bed in" into the ballast were consistent results achieved for successive drops.

Each set of results for a crib gave fairly consistent results, but there was significant variation between sets of results for different cribs. The results can be seen in Table 6.3 – note the categorisation of Crib 11 due to the PSD results (cf. *2.5 Particle Size Distribution Analysis*) (full results can be seen in Appendix 4).

	Clean							Mixed				Spent				
Crib	**1**	**2**	**3**	**4**	**5**	**6**	**11**	**7**	**8**	**9**	**10**	**12**	**13**	**14**	**15**	**16**
Max Stiffness (MPa)	55	134	112	56	63	62	45	121	121	93	80	84	47	48	94	52
Ave Stiffness (MPa)	45	100	97	50	59	49	43	99	85	86	60	72	42	38	77	65
Min Stiffness (MPa)	23	72	78	42	49	32	40	84	38	66	43	59	34	30	72	40
Max Peak Defl (μm)	1512	514	512	937	830	1249	997	478	986	577	950	676	1193	1322	548	991
Ave Peak Defl (μm)	893	403	426	803	707	859	935	426	554	465	704	560	987	1101	516	838
Min Peak Defl (μm)	681	288	370	742	654	696	888	350	333	431	492	481	886	863	420	778

Table 6.3 Results of all tests on each crib

The significant variation between cribs was suspected to arise not only because of the different condition of the ballast present, but because stiffness results achieved only related to the small area of ballast tested, which could vary significantly in stiffness, i.e., the mini-FWD was not large enough to impart and measure forces throughout the whole track structure.

Again, the averages for each ballast category are taken, as can be seen in Table 6.4.

Ballast Material	Clean	Mixed	Spent
Max Stiffness (MPa)	134	121	94
Ave Stiffness (MPa)	63	82	59
Min Stiffness (MPa)	23	38	30
Max Peak Defl (μm)	1512	986	1322
Ave Peak Defl (μm)	718	537	800
Min Peak Defl (μm)	288	333	420

Table 6.4 Summary of crib results

From the table it can be seen that there is no clear trend; the clean ballast features the highest and lowest stiffness values, the mixed ballast has the highest average stiffness

value, and similar results can be seen with the deflection values. Therefore, it can be concluded that the mini-FWD is not suited for testing ballast.

6.2.5 Mini-FWD Confidence Tests

In order to determine the effects of undertaking multiple sets of drops on the same surface area with each set being slightly repositioned, a series of "confidence tests" were carried out, i.e., this is to determine the ability to achieve consistent results in separate sets of drops with each set having the mini-FWD repositioned.

The confidence tests were carried out on Sleeper 6 with multiple drops undertaken and then the mini-FWD slightly moved and several more drops taken, etc (between 4 and 8 successful drops were carried at each position).

The results were generally consistent regardless of the mini-FWD being moved. The averaged results for each sleeper test can be seen in Table 6.5 (full results can be seen in Appendix 5).

Multiple Drops on Position	1	2	3	4	5
Max Stiffness (MPa)	170	146	141	153	174
Ave Stiffness (MPa)	158	142	138	145	159
Min Stiffness (MPa)	149	138	136	141	152
Max Peak Defl (μm)	272	296	308	286	269
Ave Peak Defl (μm)	258	290	300	280	248
Min Peak Defl (μm)	242	277	289	271	222

Table 6.5 Sleeper 6: confidence tests 1-5

A confidence test was carried out on Crib 6 with multiple drops undertaken and then the FWD slightly moved and several more drops taken, etc (between 4 and 6 successful drops were carried at each position). Where results were for the same position, there was a degree of consistency, but where the mini-FWD was moved to a new position, the results were then fairly consistent to a new but often quite different value.

The averaged results for each crib test can be seen in Table 6.6 (the full results can be seen in Appendix 6).

Multiple Drops on Position	1	2	3	4	5
Max Stiffness (MPa)	70	103	48	123	64
Ave Stiffness (MPa)	54	96	45	102	55
Min Stiffness (MPa)	44	81	42	85	41
Max Peak Defl (μm)	906	486	975	452	983
Ave Peak Defl (μm)	752	427	911	392	761
Min Peak Defl (μm)	576	402	838	321	644

Table 6.6 Crib 6: confidence tests 1-5

6.3 Conclusions

The results showed that consistent and meaningful responses could be gained from multiple mini-FWD drops on sleepers but not on ballast. Given the small size of the geophone sensor area (about $1cm^2$), the mini-FWD only seemed to test the stiffness of that small localised surface area over which it was placed. The uniform nature of the sleeper meant that this did not prevent consistent results from being achieved; however, it was concluded that given the loose unbound nature of ballast, this meant that the mini-FWD was essentially only testing the individual piece of ballast stone it happened to be placed upon. This individual piece of ballast could be loose or tightly wedged in its location and this would significantly affect the results but give no real indication as to the properties of the ballast as a whole.

It is clear that the mini-FWD had significant advantages over the full-sized FWD in terms of being easily deployable on site; although, its lack of mass and the device's fixed unitary form restricted its effectiveness in testing railway ballast and structure.

However, the technique of measuring impact forces and their response from a portable device is worth further investigation.

CHAPTER 7 IMPULSE RESPONSE

7.1 Impulse Response History and Application

A well-documented area of research to determine the stiffness of concrete structures, as well as analysis of other structures and material properties, is Impulse Response testing: where an instrumented hammer is used to excite a structure and the response of the structure is measured with a transducer.

One of the first companies involved in the field were PCB Piezotronics, Inc (Walter, 2007). They were founded 1967 and are based in Buffalo, New York, USA. They researched and produced electronic testing and measurement devices, and in 1972 worked with the University of Cincinnati's Structural Dynamics Research Laboratory (UCSDRL) to develop a "modally tuned" impulse hammer with integral force transducer to provide structural system excitation.

The technique, developed through experimental modal analysis, used the "modally tuned" hammer to test structures in order to extract modal parameters, such as resonant frequencies, damping, and vibratory mode shapes, for the purposes of enhancing the modelling process (Walter, 2007).

However, the Impulse Response testing method itself was originally developed from non-destructive steady-state vibration testing of piles in France (Davis & Dunn, 1974), where a controlled force was applied to the shaft head by a frequency generator.

The input force from the frequency generator was monitored and the vertical shaft response was recorded by velocity transducers. The ratio of the response velocity to the vibration force applied was plotted against frequency, and the resulting curve termed "mobility", with a useful frequency range of about 0-2000Hz (Davis & Dunn, 1974).

It was the later combination of the modally tuned hammer and the impulse response testing method, along with the dramatic increase in electronic data-processing performance of computers in the 1980s and 1990s, which permitted the on-site processing of the hammer impact and geophone responses into the frequency domain, that created the current technique of impulse response testing (ACI 228.2R S2.2, 2011).

This all made the testing method much more capable in the field, rather than being reliant on post-analysis after the collection of field data.

Consequently, there was a significant growth in the range of applications to which the impulse response method was put. Applications have included the testing of pre-cast concrete slab pavements (Pederson & Senkowski, 1986), voiding beneath concrete pavements, spillway and floor slabs (Davis & Hertlein, 1987), integrity testing and assessment of bridge decks (Davis & Hertlein, 1990), delamination of concrete around steel reinforcement in slabs, walls and large structures such as dams, chimney stacks and silos (Davis & Hertlein, 1995), location of "honeycombed" (low density) concrete and cracking in large concrete foundations (Davis & Hertlein, 1997), debonding of asphalt and concrete overlays to concrete substrates (Davis et al., 1996), and depth of alkali-silica reaction attack in drilled shafts used as pylon foundations (Davis & Kennedy, 1998).

American ASTM standards cover impulse response testing in relation to concrete testing (ASTM C1740, 2010), and in relation to piles (ASTM D5882, 2007), where it is referred to as the transient response method.

7.2 Impulse Response Principles

To determine the impulse response of a material or structural element it is impacted by a hammer equipped with a force transducer to generate a low-strain stress wave with a wide frequency content. The resultant bending behaviour of the element is analysed to characterize the integrity of the element. There are many different hammer sizes (varying in weight) and tip materials (varying in hardness) available.

The maximum compressive stress at the impact point, and the range of frequencies imparted, is related directly to the elastic properties of the impactor tip. The hammer impact frequency content can vary from 0 to 1000 Hz for soft rubber-tipped hammers, and from 0 to 3000 Hz or higher for metal-tipped hammers (Chan, 1987).

For the purposes of impulse response, a low enough frequency must be used so that the structure responds to the impact in a bending mode rather than a reflective mode (ACI 228.2R S2.2, 2011).

The load cell measures the force input, and the response is measured by a transducer.

The transducer is generally either a displacement transducer (measuring displacement), a geophone (measuring velocity), or an accelerometer (measuring acceleration).

The force and transducer time-domain signals are recorded by a digital acquisition device, and converted into the frequency-domain by computer using a Fast Fourier Transform (FFT) algorithm. At each frequency value, the transducer value is divided by the force value to provide a normalised response, or a Frequency Response Function (FRF), which is displayed as a graph in the frequency domain; thus, the FRF discards the effects of magnitude and type of loading (Ewins, 1984) permitting consistent analysis of the material or element tested.

For different transducers used, the resultant FRF value plotted against frequency can be referred to by different terms (Ewins, 1984) (numerous other names exist for the below FRF terms, or their inverse). The most common names are shown in Table 7.1

Transducer	Frequency Response Function
Displacement	Receptance
Velocity	Mobility
Acceleration	Inertance

Table 7.1 Terms for various FRFs

Given that receptance, mobility, and inertance, are, respectively, derived from the "zero'th", first, and second derivatives of position, the parameters are mathematically closely related, and, consequently, inertance can be integrated for mobility, and mobility can be integrated for receptance.

7.3 Mass-Spring Model

Various mass-spring models exist to describe and analyse the dynamic system of a railway track.

When simulating ground response from freight trains (Jones & Block, 1996), railway track harmonic loading (Sheng et al., 1999), or the influence of the track in relation to train-induced ground vibrations (Sheng et al., 2004), the whole dynamic system can be modelled. Such models generally feature the rails, rail pads, sleepers, ballast and underlying layers on a half-space.

An example of such a model can be seen in Figure 7.1.

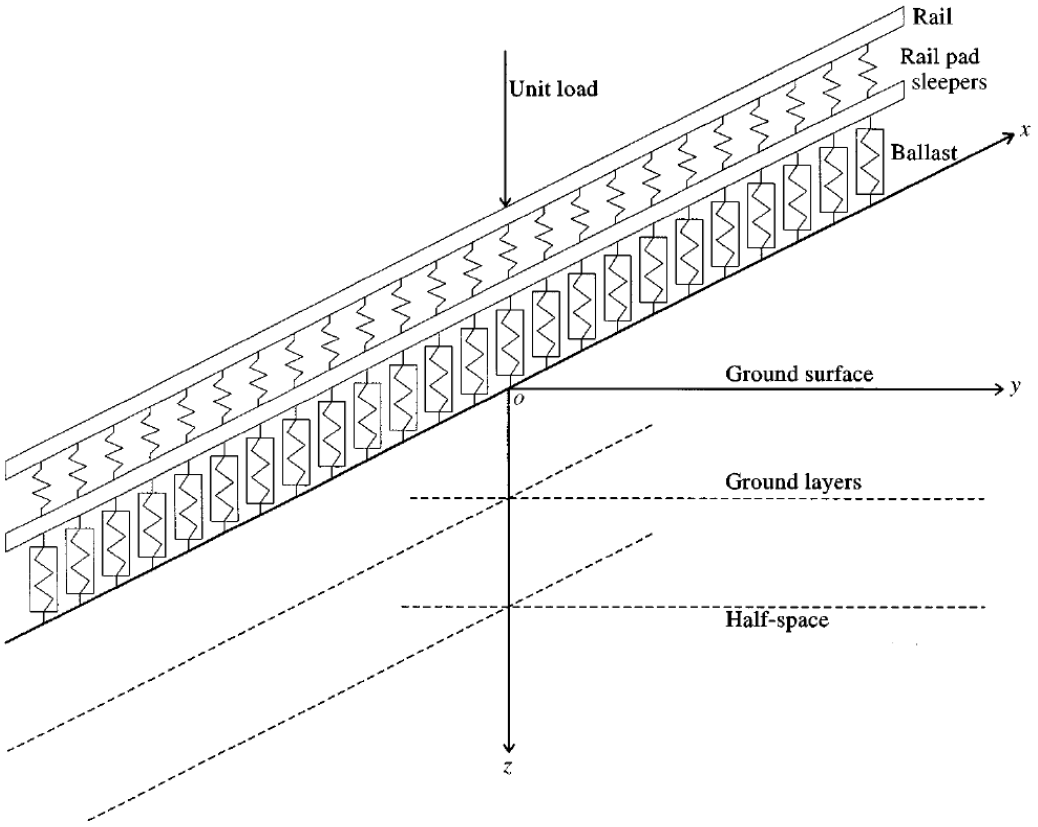

Figure 7.1 The railway-ground system (Sheng et al., 1999)

These models attempt to simulate the whole dynamic system from train-rail interactions through to the response of layered ground; however, this research is concerned with the response and properties of the ballast only.

The impulse response method applies a vertical force and measures the corresponding vertical ground response with a transducer. Consequently, any model of ballast behaviour should incorporate only the ballast and the linear forces acting upon the ballast, meaning that when vertically excited, horizontal and lateral movement can be taken as zero.

Where the dynamic stiffness of the ballast is of interest, other models (Jones, 2010) have reduced to a linear model of ballast-sleeper interaction, as can be seen in Figure 7.2.

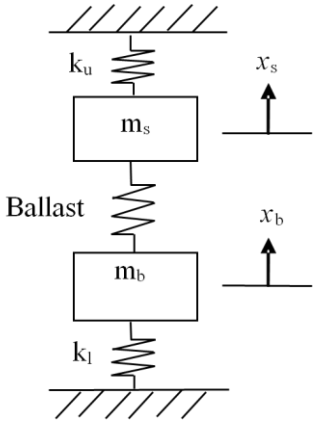

Figure 7.2 Dynamic stiffness of ballast model (Jones, 2010)

Furthermore, it is not intended to use the impulse response method to simulate train loading, but rather to use the force and frequency of the vertical impact and vertical response to determine the ballast properties. This vertical impact force may be applied directly to the ballast or via the track structural components.

A commonly used model for analyzing the dynamic responses of linear systems is the single degree of freedom (SDOF) mechanical system containing three elements: stiffness, mass, and damping coefficient (Hoffmann et al., 2004).

Single degree of freedom models have been used for impulse response testing on concrete (McCavitt et al., 1992), or for FWD testing on pavements (Westover et al., 2007) as can be seen in Figure 7.3.

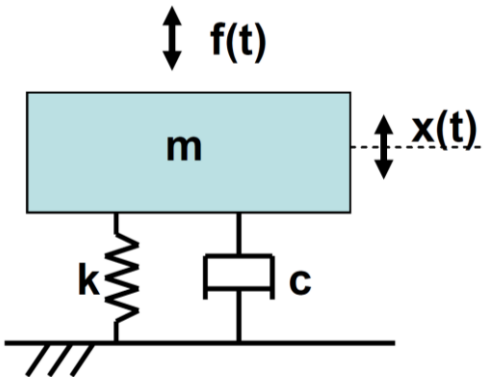

Where, c = damping co-efficient
m = mass of the entire system
k = stiffness of the spring

Figure 7.3 SDoF system (Westover et al., 2007)

Again, differential Equation 6.1 governs the dynamic response of a SDOF system: -

$$m\ddot{x} + c\dot{x} + kx = f(t) \qquad \text{Equation 6.1}$$

Where, x = displacement;
$\dot{x}$ = velocity; and,
$\ddot{x}$ = acceleration.

Note that stiffness (K) is defined as "the ratio of a steady force (P) acting on a deformable elastic medium to the resulting displacement" (Rasmussen & De Man, 2000). This means that if the track has high stiffness, then when a train passes, the track deformation will be low; and if the track has low stiffness, then when a train passes, the track deformation will be high.

The force applied to the mass represents the hammer blow and is defined as $f(t)$, and the mass's position is defined solely in the vertical axis by $x(t)$.

Such a method assumes that the model is a single degree of freedom system and when analysing concrete slabs or pavements, this is very often taken as the case; whereas, clean ballast is an unbound material. However, once the ballast particles mechanically interlock, and particularly when fouled, then at low strains, it may act as a single degree of freedom system when excited by a hammer and the response measured with a geophone.

In this research, the ballast is impacted by a hammer and the response is measured on the ballast by a geophone. Thus, the single degree of freedom model is considered to be an acceptable approximation.

7.4 Impulse Response Theory

Previous research has analysed the mass-spring system using the excitation force and the structural response to derive the FRF to determine concrete material properties (McCavitt et al., 1992). Therefore, this can be developed further (Ewins, 1984) and applied to ballast. In terms of Receptance, for the case of no damping, the FRF is calculated with the damping force considered to be zero.

If no excitation force is applied, then ..... $f(t) = 0$ and $c\dot{x} = 0$

So the equation of motion becomes ..... $m\ddot{x} + kx = 0$

Which has the solution ..... $x = -e^{-i\omega t}$

Now, consider an excitation of the form ..... $f(t) = fe^{i\omega t}$

Then, using trial solution (x independent of time and contains information on phase and magnitude) ..... $x(t) = xe^{i\omega t}$

Gives..... $k - \omega^2 m = 0$

Therefore, the modal model consists of one mode of vibration with a natural frequency given by..... $\omega_0 = \left(\frac{k}{m}\right)^{0.5}$

The equation of motion then becomes ..... $(k - \omega^2 m)xe^{i\omega t} = fe^{i\omega t}$

Therefore, this can be solved and is the equivalent to the ballast vibration divided by the input (Ewins, 1984): -

$$\alpha(\omega) = \frac{x}{f} = \frac{1}{k - \omega^2 m} \qquad \textbf{Equation 7.1}$$

With the inclusion of damping (Ewins, 1984), this becomes: -

$$\alpha(\omega) = \frac{1}{(k - \omega^2 m) + i(\omega c)} = \frac{\text{Displacement transducer response}}{\text{Hammer response}} \qquad \textbf{Equation 7.2}$$

Given that: -

$$Y(\omega) = \frac{v}{f} = \mathrm{i}\omega\, \frac{x}{f} = \mathrm{i}\omega\alpha(\omega) \qquad \textbf{Equation 7.3}$$

Then,

$$Y(\omega) = \frac{v}{f} = \frac{\mathrm{i}\omega}{k - \omega^2 m + i\omega c} = \frac{\text{Velocity transducer response}}{\text{Hammer response}} \qquad \textbf{Equation 7.4}$$

7.5 Impulse Response on Railways

A number of other researchers in recent years have investigated the use of an instrumented hammer being used to determine the dynamic properties of railway track components.

A system was developed by Delft University of Technology, called Dynatrack (de Man & Esveld, 2001), which used an instrumented hammer and several accelerometers to

record the dynamic behaviour of railway track superstructure components. This data was used to calculate the FRF, which was then further analysed to compare resonant frequencies and vibration modes of different components for the purpose of assessing track fastening systems. Earlier research at Delft had used the same technique to analyse the dynamic behaviour of ballastless track components compared to those on ballasted track (Oostermeijer & Kok, 2000).

Similarly, further research (amongst numerous related papers) at the University of Wollongong (Kaewunruen & Remennikov, 2005), found that the technique could be used to derive FRF curves for rail pads on concrete sleepers and that these curves could be used to determine the condition of aged pads.

A continuation of this work undertook field trials for dynamic characteristics on a ballasted track in Central Queensland and found that the results could provide "important input for determining the maximum speed and axle load for the future track upgrades" (Kaewunruen & Remennikov, 2007).

The work by Jones and Sheng and others (Jones & Block, 1996)(Sheng et al., 1999)(Sheng et al., 2004)(Jones, 2010) models the rail-pad-sleeper-ballast-ground system and the ballast system – but from the standpoint of vibration transmission. They were not investigating ballast fouling.

The above hammer impact techniques concentrate on testing the railway track superstructure components without direct measurement of the ballast; whereas, the FWD measures the ballast exclusively whilst decoupling the superstructure. A combination of aspects of both techniques could be considered.

CHAPTER 8 IMPULSE RESPONSE ANALYSIS

8.1 Impulse Response Analysis Development

It was determined that impulse response tests were to be conducted on the University of Edinburgh railway track. In order to undertake such experiments, the testing procedure had to be developed.

An instrumented 12lb (5.44kg) impulse hammer with built-in load cell that converted the impact force into an electrical signal was used to impact various parts of the track and the vibration response was recorded using a nearby transducer. The 12lb hammer was chosen over smaller models because it imparts the largest force and has the lowest frequency content (Rausche et al., 1992).

Two different hammer tips were used; one made from rubber and one made from vinyl. A metal tip was found to be unsuitable due to it tendency to cause localised aggregate crushing damage on impact giving rise to randomly variable and noisy results.

A velocity transducer (geophone) and a displacement transducer were used to record the hammer impact responses. Later analysis found that the displacement transducer data was not suitable as the low frequency performance was less linear. The geophone used was a low frequency model and captured the data of interest, i.e., less than 100Hz, whereas the displacement transducer did not.

A National Instruments dynamic signal conditioning unit with USB connectivity was used to supply power and condition the signals from the hammer and geophone. National Instruments software was used to record the data on a laptop PC. A programme was constructed with the software to manage the devices and collect, analyse, display, and record the data.

The experimental setup is shown in Figure 8.1 and Figure 8.2.

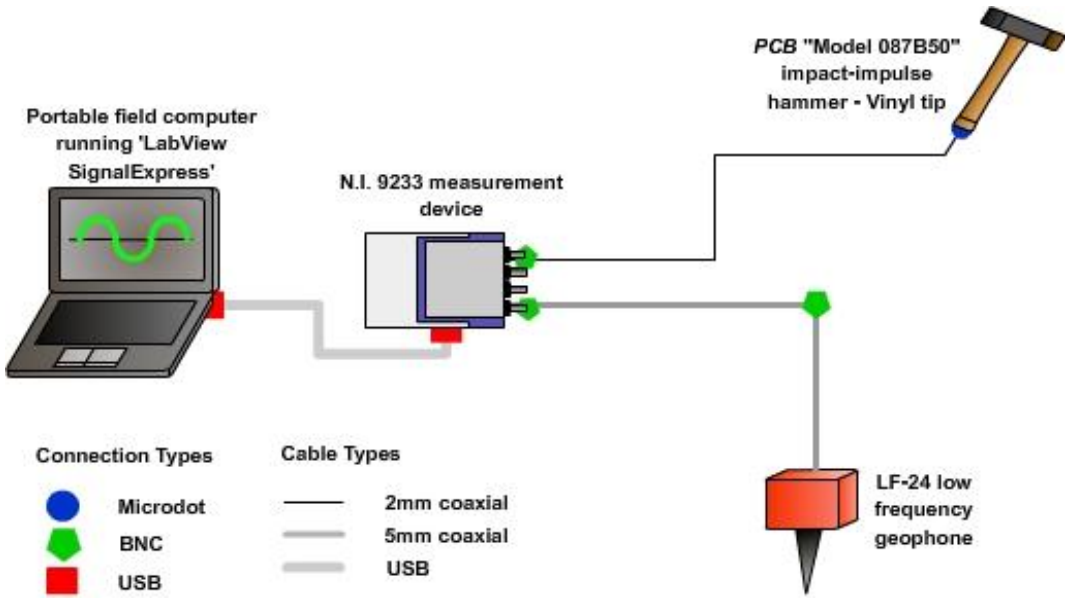

Figure 8.1 Experimental setup schematic

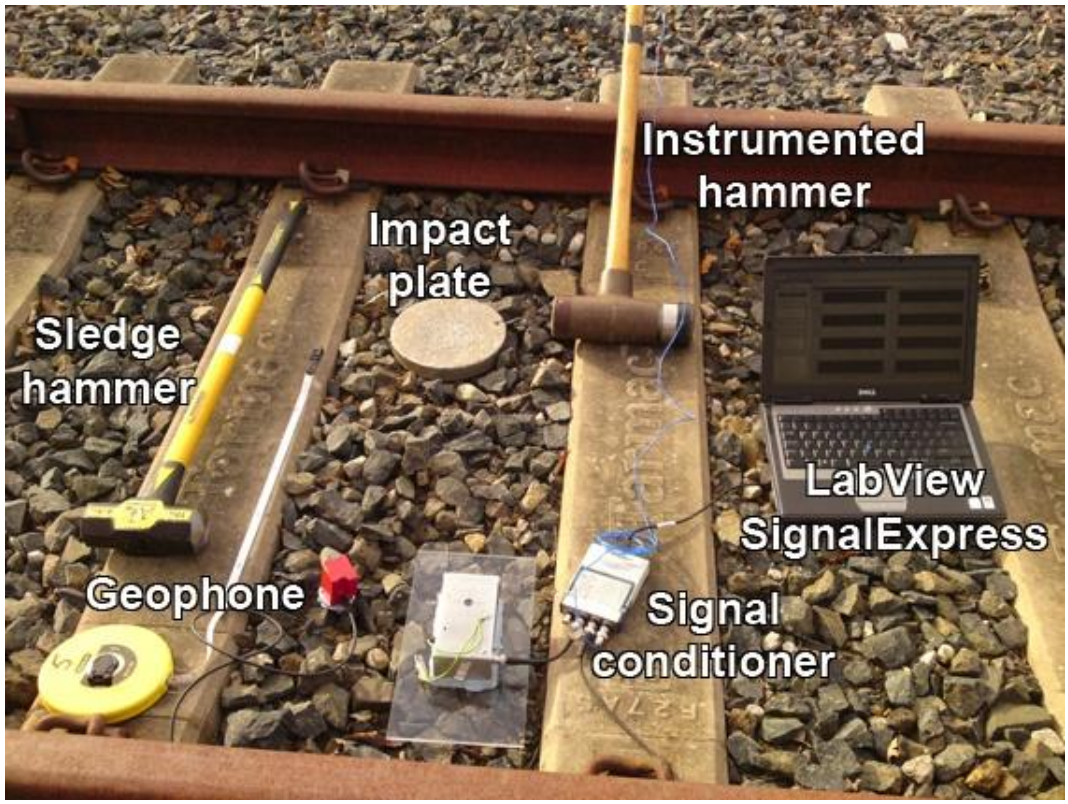

Figure 8.2 Experimental setup photograph

8.2 Impulse Response Testing Method Validation

8.2.1 Beam Tests

In order to validate the testing method prior to experimentation on the railway track, tests were conducted on a 1.5m long concrete beam, supported by three wooden strips, in order to determine the effects of orientation of the geophone's response. A thick strip of plasticine was used as an effective coupling material to attach the geophone (Colombo et al., 2005). The geophone was connected horizontally and vertically to the concrete beam with the hammer used to impact the far end of the beam (Figure 8.3).

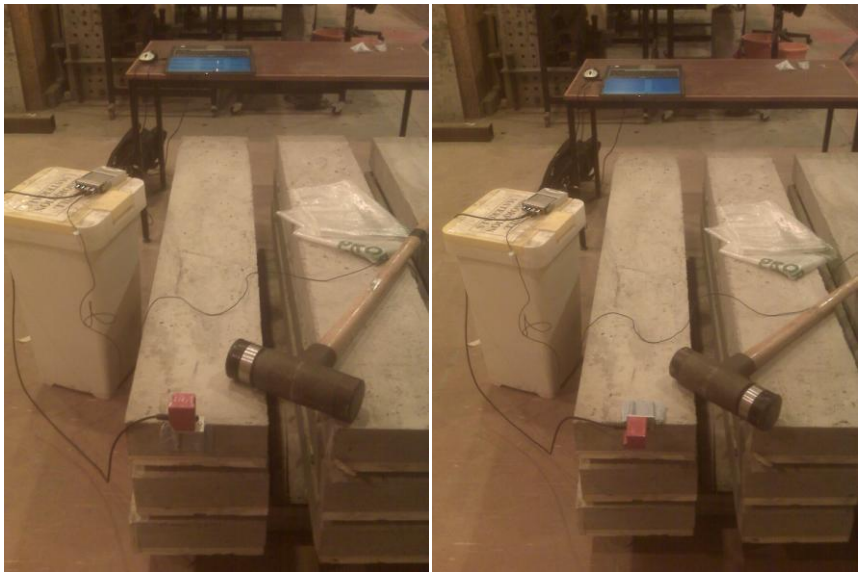

Figure 8.3 Testing vertical and horizontal geophone orientation on beam

When the beam was impacted with the hammer horizontally, such that the impact force of the hammer travelled horizontally along the length of the beam, the response was picked up by the geophone in the vertical orientation (Figure 8.4).

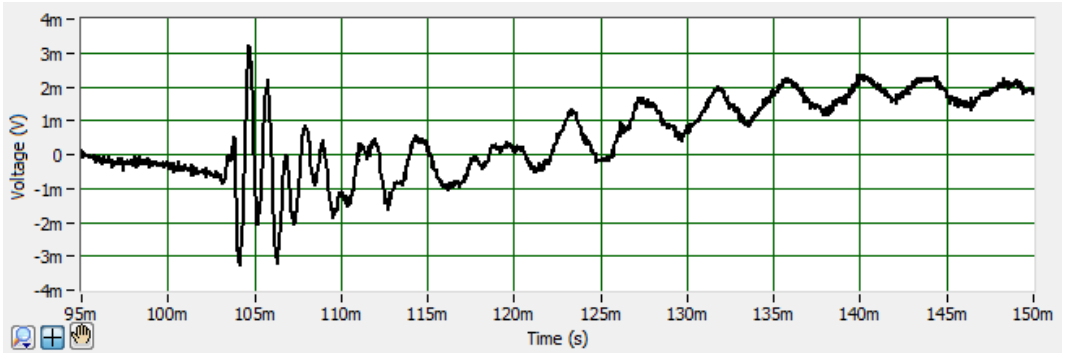

Figure 8.4 Vertical geophone response to horizontal hammer impact

However, when the beam was again impacted with the hammer horizontally, such that the impact force of the hammer travelled horizontally along the length of the beam, the response picked up by the geophone when in the horizontal orientation was considerably stronger – by a factor of over 25 (Figure 8.5).

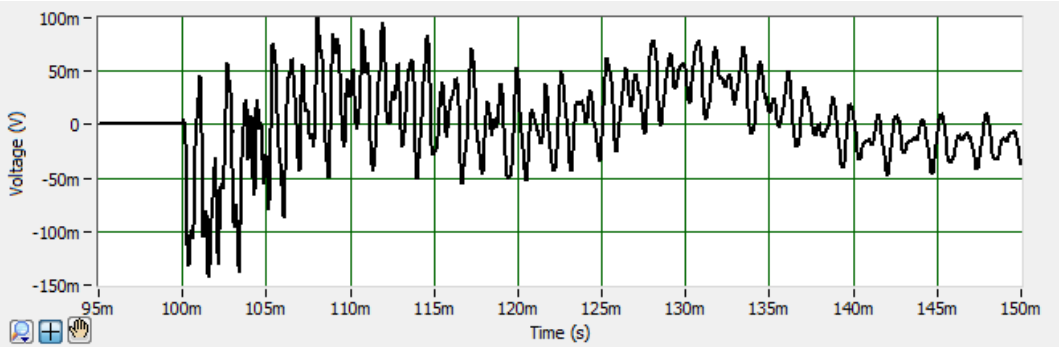

Figure 8.5 Horizontal geophone response to horizontal hammer impact

From this, it can be seen that the geophone responses are primarily due to movements in a single plane of orientation to the geophone, and out of plane movements are largely not recorded. However, both responses clearly demonstrated anomalous recurring peaks.

8.2.2 No Action Tests

The recurring peaks in the geophone response were also evident in the FFT of the geophone response; in the frequency domain, they appeared as 50Hz recurring peaks (50Hz obviously being the frequency of mains supply).

This was even detected when a test was conducted where no hammer impact was undertaken (a "no action test"); that is, only background noise was recorded by the geophone (Figure 8.6).

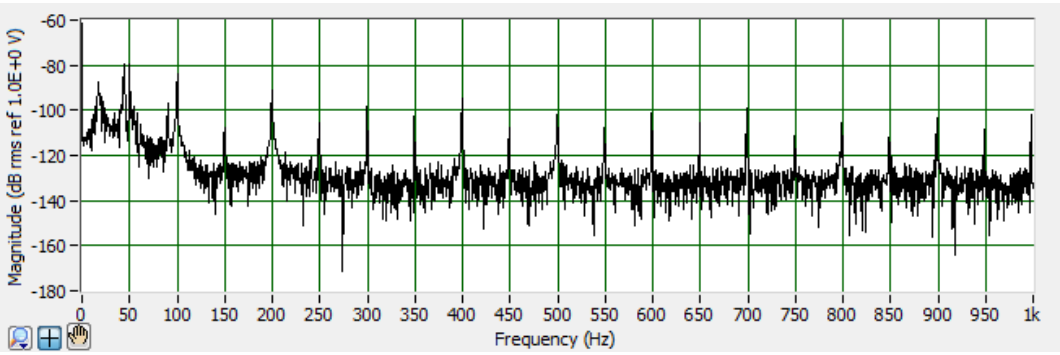

Figure 8.6 FFT of geophone response under AC power

It was eventually determined that this anomaly was caused whenever the laptop that powered the experimental devices was connected to the 50Hz AC (alternating current) mains electricity power supply. Thus, it was presumed that there was a degree of "AC leakage" from the mains electricity interfering with the geophone response. It was found that the simplest and easiest way to remove this "AC leakage" was to ensure that future experiments were conducted under the battery power of the laptop, which provides a non-alternating DC (direct current) power supply.

8.2.3 Pile Tests

Further tests of the experimental procedure were undertaken on some buried 10m long, 0.4m diameter, concrete piles. The tests were undertaken with a 1kg hammer using the metal and vinyl hammer tips (Figure 8.7).

Figure 8.7 Testing geophone and medium hammer on pile head

The typical results where a vinyl-tipped hammer was used are shown in Figure 8.8 and Figure 8.9.

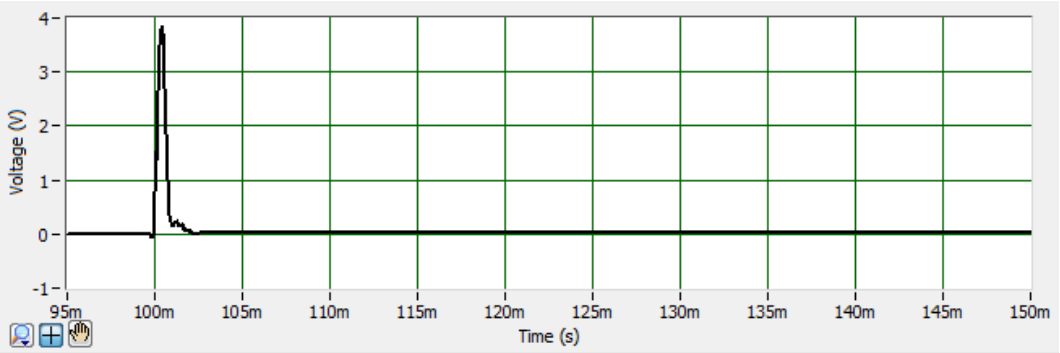

Figure 8.8 Typical vinyl-tipped hammer response

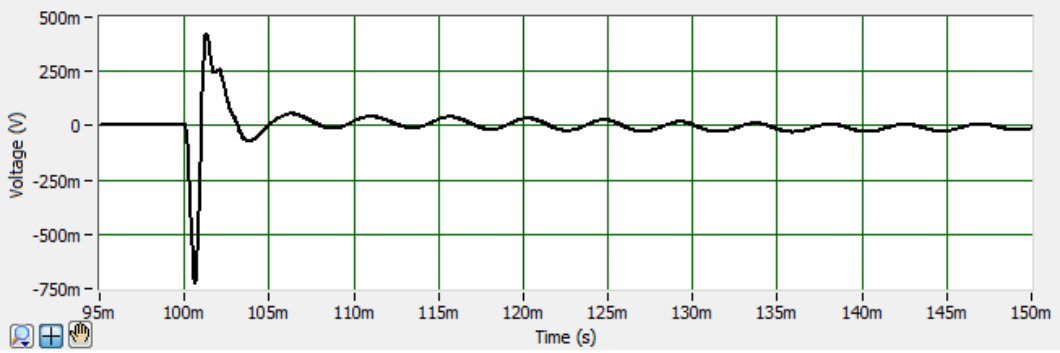

Figure 8.9 Typical geophone response from vinyl-tipped hammer

However, where a metal-tipped hammer was used it could be seen that localised concrete crushing damage was caused to the pile head. Evidence of this could also be seen in the hammer response, where the load cell trace did not return to zero (Figure 8.10), and in the geophone response, where the peak positive response was curtailed (Figure 8.11).

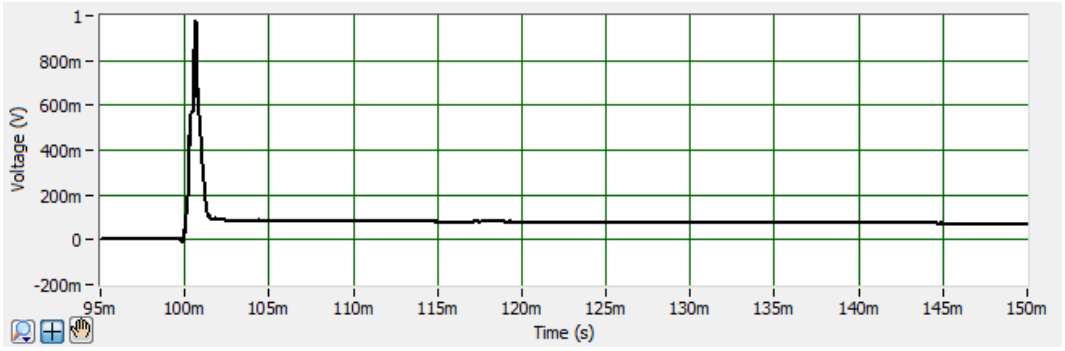

Figure 8.10 Metal-tipped hammer response featuring concrete crush

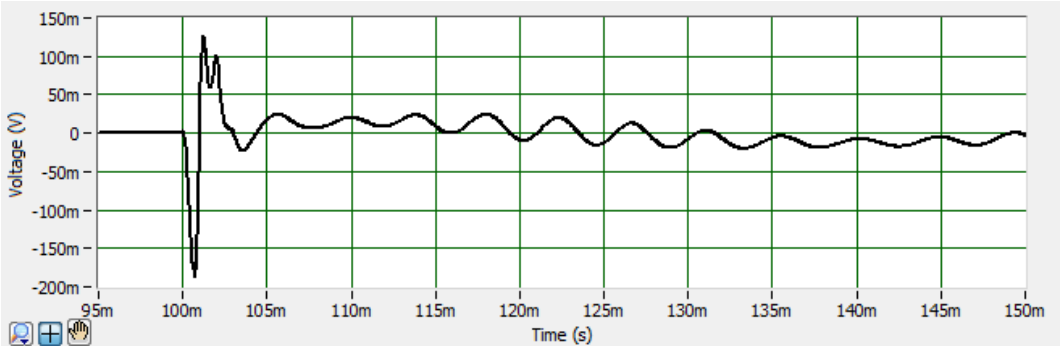

Figure 8.11 Metal-tipped hammer geophone response featuring concrete crush

Given the concrete crush damage caused by the hammer with the metal tip, it became apparent that the metal tip would not likely be suitable for testing on the stone, concrete, and wooden structures of a railway.

After several "forceful" uses of the vinyl-tipped hammer, a portion of the tip head fractured and sheared off. Two vinyl-tipped hammers failed in such a fashion. The hammer response and geophone response of these incidents was also recorded: the hammer load cell trace returned to below zero (Figure 8.15) and, again, the geophone peak response was curtailed (Figure 8.13).

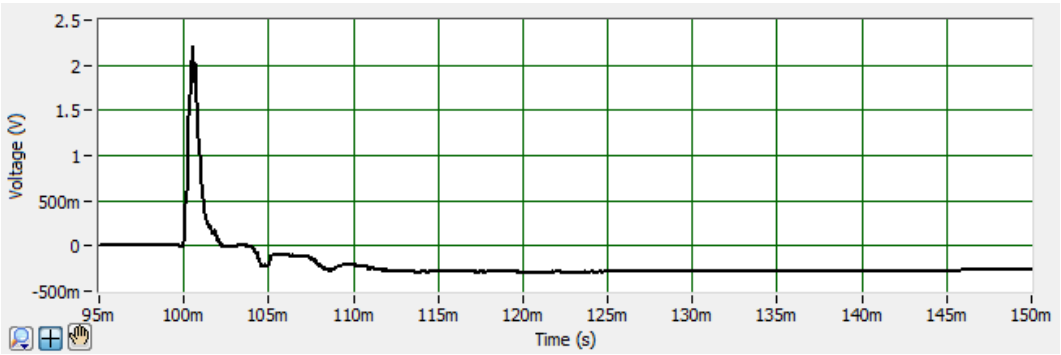

Figure 8.12 Vinyl-tipped hammer response featuring tip breakage

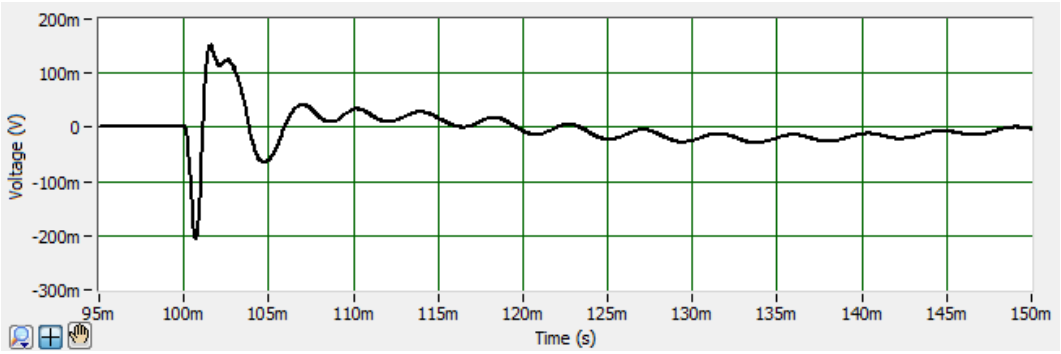

Figure 8.13 Vinyl-tipped hammer geophone response featuring breakage

Given the breakages of the 1kg medium hammer vinyl tip, it became apparent that a more robust larger hammer (with a larger vinyl tip) may be required. Also, a larger hammer would be anticipated to input more energy at a lower frequency.

8.3 Experiment Setup

The general testing procedure for each crib was to impart a force into the structure using both the vinyl and rubber hammer tip.

The test was repeated three times at cribs 1, 2, 3, 4, 6, 8, 10, 12, 14, and 16.

The three main structural components were tested using the following setup configurations: -

Setup 1 Ballast impacted with hammer, response from ballast measured – "Hit Ballast, Measure Ballast".

Setup 2 Ballast impacted with hammer, response from sleeper measured – "Hit Ballast, Measure Sleeper".

Setup 3 Ballast impacted with hammer, response from rail measured – "Hit Ballast, Measure Rail".

Setup 4 Rail impacted with hammer, response from ballast measured – "Hit Rail, Measure Ballast".

Setup 5 Sleeper impacted with hammer, response from ballast measured – "Hit Sleeper, Measure Ballast".

When the impulse hammer was impacted on the ballast, an 8" (20.5cm) diameter, 1" (2.5cm) thick, 2.6kg aluminium metal disc was used as a strike plate. The plate would rest on the surface of the ballast after being bedded into the ballast with a sledgehammer prior to testing.

Given that the metal strike plate is acting as a hard couplant material between the hammer and the ballast, it is anticipated that there will not be significant attenuation or filtering of the frequencies of the impact force imparted into the ballast (Colombo et al., 2005).

When the response from the ballast was measured, the geophone would be affixed to a 15cm spike with a square flat head that would be driven into the ballast with a sledgehammer prior to testing (Figure 8.14).

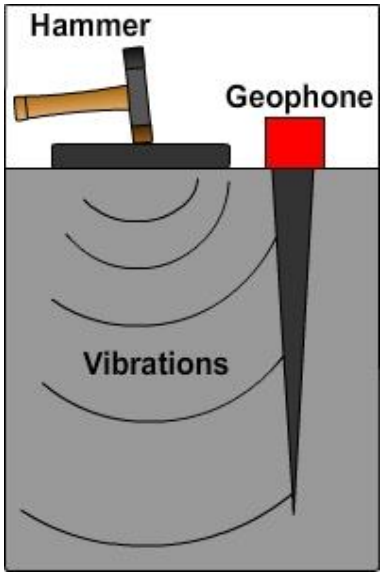

Figure 8.14 Long spike

The geophone would be located at a distance of 500mm from the edge of the strike plate (this distance was found to produce the clearest and most consistent results).

Again, plasticine was used as an effective coupling material (Colombo et al., 2005).

8.4 Signal Analysis

8.4.1 FRF Generation

The analysis software converted the hammer and transducer responses from the time domain into the frequency domain using a Fast Fourier Transform (FFT). The transducer FFT response was divided by the hammer's FFT response in order to produce the Frequency Response Function (FRF) (Figure 8.15).

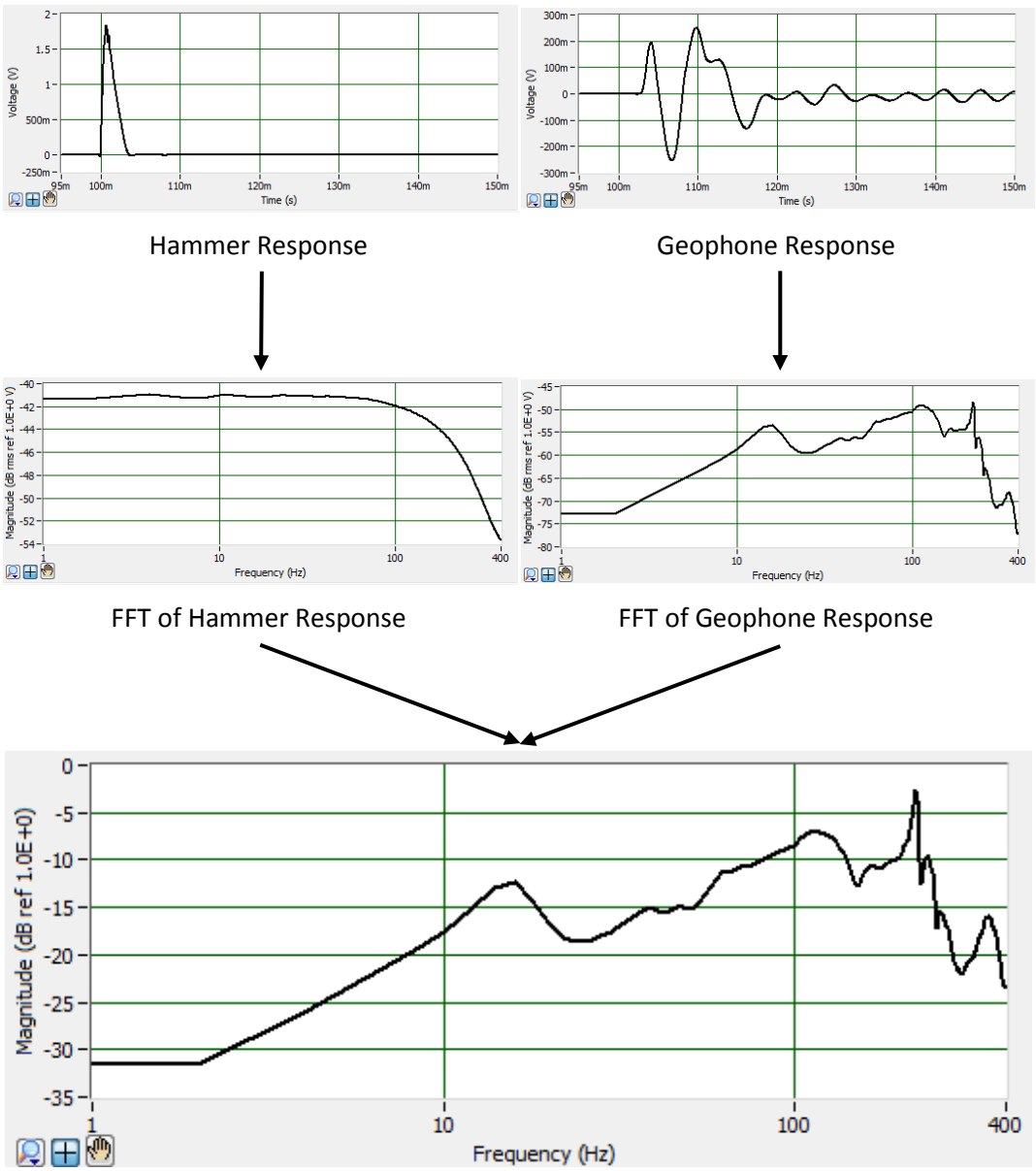

Figure 8.15 FRF generation (Crib 10, vinyl hammer tip onto strike plate on ballast)

8.4.2 Units

The hammer sensitivity is 0.17mV/N, and the geophone sensitivity is 20mV/m/s; therefore, the conversion factor from mobility voltage values to mobility units is: -

$$\text{Factor} = \frac{\text{Hammer Sensitivity}}{\text{Geophone Sensitivity}} = \frac{0.17}{20}\frac{mV}{N}\frac{m/s}{mV} = 0.0085\frac{m}{sN} \text{ per output unit}$$

8.5 Characteristics of Ballast

The two main characteristics of dry spent ballast are an increase in strength and an increase in stiffness: -

Increased fouling in dry ballast increases stiffness..... $\uparrow$ Fouling $\overset{dry}{\Rightarrow} \uparrow$ Stiffness

However, fouled wet ballast at, or nearing saturation, may have a lower stiffness than dry ballast. Where the immediate passage of a train causes intensive repeat loading of spent wet ballast, then this can give rise to an increase in pore water pressure (PWP), and, thus, a reduced effective stress leading to a reduction in shear strength and stiffness – as demonstrated by Wood in relation to clay (Wood, 1994): -

Increased fouling in wet ballast under traffic increases PWP,..... $\uparrow$ Fouling $\overset{wet + trafficking}{\Longrightarrow} \uparrow$ PWP

And, increased PWP in wet ballast decreases stiffness..... $\uparrow$ PWP $\overset{wet}{\Rightarrow} \downarrow$ Stiffness

Therefore, increased fouling in wet ballast decreases stiffness..... $\uparrow$ Fouling $\overset{wet}{\Rightarrow} \downarrow$ Stiffness

However, this condition will not normally be encountered during routine FRF testing during track possessions. Therefore, for normal FRF testing, in the absence of a build-up of positive pore water pressure from a passing train, spent ballast would not lose significant stiffness due to being wet.

Returning to the original assertion that the two main characteristics of dry spent ballast are an increase in strength and an increase in stiffness; then, if track stiffness can be quantified, as it is related to ballast condition, the spentness of the ballast can also be established.

From control experiments of a sleeper being impacted with a hammer and the response from the sleeper being measured, it was found that tests featuring ballast had a significantly lower response beyond 150Hz; therefore, it can be noted that the ballast damps, or otherwise filters, the higher frequency signal propagation.

8.6 Impulse Response Results Interpretation

The FRF contains information on the condition and the integrity of the tested element (ACI 228.2R S2.2, 2011), and a typical mobility plot of a concrete structure can be broken down into three regions (Davis et al., 2004). This research has been summarised to depict the regions in Figure 8.16.

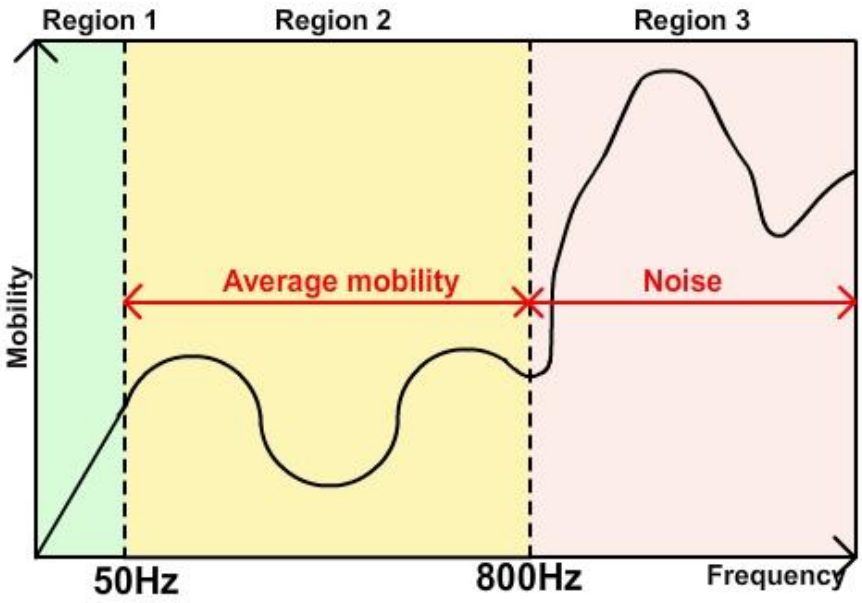

Figure 8.16 Typical concrete element FRF

Region 1 Below 100Hz – the gradient of this portion of the mobility plot defines the static compliance or flexibility of the area around the test point for a normalized force input; the inverse of this is the "dynamic stiffness". The dynamic stiffness of a plate-like element depends on its physical characteristics: the thickness of the plate, the density and elastic modulus of the material, support conditions, and presence of internal defects.

Region 2 100Hz to 800Hz – the mean mobility value inside this range is related to stiffness; a higher mobility indicates that the test element is relatively more flexible at that test point. The response of a test element to an impact-generated elastic wave will be damped by the intrinsic rigidity of the element, i.e., "body damping", again determined by the physical characteristics of the test element.

*Region **3*** Above 800Hz – data in this region not related to stiffness.

It is understood that the FRF of components of a railway track when tested would potentially differ significantly from the above model, but it is the attempt of this research to determine if any parallels can be made.

The early research from the 1970s into vibration testing of piles (Davis & Dunn, 1974), used the below equation to calculate dynamic stiffness: -

$$E' = \frac{2\pi}{M}$$ Where, E' = dynamic stiffness; and, M = gradient of initial slope of FRF. **Equation 8.1**

Further research explained that when a structure is excited at low frequencies, the inertia effects are negligible causing the structure to behave like a spring, and that the initial slope up to 100Hz defines the structures static compliance and that the slope's inverse is proportional to the dynamic stiffness (Davis et al., 2001).

Continuation of the research into concrete tunnel linings looked at other structural properties that can be determined from an FRF plot (Davis et al., 2004). This found that the mean mobility over the 100-800Hz range can also be used as an indicator of stiffness.

An example of such a plot of mobility (vertical axis in units of speed per unit of force) versus frequency (horizontal axis) for a concrete slab can be seen in Figure 8.17.

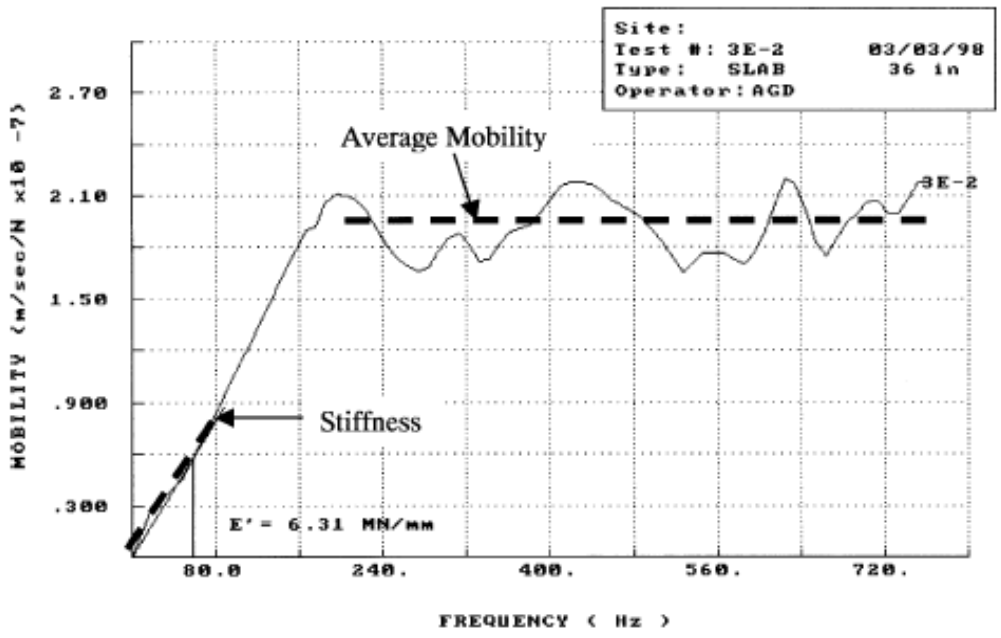

Figure 8.17 Initial gradient and average mobility (Davis et al., 2001)

Later research into concrete tunnel linings found that the gradient to 50Hz (Ottosen et al., 2004) is the range over which stiffness can be calculated, and further states that there is a difference in FRF response between "honeycombed" concrete, with higher mobility values, and "sound" concrete, with lower mobility values (Figure 8.18).

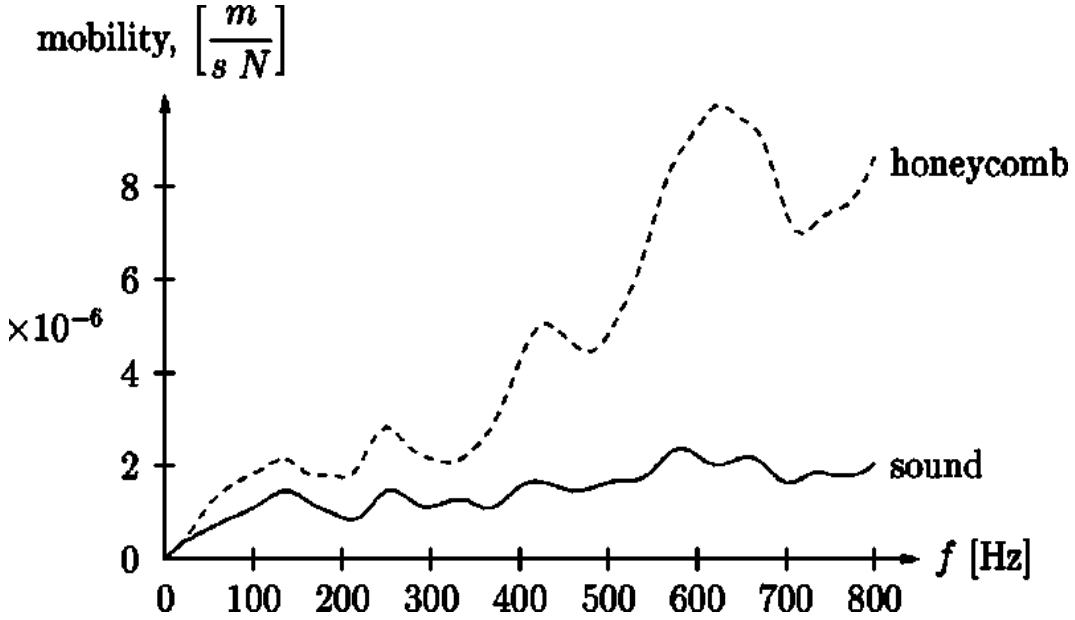

Figure 8.18 Honeycombed and sound concrete FRF (Ottosen et al., 2004)

Where there is a reduction in thickness, or a debonding of an upper layer, loss of support, or the intrinsic rigidity of the test element has been reduced by cracking or honeycombing, then an increase in the mean mobility becomes apparent from the mean mobility value between 100Hz and 800Hz. It is also apparent from the mobility value at 100Hz, that under such conditions the dynamic stiffness has similarly decreased.

Where debonding or delamination has occurred in a concrete slab, it is the uppermost layer that determines the impulse response test result. The higher the ratio of the mean 100Hz to 800Hz mobility to the initial 100Hz peak, then the greater the indication of one of the noted forms of failure (ASTM C1740, 2010).

The method can applied in a grid formation over a test element surface, with the results plotted on a two-dimensional contour chart, thus allowing comparative evaluation of the findings.

Figure 8.19 shows an example of a contour plot of average mobility obtained from testing a concrete floor.

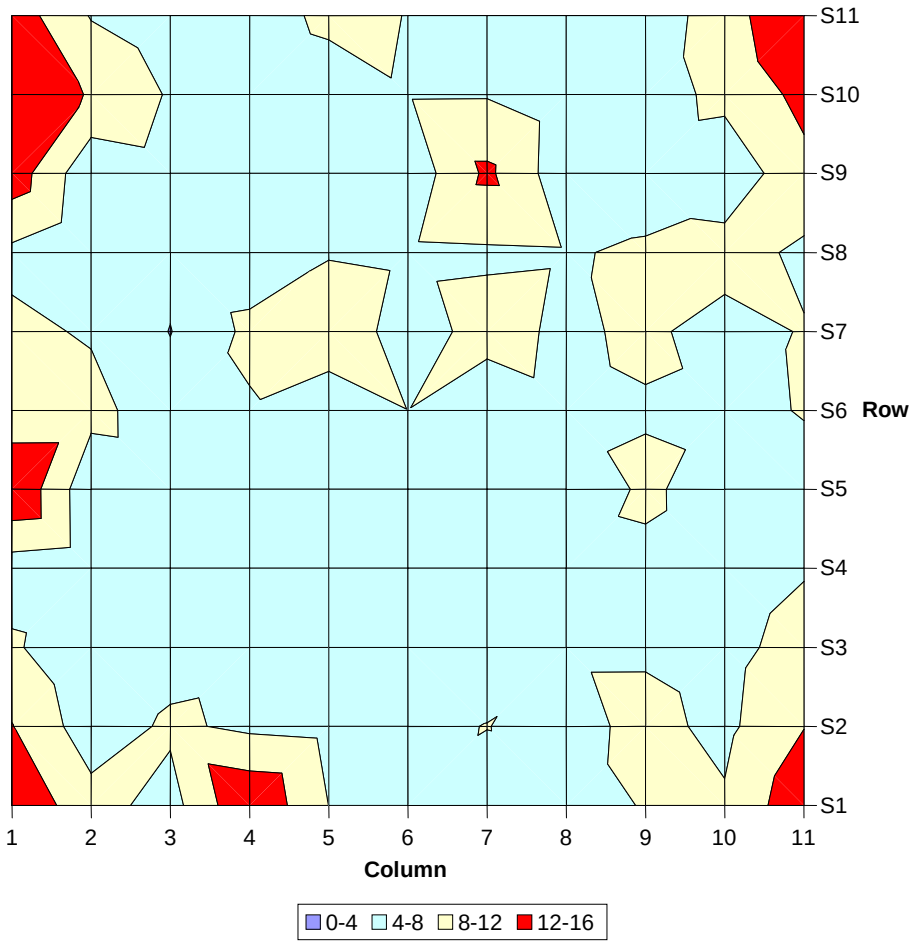

Figure 8.19 Concrete floor slab mean mobility contour plot (ACI 228.2R S2.2, 2011)

The darker colouration shows the areas of higher mobility. It can be seen that this example slab had higher mobility at the corners, which possibly indicates lifting off the ground at those points; and also an anomaly at Column 7, Row 9, which may require further investigation.

It should be noted that it is explicitly stated in most modern guides to impulse response (ACI 228.2R S2.2, 2011) (ASTM C1740, 2010) that the results from impulse response tests, such as the dynamic stiffness or average mobility, cannot readily be predicted from engineering mechanics theory due to the potential variation in support and sub-grade conditions; and that, therefore, the evaluation of impulse-response tests is typically performed as a comparative indicator, with the change or variation in results between test points used to identify anomalous conditions.

8.7 Application of Impulse Response Testing to Ballast

Ballast contains many voids and, therefore, this method could be applicable to ballast if one considers clean ballast analogous to honeycombed concrete and spent ballast analogous to sound concrete.

Historical research on vibration testing of piles used the gradient of the initial mobility line before the first peak on a mobility plot to calculate stiffness (Davis & Dunn, 1974). Through visual inspection, it was found that this peak occurred at 18Hz on tests at the Edinburgh track using a vinyl tipped hammer.

Similarly, the previous method that used the mean mobility over 100-800Hz range, used the 100Hz value as this was where the first peak in the mobility graph occurred. If this method is scaled, given that the first peak in the Edinburgh track experiments occurs at 18Hz, then, if the relationship is considered to be linear, then a range of 18-144Hz may be more appropriate for the Edinburgh track using this method.

However, as noted in Figure 8.17, there is the apparent assumption that the mobility plot "plateaus" after the peak value is reached. In the results from the Edinburgh track, this behaviour is not always present, but when it is, it is only true to 50Hz, after which there is often a surge in value that trails off and eventually becomes noise dominant. This behaviour is more consistent with Hit Ballast, Measure Ballast tests.

The initial peak at 18Hz, "plateau", and surge can be seen in two examples in Figure 8.20.

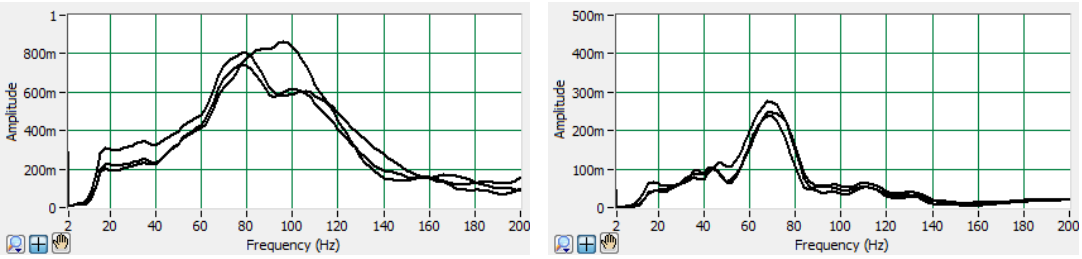

Crib 6: Hit Ballast, Measure Ballast Crib 8 Hit Ballast, Measure Rail

Figure 8.20 Typical railway track FRF curves

It can be seen that Figure 8.16 closely resembles Figure 8.20 but over a smaller frequency range where 18-50Hz would be comparable to 50-800Hz for Region 2. It can also be seen that the more direct measurement of Hit Ballast, Measure Ballast has a

greater amplitude than Hit Ballast, Measure Rail, where the impact forces travel and dissipate through the ballast, sleeper, and rail. This is unsurprising given that the FRF technique normalises per the input (the impact).

8.8 Hammer tip analysis

As can be seen on Figure 8.21, different hammer tips impart the impact force over different periods of time, with the rubber tip (shown as red) having a longer contact time than the vinyl tip (shown as blue). The resultant different FFT results of the hammer response can be seen on Figure 8.22.

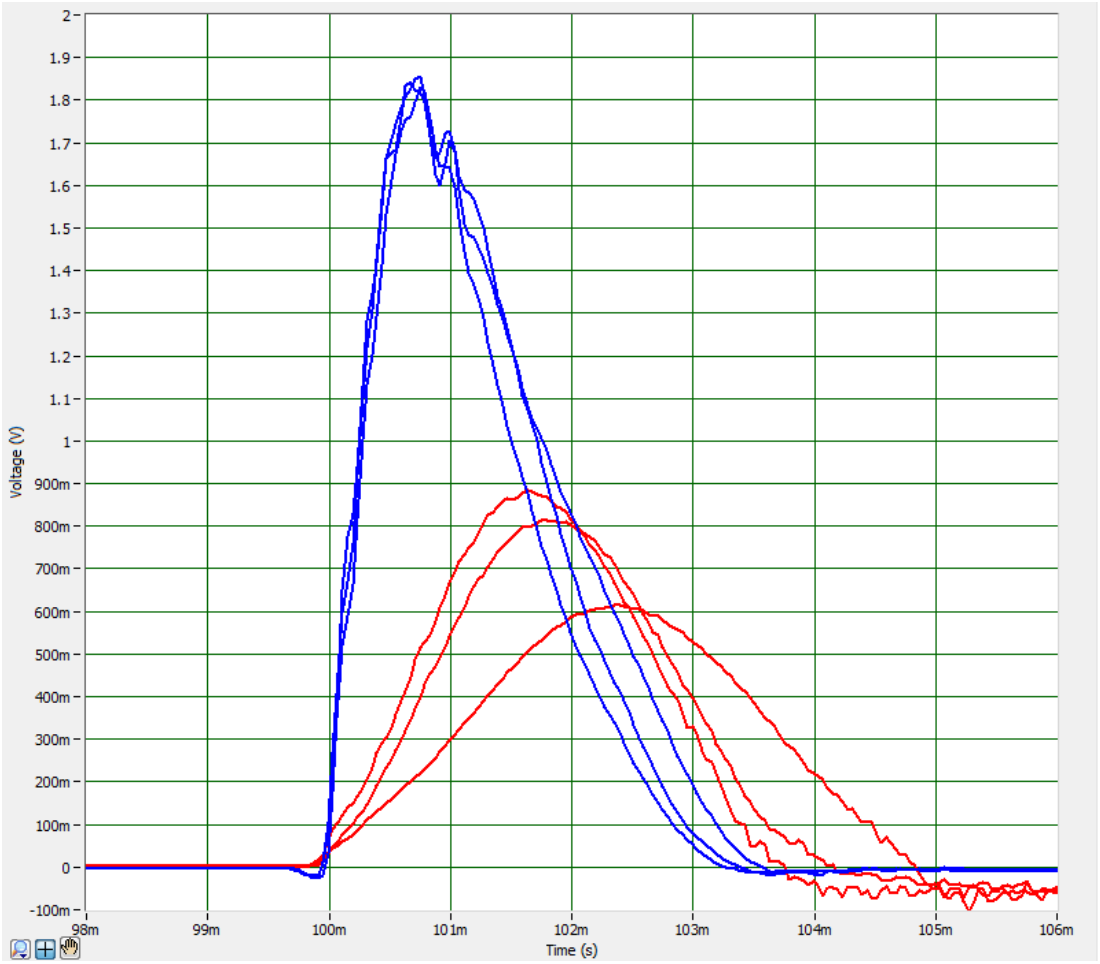

Figure 8.21 Hammer response (Crib 10, hit ballast)

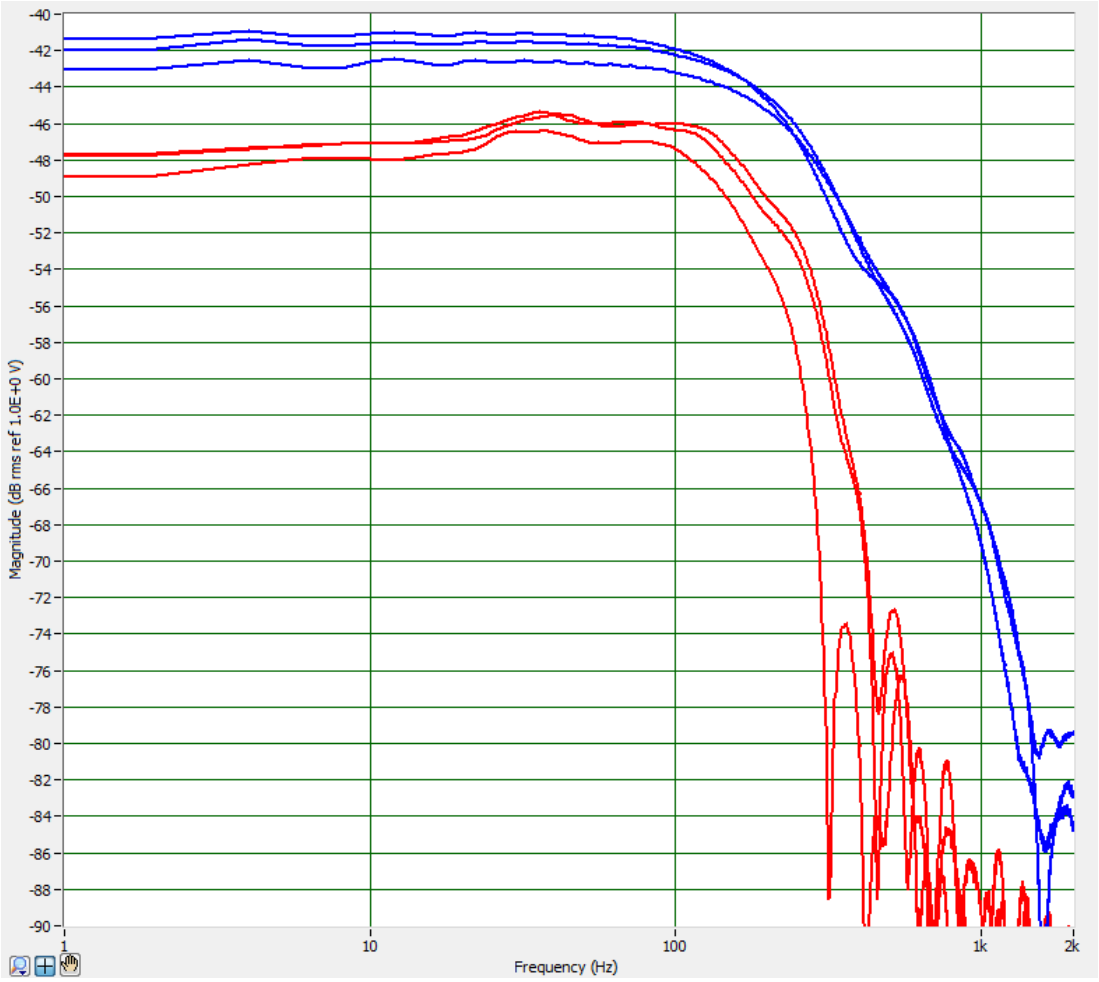

Figure 8.22 FFT of hammer response (Crib 10, hit ballast)

Therefore, as expected, if the tip is constructed from a hard material, then the hammer impact will impart higher frequencies. If it is soft, it will impart lower frequencies.

The FFT produced by softer tips, e.g., rubber (shown in red, vinyl shown in blue), are only accurate to lower frequencies before succumbing to noise. Therefore, FRFs can only be accurate to the instrumented hammer's useful frequency range.

Chan (Chan, 1987) showed that a 10dB drop in the hammer response can be used to determine the upper limit in the useful range of frequencies to determine stiffness. Data collected at higher frequencies is outside the useable range of the impulse hammer and is therefore unstable and unreliable and should be ignored. The most important criteria in deciding this useful range is the minimal loss of power.

Inspection of the hammer FFTs showed that the 10dB drop in the rubber-tipped hammer responses generally occurred between 250Hz and 300Hz and became noise

dominant between 300Hz and 400Hz, and the 10dB drop in the vinyl-tipped hammer response occurred generally between 375Hz and 425Hz and became noise dominant between 1,500Hz and 2,000Hz.

8.9 Summary of Hypotheses

From the FRF of ballast, it may be possible to determine its stiffness using these methods. However, these assessments are based on research into concrete structures being excited with a 1kg hammer with an aluminium tip.

Testing on the Edinburgh track was undertaken with a 12lb hammer with vinyl and rubber tips and used to impart force onto three different components (made of four different materials): rail (steel), sleeper (concrete or wood), and ballast (crushed stone). Consequently, the nature of the frequency and depth of penetration of the excitation forces imparted will be considerably different.

Therefore, to investigate the application of impulse response on railway ballast, an FRF was calculated for most cribs of the Edinburgh track and the noted hypotheses for relating stiffness to the FRF plots were investigated: -

Hypothesis 1 Stiffness is related to the gradient of the initial line between 0-18Hz; that is, the gradient to the frequency at which the first peak occurs in the FRF.

Hypothesis 2 Stiffness is related to average mobility between 18-50Hz; that is, the average value of the "plateau" between the first peak and first drop in value of the FRF.

The techniques of gradient to 50Hz or 100Hz (a purely mathematical exercise since no peak value is present at these frequencies) and average values between 100-800Hz or 18-144Hz (despite the ranges including noise dominant data) were also investigated but yielded expectedly poor results.

8.10 Mobility analysis

8.10.1 Hammer Tip Comparison

Both the hammer's vinyl and rubber tips were used in the testing. The hammer response results with the vinyl tip were found to be generally similar in form but more

consistent than the hammer responses with the rubber tip. Both sets of results were analysed to determine how they correlated with the fouling index results. The vinyl tip results in all cases had a clearly stronger correlation with the fouling index values (it was later speculated that the connection between the vinyl tip and the hammer was superior to the rubber tip). Therefore, hypothesis comparisons are noted with the vinyl tip results.

8.10.2 Testing

Each hypothesis was tested to determine whether the results would correlate with the fouling index values for each crib using each test setup. Each setup was tested multiple times with three clear and consistent readings free of noise or aberrations being retained for analysis.

Then to determine the closeness of results, the median of the three readings derived from each hypothesis were compared to the results from the soil classification tests using the Pearson correlation co-efficient (the mean of the three readings was not used due to the occasional presence of large outlier values that could considerably skew the result).

As per Equation 5.1, the Pearson correlation co-efficient describes the quality of the correlation between the impulse response test results and fouling index. The strength of the correlation is represented by a number between -1 and 1 where "1" indicates a strong positive linear relationship, "0" indicates zero linear relationship and -1 indicates a strong negative linear relationship.

The impulse response data for Cribs 1 and 16 was discarded and not used in correlation calculations. This was because of the presence of boundary effects that caused results from these two locations to be often radically different from adjoining cribs and unpredictable.

8.10.3 Full Results

Full results (table and graphs) for each *Hypothesis* and *Setup* are shown in Appendix 7.

8.10.4 Summary of Results

The correlations between Hypothesis 1 and 2 and the fouling index for each crib is shown in Table 8.1.

Test Setup	Impact Comp	Measured Comp	Hypothesis		Steps Removed From Direct Measurement of Ballast
			1	2	
			18Hz Gradient Correl	18-50Hz Ave Val Correl	
1	Ballast	Ballast	-0.944	-0.909	0
2	Sleeper	Ballast	-0.376	-0.798	1
3	Ballast	Sleeper	-0.481	-0.618	
4	Rail	Ballast	-0.444	-0.431	2
5	Ballast	Rail	0.297	-0.022	

Table 8.1 Hypothesis 1 to 2 Vs fouling index

The column on the right of the table notes the degree to which either the impact or measurement component is not directly coupled with the ballast. That is, where the sleeper is either impacted or measured, this is termed as the measurement being one step removed from direct measurement of the ballast, as the forces have to travel through the tie.

Similarly, where the rail is either impacted or measured, this is termed as the measurement being two steps removed from direct measurement of the ballast, as the forces have to travel through the rail and the sleeper.

It is clear, especially in the average value calculations, that the more steps removed from direct measurement, the lesser the correlation with fouling index. This is not particularly surprising, as one would expect that the more steps removed from direct measurement of ballast would result in experimental data that related to the larger railway track system rather than only the properties of the ballast.

Moreover, because the rail and tie components are connected, it is impossible to isolate any impact or measurement exclusively to specific components or crib without disconnecting them.

These findings tie in with the discussion in Chapter 7 regarding theoretical models. One would expect the best results with the simpler single degree of freedom model: hit ballast, measure response on the ballast.

The majority of the correlations are negative indicating an inverse relationship between the two variables, thus giving some credence to the analogous comparison of clean ballast to honeycombed concrete and spent ballast to sound concrete: spent ballast (the "sound concrete") with a high fouling index has a lower mobility than clean ballast with a low fouling index (the "honeycombed concrete").

The correlation between the initial 18Hz gradient and fouling index is low for each testing condition except when the ballast was excited and the ballast vibration measured. In this case, the correlation coefficient is -0.944.

A graph of the results can be seen in Figure 8.23.

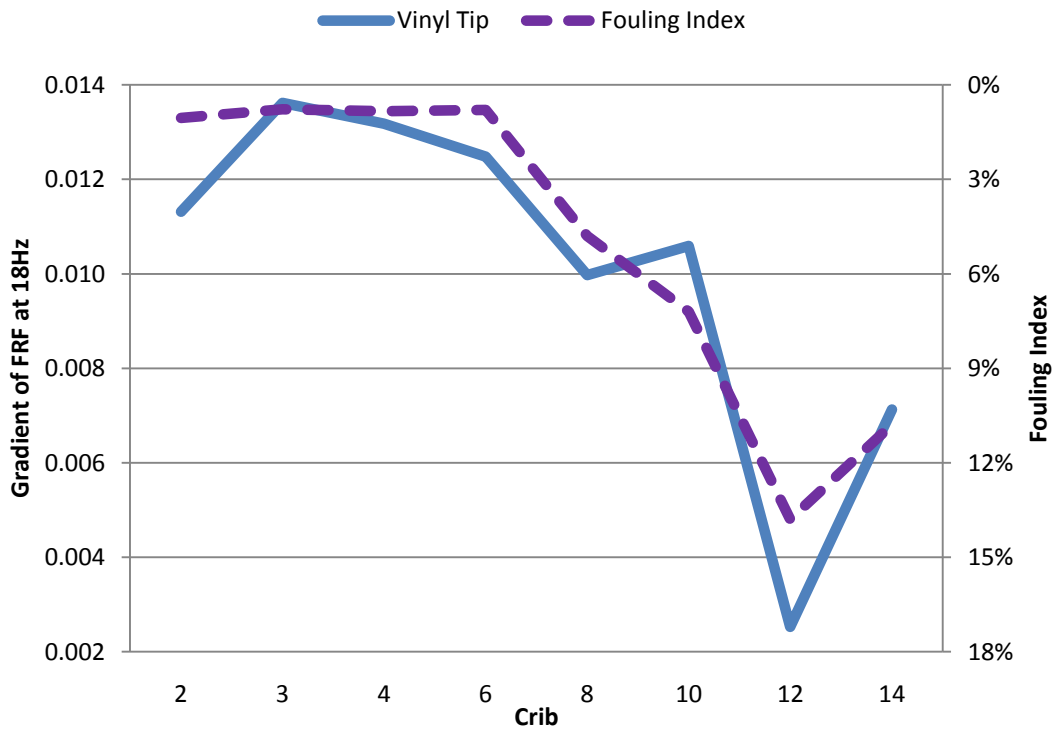

Figure 8.23 Hit ballast, measure ballast 18Hz gradient results

8.11 Mapping mobility to fouling index

The reason for the mobility-fouling relationship can be summarised below: -

From Davis, 2001, mobility is inversely proportional to stiffness	Mobility $\propto {}^{1}/_{\text{Stiffness}}$
And if stiffness is proportional to spentness	Stiffness $\propto$ Spentness
And spentness is proportional to the fouling index	Spentness $\propto F_i$
Then, mobility is inversely proportional to the fouling index	Mobility $\propto {}^{1}/_{F_i}$
Therefore, in ballast, this would mean that a decrease in mobility would result in an increase in stiffness	$\downarrow$ Mobility $\overset{dry}{\Longrightarrow} \uparrow$ Stiffness
From Wood 1994	$\uparrow$ Fouling $\overset{dry}{\Longrightarrow} \uparrow$ Stiffness
Therefore	$\downarrow$ Mobility $\overset{dry}{\Longrightarrow} \uparrow$ Fouling

Thus, the two hypotheses were: -

The average mobility used was between 18Hz and 50Hz of the Frequency Response Function value (Hypothesis 2)	$\downarrow {}^{18\text{Hz}}_{50\text{Hz}}\overline{\text{FRF}} \overset{dry}{\Longrightarrow} \uparrow F_i$
Or,	
The mobility used was the gradient of the Frequency Response Function value at 18Hz (Hypothesis 1)	$\downarrow \left.\frac{\text{FRF}_{18\text{Hz}}}{\Delta\text{f}}\right\vert_{\text{f=18Hz}} \overset{dry}{\Longrightarrow} \uparrow F_i$

This relationship has been best demonstrated in the results of Test Setup 1 using Hypothesis 1 with a correlation of -0.944.

8.12 Conclusions

An experimental study was conducted to establish correlations between ballast stiffness when excited by a modally tuned instrumented hammer, using the Frequency Response Function (FRF) method.

The strongest mobility correlation was exhibited when the ballast was impacted and the ballast vibration measured. This is unsurprising, as one would expect the best results with the simpler single degree of freedom model: Hit Ballast, Measure Ballast

This measurement of mobility correlated with the ballast fouling index with a coefficient of -0.944.

Through the measurement of mobility to determine comparative levels of ballast fouling, stiffness was related to ballast fouling in an absolute context.

It is recognised that different fouling agents, different moisture conditions, and even different ballast aggregate void structures would yield different ballast mobility values.

It is considered that this FRF impulse response method is a useful additional, low cost, rapid tool for use by the railway industry – for at best quantitative decisions and at a minimum as a comparative tool for investigating adjacent areas of ballast for fouling.

A peer-reviewed paper of this research can be seen in Appendix 11 (De Bold et al., 2010b).

CHAPTER 9 DYNAMIC TRACK MODULUS FROM GPR

9.1 Railroad Track Modulus Estimation at TTCI, Pueblo, CO, USA

Previous experimental research in the field of statistical analysis of radar data from railway tracks was undertaken Dr Ram Narayanan of Pennsylvania State University (PSU) (Narayanan et al., 1999) (Narayanan et al., 2002) (Narayanan et al., 2004).

The research investigated the use of numerically correlating measured stiffness of railway ballast with the weighted average of subsurface 400MHz GPR reflectivities (Narayanan et al., 2002). This was done by using multivariate linear regression of the time-domain radar scan data with stiffness measurements acquired by traditional intrusive means.

The rationale for using GPR images to estimate track modulus was based on the supposition that GPR responses can be related directly to the formation and composition of the track substructure (e.g., layering characteristics, heterogeneities, material distribution, etc.), which can then be related directly to the strength of that track substructure, and, therefore, the track modulus. Thus, it was hypothesised that track modulus can be inferred indirectly from analysis of GPR responses.

The GPR data was collected on controlled tracks at the Transportation Technology Center, Inc., (TTCI) in Pueblo, Colorado, USA. The formation was universally silty sand, but the trackbeds tested varied radically in their layer composition over their lengths: -

- 10cm subballast and 30cm ballast separated by 10cm asphalt;
- 10cm subballast and 20cm ballast separated by 20cm asphalt;
- 15cm subballast and 30cm ballast separated by 20cm Geocell;
- 15cm subballast and 30cm ballast separated by 20cm asphalt;
- 15cm subballast and 20cm ballast separated by 30cm concrete slab; and,
- 15cm subballast below 50cm ballast.

The GPR system used was the GSSI SIR-10B (the same as used by Gallagher, 1999, at the University of Edinburgh) with monostatic dipole antennas with a front-to-back beam extent of 90 degrees, and a side-to-side beam extent of 60 degrees. A cart was used that was capable of being pulled behind a hi-rail vehicle along the railway track.

The railway track was tested to determine the track modulus at numerous locations, with values ranging from 13.7MPa to 34.4MPa. The GPR images of the locations featuring high and low values of track modulus were extracted.

It was established from numerous field measurements, that track modulus values of less than 13.7MPa indicate poor performance, 13.7MPa to 27.5MPa indicate average performance, and values greater than 27.5MPa indicate good performance (Ahlf, 1975).

Noticeable differences between high and low modulus images were observed. The high track modulus GPR images showed many "bright bands", or high amplitude signals, indicative of strong reflections from distinct layers. The low track modulus GPR images did not have such "bright bands" and showed greater heterogeneity – it was conjected that this was due to material migration between layers.

The GPR data consisted of vertical scans composed of 512 voltage sample values. Each voltage sample was representative of a reflectivity at a different depth. Thus, a known track modulus value could be analysed against an array of numerical values descriptive of the physical cross-section at that location.

Given that there were several track modulus records that could each be analysed against an array of numerical values, multivariate linear regression was used to determine if a relationship existed. A numerical model (Equation 9.1) was created that stated that a vector $[Y]$ containing the track modulus at locations $1, 2, \dots m$, could be equated to a matrix $[X]$, which contained the GPR reflectivities at different depths $1, 2, \dots n$ and at locations $1, 2, \dots m$, multiplied by an unknown vector $[b]$, which, when solved, would relate the GPR reflectivities at each location to the track modulus: -

$$\begin{bmatrix} Y_1 \\ Y_2 \\ \vdots \\ Y_m \end{bmatrix} = \begin{bmatrix} X_{11} & \cdots & X_{1n} \\ X_{21} & \cdots & X_{2n} \\ \vdots & \ddots & \vdots \\ X_{m1} & \cdots & X_{mn} \end{bmatrix} \begin{bmatrix} b_1 \\ b_2 \\ \vdots \\ b_n \end{bmatrix} \qquad \textbf{Equation 9.1}$$

Only 11 (of the available 512) n-values were used in the calculation. At 400MHz, this was enough to cover 220cm depth penetration, which was significantly greater than the maximum 65cm of ballast and subballast used in the experiment. It was stated that this was necessary because the formation played a significant role in determining the track modulus and, therefore, had to be included in the calculation. 13 locations had been included in the track modulus measurements; therefore, there were 13 m-values.

Where the [b]-vector was derived from a set of track modulus values and GPR responses, and then used to re-calculate the track modulus values from those same GPR values, the plotted relationship between the measured (i.e., actual) modulus and the computed (i.e., modelled) track modulus was within ±3.4MPa from the 1:1 line, which was stated to be within acceptable errors for modulus estimation. This is a case where the testing and the training data sets were the same (Figure 9.1).

Where the [b]-vector was derived from a set of track modulus values and GPR responses, and then used to re-calculate the track modulus values from a different set of GPR values on the track, the results were not so encouraging (Figure 9.2).

It is considered that the above work has certain limitations: -

1. The tests were conducted in desert conditions devoid of moisture content.
2. The method worked best where the data set for the training data sets were the same – where the model is calibrated to confirm and recalculate the original results.
3. Using GPR data to a depth of 220cm, whereby responses from the formation layer would be two-thirds of the numerical model's data, seemed arbitrary.
4. There is no theoretical justification for the methods of the model in determining the track modulus.
5. The radar waveforms used were only composed of 11 points (sample values); therefore, the resolution of the data is questionable.

On the positive side: -

6. The high track modulus GPR images show many bright bands indicating strong reflections from various distinct layers. The low track modulus GPR images are much darker in intensity, and show more heterogeneity probably on account of material migration between layers.
7. Given the ability of GPR to detect layering, high track modulus areas show strong layering, and low track modulus areas show weak layering – thus, one can convert this into an empirical relationship with some degree of accuracy.

This research is an interesting concept that has not been adopted by the international community of practitioners – perhaps partly because of the complexity of the analysis and lack of research into the validity of the method.

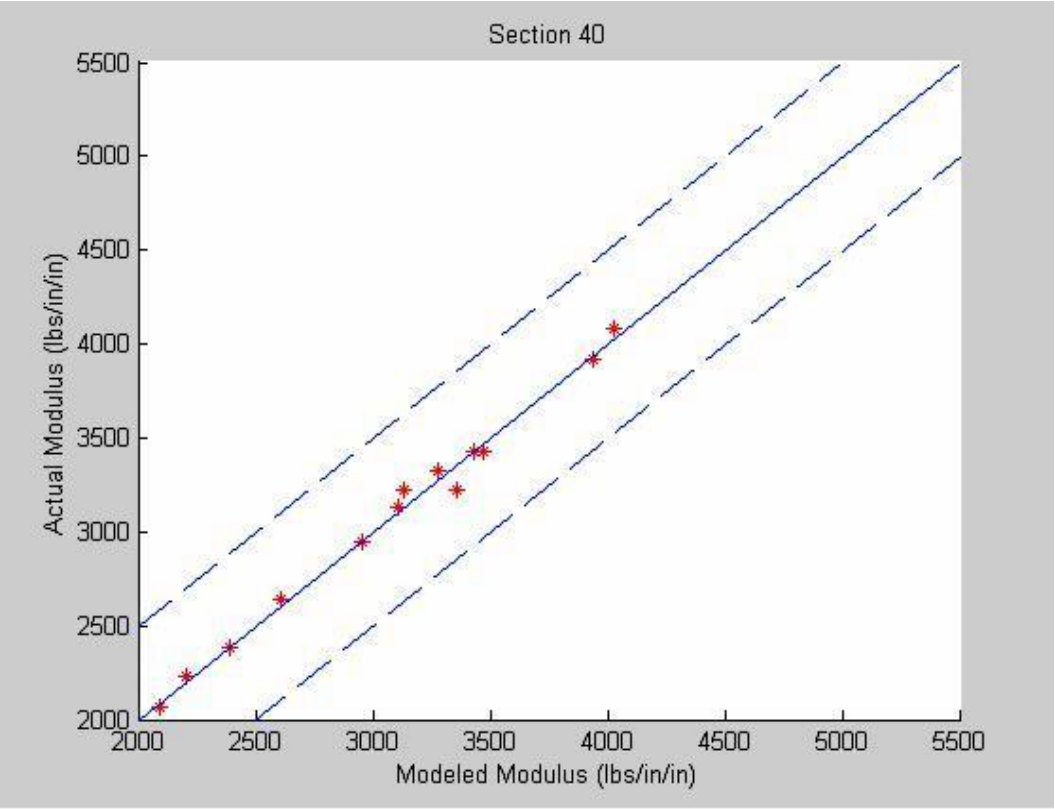

Figure 9.1 Modulus results with same testing and training sets (Narayanan, 2002)

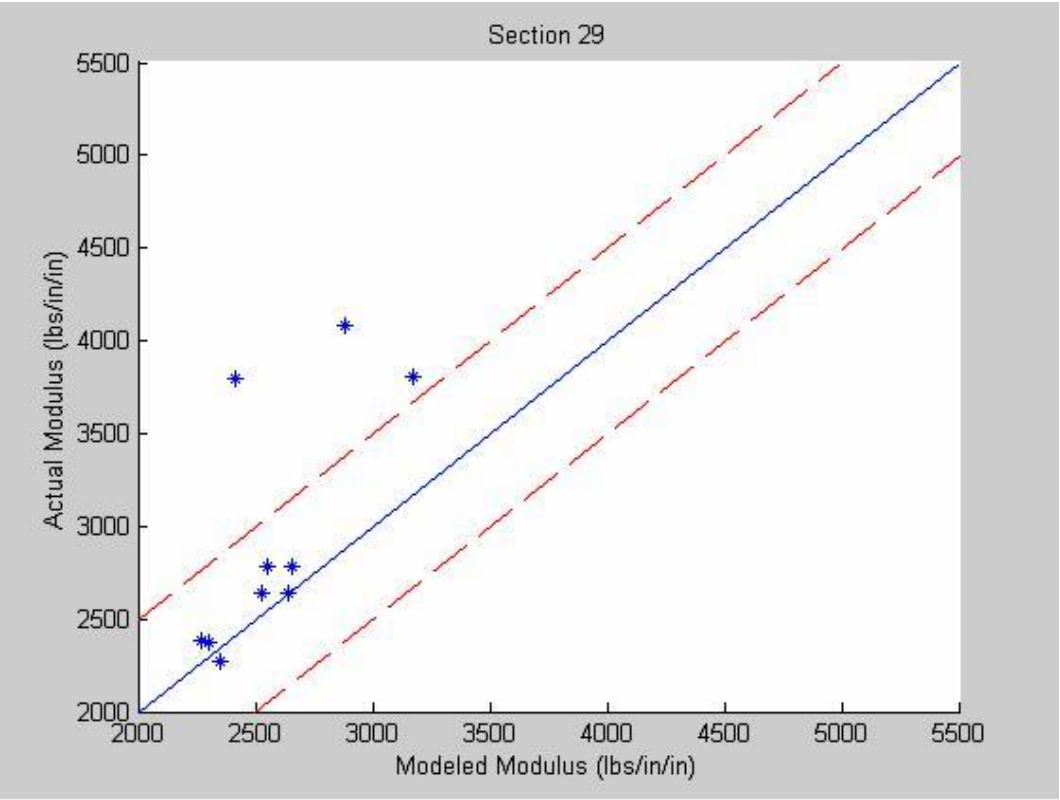

Figure 9.2 Different testing and training sets modulus results (Narayanan, 2002)

9.2 Banverket Data Analysis

Through contacts at Roadscanners, Oy, Tampere, Finland, and Banverket (Swedish National Rail Administration), approximately 300km of railway track stiffness and GSSI radar data was provided from a study of the Gävle-Sundsvall line. The stiffness data was collected using a new Rolling Stiffness Measurement Vehicle (RSMV) built by Banverket that can continuously measure vertical track stiffness.

The measurement principle for the RSMV was based on two oscillating masses used to excite the track dynamically via an ordinary wheel axle and the track stiffness was calculated from the measured axle forces accelerations (Berggren, 2005). The stiffness results were given as a magnitude and a phase variance, or phase delay. The phase delay is stated as a measure of how long it takes for the track to respond to the applied load. The phase delay can be viewed as a measure of the damping in the system (Berggren, 2005).

The frequencies of the oscillating masses were chosen to provide an appropriate spatial resolution (the minimum spatial resolution is twice the length of one period of excitation), avoid sleeper-passing frequencies and vehicle resonances, and chosen with an understanding of what the frequencies will reveal. Frequencies of 6.8Hz and 11.4Hz were used, and, thus, four data sets were generated (magnitude and phase variance values for each frequency). The stiffness data was recorded at 0.5m intervals.

A 400MHz GSSI horn antenna was located 28m behind the RSMV and approximately 10 scans per metre were taken at 512 samples per scan to a depth of 84ns. Each sample was a numerical voltage value that corresponded to a radar response from a specific depth of the scan. Banverket interpreted this data to determine the layer separation of the subsurface material (usually one, two, or three layers). The Banverket research indicated that there was not an apparent relationship between layer thicknesses and stiffness responses (Berggren, 2005).

For this research, in several experiments, the multivariate regression method used in the TTCI research (Narayanan et al., 2002) was used to compare the radar response data with the stiffness data.; although, a vastly greater quantity of data was analysed than the TTCI research, as is noted below.

For a stretch of the Banverket track data (114,530m to 121,222m), 67,039 radar scans were imported into mathematical analysis software (MatLab), and each scan was given an appropriate chainage value. Similarly, the 13,296 increments of stiffness data ("6.8Hz magnitude", "6.8Hz phase", "11.4Hz magnitude", and "11.4Hz phase" data) were imported over the same length of track with chainage values.

A function was used to interpolate the stiffness data to associate each radar scan with a stiffness value at its location. Consequently, four vectors of data were created for the length of the track investigated that associated one of the four stiffness parameters, "6.8Hz magnitude", "6.8Hz phase", "11.4Hz magnitude", and "11.4Hz phase", with a matrix of the corresponding 512 radar samples.

Given that the stiffness data started and finished at slightly different locations, i.e., offset by 28m, the radar data was cropped slightly at the start and finish, which reduced it to 66,487 scans. There were a similar number of stiffness values for each stiffness parameter. Thus, a known stiffness value could be analysed against an array of numerical values descriptive of the physical cross-section at that location in the 66,487-by-512 radar samples matrix.

A numerical model, as per Equation 9.1, was created that stated that a vector $[Y]$, containing one of the four track stiffness vectors (66,487 values) at locations $1, 2, \dots m$ (66,487 values), could be equated to a matrix $[X]$, containing the GPR reflectivities at depths $1, 2, \dots n$ (the 512 samples) and at locations $1, 2, \dots m$ (66,487 values), multiplied by an unknown vector $[b]$ (512 values), which, when solved, would relate the GPR reflectivities at each location to the track modulus.

Where the $[b]$-vector was derived for each of the four sets of stiffness values with the GPR responses, it was used to re-calculate the track modulus values from those same GPR values. The plotted relationship between the measured (i.e., "Real") stiffness and the computed (i.e., "Modelled") stiffness values was plotted and the correlation between the two was calculated (Appendix 7).

The degree of correlation between the Real and Modelled values for the 11.4Hz magnitude data was 0.6376 (as seen in Figure 9.3 and Table 9.1 under "All").

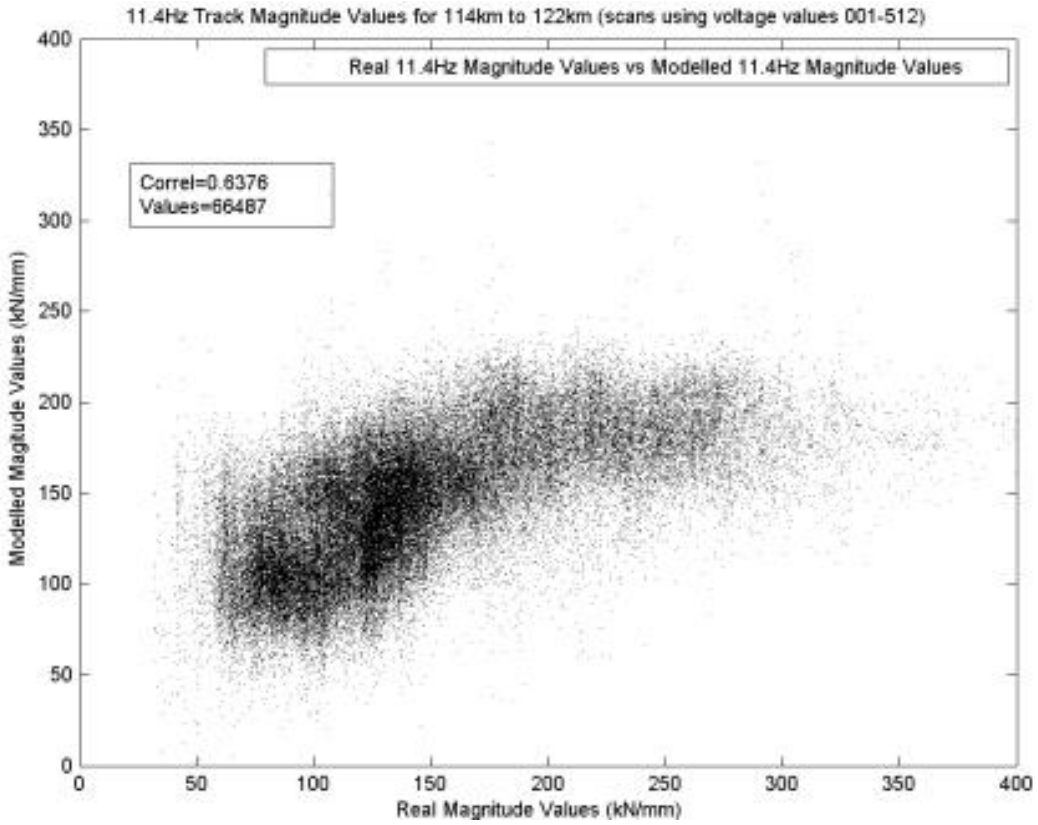

Figure 9.3 11.4Hz magnitude values for 114km to 122km

This method essentially analyses 7km of track consisting of 66,487 data points and creates a model from which any individual radar scan can be interpreted to produce a stiffness value with a correlation coefficient of 0.6376.

If there was a perfect correlation between the Real and Modelled values, the above graph would plot all the results as a 45° line. However, there is a large scatter of data as discussed below.

This work essentially repeats the Pueblo, Colorado, work but in those experiments only 11 (of the available 512) n-values were used in the calculation, and 13 locations had been included in the track modulus (stiffness) measurements; therefore, there were only 13 m-values.

9.3 Reduced Depth Analysis

It was theorised that not all the samples per scan were necessary to establish the correlation and that the near surface sample values from the radar scans contain the majority of the information that enables the correlation to be determined by the

multivariate regression method. To investigate this, the regression analysis was repeated several times. For each analysis, only certain ranges of near surface radar samples or lower samples were used. The results can be seen in the Table 9.1.

Track 114km to 122km											
	Near Surface Samples Per Scan					All	Lower Samples Per Scan				
Samples Used	1-032	1-064	1-128	1-256	1-384	1-512	33-512	65-512	129-512	257-512	385-512
11.4kHz Magnitude	0.320	0.578	0.610	0.625	0.635	0.638	0.621	0.552	0.492	0.381	0.142
11.4kHz Phase	0.210	0.359	0.388	0.422	0.435	0.439	0.403	0.344	0.276	0.194	0.091
6.8kHz Magnitude	0.314	0.556	0.577	0.590	0.596	0.598	0.582	0.519	0.459	0.335	0.125
6.8kHz Phase	0.130	0.251	0.324	0.354	0.364	0.368	0.364	0.333	0.270	0.168	0.069

Table 9.1 Measured to modelled stiffness correlation depending on samples used

Charts of the correlation results can be seen in Appendix 8, where all samples are used, and Appendix 9, where not all samples are used.

As can be seen, if only the near surface 128 sample values of each scan are used ("1-128"), very similar correlation values are achieved to using all 512 samples for each scan. When cropping samples from near surface responses and only retaining the lower values, the correlation quickly drops away. Thus, it can be assumed that the data containing the correlation relationship is mostly in the first 128 sample values of the radar responses. A graph of these relationships can be seen in Figure 9.4 and Figure 9.5.

If the data containing the stiffness correlation relationship is mostly in the first 128 sample values of the radar responses, then the 128 sample values represents a radar depth penetration of 21ns because the 512 samples values were over a stated depth penetration of 84ns. Therefore, it is hypothesised that the results could have been better if the depth penetration data to 21ns had been spread over the 512 sample values rather than the 128 sample values. That is, the subsequent 384 sample values containing the radar response down to 84ns bore no additional stiffness information yet squeezed the useful 21ns of information into 128 sample values where the quality of the waveform would have likely been better had it been recorded over 512 sample values.

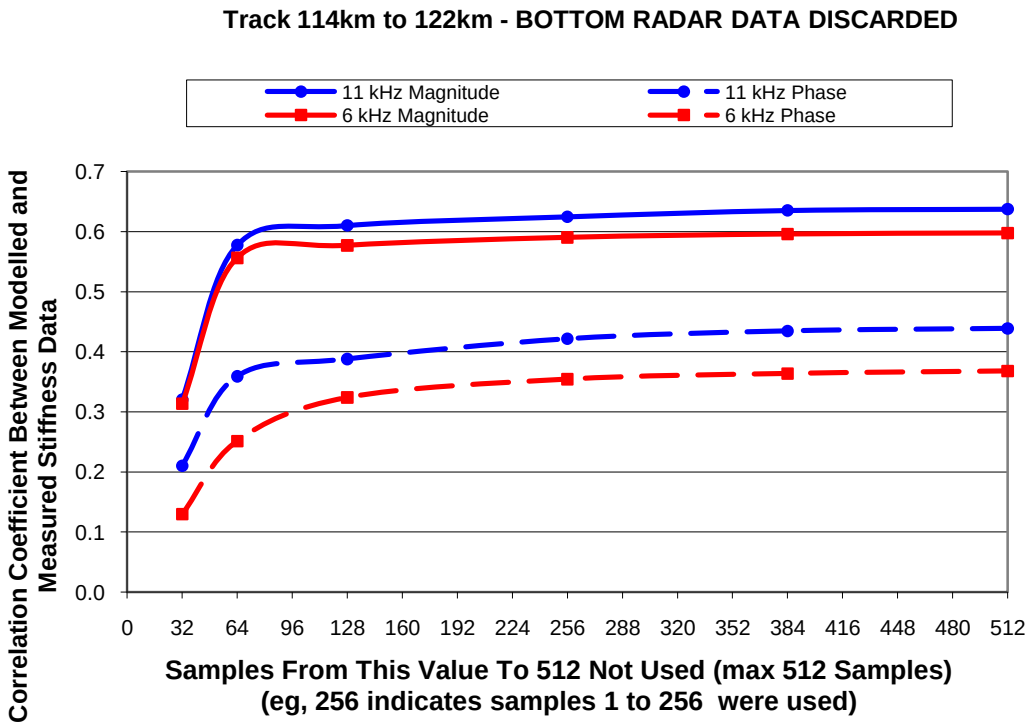

Figure 9.4 Measured to modelled stiffness data correlation – bottom data discarded

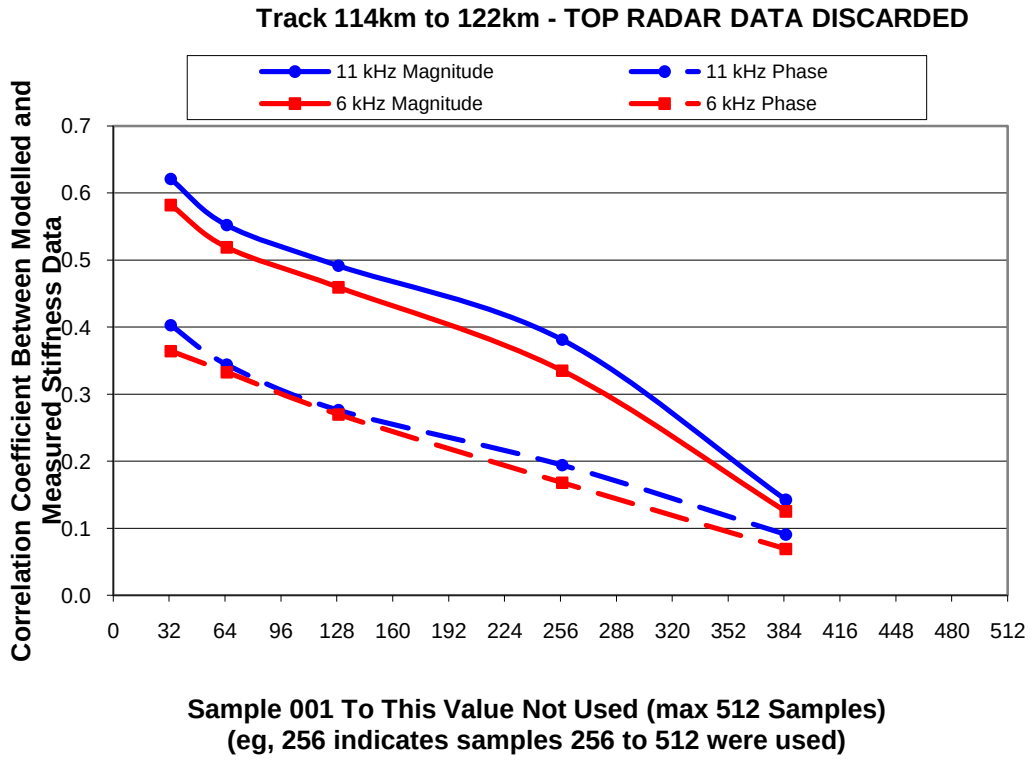

Figure 9.5 Measured to modelled stiffness data correlation – top data discarded

9.4 Reduced Length Analysis

In an attempt to improve the accuracy of the multi-variate regression, a smaller area of track was selected (120,889m to 121,009m consisting of 1,262 radar scans). This area was selected from visual inspection of the radar scan data and deemed to be an area of apparent uniform layering characteristics (Figure 9.6).

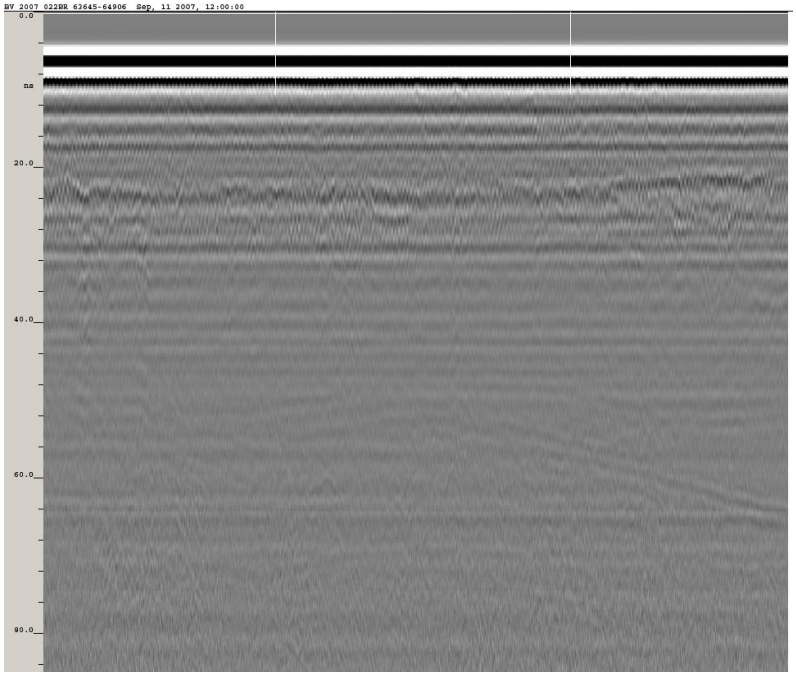

Figure 9.6 Banverket radar scan of 120.889km to 121.009km

The correlations between real and modelled data was greatly improved (Table 9.2).

Samples	1-512
11.4kHz Magnitude	0.914
11.4kHz Phase	0.870
6.8kHz Magnitude	0.858
6.8kHz Phase	0.836

Table 9.2 Banverket radar scan of 120.889km to 121.009km correlation values

The degree of correlation between the Real and Modelled values for the 11.4Hz magnitude data between 120.889km to 121.009km, can be seen in Figure 9.7.

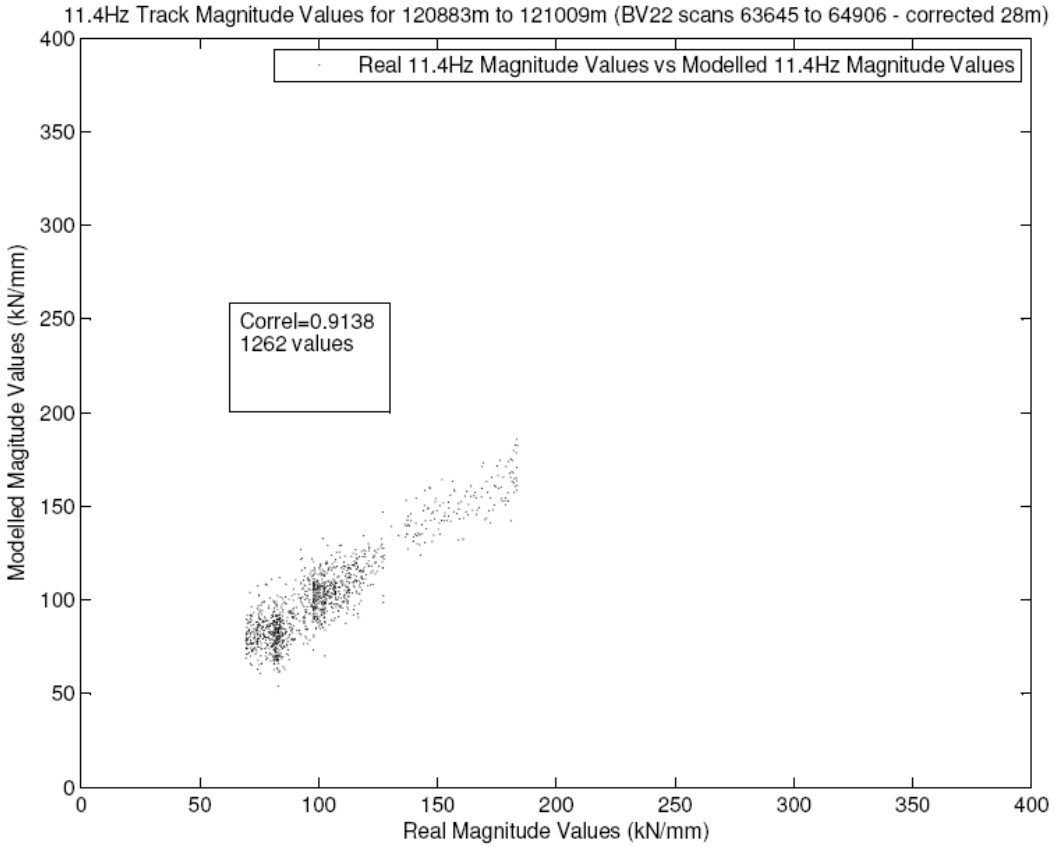

Figure 9.7 11.4Hz magnitude values for 120.889km to 121.009km

Charts of the correlation results can be seen in Appendix 10.

Thus, it can be seen that more accurate correlation results can be achieved if the model is used to evaluate more homogenous lengths of track.

9.5 Multiple Lengths Analysis

In order to determine whether this method can determine track stiffness values with a model developed on one length of track and applied to another, numerous models were created on the basis of average stiffness. Twelve different 80m lengths of track were isolated. Each section of track was selected on the basis of the average 11Hz Magnitude stiffness value. A table of the chainages and average stiffnesses for each length of track can be seen in Table 9.3.

The length of 80m was chosen as it was the longest track length where three track lengths of the three stiffness values could be found; at longer lengths, sections with overall averages of 120kN/mm or 240kN/mm could not be found.

Designation	Average Stiffness (kN/mm)	Start Chainage (m)	End Chainage (m)
120a	119.90	239776.5	239856.0
120b	120.03	240043.5	240123.0
120c	120.24	246523.5	246603.0
160a	159.78	239944.5	240024.0
160b	159.59	240313.5	240393.0
160c	159.94	242528.5	242608.0
200a	199.62	240173.5	240253.0
200b	199.77	241618.0	241697.5
200c	199.92	242093.0	242172.5
240a	240.07	242747.5	242827.0
240b	239.73	243046.0	243125.5
240c	240.14	243390.0	243469.5

Table 9.3 Selected track chainages

For each length of track, a model was produced that was then used to remodel the stiffness values from all the other lengths of track, including itself. The results of this are shown in Table 9.4. Where lengths of track are remodelled against their own data, they are highlighted orange. Where lengths are remodelled against data from equally stiff lengths, they are highlighted yellow.

A summary of the results is shown Table 9.5 where the average correlation with relation to the similarity or difference in stiffness values is calculated. It can be seen that where lengths of track are remodelled against themselves there is a very high degree of correlation. However, in general, there is no significant correlation between lengths of similar stiffness except when those stiffness values are high.

For example, for 120kN/mm lengths remodelled from other 120kN/mm lengths, the correlation coefficient value is -0.14, and for 120kN/mm lengths remodelled from 160kN/mm lengths, the correlation coefficient value is -0.16; whereas, for 200kN/mm lengths remodelled from other 200kN/mm lengths, the correlation coefficient value is 0.55, and for 240kN/mm lengths remodelled from 200kN/mm lengths, the correlation coefficient value is 0.59. Thus, it can be seen that models created from stiffer lengths of track are more accurate in determining the stiffness values of other stiffer lengths of track.

			80m stretches of track from which model is created											
			1	2	3	4	5	6	7	8	9	10	11	12
			120 kN/mm			160 kN/mm			200 kN/mm			240 kN/mm		
Remodelled 80m stretches of track	1	120 kN/mm	0.97	0.16	0.08	0.72	-0.01	0.40	0.20	0.18	0.06	0.10	0.03	0.02
	2		-0.77	0.96	-0.10	-0.76	-0.16	-0.68	-0.81	-0.55	-0.86	-0.74	-0.44	0.12
	3		-0.15	-0.07	0.97	-0.37	-0.06	-0.48	-0.54	-0.42	-0.48	-0.41	-0.55	0.00
	4	160 kN/mm	0.46	-0.15	0.16	0.99	0.05	0.41	0.33	0.39	-0.11	-0.11	-0.12	-0.08
	5		0.33	-0.15	0.04	0.53	0.92	0.64	0.38	0.40	0.11	0.09	0.14	0.01
	6		-0.18	0.12	0.19	0.40	-0.10	0.98	0.56	0.18	0.41	0.46	0.60	0.14
	7	200 kN/mm	0.22	-0.09	0.24	0.50	0.06	0.75	0.99	0.52	0.58	0.65	0.37	0.02
	8		0.52	-0.15	-0.02	0.67	0.20	0.68	0.53	0.97	0.21	0.18	0.12	0.03
	9		0.60	-0.03	-0.26	0.69	0.27	0.78	0.78	0.66	0.99	0.67	0.54	0.08
	10	240 kN/mm	0.40	-0.01	0.09	0.56	0.13	0.67	0.57	0.35	0.58	0.97	0.47	0.01
	11		0.32	-0.09	-0.11	0.64	0.11	0.80	0.75	0.59	0.72	0.73	0.96	0.08
	12		0.33	0.03	0.06	0.46	0.06	0.75	0.70	0.39	0.70	0.67	0.46	0.91

Table 9.4 Correlation values of real stiffness data and remodelled stiffness data

			Ave Correlation	
Own data		120kN/mm lengths remodelled with own data	0.97	0.96
		160kN/mm lengths remodelled with own data	0.96	
		200kN/mm lengths remodelled with own data	0.98	
		240kN/mm lengths remodelled with own data	0.95	
Similarly stiff stretch		120kN/mm lengths remodelled from other 120kN/mm lengths	-0.14	0.28
		160kN/mm lengths remodelled from other 160kN/mm lengths	0.32	
		200kN/mm lengths remodelled from other 200kN/mm lengths	0.55	
		240kN/mm lengths remodelled from other 240kN/mm lengths	0.40	
Stiffness difference (kN/mm)	40	120kN/mm lengths remodelled from 160kN/mm lengths	-0.16	0.27
		160kN/mm lengths remodelled from 120kN/mm lengths	0.09	
		160kN/mm lengths remodelled from 200kN/mm lengths	0.29	
		200kN/mm lengths remodelled from 160kN/mm lengths	0.51	
		200kN/mm lengths remodelled from 240kN/mm lengths	0.30	
		240kN/mm lengths remodelled from 200kN/mm lengths	0.59	
	80	120kN/mm lengths remodelled from 200kN/mm lengths	-0.36	0.09
		160kN/mm lengths remodelled from 240kN/mm lengths	0.13	
		200kN/mm lengths remodelled from 120kN/mm lengths	0.11	
		240kN/mm lengths remodelled from 160kN/mm lengths	0.47	
	120	120kN/mm lengths remodelled from 240kN/mm lengths	-0.21	-0.05
		240kN/mm lengths remodelled from 120kN/mm lengths	0.11	

Table 9.5 Summary of correlation values

9.6 Discussion

In terms of track stiffness calculations, the Banverket data was recorded to an unnecessary depth of 84ns. The useful stiffness correlation information was only found to a depth of 21ns. Using less than 21ns of data gave lesser results, and using more than 21ns of data did not give better results.

By collecting data to 84ns, this reduced the available sample values to record the 21ns of useful information to 128 sample values. Had the recording depth been set to 21ns, the useful information would have been collected over 512 sample values and the quality of the waveform would have likely been better, potentially giving better stiffness correlation results.

The 21ns of useful depth data corresponds with the results from Chapter 8, where the best results were achieved using the full-time range of data at 23ns with the 500MHz antenna; using less than 23ns gave lesser results. Therefore, it appears that using lower frequency antennas (400-500MHz) to determine or correlate trackbed stiffness that around 22ns of depth penetration provides the best results.

22ns of depth penetration corresponds to an actual depth range of 1.10-1.65m over a dielectric constant range of 4-9. Therefore, the useful stiffness information is derived from radar data that extends into the subballast and formation.

9.7 Conclusion

It was seen that more accurate correlation results can be achieved if the model is used to evaluate more homogenous areas of track.

Where multiple lengths of track were cross-correlated, models created from stiffer lengths of track are more accurate in determining the stiffness values of other stiffer lengths of track. It may be that stiffer lengths of track share similar properties that are discernable to this process; whereas, less stiff areas of track do not.

The low correlations for lower stiffness data demonstrates that the technique may be useful as a first pass to identify low stiffness areas of track. Where high stiffness is predicted there would be less urgency to investigate that track further.

CHAPTER 10 CONCLUSIONS

10.1 Original Objectives

The original research objectives were successfully achieved: -

- In Chapter 2 University of Edinburgh Railway, the condition of the ballast of the University of Edinburgh railway track was investigated.
- In Chapter 3 Ground Penetrating Radar, a way to take forward the previous University of Edinburgh research was determined.
- In Chapter 4 GPR Testing, the techniques of using GPR to fingerprint ballast was validated.
- In Chapter 5 GPR Analysis, new metrics were developed to determine ballast condition.
- In Chapter 6 Mini Falling Weight Deflectometer, the viability of using the Prima 100 mini-FWD on railways to measure stiffness was determined.
- In Chapter 7 Impulse Response, the applicability of impulse response techniques on railways was determined.
- In Chapter 8 Impulse Response Analysis, a method to evaluate ballast condition was developed using an instrumented hammer and geophone.
- In Chapter 9 Dynamic Track Modulus From GPR, from the Roadscanners data of the Banverket track, a method to relate radar responses to stiffness measurements was developed.

10.2 Overall Conclusions

The overall conclusions are: -

1. The need for a ballast fingerprinting system has been demonstrated.
2. The history of both stress wave and electromagnetic NDT methods for ballast characterisation were investigated
3. In the GPR analysis, a 500MHz antenna in the parallel orientation gave the best correlation (0.92) between Ionescu FI and scan area.
4. It was concluded that a simple single degree of freedom model was appropriate where the ballast is excited and response measured on the ballast

5. In the impulse response analysis, where the ballast was impacted and the response of the ballast measured using the gradient of 0-18Hz hypothesis, a correlation coefficient of -0.944 was found between the FRF and the Ionescu FI.
6. In the dynamic track modulus from GPR analysis, where multiple lengths of track were used to create multiple models, models created from stiffer lengths of track are more accurate in determining the stiffness values of other stiffer lengths of track. This could be used in order to identify low stiffness lengths.
7. The optimal depth for analysing railway track stiffness is 22ns or 1.10-1.65m.

10.3 Introduction Conclusions

In Chapter 1, it was found that there was significant demand for increased freight and passenger travel on the world's railways. A UK Department of Statistics publication showed that UK rail usage has increased since 1994/5 to 2008/9, from 28.7 to 50.7 billion passenger-kilometres. A similar trend was seen in the US where, from 1994/5 to 2008/9, freight haulage has increased from 1,201 to 1,777 billion ton-miles. These increases in freight and passenger rail travel have driven demand for more efficient and rapid investigation of trackbed ballast.

An assessment of current railway maintenance showed that track ballast deteriorates over time where ballast particles become rounded and fouling material accumulates in the void structure; and that such deteriorated ballast is defined as "spent" and fails to provide the drainage and mechanical functions required.

It was established that industry requires a method of track ballast evaluation that is non-intrusive, cheap, can appraise long stretches of track in a short period of time, and give a fingerprinting result from which time-to-maintenance can be calculated and planned, and, therefore, the objective of the research was to investigate and develop such a method.

Following a re-appraisal of University of Edinburgh research on the electrical permittivity of railway ballast and an appraisal of international work on the use of ground penetrating radar (GPR) on railway ballast – a series of large scale experiments were designed. In order to avoid boundary effects, field experiments were undertaken on the University of Edinburgh's 10m-long full-scale railway track, where previous research with ground penetrating radar (GPR) at the University could be re-evaluated

and technically extended. A key feature of the full-scale testing was the absence of boundary effects encountered in laboratory experiments.

The use of a mini falling weight deflectometer was investigated, along with the development of a new method using a frequency response function generated by a 12lb instrumented hammer and measured by a geophone.

Finally, a statistical analysis was conducted of a large amount of railway track radar and stiffness data made available from Banverket, Sweden and Road Scanners Oy, Tampere, Finland.

10.4 University of Edinburgh Railway Track Conclusions

In Chapter 2, the Fouling Index (FI) of the 10-year-old University of Edinburgh railway track was analysed through particle size distribution tests. The Selig & Waters FI analysis method was evaluated alongside the Ionescu method. It was concluded that the Ionescu method was more appropriate to the UK as UK ballast is similar to the Australian ballast used to develop the Ionescu method. The Ionescu method provided a numerical indication of track fouling condition and showed that there was a gradation from clean ballast to fouled ballast along the track length.

10.5 Ground Penetrating Radar Conclusions

In Chapter 3, the history, theory, and application of ground penetrating radar were discussed, with the previous research at the University of Edinburgh being presented. It was found that although the previous research focused on categorising the condition of track ballast using the relative electrical permittivities or dielectric constants. There had been no attempt other than visually to analyse further the waveform of the GPR signal through the ballast.

The results of the field experiments, with no boundary effects, could be used to differentiate between clean and spent ballast through a visual inspection of the radar waveform; whereas analysis of the waveform in the laboratory experiments would be hampered by the presence of the edge effects in a contained laboratory experiment.

In Chapter 4, it was shown that waveform analysis undertaken at the TTCI in Pueblo, Colorado, relied on assessing the envelope of the GPR waveform amplitude and relating

that to changes in the ballast condition through empirically derived calibrations. It was not a true numerical analysis of the GPR waveform.

In Chapter 5, three metrics were developed to analyse the GPR waveform in ballast: a calculation of the scan area, the number of axis crossings of a scan, and the number of inflection points of a scan. Five bowtie antennas (500MHz, 900MHz, 1GHz, 1.6GHz, and 2.6GHz) were used in the parallel and perpendicular orientation. The results for the several hundred or so scans associated with each crib were calculated and averaged.

It was found that using all the sample data for each scan (23ns for the 500MHz antenna) gave the most consistent results and strongest correlations.

For the axis crossings metric and the inflection points metric, with antennas of 900MHz or over, clean ballast featured more axis crossings or inflection points than the spent ballast; below 900MHz, this behaviour reversed.

There were no particularly strong correlations between fouling index and axis crossings; whereas, the 900MHz antenna in the parallel orientation gave the best correlation (-0.80) between Ionescu FI and inflection points.

For the scan area metric, the clean ballast had the smallest area with most antennas; the spent or mixed ballast had the largest areas. Using the scan area metric, the 500MHz antenna in the parallel orientation gave the best overall correlation coefficient (0.92) with the Ionescu FI.

10.6 Mini Falling Weight Deflectometer Conclusions

In Chapter 6, initial investigative work on the University of Edinburgh track, involved the use of a mini-FWD; a Prima100 6050, where all the sleepers and cribs were tested.

Each set of results for a sleeper gave fairly consistent results, but there was considerable variation between sets of results for different cribs that was suspected to be because the mini-FWD can only test a small localised area of the ballast surface at any time, which could vary significantly and give no indication as to the properties of the ballast as a whole.

The mini-FWD has poor performance on ballast and the device's fixed unitary form restricted its effectiveness in testing railway ballast and structure. However, the

technique of measuring impact forces and their response from a portable device was worth further investigation.

10.7 Impulse Response Conclusions

In Chapter 7, the history, theory, and application of impulse response techniques were discussed, with previous research at other universities and in industry presented. The characteristics of the frequency response function (FRF) generated by an impulse response test were discussed, and the three regions of the FRF were related to material properties of the test element.

Recurring 50Hz peaks in the response data was found to be due to voltage leakage when the test equipment was under mains power. This was resolved by running experiments under battery power.

Theories of rail-pad-sleeper-ballast-ground interaction were reviewed. It was concluded that a simple single degree of freedom model was appropriate where the ballast is excited and response measured on the ballast.

It was concluded with two hypothesis that stiffness can be related to the gradient of the initial line between 0-18Hz (the first peak) of the FRF; and that stiffness is related to average mobility between 18-50Hz (the "plateau" between the first peak and first drop in value) of the FRF.

To investigate the application of impulse response on railway ballast, an FRF was calculated for most cribs of the Edinburgh track.

In Chapter 8, in order to undertake such experiments, a testing procedure was developed. It featured an instrumented 12lb (5.44kg) impulse hammer with built-in load cell that was used to impact various components of the railway track where the vibration response of those or other railway track components were measured with a transducer. In the final experiments, the hammer used a plastic tip and the transducer was a low-frequency geophone. The signals from the hammer and transducer were recorded and analysed in-field on a laptop PC to create the FRFs.

The best correlation between the FRF and the Ionescu FI method was observed when the ballast was impacted and the response of the ballast measured using the gradient of 0-18Hz hypothesis. This produced a correlation coefficient of -0.944.

It is considered that this FRF impulse response method is a useful additional, low cost, rapid tool for use by the railway industry – for at best quantitative decisions and at a minimum as a comparative tool for investigating adjacent areas of ballast for fouling.

10.8 Dynamic Track Modulus from GPR Conclusion

In Chapter 9, a statistical analysis of GPR and stiffness data undertaken at TTCI, Pueblo, Colorado, using a 400MHz antenna was reviewed. Eleven radar samples per scan from 13 scans of 13 locations were analysed against 13 stiffness values from those 13 locations using multi-variate linear regression mathematics. This produced a numerical model that could re-calculate the stiffness values solely from the 11 samples per scan.

This technique was repeated with GPR (400MHz antenna) and stiffness data supplied by Banverket, Sweden and Road Scanner Oy, Tampere, Finland. However, 66,487 radar scans were provided along with 13,296 increments of stiffness data consisting of phase and magnitude readings taken from an oscillating mass at 6.8Hz or 11.4Hz, thus giving four stiffness data sets. This created a data pool far in excess of that analysed by TTCI.

Using the entirety of the data, any stiffness value at a location could be recalculated from the GPR scan data at that location with a correlation coefficient of 0.6376 using the 11.4Hz magnitude data.

The useful stiffness correlation information was only found to a depth represented by 21ns. The quality of the radar data may have been improved, in terms of stiffness calculations, had the recording been limited to this time scan or depth.

The 21ns of useful depth data corresponds with the 23ns used in Chapter 8 for best results. Therefore, when using lower frequency antennas (400-500MHz) to determine or correlate trackbed stiffness, 22ns of depth penetration may be optimal. 22ns of depth penetration corresponds to an actual depth range of 1.10-1.65m. Therefore, the useful stiffness information is derived from radar data that extends into the subballast and formation.

To investigate improvements to the accuracy of the multi-variate regression, a smaller (220m) length of track was selected consisting of 1,262 radar scans. This length was selected from visual inspection of the radar scan data to have apparent uniform

layering characteristics. Using this reduced length of track, any stiffness value at a location could be recalculated from the GPR scan data at that location with a correlation coefficient of 0.914 using the 11.4Hz magnitude data.

Where multiple lengths of track were used to create multiple models, models created from stiffer lengths of track are more accurate in determining the stiffness values of other stiffer lengths of track. This could be used to identify low stiffness lengths.

10.9 Research Impact

The original aim of this research was to develop evaluation methods for railway track ballast using non-destructive testing techniques.

As was related in Chapter 1 Introduction, railway ballast deterioration has significant cost implications for railway track operating companies; therefore, easily deployable ballast evaluation methods would offer significant cost savings.

At present, ballast is renewed after visual inspection and very often entire lengths of track are renewed without regard to localised conditions. With the development of easily deployable evaluation techniques, it would be quite feasible to develop an on-going, and constantly updated model of ballast condition throughout the network. This would allow for smaller stretches to be renewed on a needs basis.

The radar techniques potentially offers the exciting prospect of being able to attach a radar antenna to the underside of a standard train carriage whilst on normal commercial operations and for that antenna to monitor and assess ballast conditions. If successful, virtually every operating train could have such an antenna (with associated communications equipment) at low cost, giving the prospect of a network ballast condition model being updated hourly.

The impulse response technique may not offer the speedy, network-wide, assessment potential of radar, but it could be developed into a quick and simple on-site appraisal tool for operatives – conceivably to confirm the GPR findings when maintenance staff are deployed to investigate.

Similarly, the Dynamic Track Modulus from GPR work offers the potential of cross-correlating the GPR findings and the impulse response findings to further enhance any potential on-going ballast condition model.

10.10 Recommendations for Further Research

It is suggested that opportunities for future research could be: -

1. To investigate further the GPR analysis technique on operational track, noting changes in responses for known locations over time related to ballast fouling.
2. To develop further the impulse response technique to produce a hammer testing device that could give an immediate reading that is not dependent on post-experiment analysis.
3. To investigate the combination of the techniques developed in this thesis; that is, the GPR analysis, the mini-falling weight deflectometer, and the impulse response technique.
4. To investigate further the dynamic track modulus from GPR method with many more lengths of track and investigations to determine the cause of correlations between lengths of stiffer track.

REFERENCES

ACI 228.2R S2.2, 2011. Section 2.2 - Stress-wave methods for structures. In *Nondestructive Test Methods for Evaluation of Concrete in Structures - in press*.

ACI 228.2R S2.3, 2011. Section 2.3 - Stress-wave methods for deep foundations. In *Nondestructive Test Methods for Evaluation of Concrete in Structures - in press*.

ACI 228.2R S2.8, 2011. Section 2.8 - Radar. In *Nondestructive Test Methods for Evaluation of Concrete in Structures - in press*.

Ahlf, R., 1975. M/W costs: how they are affected by car weight and the track structure. *Railway Track & Structures*, 71(3), pp.34-37, 90-92.

Alexander, A.M. & Thornton, H.T.J., 1989. Ultrasonic Pitch-Catch and Pulse-Echo Measurements in Concrete. In H.S. Lew, ed. *Nondestructive Testing of Concrete, ACI SP-112*. Detroit, MI: American Concrete Institute. pp.21-40.

Al-Qadi, I., Xie, W. & Roberts, R., 2008. Scattering analysis of ground-penetrating radar data to quantify railroad. *NDT&E International*, 41, p.441– 447.

Annan, A.P., 2002. GPR - History, trends, and future developments. *Subsurface Sensing Technologies and Applications*, 3(4), pp.253-70.

Annan, A.P., 2008. Chapter 1 - Electromagnetic Principles of Ground Penetrating Radar. In H. Jol, ed. *Ground Penetrating Radar: Theory and Applications*. Elsevier Science & Technology Books.

Annan, A.P. & Davis, J.L., 1976. Impulse radar soundings in permafrost. *Radio Science*, 11, pp.383-94.

AREMA, 2003. *Practical Guide to Railway Engineering*. American Railway Engineering and Maintenance-of-Way Association.

Association of American Railroads, 2006. *Railroad Facts 2006*. Washington DC: Association of American Railroads.

Association of American Railroads, 2010. *Railroad Facts 2010*. Washington DC: Association of American Railroads.

ASTM C1740, 2010. *Standard Practice for Evaluating the Condition of Concrete Plates Using the Impulse-Response Method*.

ASTM C33, 2008. *Standard Specifications for Concrete Aggregates - Gradation 4*.

ASTM D5882, 2007. *Standard Test Method for Low Strain Impact Integrity Testing of Deep Foundations*.

ASTM D6913-04, 2009. *Standard Test Methods for Particle-Size Distribution (Gradation) of Soils Using Sieve Analysis*.

Bailey, J.T., Evans, S. & Robin, G.d.Q., 1964. Radio echo sounding of polar ice sheets. *Nature*, 204(4957), pp.420-21.

Balanis, C., 1989. *Advanced Engineering Electromagnetics*. New York: Wiley.

Bell, B., 2008. Network Rail Structures Engineer. *private communication*.

Bently, C.R., 1964. The structure of Antarctica and its ice cover. *Research in Geophysics, Volume 2: Solid Earth and Interface Phenomena*, p.335.

Berggren, E., 2005. ISSN 1651-7660 *Dynamic track stiffness measurement, A new tool for condition monitoring of track substructure*. Stockholm: KTH.

Berggren, E., 2009. *Railway Track Stiffness - Dynamic Measurements and Evaluation for Efficient Maintenance*. PhD thesis. Stockholm: KTH.

Bonnett, C.F., 2005. *Practical Railway Engineering*. Imperial College Press.

BR1203, 1988. *Ballast Specification (July 1985, amended May 1988)*. British Rail.

Bradfield, G. & Gatfield, E., 1964. Determining the Thickness of Concrete Pavements by Mechanical Waves: Directed Beam Method. *Magazine of Concrete Research*, 16(46, March), pp.49-53.

Brough, M., Stirling, A., Ghataora, G. & Madelin, K., 2003. Evaluation of railway trackbed and formation: a case study. *NDT&E International*, 36, p.145–156.

BS 1377-2, 1990. *Soils for civil engineering purposes - Part 2: Classification tests*. British Standards Institution.

BS 812-103.1, 1985. *Testing aggregates - Part 103: Methods for determination of particle size distribution - Section 103.1 Sieve tests*. British Standards Institution.

BS EN 13450, 2002. *Aggregates for railway ballast*. British Standards Institution.

Bungey, J.H. & Millard, S.G., 1993. Radar Inspection of Structures. *Proceedings of the Institution of Civil Engineers, Structures and Buildings Journal*, 99, May, pp.173-86.

Bungey, J.H. & Millard, S.G., 1995. Detecting Sub-surface Features in Concrete by Impulse Radar. *Nondestructive Testing and Evaluation*, 12, pp.33-51.

Bungey, J.H., Millard, S.G. & Grantham, M., 2006. *Testing of concrete in structures*. 4th ed. Oxford: Taylor & Francis.

Bungey, J.H., Millard, S.G. & Shaw, M.R., 1994. The influence of reinforcing steel on radar surveys of structural concrete. *Construction and Building Materials*, 8(2), pp.119-26.

Bungey, J.H., Millard, S.G. & Shaw, M.R., 1997. Radar assessment of post-tensioned concrete. In *Structural Faults & Repair 97*., 1997. Engineering Technics Press.

Cassidy, N., 2008. Introduction to GPR. In *Workshop at the 12th International Conference on Ground Penetrating Radar*. Birmingham, 2008.

Chan, H.F., 1987. *Non-Destructive Testing of Concrete Piles Using the Sonic Echo and Transient Shock Methods*. PhD thesis. Edinburgh: University of Edinburgh.

Clark, M., 2001. *Non-Destructive and Geotechnical Testing of Railway Track Bed Ballast*. PhD thesis. University of Edinburgh.

Clark, M.R. et al., 1998. Electromagnetic properties of railway ballast. In *Proceedings 1st International Railway Engineering Conference*. Brunel University, 1998. Engineering Technics Press.

Clark, M.R. et al., 2001. Electromagnetic properties of Railway Ballast. *NDT&E International*, 35, pp.83-85.

Clark, M.R., Gordon, M.O. & Forde, M.C., 2004. Issues over high-speed non-invasive monitoring of railway trackbed. *NDT&E International*, 37(2), pp.131-39.

Clark, M.R., Gordon, M.O., Giannopoulos, A. & Forde, M.C., 2003. Experimental and computer modelling of GPR to characterise trackbed ballast. In *Proceedings of World Congress of Railway Research, WCRR-2003, 28 Sept - 1 Oct 2003*. Edinburgh, CD-Rom, 2003.

Colombo, S. et al., 2005. Frequency Response of Different Couplant Materials for Mounting Transducers. *NDT&E International*, 38(3), pp.187-93.

Cook, J.C., 1973. Radar exploration through rock in advance of mining. *Trans. Society Mining Engineers, AIME*, 254, pp.140-46.

Coon, J.B., Fowler, J.C. & Schafers, C.J., 1981. Experimental uses of short pulse radar in coal seams. *Geophysics*, 46(8), pp.1163-68.

Corus, 2010. *Steel Sleepers*. [Online] Available at: http://www.corusgroup.com/en/products/rail_products_and_services/rail_products/sleepers/ [Accessed 23 August 2010].

Daniels, D.J., 2004. *Ground penetrating radar*. 2nd ed. London: The Institution of Electrical Engineers.

Daniels, D.J., Gunton, D.J. & Scott, H.F., 1988. Introduction to sub-surface radar. *Proceedings of Institution of Electrical Engineers*, August. pp.278-320.

Davidson, N.C. & Forde, M.C., 1996. A laboratory appraisal of ground-penetrating radar over water. *Nondestructive Testing and Evaluation*, 12(4), pp.219-42.

Davis, A.G., 1995. Nondestructive Evaluation of Existing Deep Foundations. *Journal of Performance of Constructed Facilities, ASCE*, 9(1, Feb), pp.57-74.

Davis, J.L. & Annan, A.P., 1986. Borehole Radar Sounding in CR-6, CR-7 and CR-8 at Chalk River, Ontario. *Technical Record TR-401, Atomic Energy of Canada Ltd*.

Davis, A.G., Carlton, A., Olson & Michols, K.A., 2001. Evaluation of historic reinforced concrete bridges. *ASCE news*, 26(11).

Davis, A.G. & Dunn, C.S., 1974. From Theory to Field Experience with the Non-Destructive Vibration Testing of Piles. *Proceedings of the Institution of Civil Engineers*, pp.571-93.

Davis, A.G. & Hertlein, B.H., 1987. Nondestructive Testing of Concrete Pavement Slabs and Floors with the Transient Dynamic Response Method. In *Proceedings International Conference on Structural Faults and Repair,*. London, July, Vol. 2, 1987.

Davis, A.G. & Hertlein, B.H., 1990. Assessment of Bridge Deck Repairs by a Nondestructive Technique. In Nowak, A.J., ed. *Proceeding of the NATO Advanced Research Workshop on Bridge Evaluation, Repair, and Rehabilitation*. Baltimore, Maryland, 1990. Kluwer Academic Publishers.

Davis, A.G. & Hertlein, B.H., 1995. Nondestructive Testing of Concrete Chimneys and Other Structures. In *Conference Nondestructive Evaluation of Aging Structures and Dams, Proceedings of SPIE 2457*. Oakland CA, June. , 1995.

Davis, A.G. & Hertlein, B.H., 1997. Evaluation of the Integrity of Some Large Concrete Foundations Using NDT. *ACI SP-168, Innovations in Nondestructive Testing of Concrete*, pp.333-356.

Davis, A.G., Hertlein, B.H., Lim, M.K. & Michols, K.A., 1996. Impact-Echo and Impulse Response Stress Wave Methods: Advantages and Limitations for the Evaluation of Highway Pavement Concrete Overlays. In *Conference Nondestructive Evaluation of Bridges and Highways, Proceedings of SPIE 2946*. Scottsdale AZ, December, 1996.

Davis, A.G. & Kennedy, J., 1998. Impulse Response Testing to Evaluate the Degree of Alkali-aggregate Reaction in Concrete Drilled-shaft Foundations for Electricity Transmission Towers. In *Conference Nondestructive Evaluation of Utilities and Pipelines II, Proc. SPIE 3398*. San Antonio, TX, April, 1998.

Davis, A.G., Lim, M.K. & Petersen, C.G., 2004. Rapid and economical evaluation of concrete tunnel linings with impulse response and impulse radar non-destructive methods. *NDT&E International*, 38(3), pp.181-86.

De Bold, R., Connolly, D., Patience, S. & Forde, M.C., 2010b. Using frequency response function testing to examine a railway trackbed. In *National Academies Transportation*

Research Board (TRB), Proc 89th Annual Meeting. Washington DC, USA, 10-14 January 2010, paper no. 10-3033, 2010b.

De Bold, R., Morrissey, J.P., O'Connor, G. & Forde, M.C., 2010a. New analysis of ground penetrating radar testing of a mixed railway trackbed. In *National Academies Transportation Research Board (TRB), Proc 89th Annual Meeting*. Washington DC, USA, 10-14 January 2010, paper no. 10-3142, 2010a.

de Man, A.P. & Esveld, C., 2001. Recording, estimating and managing the dynamic behaviour of railway structures. In *Proceedings of the International Seminar on Modal Analysis*., 2001.

Dolphin, L.T., Beatty, W.B. & Tanzi, J.D., 1978. Radar Probing of Victorio Peak, New Mexico. *Geophysics*, 43(7), pp.1441-48.

Drossaert, F.H., 2008. *Detection of Abandoned Mineshafts in the Proximity of Railways*. PhD thesis. University of Edinburgh.

Drossaert, F.H. et al., 2005. Void detection beneath the ballast using GPR and resistivity. In *Railway Engineering 2005*. London, 2005.

El Said, M., 1956. Geophysical prospection of underground water in the desert by means of electromagnetic interference fringes. *Proceedings of the IRE*, 44, pp.24-30.

Ender, J., 2002. *98 Years of the Radar Principle: The Inventor Christian Hülsmeyer*. EuroSAR.

Eriksen, A., Gascoyne, J. & Al-Nuaimy, W., 2004. Improved productivity and reliability of ballast inspection using road-rail multi-channel GPR. In *Railway Engineering 2004*. London, 2004.

Esveld, C., 2001. *Modern Railway Track*. Second Edition ed. MRT-Productions.

Eurailscout, 2009. *Eurailscout Inspection & Analysis b.v.* [Online] Available at: http://www.eurailscout.com [Accessed 25 January 2009].

Eurostat, 2007. *EU Transport in Figures - Statistical Pocketbook*. European Commission Directorate-General for Energy and Transport.

Ewins, D.J., 1984. *Modal testing: Theory and practice*. Research Studies Press.

Gallagher, G.P., 1999. *Investigation of Railway Trackbed Deterioration using Ground Penetrating Radar*. MSc Thesis. University of Edinburgh.

Gallagher, G.P., Leiper, Q., Clark, M. & Forde, M.C., 2000. Ballast Evaluation Using Ground Penetrating Radar. *Railway Gazette International*, February. pp.101-02.

Gallagher, G. et al., 1999. The application of time domain ground penetrating radar to evaluate railway track ballast. *NDT&E International*, 32(8), pp.463-68.

Giannopoulos, A., 1997. *The investigation of transmission-line matrix and finite-difference time-domain methods for the forward problem of ground probing radar*. DPhil Thesis. York, UK: University of York.

Goodwin, R. & Cassidy, N., 2008. GPR characteristics of magnetite-rich layered igneous bodies. In *Proceeding of the 12th International Conference on Ground Penetrating Radar*. Birmingham, 2008.

Grant, R.H., 2005. *GrantThe Railroad: The Life Story of a Technology*. Greenwood Press.

Halabe, U.B., Maser, K.R. & Kausel, E.A., 1995. Condition Assessment of Reinforced Concrete Structures Using Electromagnetic Waves. *ACI Materials Journal*, 92(5), pp.511-523.

Halabe, U.B., Sotoodehnia, A., Maser, K.R. & Kausel, E.A., 1993. Modeling the Electromagnetic Properties of Concrete. *ACI Materials Journal*, 90(6), pp.552-63.

Harsco Track Technologies, 2009. *On Track Machine – Stoneblower Operations*. [Online] Available at: http://www.httuk.com/otm.html [Accessed 25 January 2009].

Hay, W.W., 1982. *Railroad Engineering*. John Wiley and Sons.

Heisey, J.S., Stokoe, K.H.I. & Meyer, A.H., 1982. Moduli of Pavement Systems From Spectral Analysis of Surface Waves. *Transportation Research Record*, (853), pp.22-31.

Hertz, H.R., 1887. Ueber sehr schnelle electrische Schwingungen. *Annalen der Physik*, 267(7), pp.421-48.

Hertz, H.R., 1888a. Ueber die Ausbreitungsgeschwindigkeit der electrodynamischen Wirkungen. *Annalen der Physik*, 270(7), pp.551-69.

Hertz, H.R., 1888b. Ueber die Einwirkung einer geradlinigen electrischen Schwingung auf eine benachbarte Strombahn. *Annalen der Physik*, 270(5), pp.155-70.

Hoffmann, O.J.-M., Guzina, B.B. & Drescher, A., 2004. Stiffness Estimates Using Portable Deflectometers. *Transportation Research Record: Journal of the Transportation Research Board,* 1869, pp.59-66.

Holser, W.T. et al., 1972. Radar logging of a salt dome. *Geophysics*, 37, pp.889-906.

Hondawanderer, 2010. *Martin Loader's Railway Photography*. [Online] Available at: http://www.hondawanderer.com/Track_Machines.htm [Accessed 12 September 2010].

Hugenschmidt, J., 1999. Ballast inspection using ground penetrating radar. In *Proceedings of the Second International Conference on Railway Engineering*., 1999. Engineering Technics Press, London.

Hugenschmidt, J., 2000. Railway track inspection using GPR. *Journal of Applied Geophysics*, 43, pp.147-55.

Huille, J.-P., 1997. *Synthesis Report*. Paris: SNCF / Direction de l'Equipement European Research Project for Optimised Ballasted Tracks.

Hülsmeyer, C., 1904. German Patent no. DE165546 *Verfahren, um metallische Gegenstände mittels elektrischer Wellen einem Beobachter zu melden.* Dusseldorf. Patented on 30 April 1904.

Hunt, G.A., 2000. EUROBALT optimises ballasted track. *Railway Gazette International*.

Ionescu, D., 2004. Ballast degradation and measurement of ballast fouling. In *Proceedings of 7th International Railway Engineering Conference*. London, 2004. Engineering Technics Press.

Jack, R. & Jackson, P., 1998. Imaging attributes of railway track formation using ground probing radar (GPR). In *Proceedings of the First International Conference on*

Maintenance and Renewal of Permanent Way and Structures. London, 1998. Engineering Technics Press, Brunel University.

Jones, R., 1949. The Non-destructive Testing of Concrete. *Magazine of Concrete Research*, (2, June), pp.67-78.

Jones, C.J.C., 2010. *WA3 Noise and vibration*. Presentation. Track 21.

Jones, C.J.C. & Block, J.R., 1996. Prediction of ground vibration from freight trains. *Journal of Sound and Vibration*, 193(1), pp.205-13.

Kaewunruen, S. & Remennikov, A.M., 2005. Application of Experimental Modal Testing for Estimating Dynamic Properties of Structural Components. *University of Wollongong - Research Online*, Available at: http://ro.uow.edu.au/engpapers/283.

Kaewunruen, S. & Remennikov, A.M., 2007. Field Trials for Dynamic Characteristics of Railway Track and its Components Using Impact Excitation Technique. *NDT&E International*, 40, pp.510-19.

Kathage, A., Niessen, J., White, G. & Bell, N., 2005. Fast inspection of railway ballast by means of impulse GPR equipped with horn antennas. *Journal of Nondestructive Testing*, 10(9), p.1.

Kozlov, V.N., Samokutov, A.A. & Shevaldykin, V., 1997. Thickness Measurement and Flaw Detection in Concrete Using Ultrasonic Echo Method. *Nondestructive Testing and Evaluation*, 13, pp.73-84.

Lambe, T.W. & Whitman, R.V., 1979. *Soil Mechanics*. John Wiley and Sons.

Leslie, J.R. & Cheesman, W.J., 1949. An Ultrasonic Method of Studying Deterioration and Cracking in Concrete Structures. *Journal of the American Concrete Institute*, 21(1, September), pp.17-36.

Levy, J.F., 1970. Sonic Pulse Method of Testing Cast in Situ Piles. *Ground Engineering*, 3(3), pp.17-19.

Loizos, A., Boukovalas, G. & Karlaftis, A., 2003. Dynamic Stiffness Modulus for Pavement Subgrade Evaluation. *Journal of Transportation Engineering*, July-August, pp.434-43.

Löwy, H. & Leimbach, G., 1910. Eine elektrodynamische Methode zur Erforschung des Erdinneren. *Physikalische Zeitschrift*, 11, pp.697-705.

Marconi, G., 1896. British Patent No 12,039 *Improvements in Transmitting Electrical Impulses and Signals, and in Apparatus Therefor*.

Maser, K.R. & Roddis, W.M., 1990. Principles of Thermography and Radar for Bridge Deck Assessment. *Journal of Transportation Engineering (ASCE)*, Vol. 116(5), pp.583-601.

Maxwell, J.C., 1861. On Physical Lines of Force. *Philosophical Magazine*.

McCavitt, N., Yates, M.R. & Forde, M.C., 1992. Dynamic Stiffness Analysis of Concrete Paving Slabs. *Journal of Transport Engineering*, 118(4), pp.540-56.

McMichael, P. & McNaughton, A., 2003. The Stoneblower – Delivering The Promise. In *TRB Conference*., 2003.

Millard, S.G., Bungey, J.H. & Shaw, M., 1993. The Assessment of Concrete Quality Using Pulsed Radar Reflection and Transmission Techniques. In *Proceedings International Conference NDT in Civil Engineering, 14-16 April*. Liverpool, 1993. The British Institute of NDT.

Morey, R.M., 1974. Continuous subsurface profiling by impulse radar. In *Proceedings of Engineering Foundations Conference on Subsurface Exploration for Underground Excavations and Heavy Construction*. Henniker, New Hampshire, 1974.

Narayanan, R.M., Jakub, J.W., Elias, S.E.G. & Li, D., 2002. Railroad track modulus estimation using ground penetrating radar. In *Proceedings of 5th International Railway Engineering Conference 2002*. London, 4th-6th July 2002. Engineering Technics Press, UK.

Narayanan, R.M., Jakub, J.W., Li, D. & Elias, S.E.G., 2004. Railroad track modulus estimation using ground penetrating radar measurements. *NDT&E International*, 37(2), p.141–151.

Narayanan, R.N., Kumke, C.J. & Li, D., 1999. Railroad Track Monitoring Using Ground Penetrating Radar. *Simulation Study and Field Measurements*, 3752(243).

Network Rail, 2004. *Network Rail – Making a Fresh Start*. London: The Stationery Office Ordered by the House of Commons.

Network Rail, 2006. *Network Rail Business Plan 2006 – Delivering For Our Customers*.

Network Rail, 2008. *Fact & Figures: Equipment on the Network*. [Online] Available at: http://www.networkrailmediacentre.co.uk/Content/Detail.asp?ReleaseID=1850&NewsAreaID=22&SearchCategoryID=-1 [Accessed 2008 September 15].

Newland, D.E., 1989. *Mechanical vibration response and computation*. London, England: Longman Scientific & Technical.

Ogilvie, N. & Quante, F., 2001. *Innovative Track Systems - Criteria for their Selection*. Promain.

Olhoeft, G.R., 1975. *The electrical properties of permafrost*. PhD Thesis. University of Toronto.

Olhoeft, G.R., 1987. Electrical properties from 10−3 to 10+9 Hz—physics and chemistry. *Proceedings of the American Institute of Physics 2nd International Symposium on the Physics and Chemistry of Porous Media*, 154, pp.281-98.

Olhoeft, G.R., 1996. Application of Ground Penetrating Radar. In *Proceedings of the 6th International Conference on Ground Penetrating Radar, GPR'96*. Sendai, Japan, 1996.

Oostermeijer, K.H. & Kok, A.W.M., 2000. Dynamic Behaviour of Railway Superstructures. *HERON*, 45(1).

Ottosen, N.S., Ristinmaa, M. & Davis, A.G., 2004. Theoretical interpretation of impulse response tests of embedded concrete structures. *Journal of Engineering Mechanics*, p.1062.

Padaratz, I.J. & Forde, M.C., 1995. A theoretical evaluation of impulse radar wave propagation through concrete. *Journal of Non-destructive Testing & Evaluation*, 12, pp.9-32.

Padaratz, I.J., Hardy, M.S.A. & Forde, M.C., 1997. Coupling effects of radar antennae on concrete. In *Proceedings of 4th International Conference: NDT-CE*. University of Liverpool, 8-11 April, 1997.

Page, R.M., 1962. The Early History of RADAR. *Proceedings of the IRE (special 50th Anniversary Issue)*, 50(5).

Paquet, J., 1968. Vibration Study of Concrete Piles: Harmonic Response. *Annales de l'Institut technique du Bâtiment et des Travaux publics*, 245, pp.789-803.

Paquet, J., 1991. A New Method for Testing Integrity of Piles by Dynamic Impulse: The Impedance Log. *International Colloquium on Deep Foundations*, (March), pp.1-10.

Parker, S.P., 1997. *Dictionary of Engineering*. 5th ed. McGraw-Hill.

Pederson, C.M. & Senkowski, L.J., 1986. Slab Stabilization of PCC Pavements. In *Paper presented at TRB Annual Conference, Washington, DC, Transportation Research Record, No. 1083*. Washington DC, 1986. National Research Council, Washington DC.

Railway Technical, 2010. *Railway Technical Web Pages*. [Online] Available at: http://www.railway-technical.com/track.shtml [Accessed 3 August 2010].

Rasmussen, S. & De Man, A., 2000. Two new techniques for measurement of vertical track stiffness of railway tracks. In *3rd International Railway Engineering Conference*. London, 2000. Technics Press, UK.

Rausche, F., Likins, G. & Shen, R.K., 1992. Pile Integrity Testing and Analysis. In *Proceedings of the 4th International Conference on the Application of Stress-Wave Theory to Piles*. The Hague, 1992.

Roberts, R. et al., 2006b. Railroad Ballast Fouling Detection Using Ground Penetrating Radar – A New Approach Based on Scattering from Voids. In *Ninth European Conference on NDT*. Berlin, 2006b.

Roberts, R. et al., 2006a. Advances in Railroad Ballast Evaluation Using 2GHz Horn Antennas. In *11th International Conference on Ground Penetrating Radar*. Columbus, 2006a.

Roesset, J.M. et al., 1994. Impact of weight falling onto the ground. *Journal of Geotechnical Engineering*, 120(8), p.1394–1412.

Roesset, J.M. et al., 1996. Closure to "Impact of weight falling onto the ground". *Journal of Geotechnical Engineering*, 122(5), p.416–417.

Schoech, W., 2004. Track Maintenance and Rail Grinding - An Integrated Approach. In *International Railway Engineering Conference 2004*. London, 2004.

Schoech, W., 2005. Grinding Specific Profiles Helps Solving Rail Problems. In *International Railway Engineering Conference 2005*. London, 2005.

Schut, J.H., 2004. *They've Been Working on the Railroad*. [Online] Available at: http://www.ptonline.com/articles/200404fa3.html [Accessed 23 August 2010].

Selig, E.T. & Waters, J.M., 1994. *Track Geotechnology and Substructure Management*. Thomas Telford.

Sharpe, P., 2000. Trackbed investigation. *Journal and report of proceedings - Permanent Way Institution*, 118(3), pp.238-54.

Sharpe, P. & Collop, A.C., 1998. Trackbed investigation - a modern approach. In *Proceedings of the First International Conference on Railway Engineering*. London, 1998. Engineering Technics Press, Brunel University.

Shaw, M.R. et al., 1993. A Large Diameter Transmission Line for the Measurement of Relative Permittivity of Construction Materials. *British Journal of NDT*, 35(12), pp.696-704.

Sheng, X., Jones, C.J.C. & Petyt, M., 1999. Ground vibration generated by a harmonic load acting on a railway track. *Journal of Sound and Vibration*, 225(1), pp.3-28.

Sheng, X., Jones, C.J.C. & Thompson, D.J., 2004. A theoretical study on the influence of the track on train-induced ground vibration. *Journal of Sound and Vibration*, 272(3-5), pp.909-36.

Simmons, G. et al., 1973. Surface Electrical Properties Experiment, in Apollo 17. *Preliminary Science Report, Scientific and Technical Office, NASA*, pp.15-1 to 15-14.

Skolnik, M.I., 1980. *Introduction to Radar Systems*. New York: McGraw-Hill.

Solomon, B., 2001. *Railway Maintenance Equipment: The Men and Machines that Keep the Railroads Running*. MBI Publishing Company.

Steinbach, J. & Vey, E., 1975. Caisson Evaluation by Stress Wave Propagation Method. *Journal of Geotechnical Engineering (ASCE)*, 101(GT4, April), pp.361-78.

Steinway, W.J., Echard, J.D. & Luke, C.M., 1981. *Locating Voids Beneath Pavements Using Pulsed Electromagnetic Waves*. Washington, DC: National Research Council Transportation Research Board.

Stern, W., 1929. Versuch einer elektrodynamischen Dickenmessung von Gletschereis. *Ger. Beitr. zur Geophysik*, 23, pp.292-333.

Stern, W., 1930. Uber Grundlagen, Methodik und bisherige Ergebnisse elektrodynamischer Dickenmessung von Gletschereis. *Z. Gletscherkunde*, 15, pp.24-42.

Sussmann, T.R., 1999. *Application of Ground Penetrating Radar to Railway Track Substructure Maintenance Management*. PhD thesis. University of Massachusetts.

Thierbach, R., 1973. Electromagnetic reflections in salt deposits. *Journal of Geophysical Research*, 40, pp.633-37.

Thilakasiri, S., Mullins, G., Stinnette, P. & Gunaratne, M., 1996. Discussion of "Impact of weight falling onto the ground" by Roesset, et al. *Journal of Geotechnical Engineering*, 122(5), p.415–417.

UIC, 2010. *International Union of Railways – Railisa Database*. [Online] Available at: http://www.uic.org/spip.php?article1352 [Accessed 23 August 2010].

UK Department of Statistics, 2007. *Transport Trends: 2007 Edition - Section 3: Public Transport, Trend 3.4b - Distance travelled by National Rail passengers: 1980 to 2006/07*. [Online] Available at: http://www.dft.gov.uk/162259/162469/221412/190425/220778/trends2007 [Accessed 18 September 2008].

UK National Statistics, 2010. *Transport Trends: 2009 Edition*. Department for Transport.

Waite, A.H. & Schmidt, S.J., 1961. Gross errors in height indication from pulsed radar altimeters operating over thick ice or snow. *IRE International Convention Record, Part 5*, pp.38-54.

Walford, M.E.R., 1964. Radio echo sounding through an ice shelf. *Nature*, 204(4956), pp.317-19.

Walter, P.L., 2007. The History of the Accelerometer: 1920s-1996 – Prologue and Epilogue, 2006. *Sound and Vibration*, January. pp.84-92.

Ward, S.H. et al., 1973. Apollo lunar sounder experiment, in Apollo 17. *Prliminary Science Report, Scientific and Technical Office, NASA*, pp.22-1 to 22-26.

Westover, T.M., Labuz, J.F. & Guzina, B.B., 2007. *Resilient Modulus Development of Aggregate Base and Subbase Containing Recycled Bituminous and Concrete for 2002 Design Guide and Mn/Pave Pavement Design*. Minnesota: Minnesota Department of Transportation University of Minnesota.

Wikipedia, 2010. *Continuously welded rail*. [Online] Available at: http://en.wikipedia.org/wiki/Continuously_welded_rail [Accessed 3 August 2010].

Wikipedia, 2010. *Fishplate*. [Online] Available at: http://en.wikipedia.org/wiki/Fishplate [Accessed 3 August 2010].

Wikipedia, 2010. *Rail fastening system*. [Online] Available at: http://en.wikipedia.org/wiki/Rail_fastening_system [Accessed 3 August 2010].

Wikipedia, 2010. *Rail Tracks*. [Online] Available at: http://en.wikipedia.org/wiki/Rail_tracks [Accessed 2 August 2010].

Wood, G.S., 1994. *The Rolling Resistance of Articulated Dump Trucks on Haul Roads*. PhD thesis. Edinburgh: University of Edinburgh.

Woodward, P.K., Nicholl, G. & Zettor, B., 2004. Application of XiTRACK GeoComposite Technology to Bletchley Points on the West Coast Main Line. In *Proceedings of 7th International Conference on Railway Engineering*. London, 2004.

Xie, W., Al-Qadi, I., Jones, D. & Roberts, R., 2008. Development of a time-frequency approach to quantify railroad ballast fouling condition using UWB GPR data. In *TRB 87th Annual Meeting Compendium of Papers*. Washington DC, 2008.

Zarembski, A.M., 1987. Performance Characteristics for Concrete Tie Fasteners. *Rail International*, 18(3), pp.41-49.

Zarembski, A.M. & Newman, G.R., 2008. Comparative Technical and Economic Analysis Of Stoneblowing vs. Tamping. In *AREMA Conference*., 2008.

Zervos, A., 2011. *Ballast and Sleepers, Track 21 - Railway Track for the 21st Century*. [Online] Available at: http://www.track21.org.uk/ballast.htm [Accessed 16 April 2011].

APPENDIX 1 WORK PLAN

	Activity	2007	2008										2009												2010												2011											
			Year 1										Year 2												Year 3												Year 4											
		O	N	D	J	F	M	A	M	J	J	A	S	O	N	D	J	F	M	A	M	J	J	A	S	O	N	D	J	F	M	A	M	J	J	A	S	O	N	D	J	F	M	A	M	J	J	A	S
1	Identify and develop programme																																															
2	Preliminary field trials of UoE track																																															
3	Undertake literature search of publications																																															
4	Prepare state-of-the-art review paper																																															
5	Confirm access to 3rd party radar data																																															
6	Confirm collaborative working																																															
7	Apply for travel funding																																															
8	Refine field trial on UoE track																																															
9	Develop new objectives																																															
10	Search objectives within Innotrack web site																																															
11	Make contact with Networkrail and Carillion																																															
12	Co-author EPSRC proposal for funding																																															
13	Undertake Banverket-Roadscanners research																																															
14	Write up preliminary literature review																																															
15	Possible field trips																																															
16	Develop numerical modelling from data																																															
17	Refine GPR collection method																																															
18	Develop fines detection technique																																															
19	Refine FWD collection technique																																															
20	Develop FWD-GPR correlation technique																																															
21	Investigate continuous surface measurements																																															
22	Publication work																																															
23	Thesis write-up																																															
24	RA work																																															

NOW

The bar "NOW" denotes when the work plan was produced.

APPENDIX 2 PARTICLE SIZE DISTRIBUTION CHARTS

The University of Edinburgh

School of Engineering and Electronics

Determination of Particle Size Distribution | *BS 1377 : Part 2 : 1990 : Cl. 9.3*

Job Number	1	**Location**	The University of Edinburgh Test Track
Sample Number	1		King's Buildings,
Sample Date	23/03/2009		Edinburgh,
Sampled By	G O' Connor		EH9 3JF

Soil Description

The Sample was taken from Crib 1 of the test track. From previous research the sample was considered to be clean ballast

Grading Envelopes

BS EN 13450:2002 Envelope

RT/CE/S/006 Envelope

Sieve Size	75 mm	63 mm	50 mm	37.5 mm	28 mm	20mm	14mm	10mm	6.3mm	3.35 mm	2 mm	600 µm	63 µm	31.5mm - 50mm
% Passing	100.00	100.00	94.68	57.58	21.06	4.03	0.88	0.53	0.41	0.35	0.31	0.24	0.02	60.2

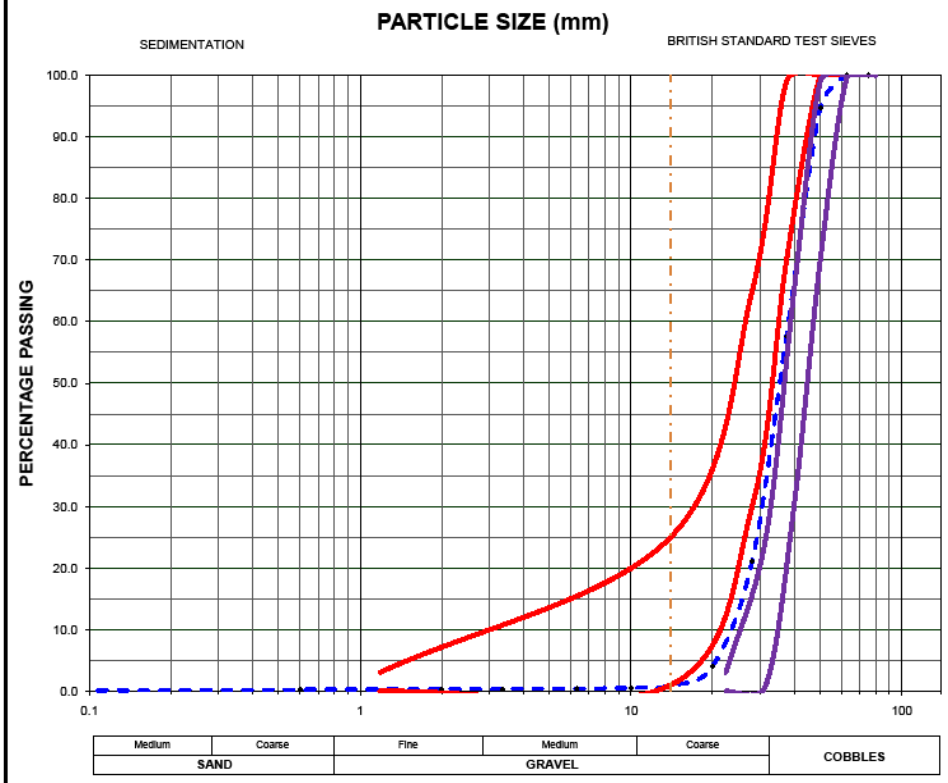

Comments

Tested By	Date	Checked By	Date	Signed	Position
G O' Connor	23-Mar-09	JP Morrissey	23-Mar-09		

The University of Edinburgh

School of Engineering and Electronics

Determination of Particle Size Distribution | *BS 1377 : Part 2 : 1990 : Cl. 9.3*

Job Number	1	**Location**	The University of Edinburgh Test Track
Sample Number	2		King's Buildings,
Sample Date	23/03/2009		Edinburgh,
Sampled By	G O' Connor		EH9 3JF

Soil Description

The Sample was taken from Crib 2 of the test track. From previous research the sample was considered to be clean ballast

Grading Envelopes

BS EN 13450:2002 Envelope
RT/CE/S/006 Envelope

Sieve Size	75 mm	63 mm	50 mm	37.5 mm	28 mm	20mm	14mm	10mm	6.3mm	3.35 mm	2 mm	600 µm	63 µm	31.5mm - 50mm
% Passing	100.00	100.00	95.37	74.83	32.19	6.27	1.05	0.53	0.38	0.32	0.31	0.27	0.00	47.5

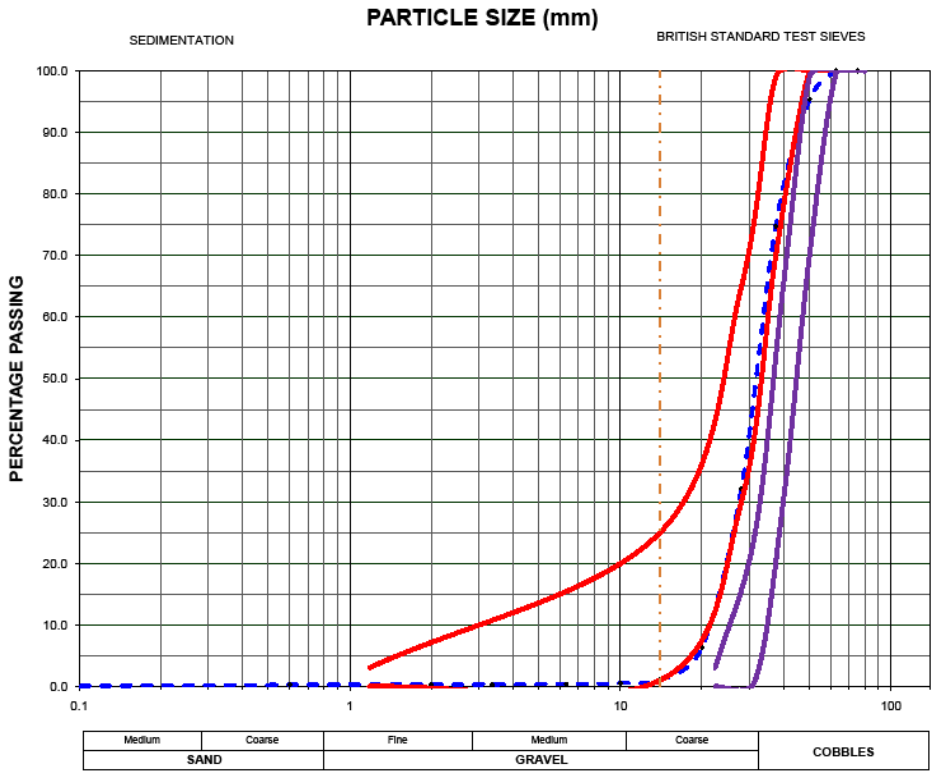

Comments

Tested By	Date	Checked By	Date	Signed	Position
G O' Connor	23-Mar-09	JP Morrissey	23-Mar-09		

The University of Edinburgh

School of Engineering and Electronics

Determination of Particle Size Distribution | *BS 1377 : Part 2 : 1990 : Cl. 9.3*

Job Number	1	**Location**	The University of Edinburgh Test Track
Sample Number	3		King's Buildings,
Sample Date	23/03/2009		Edinburgh,
Sampled By	G O' Connor		EH9 3JF

Soil Description

The Sample was taken from Crib 3 of the test track. From previous research the sample was considered to be clean ballast

Grading Envelopes

BS EN 13450:2002 Envelope

RT/CE/S/006 Envelope

Sieve Size	75 mm	63 mm	50 mm	37.5 mm	28 mm	20mm	14mm	10mm	6.3mm	3.35 mm	2 mm	600 µm	63 µm	31.5mm - 50mm
% Passing	100.00	100.00	89.39	56.34	20.42	3.64	0.67	0.52	0.41	0.35	0.33	0.28	0.10	55.7

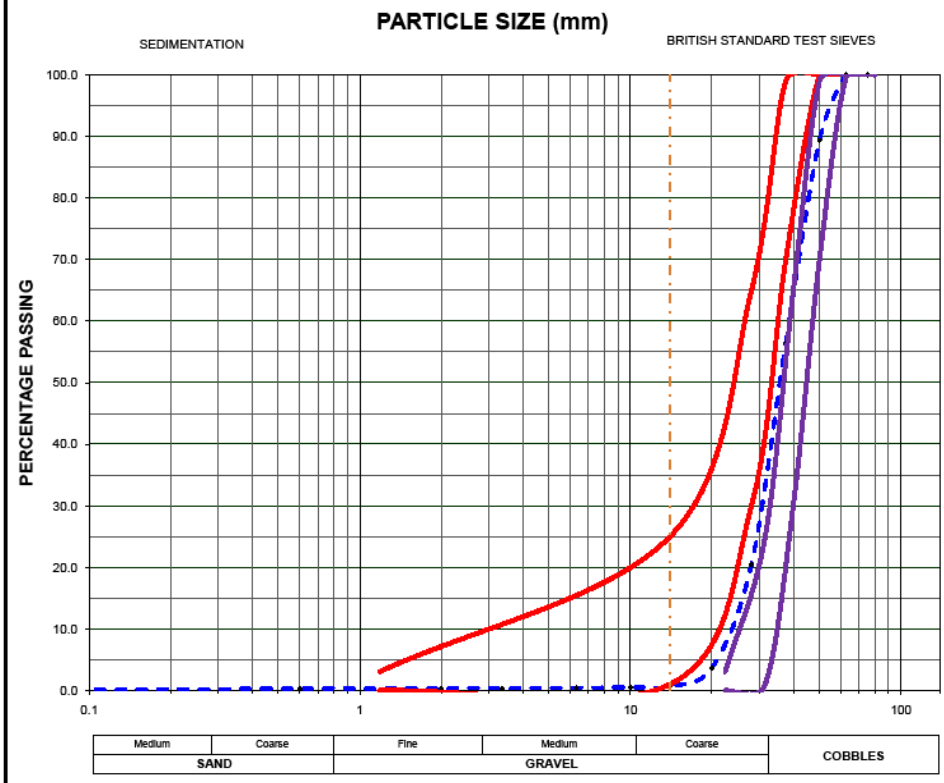

Comments

Tested By	Date	Checked By	Date	Signed	Position
G O' Connor	23-Mar-09	JP Morrissey	23-Mar-09		

The University of Edinburgh

School of Engineering and Electronics

Determination of Particle Size Distribution | *BS 1377 : Part 2 : 1990 : Cl. 9.3*

Job Number	1	**Location**	The University of Edinburgh Test Track
Sample Number	4		King's Buildings,
Sample Date	23/03/2009		Edinburgh,
Sampled By	G O' Connor		EH9 3JF

Soil Description

The Sample was taken from Crib 4 of the test track. From previous research the sample was considered to be clean ballast

Grading Envelopes

BS EN 13450:2002 Envelope
RT/CE/S/006 Envelope

Sieve Size	75 mm	63 mm	50 mm	37.5 mm	28 mm	20mm	14mm	10mm	6.3mm	3.35 mm	2 mm	600 µm	63 µm	31.5mm - 50mm
% Passing	100.00	100.00	96.98	44.79	12.89	3.24	0.62	0.34	0.22	0.22	0.22	0.22	0.22	72.3

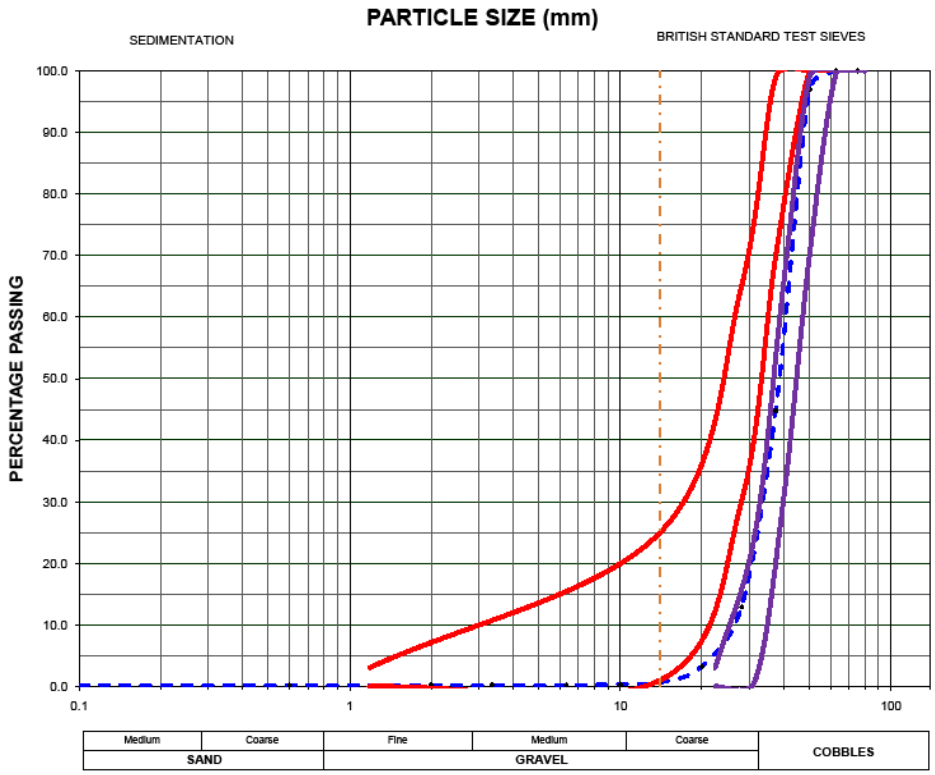

Comments

Tested By	Date	Checked By	Date	Signed	Position
G O' Connor	23-Mar-09	JP Morrissey	23-Mar-09		

The University of Edinburgh

School of Engineering and Electronics

Determination of Particle Size Distribution | *BS 1377 : Part 2 : 1990 : Cl. 9.3*

Job Number	1	**Location**	The University of Edinburgh Test Track
Sample Number	5		King's Buildings,
Sample Date	23/03/2009		Edinburgh,
Sampled By	G O' Connor		EH9 3JF

Soil Description

The Sample was taken from Crib 5 of the test track. From previous research the sample was considered to be clean ballast

Grading Envelopes

BS EN 13450:2002 Envelope

RT/CE/S/006 Envelope

Sieve Size	75 mm	63 mm	50 mm	37.5 mm	28 mm	20mm	14mm	10mm	6.3mm	3.35 mm	2 mm	600 µm	63 µm	31.5mm - 50mm
% Passing	100.00	100.00	93.28	49.05	17.91	2.78	1.37	0.84	0.63	0.48	0.40	0.20	0.00	63.9

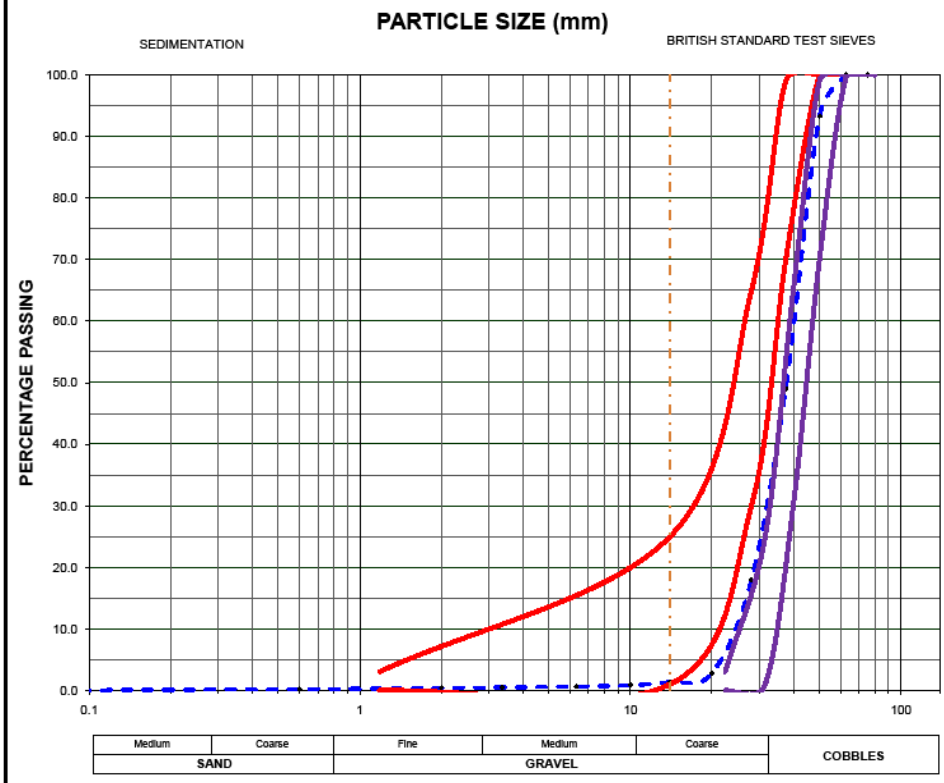

Comments

Tested By	Date	Checked By	Date	Signed	Position
G O' Connor	23-Mar-09	JP Morrissey	23-Mar-09		

The University of Edinburgh

School of Engineering and Electronics

Determination of Particle Size Distribution | *BS 1377 : Part 2 : 1990 : Cl. 9.3*

Job Number	1	**Location**	The University of Edinburgh Test Track
Sample Number	6		King's Buildings,
Sample Date	23/03/2009		Edinburgh,
Sampled By	G O' Connor		EH9 3JF

Soil Description

The Sample was taken from Crib 6 of the test track. From previous research the sample was considered to be clean ballast

Grading Envelopes

BS EN 13450:2002 Envelope

RT/CE/S/006 Envelope

Sieve Size	75 mm	63 mm	50 mm	37.5 mm	28 mm	20mm	14mm	10mm	6.3mm	3.35 mm	2 mm	600 µm	63 µm	31.5mm - 50mm
% Passing	100.00	100.00	92.65	45.26	11.53	2.48	0.89	0.53	0.45	0.40	0.37	0.31	0.13	68.7

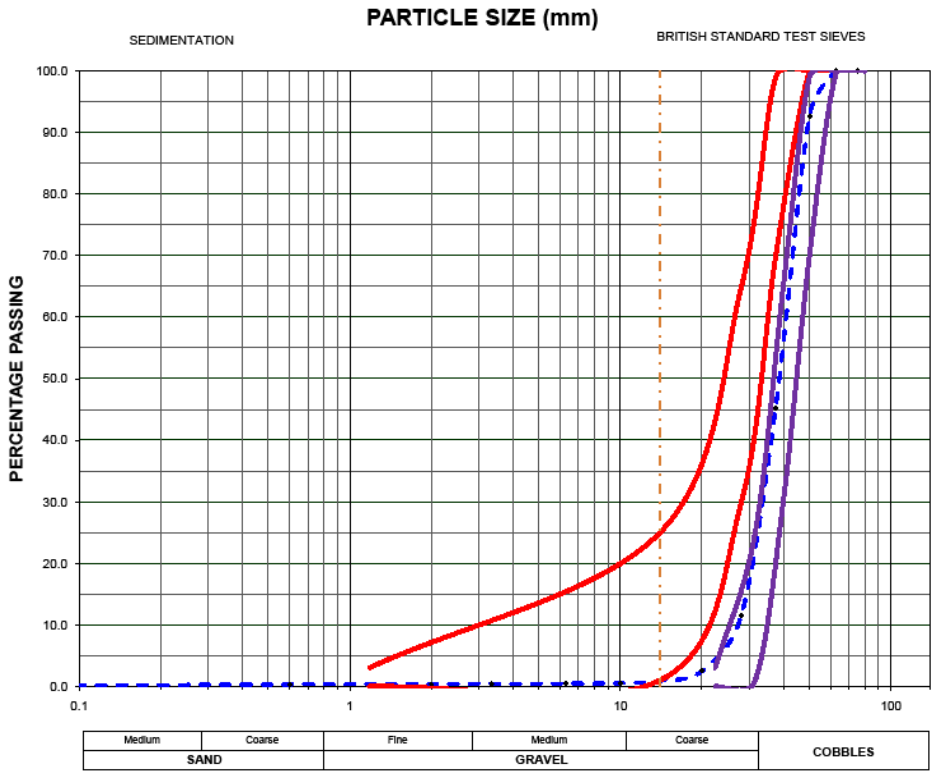

Comments

Tested By	Date	Checked By	Date	Signed	Position
G O' Connor	23-Mar-09	JP Morrissey	23-Mar-09		

The University of Edinburgh

School of Engineering and Electronics

Determination of Particle Size Distribution | *BS 1377 : Part 2 : 1990 : Cl. 9.3*

Job Number	1	**Location**	The University of Edinburgh Test Track
Sample Number	7		King's Buildings,
Sample Date	23/03/2009		Edinburgh,
Sampled By	G O' Connor		EH9 3JF

Soil Description

The Sample was taken from Crib 7 of the test track. From previous research the sample was considered to be clean ballast

Grading Envelopes

BS EN 13450:2002 Envelope

RT/CE/S/006 Envelope

Sieve Size	75 mm	63 mm	50 mm	37.5 mm	28 mm	20mm	14mm	10mm	6.3mm	3.35 mm	2 mm	600 µm	63 µm	31.5mm - 50mm
% Passing	100.00	100.00	100.00	65.25	29.97	8.06	2.98	2.00	1.22	0.58	0.21	0.04	0.02	57.0

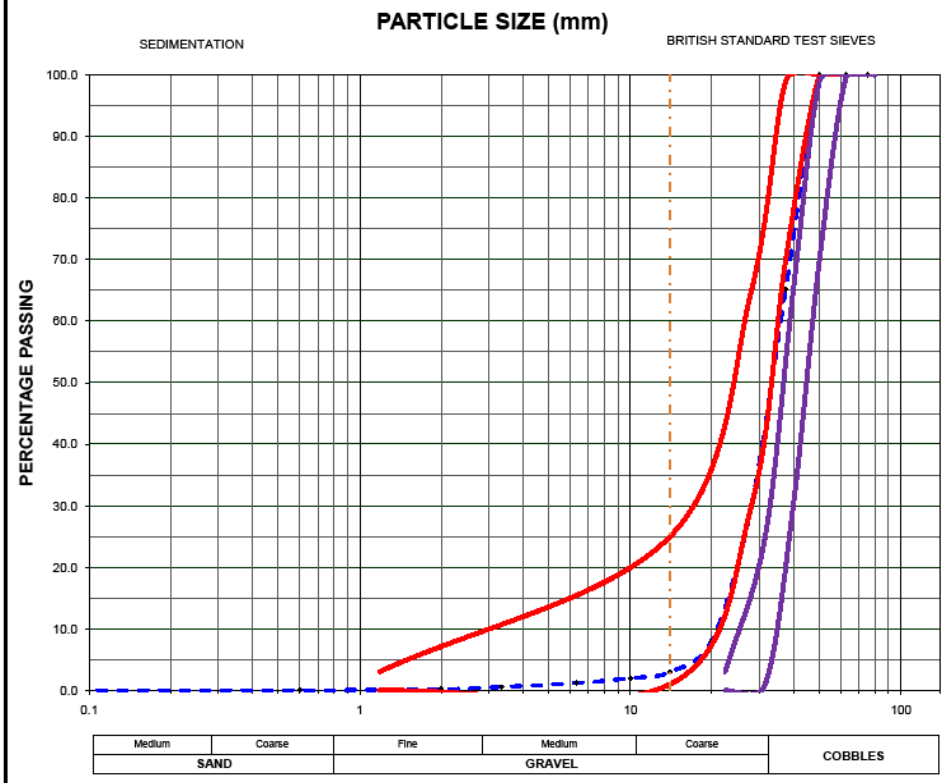

Comments

Tested By	Date	Checked By	Date	Signed	Position
G O' Connor	23-Mar-09	JP Morrissey	23-Mar-09		

The University of Edinburgh

School of Engineering and Electronics

Determination of Particle Size Distribution | *BS 1377 : Part 2 : 1990 : Cl. 9.3*

Job Number	1	**Location**	The University of Edinburgh Test Track
Sample Number	8		King's Buildings,
Sample Date	23/03/2009		Edinburgh,
Sampled By	G O' Connor		EH9 3JF

Soil Description

The Sample was taken from Crib 8 of the test track. From previous research the sample was considered to be clean ballast

Grading Envelopes

BS EN 13450:2002 Envelope

RT/CE/S/006 Envelope

Sieve Size	75 mm	63 mm	50 mm	37.5 mm	28 mm	20mm	14mm	10mm	6.3mm	3.35 mm	2 mm	600 µm	63 µm	31.5mm - 50mm
% Passing	100.00	100.00	95.93	53.64	22.27	20.79	17.89	17.09	16.59	16.00	15.53	14.10	13.09	62.1

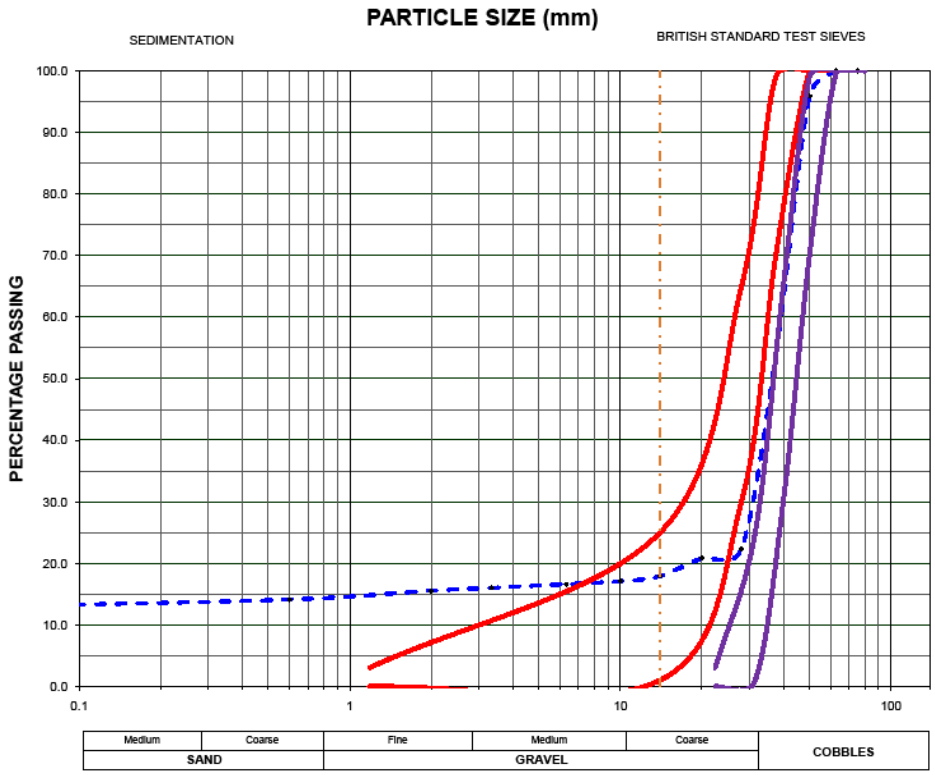

Comments

Tested By	Date	Checked By	Date	Signed	Position
G O' Connor	23-Mar-09	JP Morrissey	23-Mar-09		

The University of Edinburgh

School of Engineering and Electronics

Determination of Particle Size Distribution | *BS 1377 : Part 2 : 1990 : Cl. 9.3*

Job Number	1	**Location**	The University of Edinburgh Test Track
Sample Number	9		King's Buildings,
Sample Date	23/03/2009		Edinburgh,
Sampled By	G O' Connor		EH9 3JF

Soil Description

The Sample was taken from Crib 9 of the test track. From previous research the sample was considered to be clean ballast

Grading Envelopes

BS EN 13450:2002 Envelope

RT/CE/S/006 Envelope

Sieve Size	75 mm	63 mm	50 mm	37.5 mm	28 mm	20mm	14mm	10mm	6.3mm	3.35 mm	2 mm	600 µm	63 µm	31.5mm - 50mm
% Passing	100.00	100.00	97.37	61.97	29.78	13.27	7.12	5.38	4.60	3.72	3.18	1.58	0.00	55.7

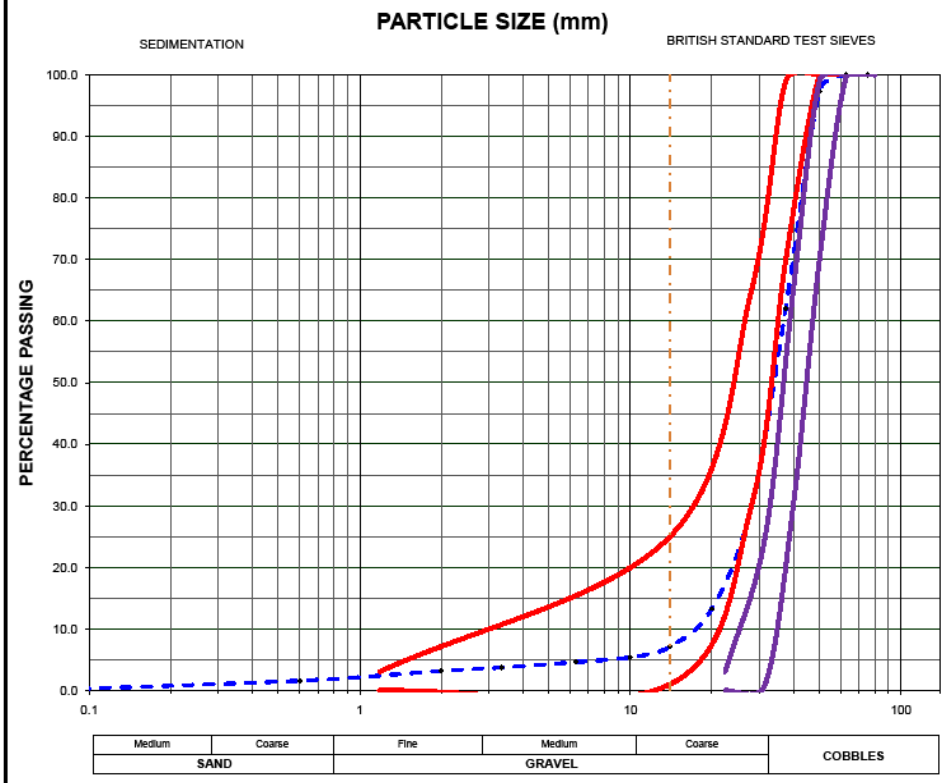

Comments

Tested By	Date	Checked By	Date	Signed	Position
G O' Connor	23-Mar-09	JP Morrissey	23-Mar-09		

The University of Edinburgh

School of Engineering and Electronics

Determination of Particle Size Distribution | *BS 1377 : Part 2 : 1990 : Cl. 9.3*

Job Number	1	**Location**	The University of Edinburgh Test Track
Sample Number	10		King's Buildings,
Sample Date	23/03/2009		Edinburgh,
Sampled By	G O' Connor		EH9 3JF

Soil Description

The Sample was taken from Crib 10 of the test track. From previous research the sample was considered to be clean ballast

Grading Envelopes

BS EN 13450:2002 Envelope

RT/CE/S/006 Envelope

Sieve Size	75 mm	63 mm	50 mm	37.5 mm	28 mm	20mm	14mm	10mm	6.3mm	3.35 mm	2 mm	600 µm	63 µm	31.5mm - 50mm
% Passing	100.00	100.00	100.00	78.52	42.06	17.23	7.20	4.31	3.03	1.89	1.27	0.33	0.00	44.5

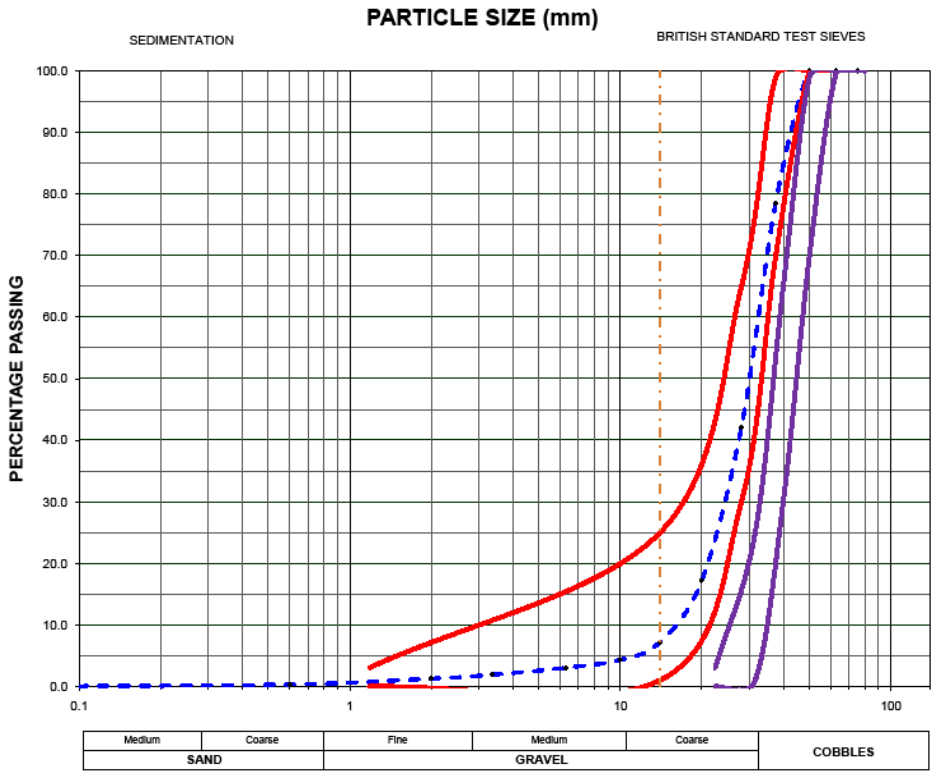

Comments

Tested By	Date	Checked By	Date	Signed	Position
G O' Connor	23-Mar-09	JP Morrissey	23-Mar-09		

The University of Edinburgh

School of Engineering and Electronics

Determination of Particle Size Distribution | *BS 1377 : Part 2 : 1990 : Cl. 9.3*

Job Number	1	**Location**	The University of Edinburgh Test Track
Sample Number	11		King's Buildings,
Sample Date	23/03/2009		Edinburgh,
Sampled By	G O' Connor		EH9 3JF

Soil Description

The Sample was taken from Crib 11 of the test track. From previous research the sample was considered to be clean ballast

Grading Envelopes

BS EN 13450:2002 Envelope

RT/CE/S/006 Envelope

Sieve Size	75 mm	63 mm	50 mm	37.5 mm	28 mm	20mm	14mm	10mm	6.3mm	3.35 mm	2 mm	600 µm	63 µm	31.5mm - 50mm
% Passing	100.00	100.00	96.87	52.09	15.71	3.30	0.99	0.60	0.53	0.45	0.41	0.27	0.00	67.8

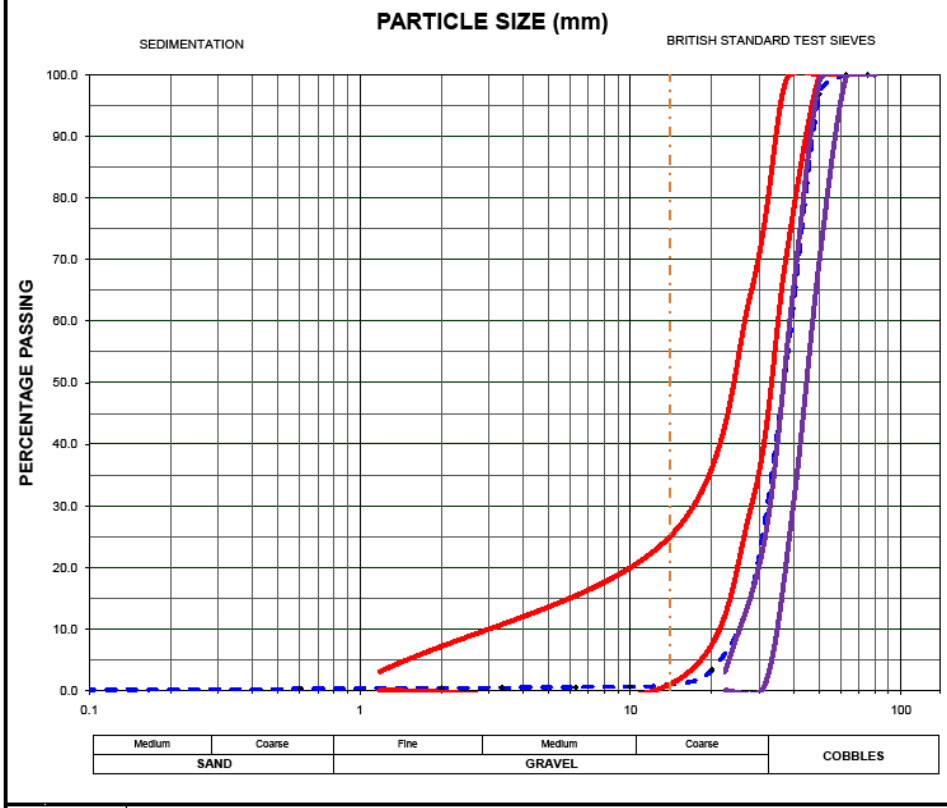

Comments

Tested By	Date	Checked By	Date	Signed	Position
G O' Connor	23-Mar-09	JP Morrissey	23-Mar-09		

The University of Edinburgh

School of Engineering and Electronics

Determination of Particle Size Distribution | *BS 1377 : Part 2 : 1990 : Cl. 9.3*

Job Number	1	**Location**	The University of Edinburgh Test Track
Sample Number	12		King's Buildings,
Sample Date	23/03/2009		Edinburgh,
Sampled By	G O' Connor		EH9 3JF

Soil Description

The Sample was taken from Crib 13 of the test track. From previous research the sample was considered to be clean ballast

Grading Envelopes

BS EN 13450:2002 Envelope
RT/CE/S/006 Envelope

Sieve Size	75 mm	63 mm	50 mm	37.5 mm	28 mm	20mm	14mm	10mm	6.3mm	3.35 mm	2 mm	600 µm	63 µm	31.5mm - 50mm
% Passing	100.00	100.00	100.00	86.96	58.86	26.43	13.79	9.20	6.66	3.97	1.78	0.00	0.00	30.8

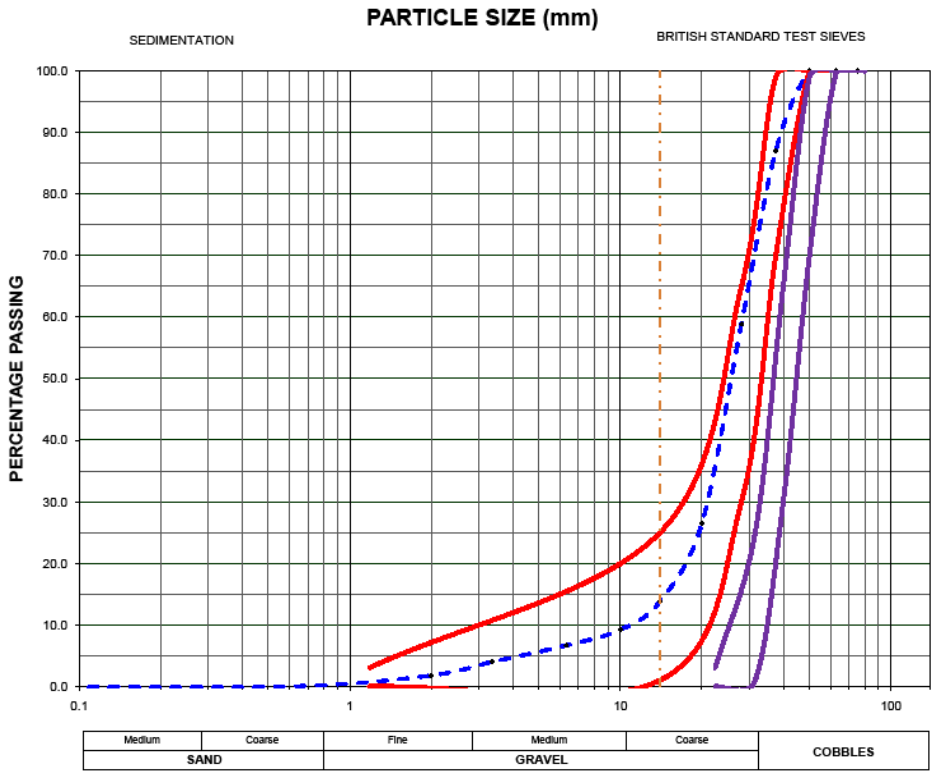

Comments

Tested By	Date	Checked By	Date	Signed	Position
G O' Connor	23-Mar-09	JP Morrissey	23-Mar-09		

The University of Edinburgh

School of Engineering and Electronics

Determination of Particle Size Distribution | *BS 1377 : Part 2 : 1990 : Cl. 9.3*

Job Number	1	**Location**	The University of Edinburgh Test Track
Sample Number	13		King's Buildings,
Sample Date	23/03/2009		Edinburgh,
Sampled By	G O' Connor		EH9 3JF

Soil Description

The Sample was taken from Crib 13 of the test track. From previous research the sample was considered to be clean ballast

Grading Envelopes

BS EN 13450:2002 Envelope

RT/CE/S/006 Envelope

Sieve Size	75 mm	63 mm	50 mm	37.5 mm	28 mm	20mm	14mm	10mm	6.3mm	3.35 mm	2 mm	600 µm	63 µm	31.5mm - 50mm
% Passing	100.00	100.00	100.00	92.85	72.61	35.90	17.17	11.19	6.94	3.17	0.83	0.45	0.28	19.9

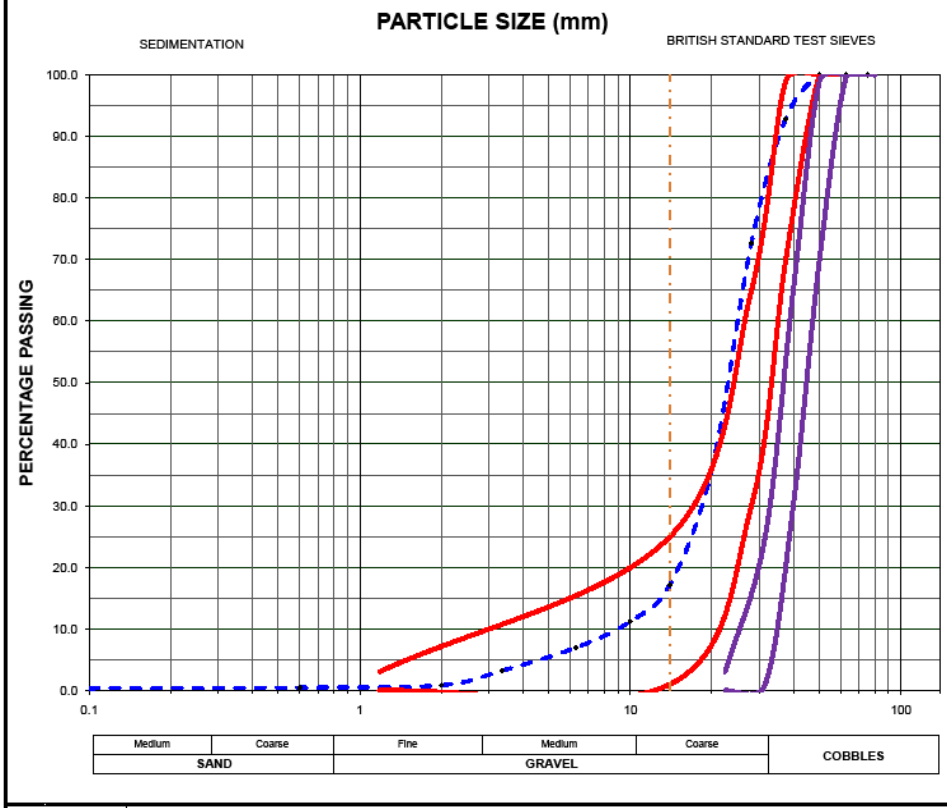

Comments

Tested By	Date	Checked By	Date	Signed	Position
G O' Connor	23-Mar-09	JP Morrissey	23-Mar-09		

The University of Edinburgh

School of Engineering and Electronics

Determination of Particle Size Distribution | *BS 1377 : Part 2 : 1990 : Cl. 9.3*

Job Number	1	**Location**	The University of Edinburgh Test Track
Sample Number	14		King's Buildings,
Sample Date	23/03/2009		Edinburgh,
Sampled By	G O' Connor		EH9 3JF

Soil Description

The Sample was taken from Crib 14 of the test track. From previous research the sample was considered to be clean ballast

Grading Envelopes

BS EN 13450:2002 Envelope
RT/CE/S/006 Envelope

Sieve Size	75 mm	63 mm	50 mm	37.5 mm	28 mm	20mm	14mm	10mm	6.3mm	3.35 mm	2 mm	600 µm	63 µm	31.5mm - 50mm
% Passing	100.00	100.00	100.00	91.57	66.17	27.41	10.79	5.95	3.77	2.21	1.34	0.07	0.00	24.5

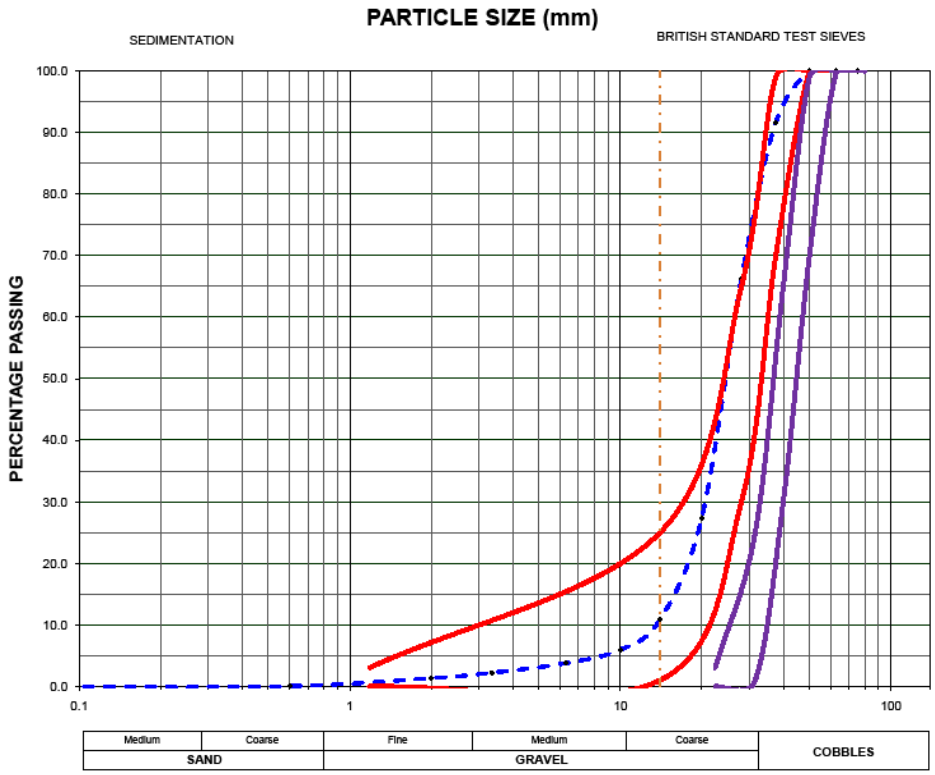

Comments

Tested By	Date	Checked By	Date	Signed	Position
G O' Connor	23-Mar-09	JP Morrissey	23-Mar-09		

The University of Edinburgh

School of Engineering and Electronics

Determination of Particle Size Distribution | *BS 1377 : Part 2 : 1990 : Cl. 9.3*

Job Number	1	**Location**	The University of Edinburgh Test Track
Sample Number	15		King's Buildings,
Sample Date	23/03/2009		Edinburgh,
Sampled By	G O' Connor		EH9 3JF

Soil Description

The Sample was taken from Crib 15 of the test track. From previous research the sample was considered to be clean ballast

Grading Envelopes

BS EN 13450:2002 Envelope

RT/CE/S/006 Envelope

Sieve Size	75 mm	63 mm	50 mm	37.5 mm	28 mm	20mm	14mm	10mm	6.3mm	3.35 mm	2 mm	600 µm	63 µm	31.5mm - 50mm
% Passing	100.00	100.00	100.00	96.26	73.46	31.99	11.63	6.97	4.25	2.13	1.19	1.02	0.08	18.1

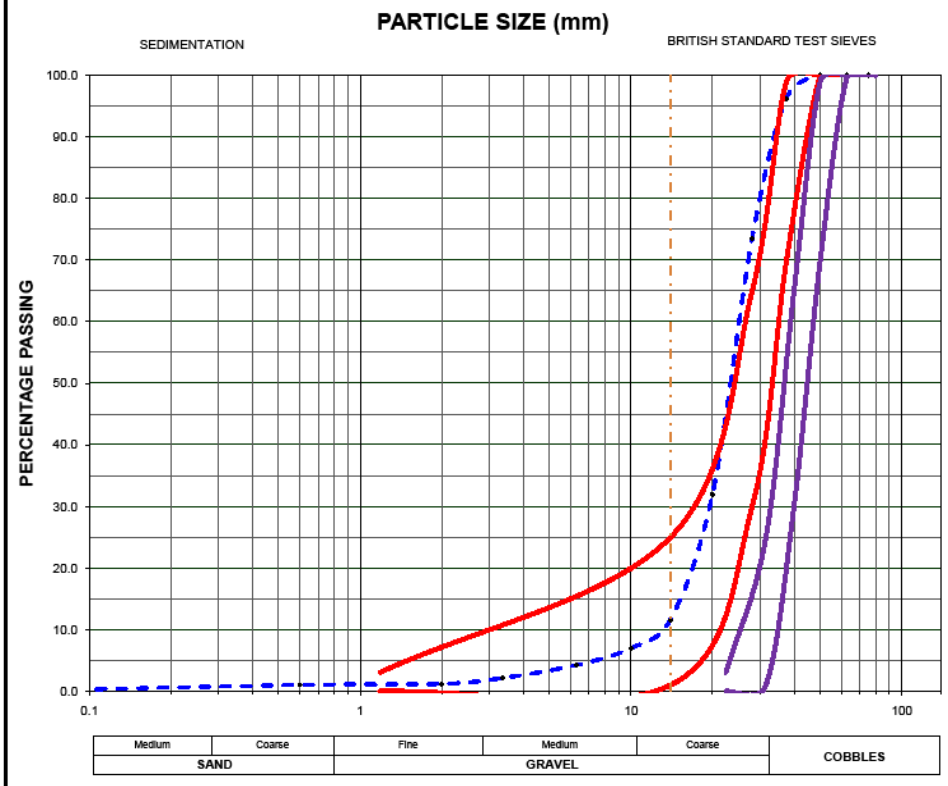

Comments

Tested By	Date	Checked By	Date	Signed	Position
G O' Connor	23-Mar-09	JP Morrissey	23-Mar-09		

The University of Edinburgh

School of Engineering and Electronics

Determination of Particle Size Distribution | *BS 1377 : Part 2 : 1990 : Cl. 9.3*

Job Number	1	**Location**	The University of Edinburgh Test Track
Sample Number	16		King's Buildings,
Sample Date	23/03/2009		Edinburgh,
Sampled By	G O' Connor		EH9 3JF

Soil Description

The Sample was taken from Crib 16 of the test track. From previous research the sample was considered to be clean ballast

Grading Envelopes

BS EN 13450:2002 Envelope

RT/CE/S/006 Envelope

Sieve Size	75 mm	63 mm	50 mm	37.5 mm	28 mm	20mm	14mm	10mm	6.3mm	3.35 mm	2 mm	600 µm	63 µm	31.5mm - 50mm
% Passing	100.00	100.00	100.00	93.99	75.81	42.49	20.47	11.68	7.48	4.57	2.78	0.04	0.00	17.5

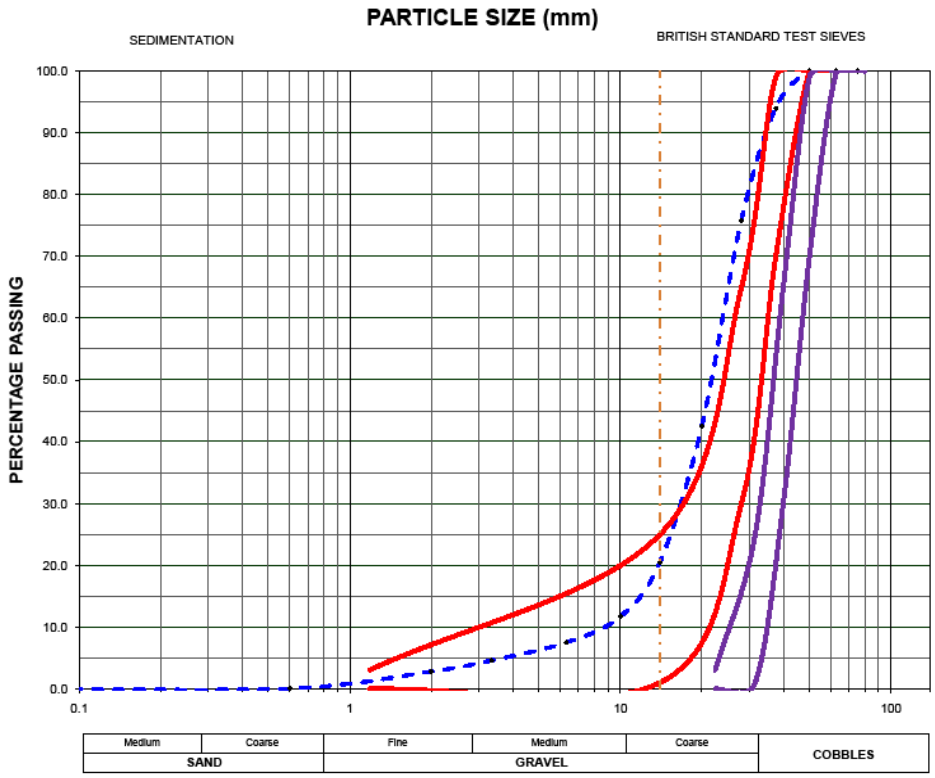

Comments

Tested By	Date	Checked By	Date	Signed	Position
G O' Connor	23-Mar-09	JP Morrissey	23-Mar-09		

APPENDIX 3 FWD DROPS ON FIXED POSITIONS ON SLEEPERS

Prima100 FWD (2007.11.13)			
Sleepers 1-6			
Sleeper	Stiffness (MPa)	Max Force (kN)	Max Defl (μm)
1	30.4	8.9	1130
1	30.4	8.9	1136
1	30.7	9.2	1158
1	31.1	9.4	1166
1	29.8	9.0	1166
1	30.9	9.2	1154
1	29.6	9.2	1206
1	30.0	9.2	1181
1	30.2	9.2	1184
1	29.4	8.9	1173
2	49.9	9.7	752
2	46.9	9.9	813
2	43.6	9.9	876
2	41.8	9.9	915
2	40.6	9.9	945
2	40.1	9.9	954
2	39.5	9.8	962
2	39.3	10.0	986
2	34.0	8.5	966
2	39.0	10.0	989
3	163.0	10.5	250
3	162.1	10.9	260
3	163.9	10.8	254
3	164.2	10.8	255
3	160.8	10.8	259
3	121.5	10.4	330
3	163.0	10.7	253
4	255.3	10.4	157
4	249.1	10.8	168
4	285.1	11.0	149
4	274.6	10.8	151
4	257.9	10.5	157
4	232.4	10.8	179
4	257.3	10.6	159
4	254.7	10.8	163
4	252.2	10.8	166
5	238.9	10.9	176
5	242.9	11.1	176
5	282.1	10.9	150
5	322.0	10.9	131
5	296.9	11.0	143
6	264.4	10.5	154
6	277.1	11.0	154
6	247.9	10.7	166
6	254.5	10.9	165
6	280.5	11.4	157
6	256.9	10.8	162
6	227.1	11.0	188
6	268.5	11.2	161
6	236.1	10.8	177

Prima100 FWD (2007.11.13)			
Sleepers 6-11			
Sleeper	Stiffness (MPa)	Max Force (kN)	Max Defl (μm)
7	151.5	10.5	268
7	148.4	11.0	287
7	145.3	10.8	288
7	140.7	10.7	293
7	145.4	10.9	290
7	146.3	10.9	287
7	146.2	10.8	286
7	146.8	10.9	287
7	141.2	10.7	294
7	138.1	10.8	303
7	137.0	10.9	306
8	141.2	10.3	281
8	141.4	10.7	293
8	141.0	10.8	295
8	139.5	10.8	298
8	141.2	10.9	297
8	141.0	11.0	301
8	139.7	10.8	298
8	137.8	10.7	301
8	141.0	10.9	297
8	138.1	10.5	295
8	138.1	11.0	307
8	138.5	10.9	305
9	161.8	10.6	254
9	196.1	10.6	209
9	157.3	10.7	262
9	155.6	10.7	267
9	155.8	10.7	266
9	155.5	10.7	265
9	158.5	11.0	269
9	151.9	10.7	272
9	155.0	10.9	273
9	152.3	10.8	274
10	365.6	11.0	116
10	349.2	11.0	122
10	344.4	11.1	124
10	361.9	11.2	120
10	345.4	10.9	122
10	358.5	11.3	122
10	344.8	11.1	124
10	355.9	11.0	120
11	239.3	11.1	179
11	266.0	10.7	156
11	206.2	10.9	203
11	224.5	10.9	188
11	235.4	10.8	177
11	257.5	10.6	159

Prima100 FWD (2007.11.13)			
Sleepers 11-17			
Sleeper	Stiffness (MPa)	Max Force (kN)	Max Defl (μm)
12	188.0	10.8	221
12	165.5	11.1	259
12	169.8	11.5	261
12	161.3	11.2	269
12	158.4	11.1	271
12	157.4	11.2	276
12	175.3	11.0	242
13	173.3	10.1	224
13	160.7	9.5	228
13	171.8	10.4	233
13	152.2	10.6	270
13	155.0	10.9	271
13	152.8	10.2	259
13	169.7	10.6	241
13	152.1	10.8	274
13	163.8	10.8	254
13	141.8	11.0	300
14	204.8	11.0	208
14	202.1	11.2	214
14	211.0	11.0	201
14	254.6	10.8	163
15	277.8	11.1	154
15	298.0	11.4	147
15	271.2	11.1	158
15	275.4	11.0	154
15	279.2	11.2	155
16	53.3	10.4	757
16	52.1	10.5	776
16	50.7	10.4	788
16	50.0	10.4	806
16	49.3	10.4	812
16	48.7	10.4	825
16	48.4	10.4	828
16	48.1	10.5	842
17	30.7	9.2	1161
17	17.8	9.8	2129
17	16.9	9.8	2238
17	16.9	9.6	2202
17	22.9	9.5	1612
17	18.1	9.4	2014
17	17.1	9.5	2150
17	19.9	9.5	1848
17	20.0	9.6	1854

Sleepers 1, 2, 16, and 17 were made of wood. All other sleepers pre-cast concrete.

APPENDIX 4 FWD DROPS ON FIXED POSITIONS ON CRIBS

Prima100 FWD (2007.11.13)			
Cribs 1-2 to 5-6			
Crib	Stiffness (MPa)	Max Force (kN)	Max Defl (μm)
1	29.4	9.5	1244
1	49.0	9.5	752
1	22.5	8.8	1512
1	48.1	9.9	797
1	51.7	9.8	731
1	53.7	10.0	717
1	52.7	9.7	712
1	55.3	9.7	681
2	72.1	9.6	514
2	100.0	10.0	387
2	75.3	9.6	494
2	134.3	10.0	288
2	118.5	10.2	331
3	82.5	10.1	475
3	78.1	10.4	512
3	87.5	10.6	468
3	99.0	10.6	413
3	106.8	10.7	387
3	109.2	10.5	373
3	112.4	10.8	370
3	101.8	10.8	409
4	42.0	10.2	937
4	49.4	9.9	777
4	50.6	10.4	796
4	48.1	10.4	834
4	51.0	10.4	791
4	50.4	10.6	812
4	52.7	10.6	776
4	56.1	11.0	755
4	53.3	10.2	742
4	48.9	10.6	838
4	52.8	10.5	769
5	48.6	10.4	830
5	51.9	10.6	789
5	56.3	10.6	730
5	56.1	10.7	737
5	59.3	10.8	702
5	60.6	10.7	680
5	58.4	10.7	707
5	62.3	10.8	668
5	62.4	10.6	654
5	60.5	10.7	684
5	61.9	10.8	677
5	62.5	10.8	667
5	61.9	10.8	672

Prima100 FWD (2007.11.13)			
Cribs 6-7 to 10-11			
Crib	Stiffness (MPa)	Max Force (kN)	Max Defl (μm)
6	32.2	10.4	1249
6	36.9	10.4	1089
6	40.9	10.4	983
6	42.1	10.5	966
6	48.7	10.6	838
6	49.2	10.6	830
6	48.4	10.6	846
6	55.3	11.3	786
6	51.9	10.6	787
6	57.1	10.8	733
6	53.0	10.6	775
6	56.8	10.7	727
6	58.5	10.9	718
6	61.6	11.1	696
7	94.5	10.3	421
7	84.3	10.3	473
7	86.8	10.7	477
7	88.0	10.9	478
7	92.2	10.9	455
7	95.7	10.8	436
7	110.7	10.9	379
7	120.8	10.9	350
7	106.1	11.0	400
7	108.5	11.1	393
8	39.1	9.5	935
8	38.4	9.8	986
8	69.6	9.8	542
8	115.2	10.3	346
8	120.7	10.4	333
8	106.3	10.2	371
8	106.0	10.1	369
9	66.4	9.9	577
9	85.9	10.0	450
9	87.4	10.2	450
9	92.6	10.4	433
9	87.1	10.3	458
9	92.9	10.4	431
9	87.3	10.5	463
9	88.1	10.4	457
10	80.3	10.2	492
10	71.5	10.5	570
10	61.9	10.2	636
10	60.0	10.6	679
10	53.4	10.7	777
10	49.3	10.5	823
10	42.8	10.5	950

Prima100 FWD (2007.11.13)			
Cribs 11-12 to 16-17			
Crib	Stiffness (MPa)	Max Force (kN)	Max Defl (μm)
11	40.0	10.3	997
11	43.6	10.4	923
11	43.6	10.5	933
11	42.3	10.5	957
11	44.8	10.5	905
11	42.9	10.5	943
11	45.3	10.4	888
12	58.9	10.3	676
12	62.0	10.3	644
12	75.6	10.5	534
12	77.5	10.2	509
12	83.5	10.4	481
12	74.6	10.3	536
12	74.3	10.4	541
13	33.6	10.4	1193
13	46.6	10.7	886
13	44.3	10.5	916
13	39.9	10.7	1033
13	45.3	10.5	895
13	40.5	10.5	997
14	47.9	10.7	863
14	29.9	10.2	1322
14	36.8	10.6	1112
14	37.7	10.5	1079
14	34.6	10.4	1165
14	38.1	10.5	1066
15	74.6	9.9	512
15	77.0	10.2	510
15	74.3	10.2	528
15	73.0	10.1	534
15	72.1	10.2	548
15	73.8	10.2	534
15	75.2	10.2	526
15	76.9	10.5	527
15	93.7	10.2	420
16	39.7	10.2	991
16	50.6	10.3	788
16	49.9	10.3	796
16	51.8	10.4	778

APPENDIX 5 FWD DROPS ON DIFFERENT POSITIONS ON SLEEPER 6

Prima100 FWD (2007.11.14)				
Sleeper 6: Conf Tests 1-5				
Position	Drop	Stiffness (MPa)	Max Force (kN)	Max Defl (μm)
1	3	169.9	10.6	242
1	4	155.6	10.6	263
1	5	149.4	10.5	272
1	6	155.1	10.5	261
1	7	162.1	10.6	252
1	10	157.2	10.4	256
2	3	146.0	10.5	277
2	4	143.8	10.8	289
2	7	140.6	10.8	296
2	11	141.0	10.7	292
2	14	137.8	10.5	294
3	1	141.1	10.6	289
3	4	138.2	10.7	299
3	9	138.1	10.8	303
3	12	136.2	10.8	308
4	1	140.5	10.0	276
4	2	144.1	10.5	282
4	5	142.0	10.5	286
4	6	152.6	10.7	271
4	9	147.7	10.8	282
4	10	144.6	10.5	281
5	3	156.0	10.9	269
5	7	174.1	10.0	222
5	12	151.8	10.0	255
5	13	155.8	10.2	253
5	15	154.9	10.2	255
5	16	156.0	10.1	249
5	17	166.5	10.4	241
5	18	160.0	10.0	241

APPENDIX 6 FWD DROPS ON DIFFERENT POSITIONS ON CRIB 6

Prima100 FWD (2007.11.14)				
Crib 6: Conf Tests 1-5				
Position	Drop	Stiffness (MPa)	Max Force (kN)	Max Defl (μm)
1	9	53.7	10.0	719
1	10	57.7	10.4	695
1	14	70.2	10.5	576
1	15	44.4	10.4	906
1	16	45.5	10.2	864
2	3	80.9	10.2	486
2	6	93.3	10.5	433
2	7	97.4	10.6	421
2	8	99.4	10.6	413
2	9	100.8	10.7	408
2	10	102.7	10.7	402
3	4	41.5	10.5	975
3	5	46.7	10.6	878
3	6	42.8	10.5	951
3	7	48.2	10.5	838
4	2	85.4	10.0	452
4	3	122.6	10.2	321
4	4	99.3	10.1	395
4	9	101.2	10.3	393
4	10	105.7	10.5	383
4	11	98.0	10.4	412
5	5	59.6	10.5	683
5	6	41.4	10.5	983
5	7	57.3	10.6	713
5	8	52.7	10.6	781
5	9	63.7	10.6	644

APPENDIX 7 FULL IMPULSE RESPONSE RESULTS

Hit Ballast, Measure Ballast Mobility Graphs – amplitude values ×*0.0085m/sN for units*

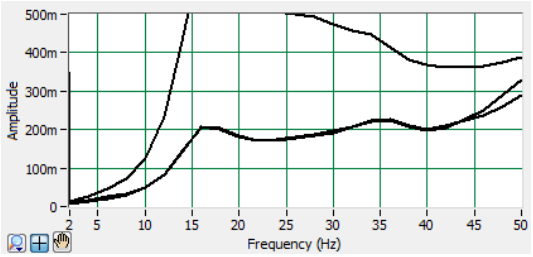

Crib 2: FI=1.05%

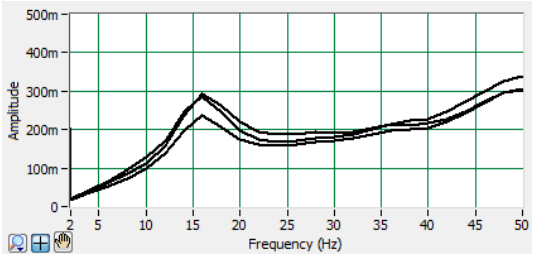

Crib 3: FI=0.77%

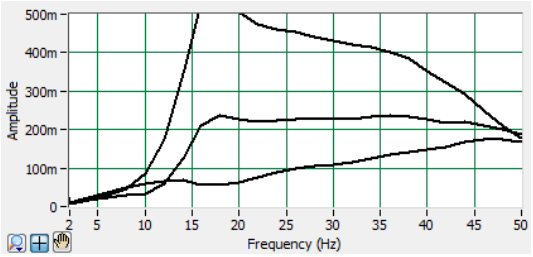

Crib 4: FI=0.84%

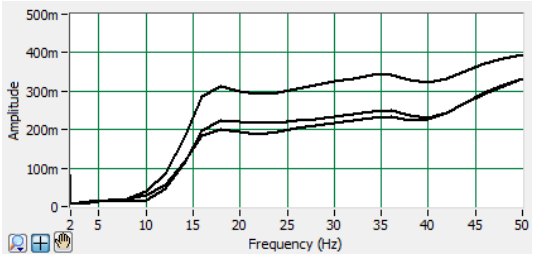

Crib 6: FI=0.79%

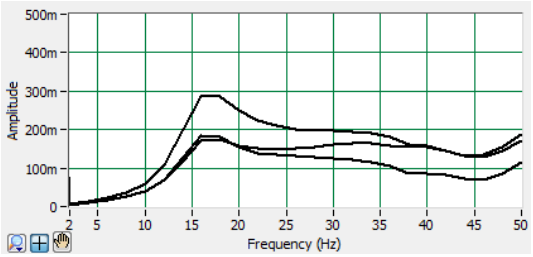

Crib 8: FI=4.80%

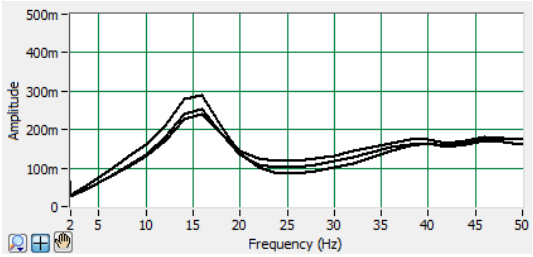

Crib 10: FI=7.20%

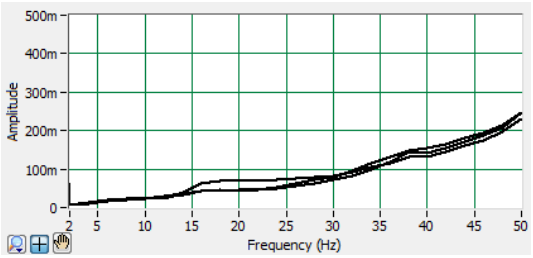

Crib 12: FI=13.79%

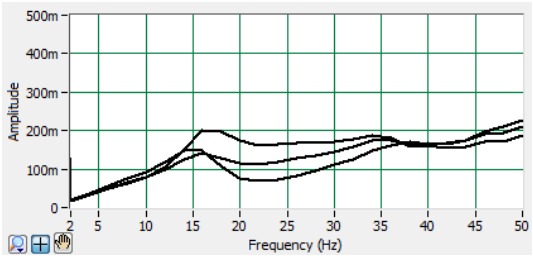

Crib 14: FI=10.79%

Hit Ballast, Measure Ballast Full Result									
		Gradient to 18Hz				Mean 18Hz to 50Hz			
		Test			Mid	Test			Mid
Crib	Fouling Index, FI	1	2	3	Value	1	2	3	Value
2	1.05%	0.036	0.011	0.011	*0.011*	0.45	0.21	0.21	*0.21*
3	0.77%	0.015	0.012	0.014	*0.014*	0.23	0.21	0.23	*0.23*
4	0.84%	0.003	0.013	0.030	*0.013*	0.12	0.22	0.38	*0.22*
6	0.79%	0.017	0.011	0.012	*0.012*	0.33	0.24	0.25	*0.25*
8	4.80%	0.016	0.010	0.010	*0.010*	0.19	0.11	0.16	*0.16*
10	7.20%	0.011	0.011	0.012	*0.011*	0.15	0.14	0.14	*0.14*
12	13.79%	0.003	0.002	0.004	*0.003*	0.11	0.12	0.12	*0.12*
14	10.79%	0.011	0.007	0.006	*0.007*	0.17	0.16	0.14	*0.16*
		Correlation with FI:			**-0.944**	**Correlation with FI:**			**-0.909**

Hit Sleeper, Measure Ballast Mobility Graphs – amplitude values ×*0.0085m/sN for units*

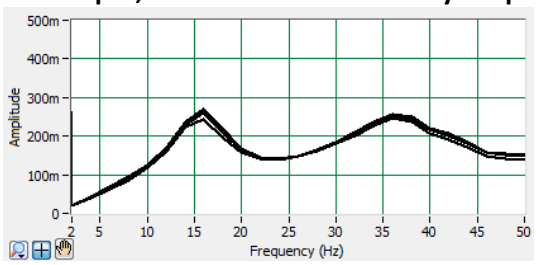

Crib 2: FI=1.05%

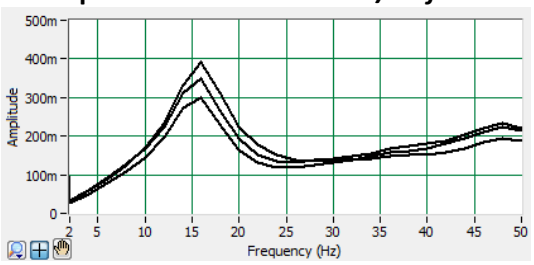

Crib 3: FI=0.77%

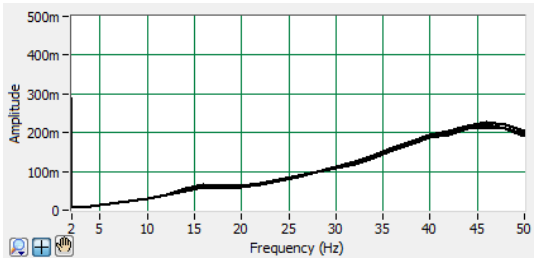

Crib 4: FI=0.84%

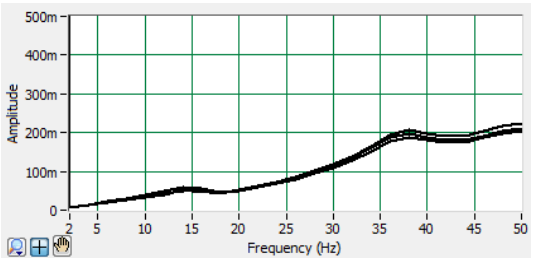

Crib 6: FI=0.79%

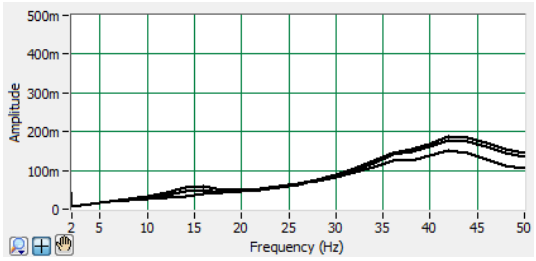

Crib 8: FI=4.80%

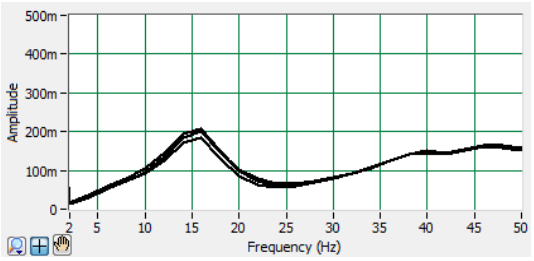

Crib 10: FI=7.20%

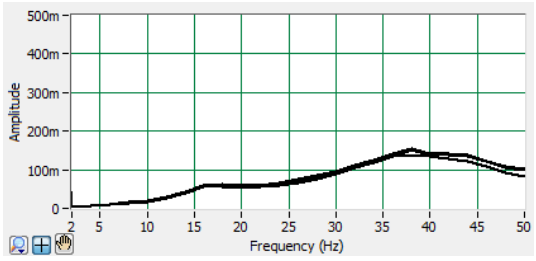

Crib 12: FI=13.79%

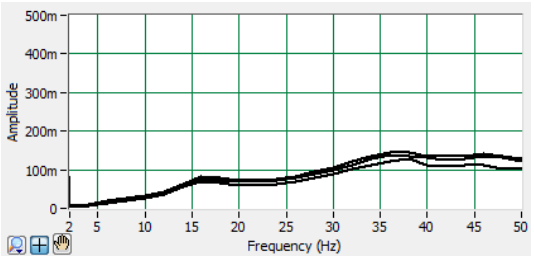

Crib 14: FI=10.79%

Hit Sleeper, Measure Ballast Full Results									
		Gradient to 18Hz				Mean 18Hz to 50Hz			
		Test			Mid	Test			Mid
Crib	Fouling Index, FI	1	2	3	Value	1	2	3	Value
2	1.05%	0.012	0.012	0.011	*0.012*	0.18	0.18	0.19	*0.18*
3	0.77%	0.017	0.015	0.013	*0.015*	0.17	0.18	0.17	*0.17*
4	0.84%	0.003	0.003	0.003	*0.003*	0.14	0.14	0.14	*0.14*
6	0.79%	0.003	0.003	0.002	*0.003*	0.14	0.13	0.14	*0.14*
8	4.80%	0.002	0.003	0.002	*0.002*	0.10	0.12	0.11	*0.11*
10	7.20%	0.007	0.008	0.008	*0.008*	0.11	0.12	0.12	*0.12*
12	13.79%	0.003	0.003	0.003	*0.003*	0.10	0.10	0.10	*0.10*
14	10.79%	0.004	0.004	0.004	*0.004*	0.09	0.11	0.11	*0.11*
		Correlation with FI:			**-0.376**	**Correlation with FI:**			**-0.798**

Hit Ballast, Measure Sleeper Mobility Graphs – amplitude values ×*0.0085m/sN for units*

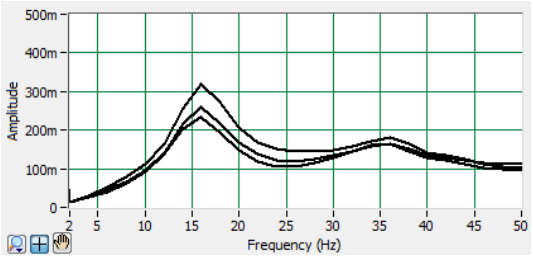

Crib 2: FI=1.05%

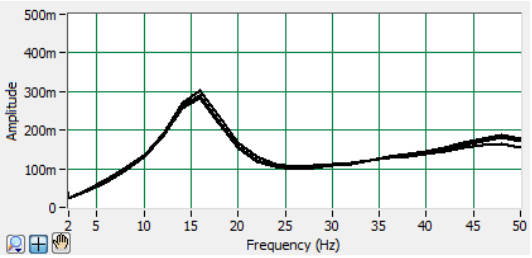

Crib 3: FI=0.77%

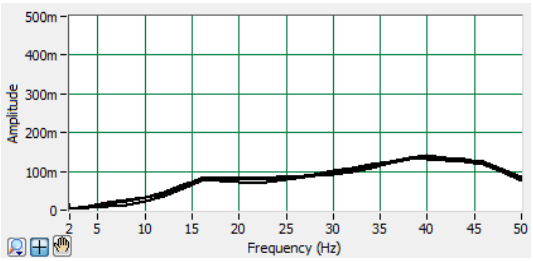

Crib 4: FI=0.84%

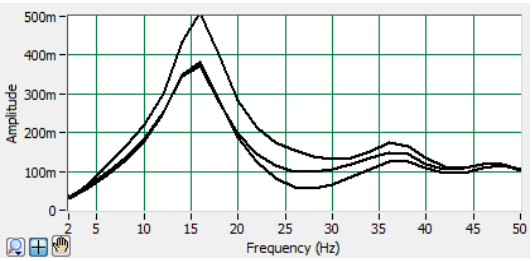

Crib 6: FI=0.79%

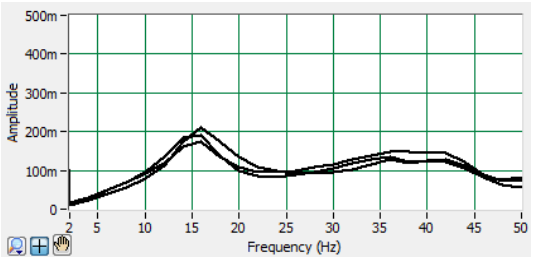

Crib 8: FI=4.80%

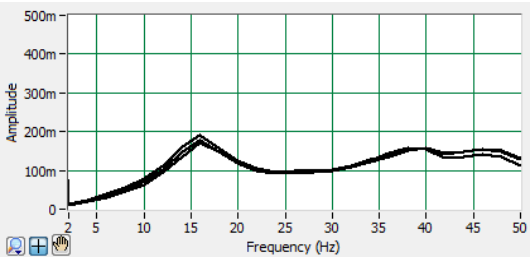

Crib 10: FI=7.20%

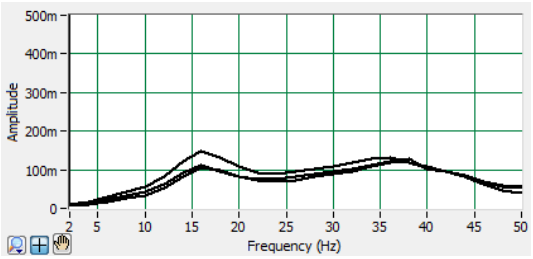

Crib 12: FI=13.79%

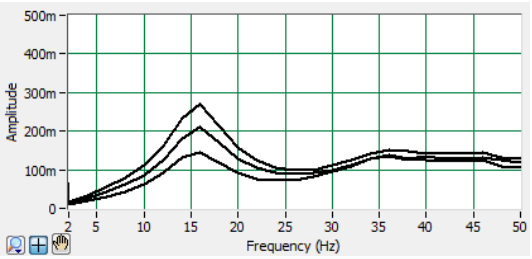

Crib 14: FI=10.79%

Hit Ballast, Measure Sleeper Full Results									
		Gradient to 18Hz				Mean 18Hz to 50Hz			
		Test			Mid	Test			Mid
Crib	Fouling Index, FI	1	2	3	Value	1	2	3	Value
2	1.05%	0.015	0.012	0.011	*0.012*	0.15	0.13	0.13	*0.13*
3	0.77%	0.012	0.013	0.013	*0.013*	0.14	0.15	0.14	*0.14*
4	0.84%	0.004	0.005	0.004	*0.004*	0.11	0.10	0.10	*0.10*
6	0.79%	0.016	0.016	0.022	*0.016*	0.13	0.11	0.17	*0.13*
8	4.80%	0.008	0.008	0.010	*0.008*	0.12	0.11	0.11	*0.11*
10	7.20%	0.008	0.009	0.008	*0.008*	0.12	0.13	0.13	*0.13*
12	13.79%	0.005	0.007	0.005	*0.005*	0.09	0.10	0.09	*0.09*
14	10.79%	0.012	0.010	0.007	*0.010*	0.14	0.12	0.11	*0.12*
		Correlation with FI:			**-0.481**	**Correlation with FI:**			**-0.618**

Hit Rail, Measure Ballast Mobility Graphs – amplitude values ×*0.0085m/sN for units*

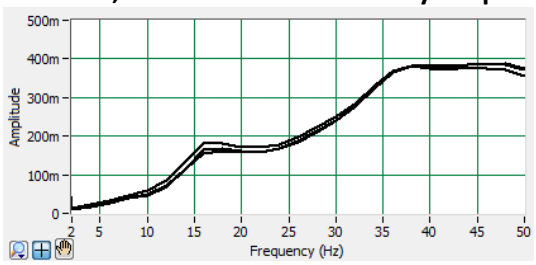

Crib 2: FI=1.05%

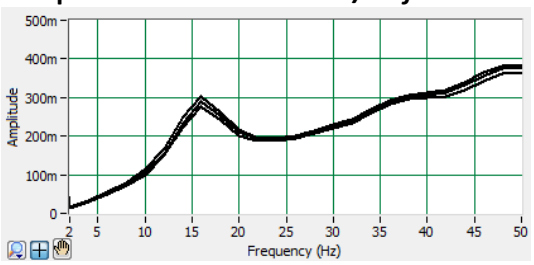

Crib 3: FI=0.77%

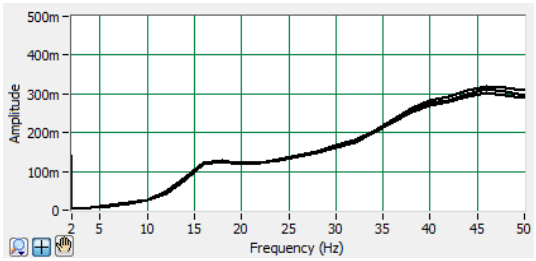

Crib 4: FI=0.84%

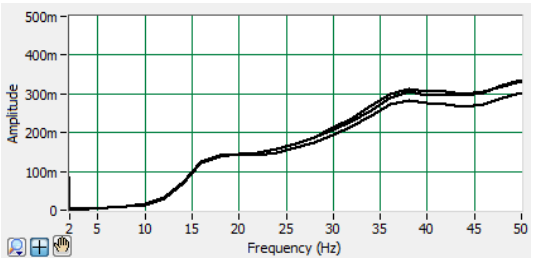

Crib 6: FI=0.79%

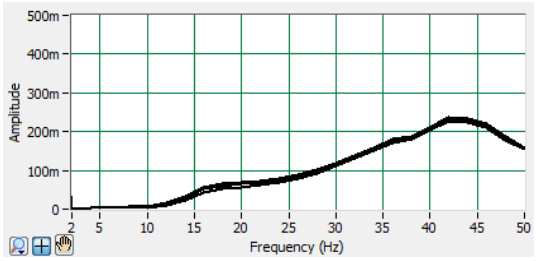

Crib 8: FI=4.80%

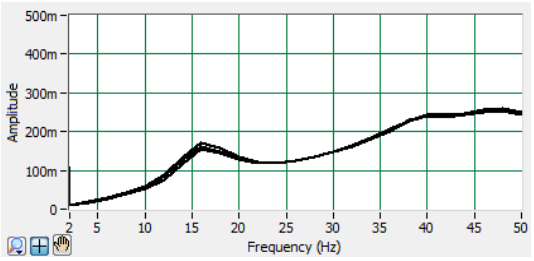

Crib 10: FI=7.20%

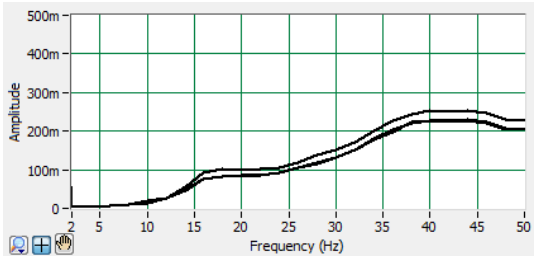

Crib 12: FI=13.79%

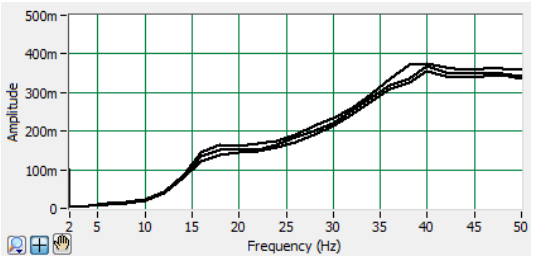

Crib 14: FI=10.79%

Hit Rail, Measure Ballast Full Results									
		Gradient to 18Hz				Mean 18Hz to 50Hz			
		Test			Mid	Test			Mid
Crib	Fouling Index, FI	1	2	3	Value	1	2	3	Value
2	1.05%	0.010	0.009	0.009	*0.010*	0.29	0.29	0.29	*0.29*
3	0.77%	0.013	0.014	0.015	*0.013*	0.26	0.28	0.27	*0.27*
4	0.84%	0.007	0.007	0.007	*0.007*	0.21	0.21	0.22	*0.21*
6	0.79%	0.008	0.008	0.008	*0.008*	0.22	0.24	0.24	*0.24*
8	4.80%	0.004	0.003	0.003	*0.004*	0.14	0.15	0.14	*0.14*
10	7.20%	0.008	0.008	0.009	*0.008*	0.19	0.19	0.19	*0.19*
12	13.79%	0.006	0.005	0.005	*0.006*	0.18	0.16	0.16	*0.16*
14	10.79%	0.009	0.008	0.008	*0.009*	0.28	0.27	0.26	*0.27*
		Correlation with FI:			**-0.444**	**Correlation with FI:**			**-0.431**

Hit Ballast, Measure Rail Mobility Graphs – amplitude values ×*0.0085m/sN for units*

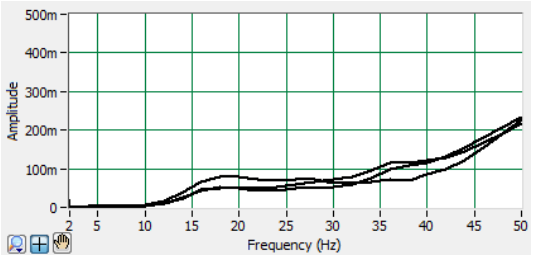

Crib 2: FI=1.05%

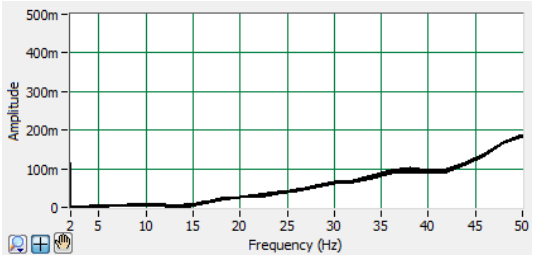

Crib 3: FI=0.77%

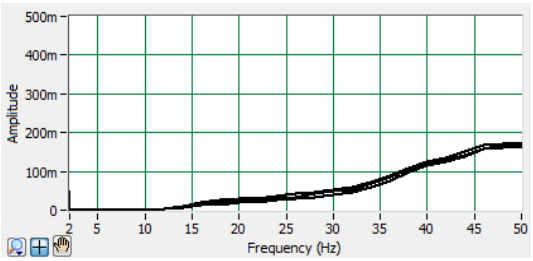

Crib 4: FI=0.84%

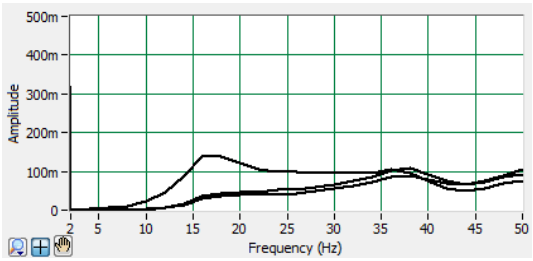

Crib 6: FI=0.79%

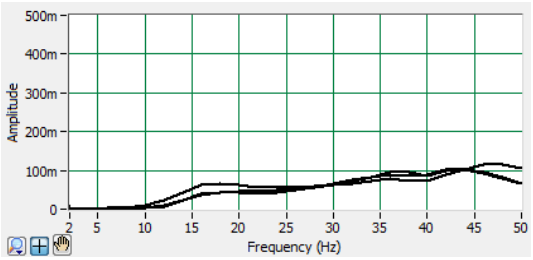

Crib 8: FI=4.80%

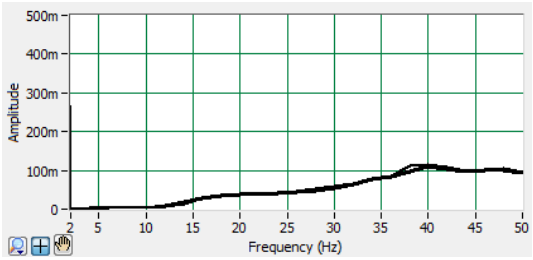

Crib 10: FI=7.20%

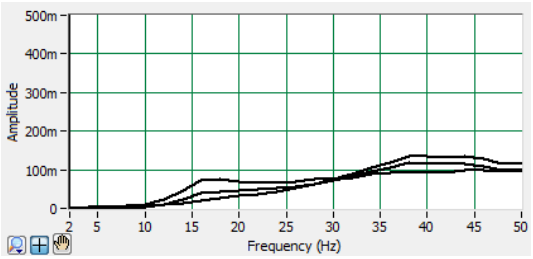

Crib 12: FI=13.79%

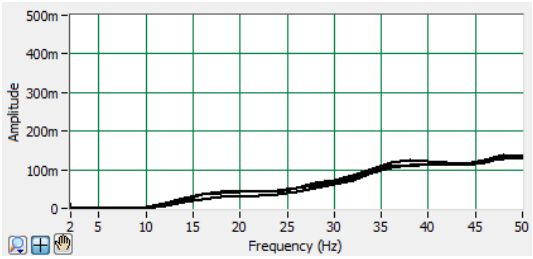

Crib 14: FI=10.79%

Hit Ballast, Measure Rail Full Results									
		Gradient to 18Hz				Mean 18Hz to 50Hz			
		Test			Mid	Test			Mid
Crib	Fouling Index, FI	1	2	3	Value	1	2	3	Value
2	1.05%	0.004	0.003	0.003	*0.003*	0.10	0.10	0.10	*0.10*
3	0.77%	0.001	0.001	0.001	*0.001*	0.08	0.08	0.08	*0.08*
4	0.84%	0.001	0.001	0.001	*0.001*	0.09	0.08	0.08	*0.08*
6	0.79%	0.008	0.002	0.002	*0.002*	0.09	0.06	0.07	*0.07*
8	4.80%	0.004	0.002	0.002	*0.002*	0.08	0.07	0.07	*0.07*
10	7.20%	0.002	0.002	0.002	*0.002*	0.07	0.07	0.07	*0.07*
12	13.79%	0.001	0.004	0.002	*0.002*	0.09	0.08	0.08	*0.08*
14	10.79%	0.002	0.002	0.002	*0.002*	0.09	0.09	0.08	*0.09*
		Correlation with FI:			**0.297**	**Correlation with FI:**			**-0.022**

APPENDIX 8 114KM TO 122KM MULTI-VARIATE REGRESSION (ALL SAMPLES)

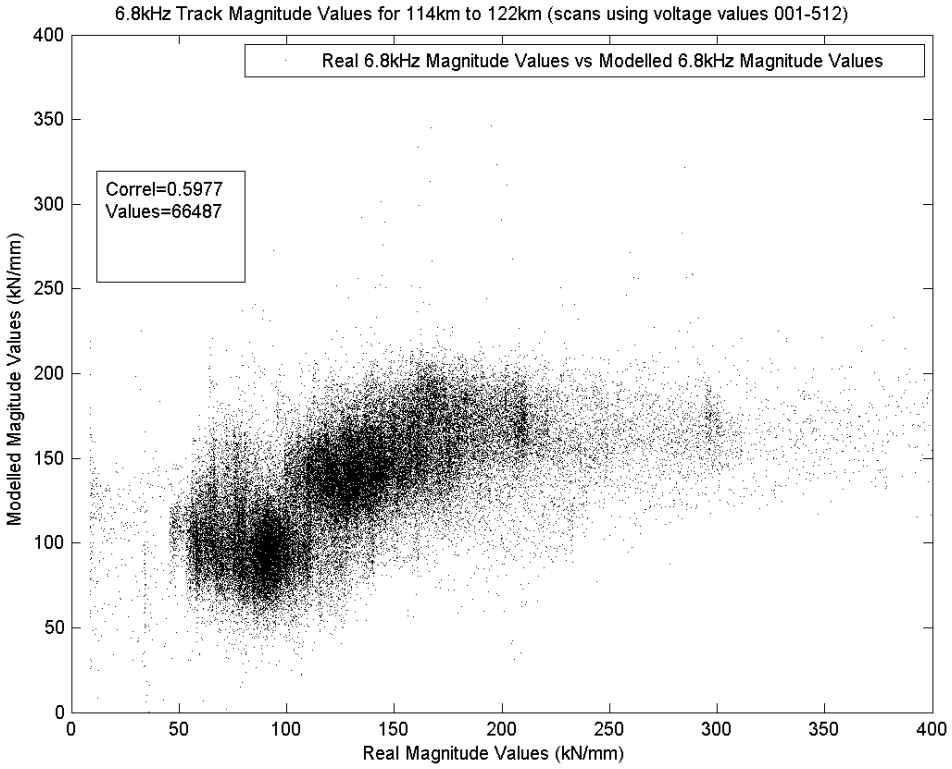
6.8kHz Track Magnitude Values for 114km to 122km (scans using voltage values 001-512)
Real 6.8kHz Magnitude Values vs Modelled 6.8kHz Magnitude Values
Correl=0.5977
Values=66487
Modelled Magitude Values (kN/mm)
Real Magnitude Values (kN/mm)
0
50
100
150
200
250
300
350
400

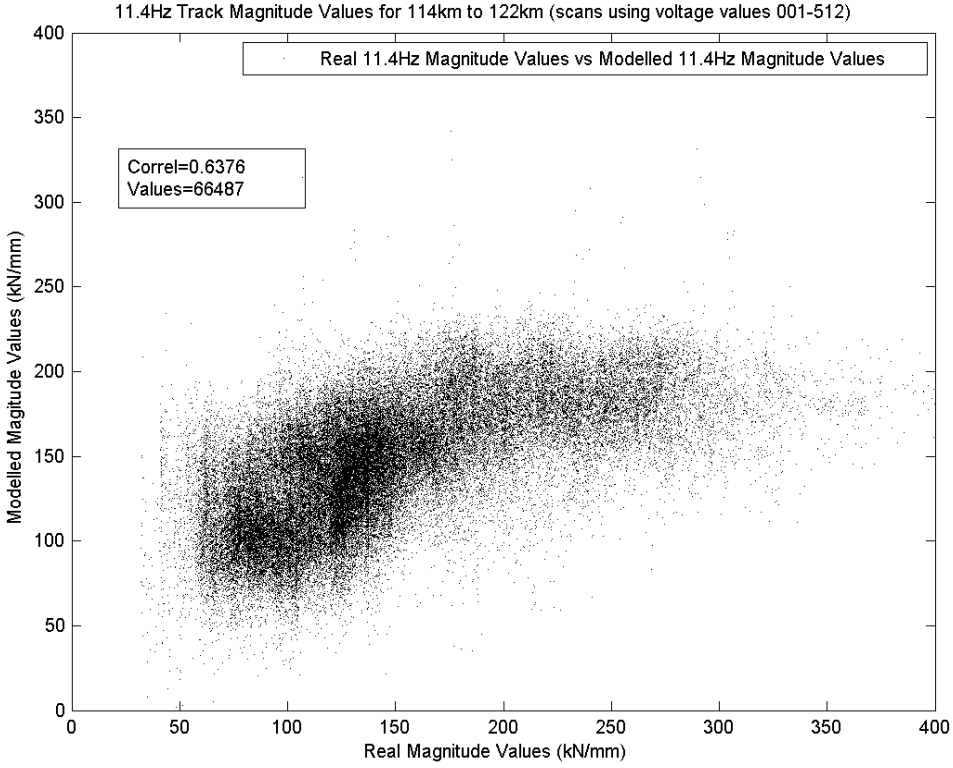
11.4Hz Track Magnitude Values for 114km to 122km (scans using voltage values 001-512)
Real 11.4Hz Magnitude Values vs Modelled 11.4Hz Magnitude Values
Correl=0.6376
Values=66487
Modelled Magitude Values (kN/mm)
Real Magnitude Values (kN/mm)
0
50
100
150
200
250
300
350
400

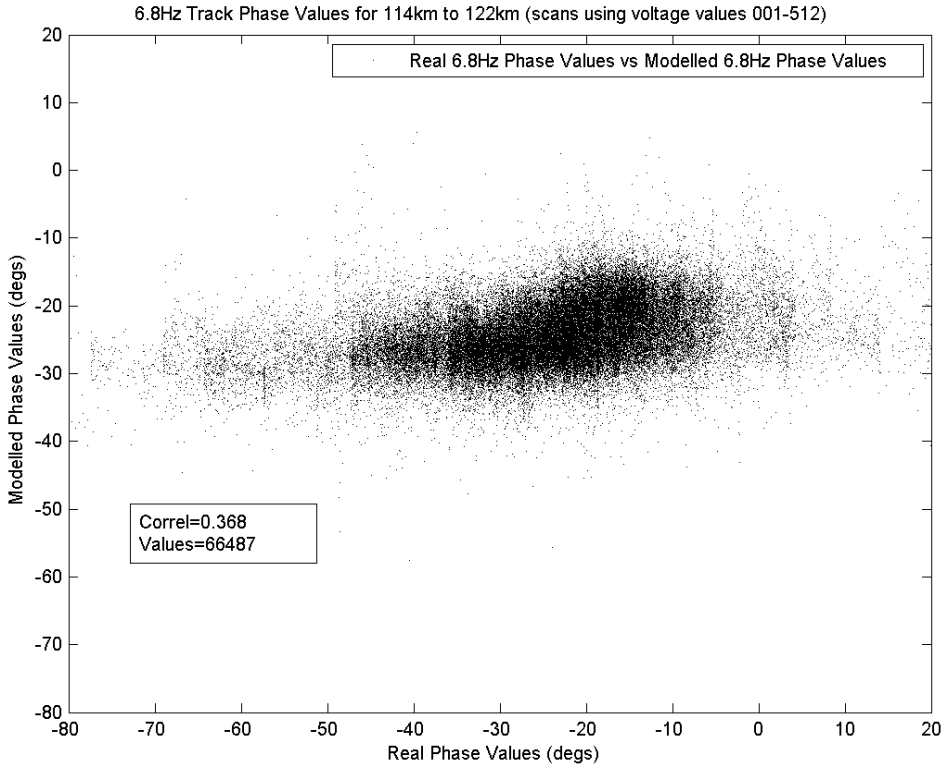
6.8Hz Track Phase Values for 114km to 122km (scans using voltage values 001-512)
Real 6.8Hz Phase Values vs Modelled 6.8Hz Phase Values
Correl=0.368
Values=66487
Modelled Phase Values (degs)
Real Phase Values (degs)
20
10
0
-10
-20
-30
-40
-50
-60
-70
-80

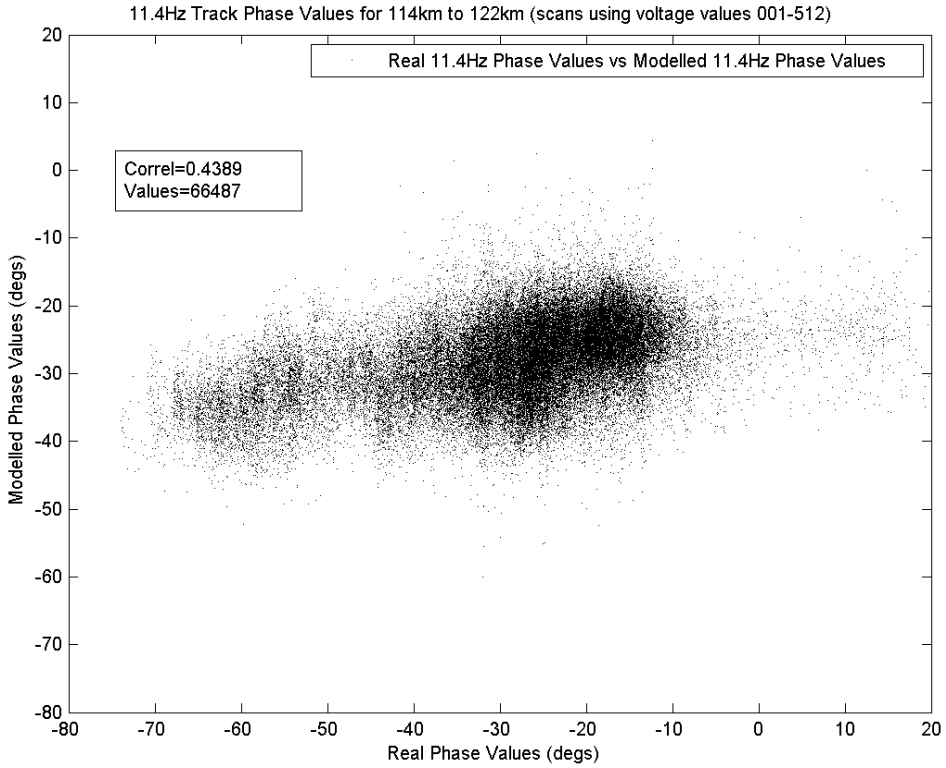
11.4Hz Track Phase Values for 114km to 122km (scans using voltage values 001-512)
Real 11.4Hz Phase Values vs Modelled 11.4Hz Phase Values
Correl=0.4389
Values=66487
Modelled Phase Values (degs)
Real Phase Values (degs)
20
10
0
-10
-20
-30
-40
-50
-60
-70
-80

APPENDIX 9 114KM TO 122KM MULTI-VARIATE REGRESSION (NOT ALL SAMPLES)

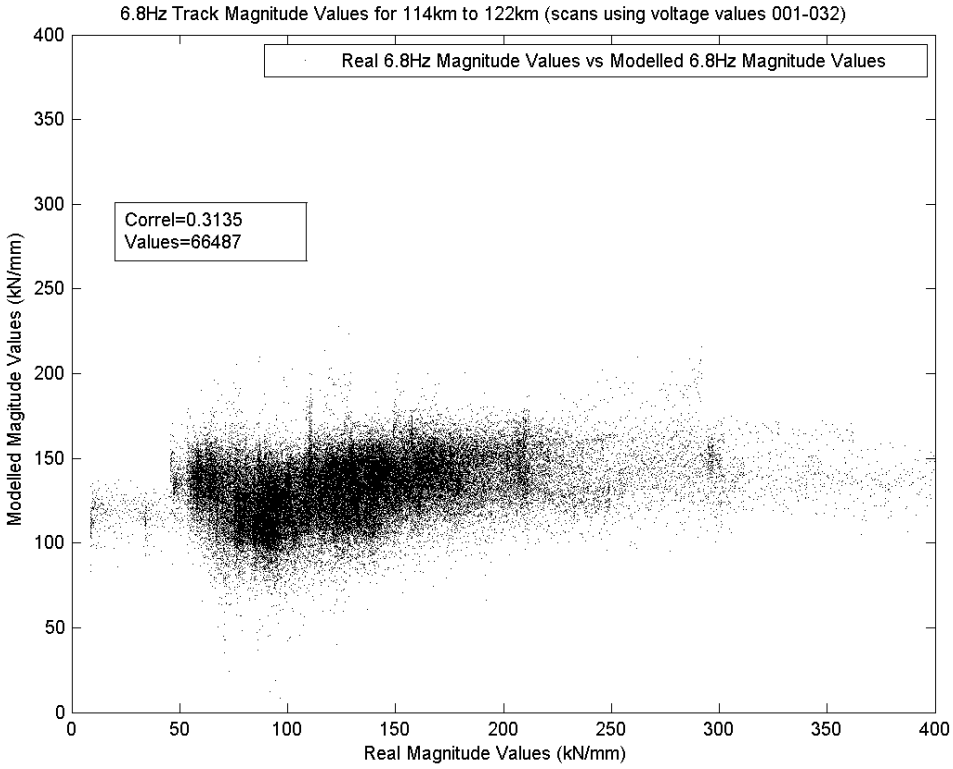
6.8Hz Track Magnitude Values for 114km to 122km (scans using voltage values 001-032)
Real 6.8Hz Magnitude Values vs Modelled 6.8Hz Magnitude Values
Correl=0.3135
Values=66487
Modelled Magitude Values (kN/mm)
Real Magnitude Values (kN/mm)
0
50
100
150
200
250
300
350
400

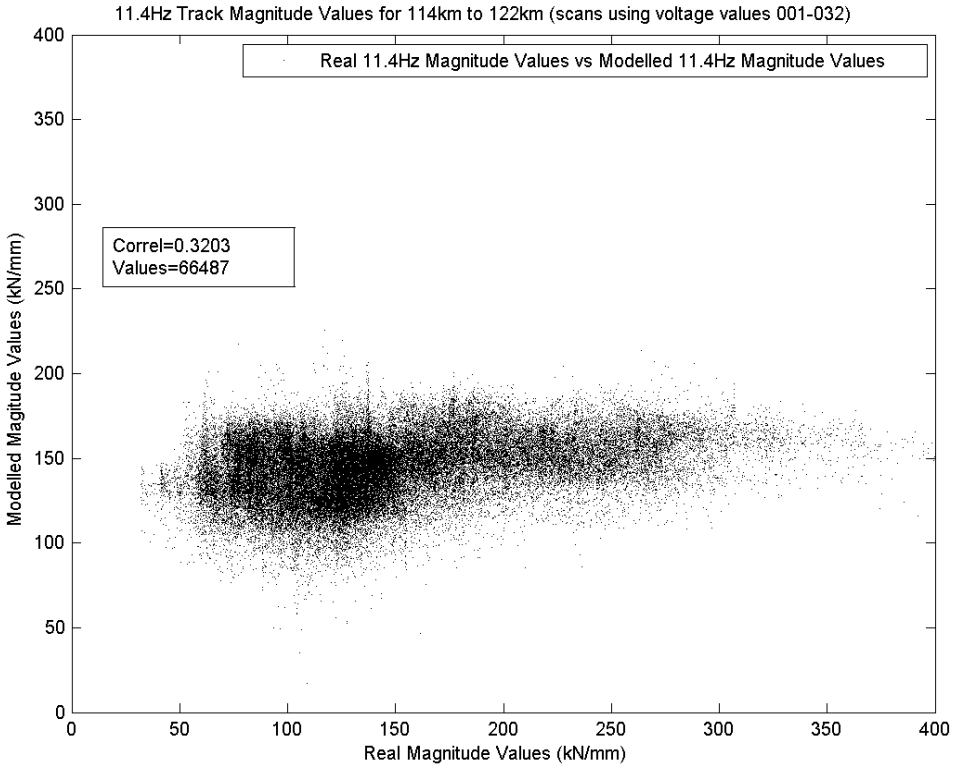
11.4Hz Track Magnitude Values for 114km to 122km (scans using voltage values 001-032)
Real 11.4Hz Magnitude Values vs Modelled 11.4Hz Magnitude Values
Correl=0.3203
Values=66487
Modelled Magitude Values (kN/mm)
Real Magnitude Values (kN/mm)
0
50
100
150
200
250
300
350
400

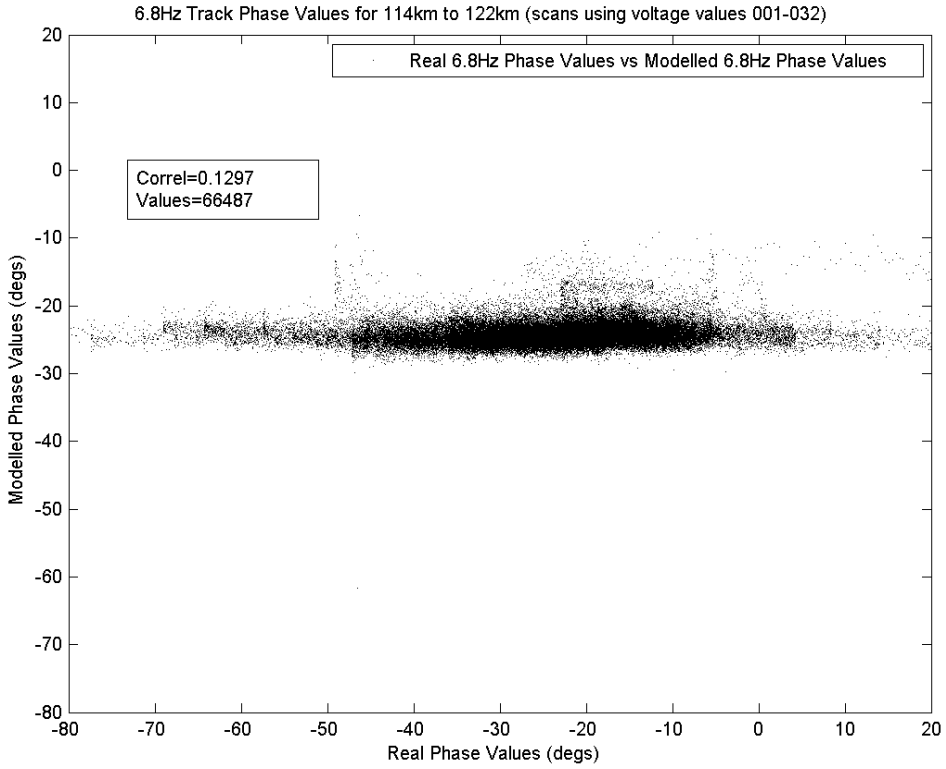
6.8Hz Track Phase Values for 114km to 122km (scans using voltage values 001-032)
Real 6.8Hz Phase Values vs Modelled 6.8Hz Phase Values
Correl=0.1297
Values=66487
Modelled Phase Values (degs)
Real Phase Values (degs)
20
10
0
-10
-20
-30
-40
-50
-60
-70
-80

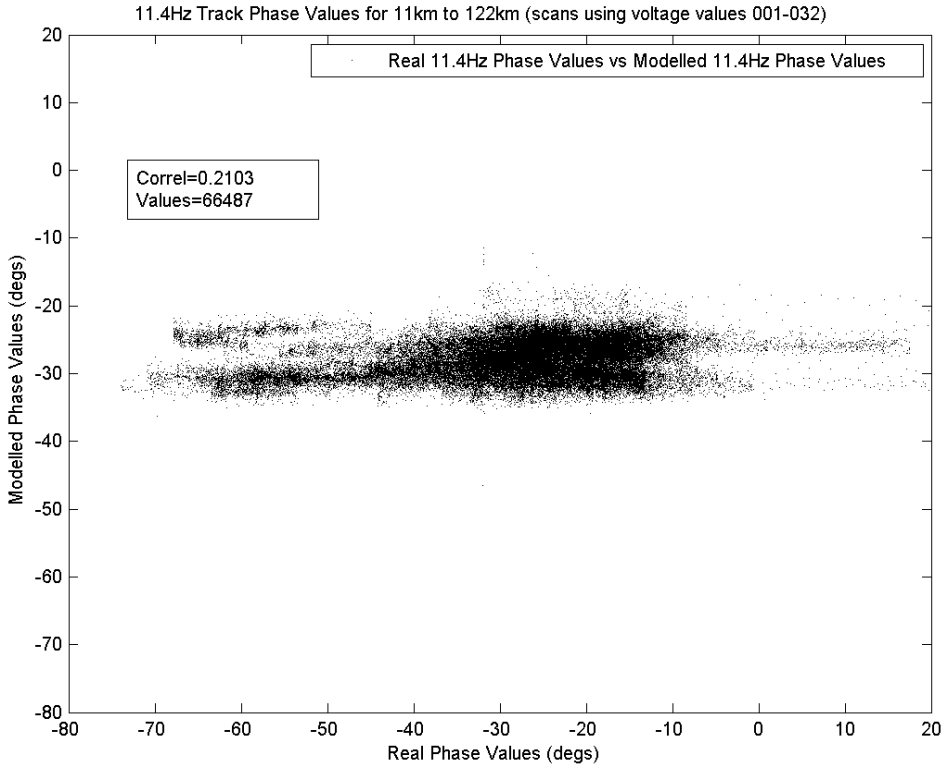
11.4Hz Track Phase Values for 11km to 122km (scans using voltage values 001-032)
Real 11.4Hz Phase Values vs Modelled 11.4Hz Phase Values
Correl=0.2103
Values=66487
Modelled Phase Values (degs)
Real Phase Values (degs)
20
10
0
-10
-20
-30
-40
-50
-60
-70
-80

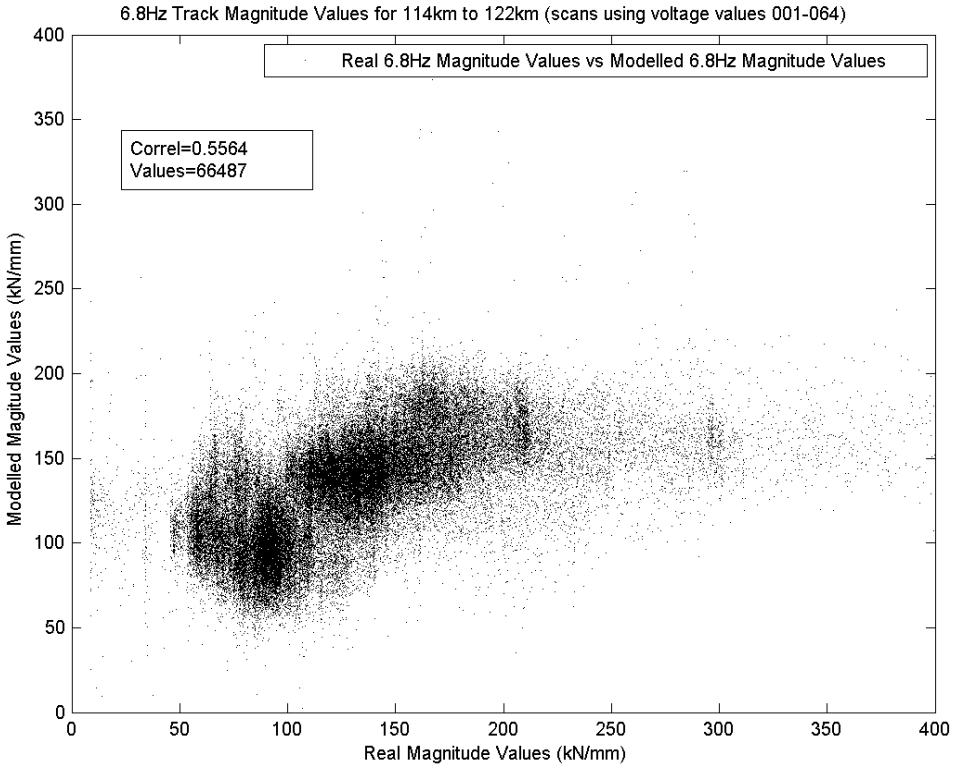
6.8Hz Track Magnitude Values for 114km to 122km (scans using voltage values 001-064)
Real 6.8Hz Magnitude Values vs Modelled 6.8Hz Magnitude Values
Correl=0.5564
Values=66487
Modelled Magitude Values (kN/mm)
Real Magnitude Values (kN/mm)
0
50
100
150
200
250
300
350
400

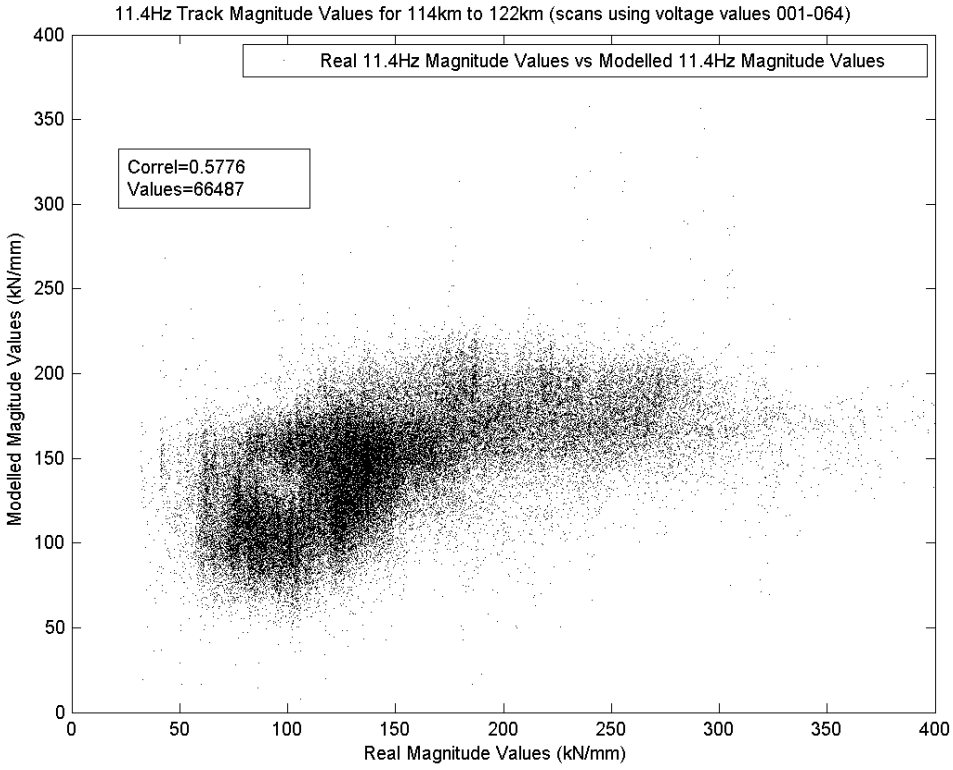
11.4Hz Track Magnitude Values for 114km to 122km (scans using voltage values 001-064)
Real 11.4Hz Magnitude Values vs Modelled 11.4Hz Magnitude Values
Correl=0.5776
Values=66487
Modelled Magitude Values (kN/mm)
Real Magnitude Values (kN/mm)
0
50
100
150
200
250
300
350
400

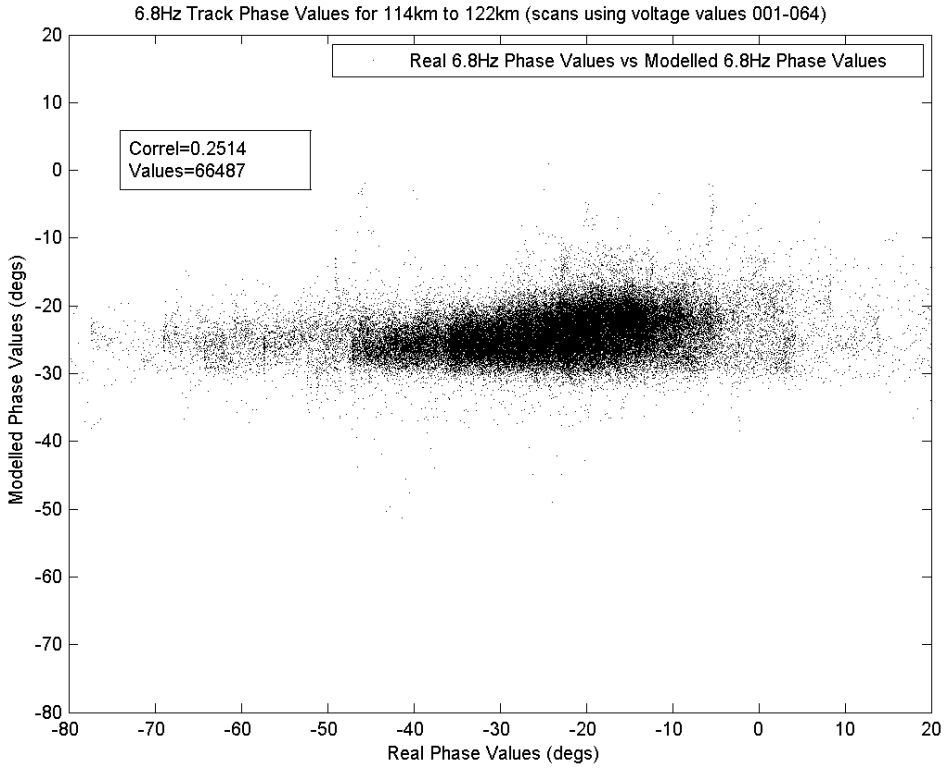
6.8Hz Track Phase Values for 114km to 122km (scans using voltage values 001-064)
Real 6.8Hz Phase Values vs Modelled 6.8Hz Phase Values
Correl=0.2514
Values=66487
Modelled Phase Values (degs)
Real Phase Values (degs)
20
10
0
-10
-20
-30
-40
-50
-60
-70
-80

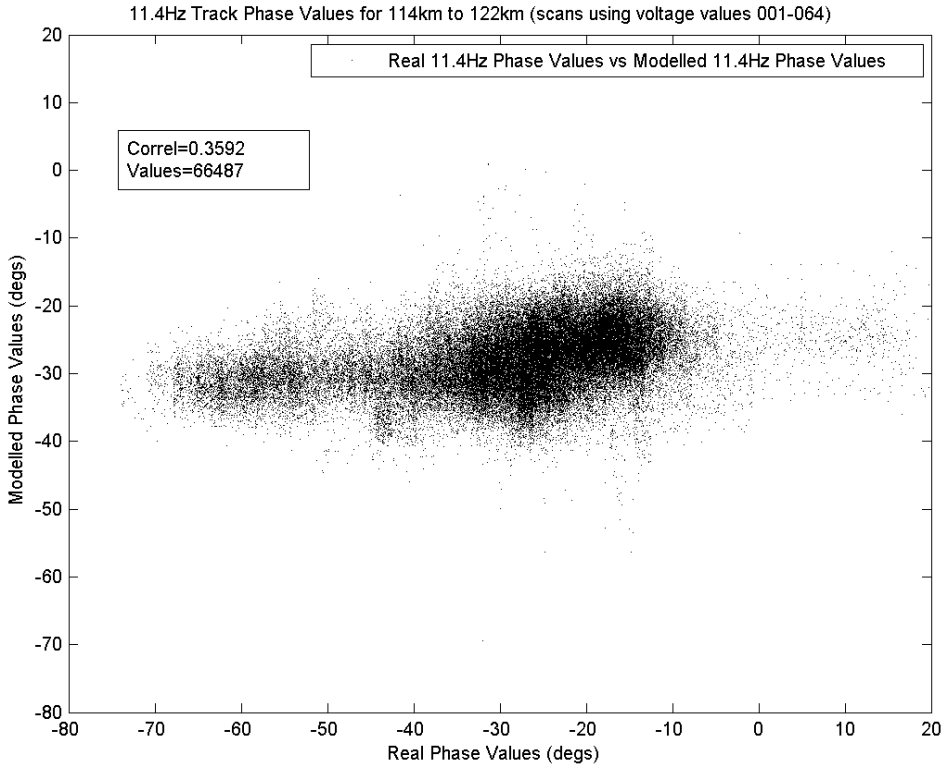
11.4Hz Track Phase Values for 114km to 122km (scans using voltage values 001-064)
Real 11.4Hz Phase Values vs Modelled 11.4Hz Phase Values
Correl=0.3592
Values=66487
Modelled Phase Values (degs)
Real Phase Values (degs)
20
10
0
-10
-20
-30
-40
-50
-60
-70
-80

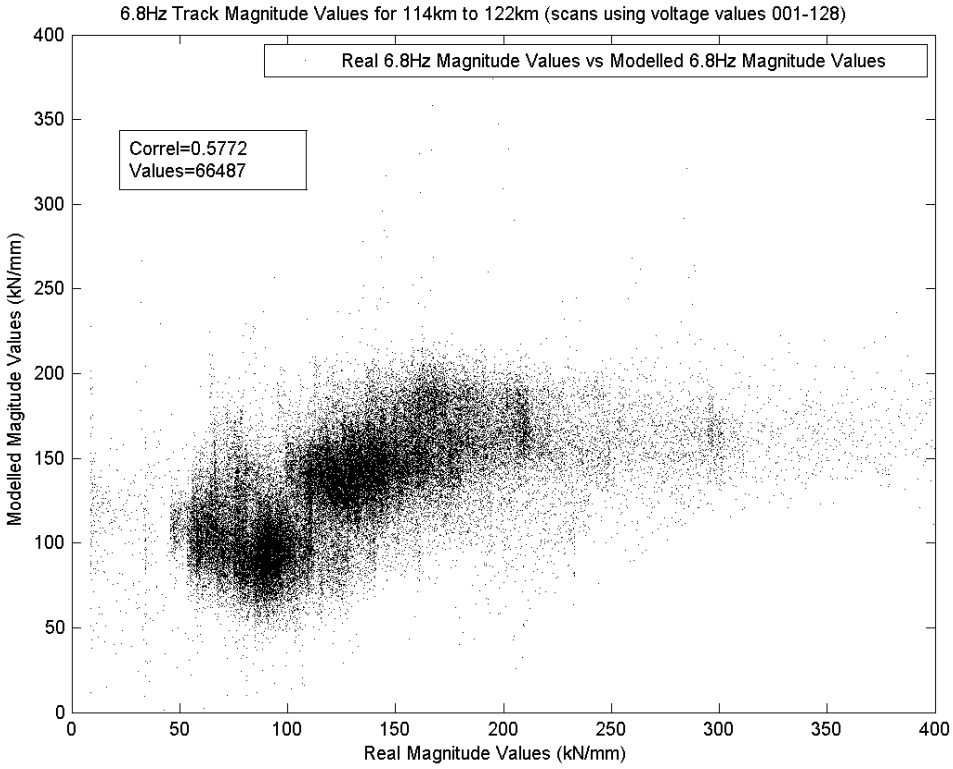
6.8Hz Track Magnitude Values for 114km to 122km (scans using voltage values 001-128)
Real 6.8Hz Magnitude Values vs Modelled 6.8Hz Magnitude Values
Correl=0.5772
Values=66487
Modelled Magitude Values (kN/mm)
Real Magnitude Values (kN/mm)
0
50
100
150
200
250
300
350
400

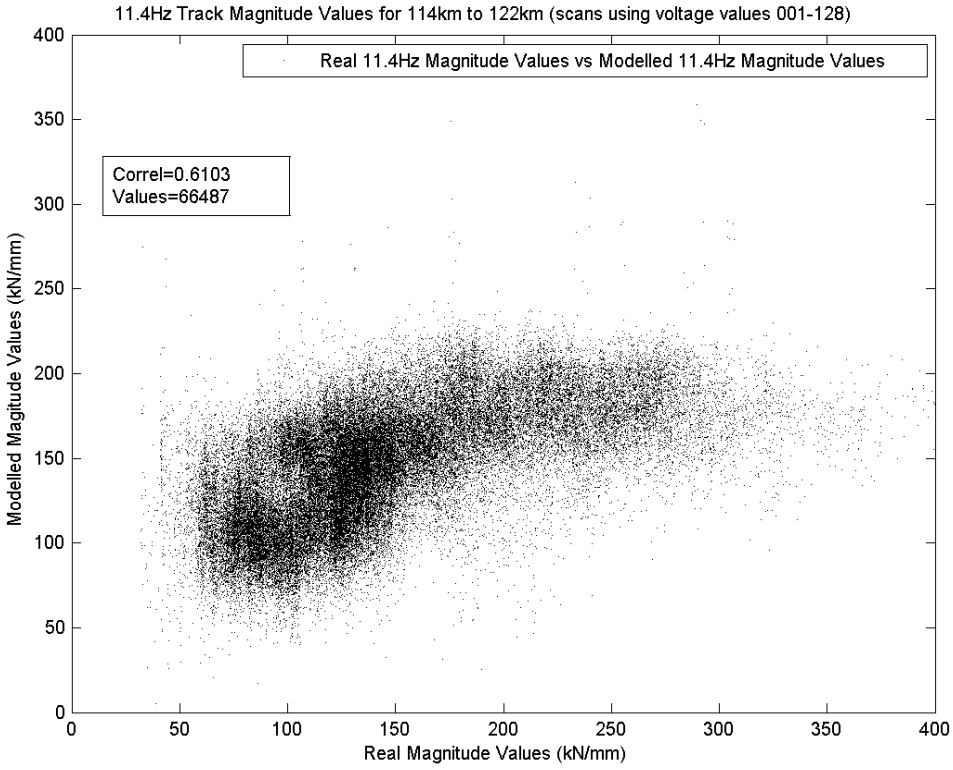
11.4Hz Track Magnitude Values for 114km to 122km (scans using voltage values 001-128)
Real 11.4Hz Magnitude Values vs Modelled 11.4Hz Magnitude Values
Correl=0.6103
Values=66487
Modelled Magitude Values (kN/mm)
Real Magnitude Values (kN/mm)
0
50
100
150
200
250
300
350
400

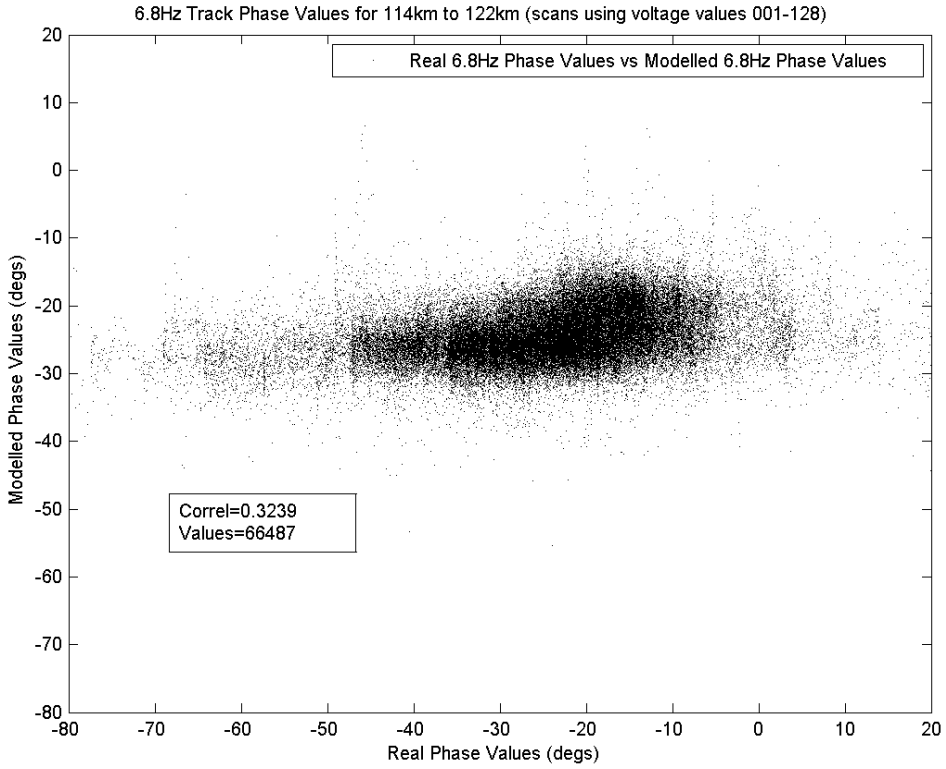
6.8Hz Track Phase Values for 114km to 122km (scans using voltage values 001-128)
Real 6.8Hz Phase Values vs Modelled 6.8Hz Phase Values
Correl=0.3239
Values=66487
Modelled Phase Values (degs)
Real Phase Values (degs)
20
10
0
-10
-20
-30
-40
-50
-60
-70
-80

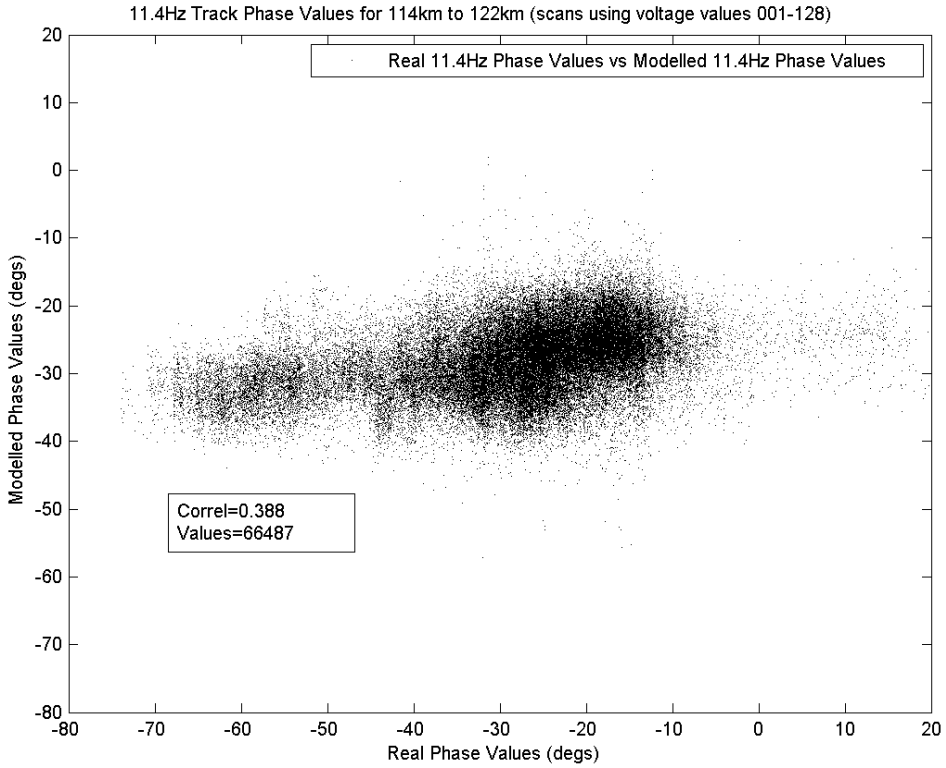
11.4Hz Track Phase Values for 114km to 122km (scans using voltage values 001-128)
Real 11.4Hz Phase Values vs Modelled 11.4Hz Phase Values
Correl=0.388
Values=66487
Modelled Phase Values (degs)
Real Phase Values (degs)
20
10
0
-10
-20
-30
-40
-50
-60
-70
-80

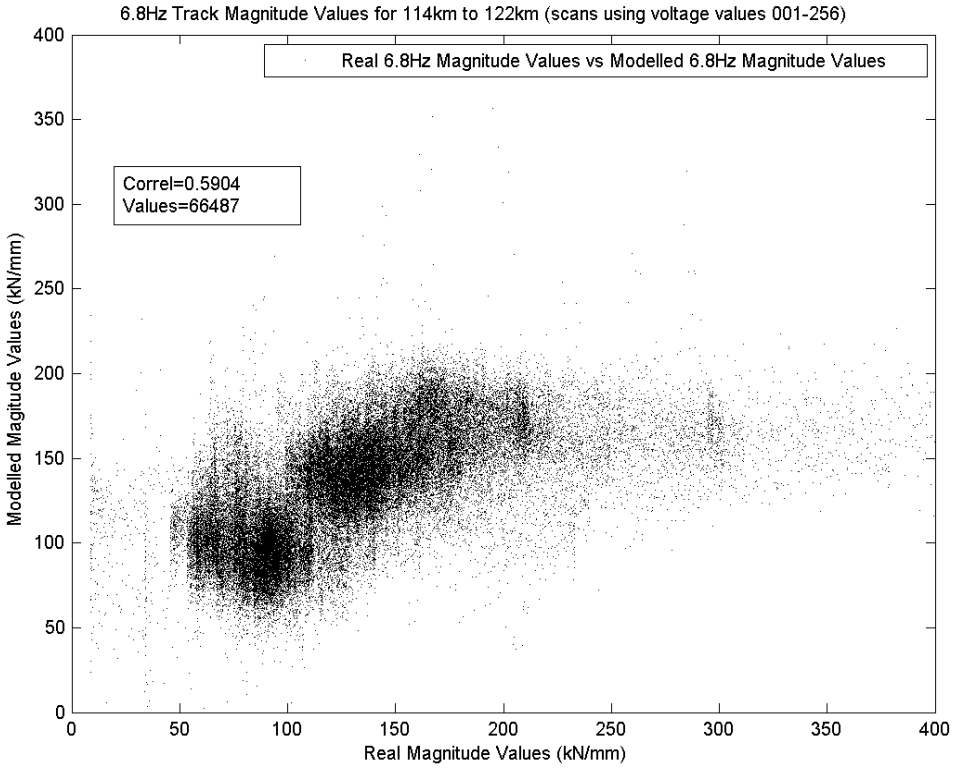
6.8Hz Track Magnitude Values for 114km to 122km (scans using voltage values 001-256)
Real 6.8Hz Magnitude Values vs Modelled 6.8Hz Magnitude Values
Correl=0.5904
Values=66487
Modelled Magitude Values (kN/mm)
Real Magnitude Values (kN/mm)
0
50
100
150
200
250
300
350
400

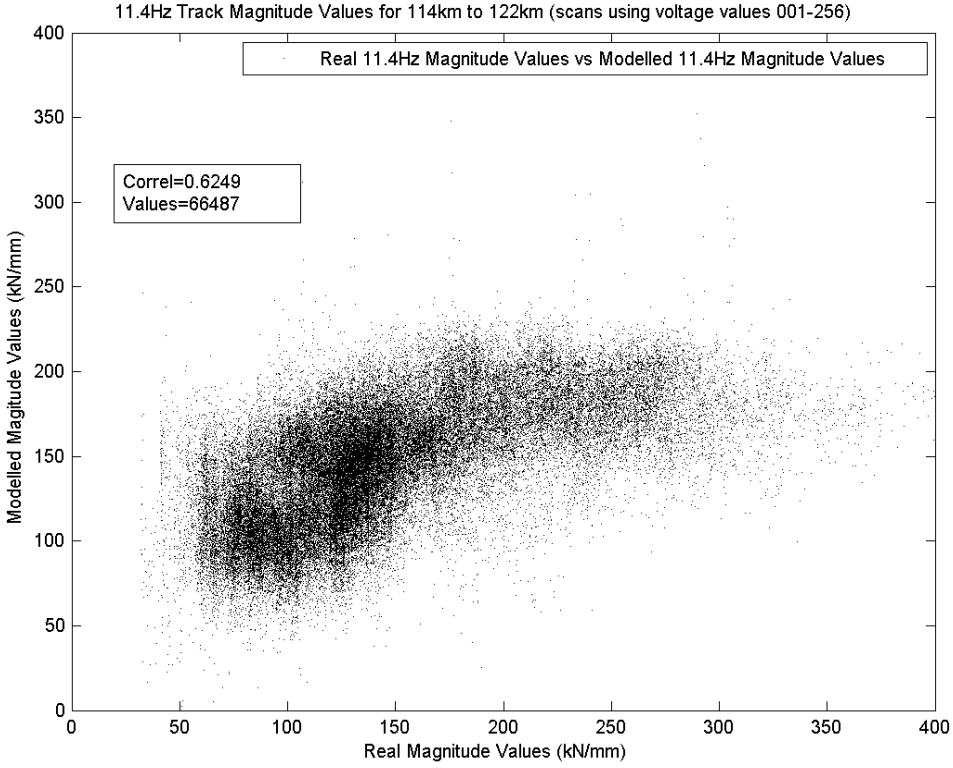
11.4Hz Track Magnitude Values for 114km to 122km (scans using voltage values 001-256)
Real 11.4Hz Magnitude Values vs Modelled 11.4Hz Magnitude Values
Correl=0.6249
Values=66487
Modelled Magitude Values (kN/mm)
Real Magnitude Values (kN/mm)
0
50
100
150
200
250
300
350
400

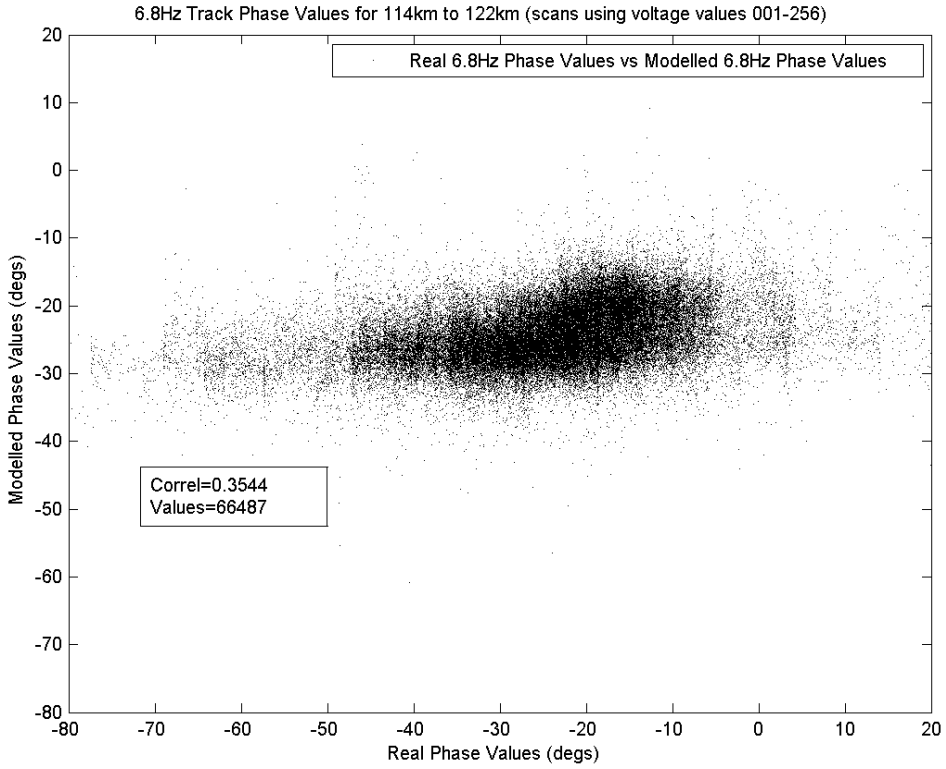
6.8Hz Track Phase Values for 114km to 122km (scans using voltage values 001-256)
Real 6.8Hz Phase Values vs Modelled 6.8Hz Phase Values
Correl=0.3544
Values=66487
Modelled Phase Values (degs)
Real Phase Values (degs)
20
10
0
-10
-20
-30
-40
-50
-60
-70
-80

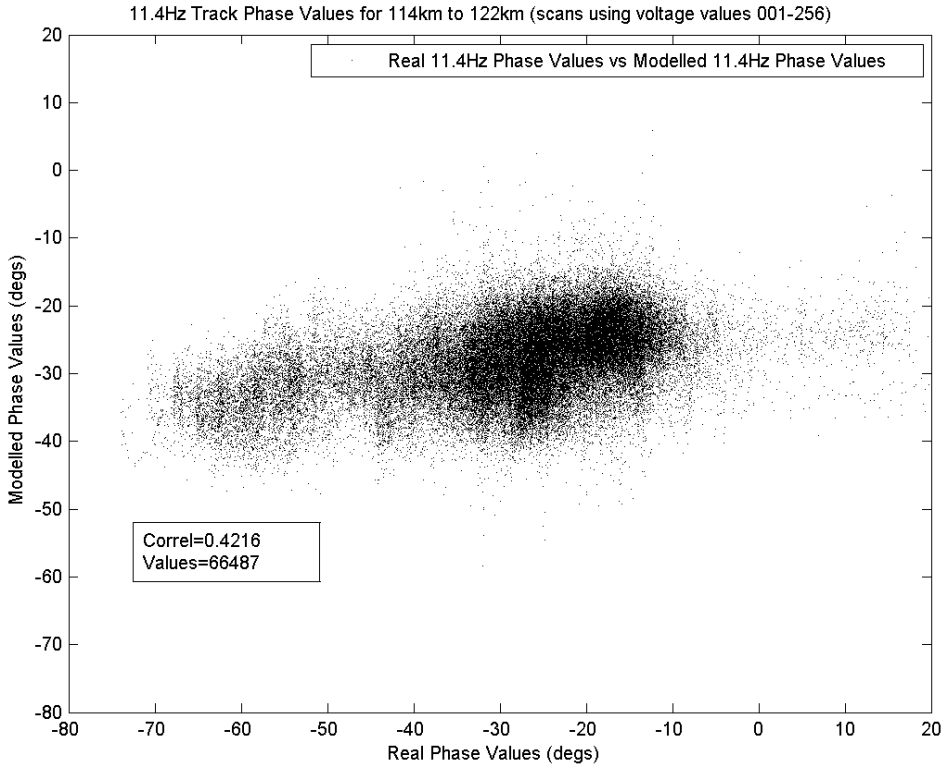
11.4Hz Track Phase Values for 114km to 122km (scans using voltage values 001-256)
Real 11.4Hz Phase Values vs Modelled 11.4Hz Phase Values
Correl=0.4216
Values=66487
Modelled Phase Values (degs)
Real Phase Values (degs)
20
10
0
-10
-20
-30
-40
-50
-60
-70
-80

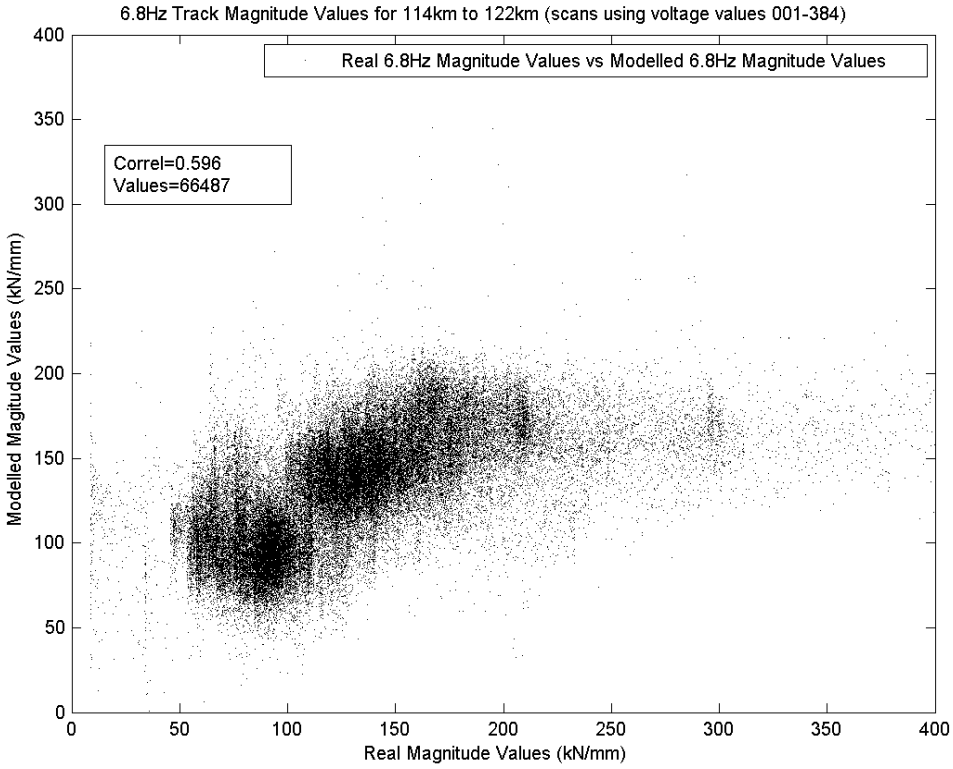
6.8Hz Track Magnitude Values for 114km to 122km (scans using voltage values 001-384)
Real 6.8Hz Magnitude Values vs Modelled 6.8Hz Magnitude Values
Correl=0.596
Values=66487
Modelled Magitude Values (kN/mm)
Real Magnitude Values (kN/mm)
0
50
100
150
200
250
300
350
400

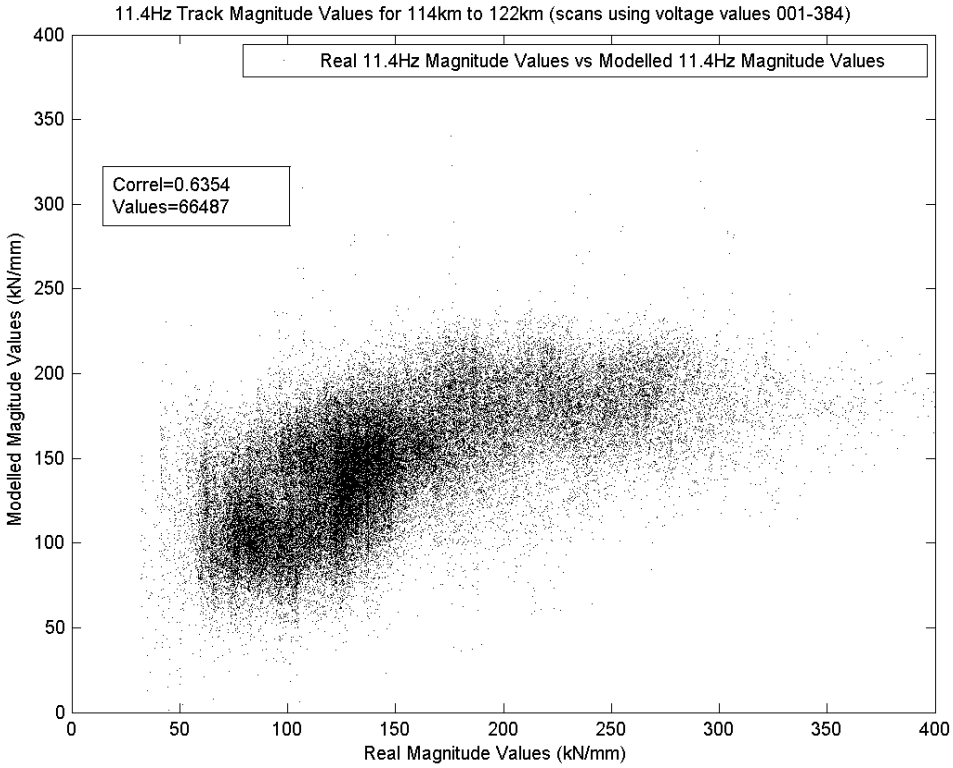
11.4Hz Track Magnitude Values for 114km to 122km (scans using voltage values 001-384)
Real 11.4Hz Magnitude Values vs Modelled 11.4Hz Magnitude Values
Correl=0.6354
Values=66487
Modelled Magitude Values (kN/mm)
Real Magnitude Values (kN/mm)
0
50
100
150
200
250
300
350
400

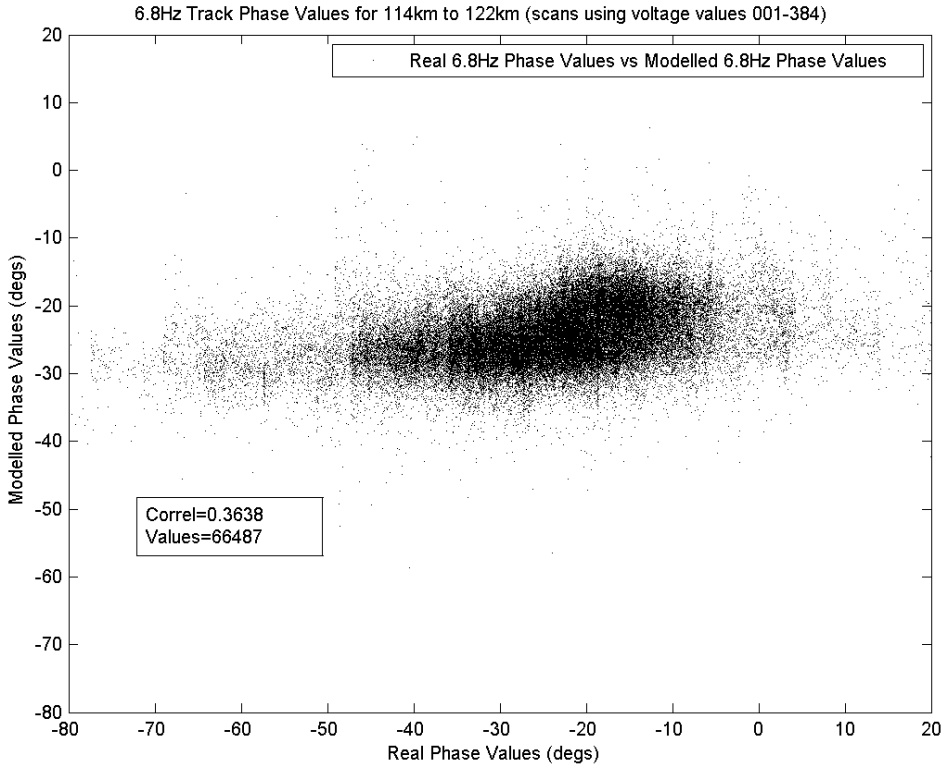
6.8Hz Track Phase Values for 114km to 122km (scans using voltage values 001-384)
Real 6.8Hz Phase Values vs Modelled 6.8Hz Phase Values
Correl=0.3638
Values=66487
Modelled Phase Values (degs)
Real Phase Values (degs)
20
10
0
-10
-20
-30
-40
-50
-60
-70
-80

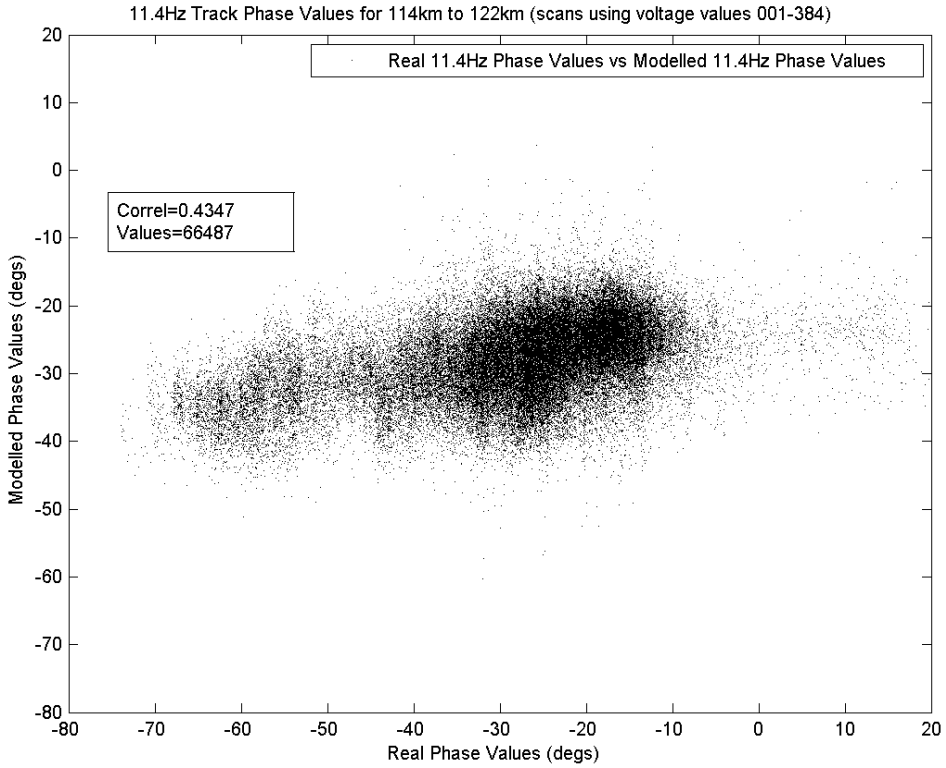
11.4Hz Track Phase Values for 114km to 122km (scans using voltage values 001-384)
Real 11.4Hz Phase Values vs Modelled 11.4Hz Phase Values
Correl=0.4347
Values=66487
Modelled Phase Values (degs)
Real Phase Values (degs)
20
10
0
-10
-20
-30
-40
-50
-60
-70
-80

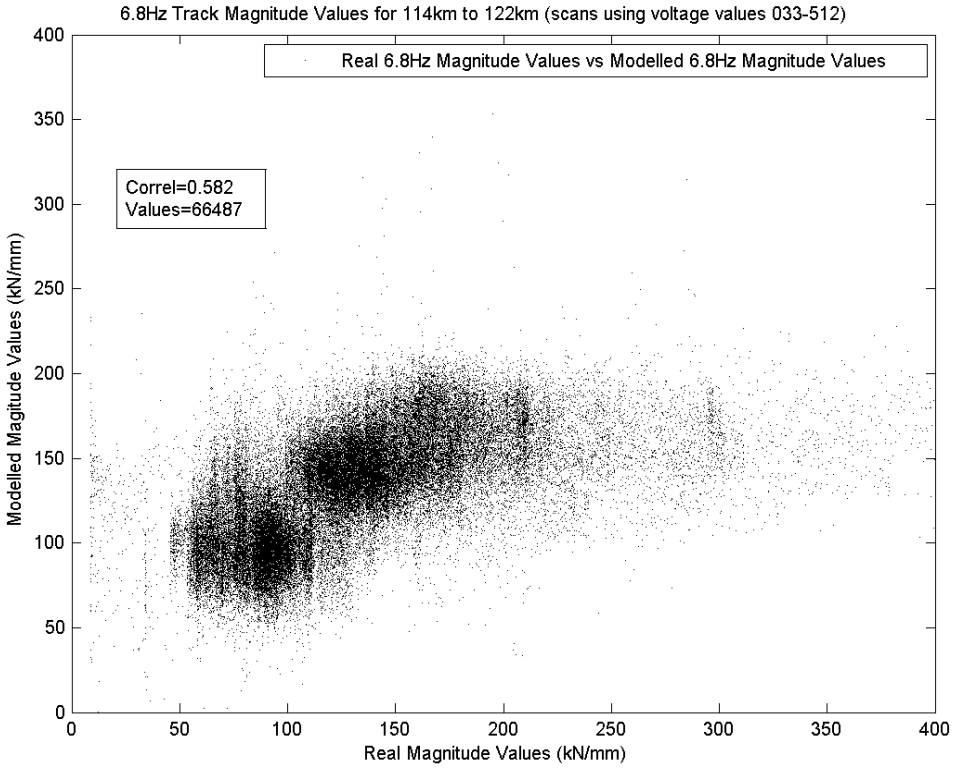
6.8Hz Track Magnitude Values for 114km to 122km (scans using voltage values 033-512)
Real 6.8Hz Magnitude Values vs Modelled 6.8Hz Magnitude Values
Correl=0.582
Values=66487
Modelled Magitude Values (kN/mm)
Real Magnitude Values (kN/mm)
0
50
100
150
200
250
300
350
400

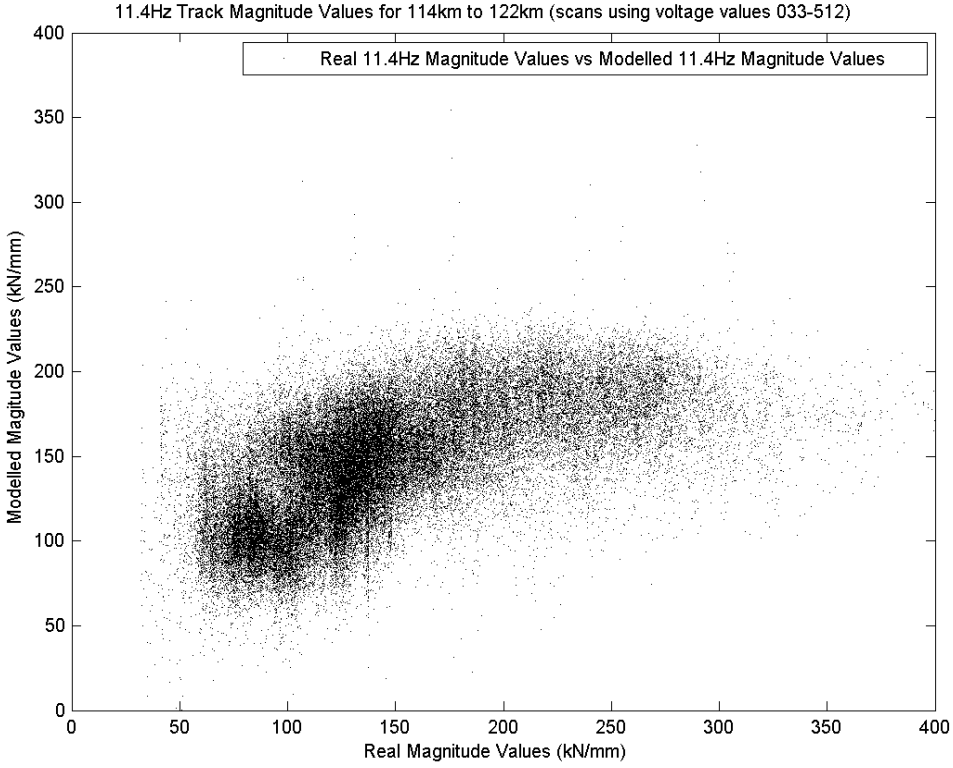
11.4Hz Track Magnitude Values for 114km to 122km (scans using voltage values 033-512)
Real 11.4Hz Magnitude Values vs Modelled 11.4Hz Magnitude Values
Modelled Magitude Values (kN/mm)
Real Magnitude Values (kN/mm)
0
50
100
150
200
250
300
350
400

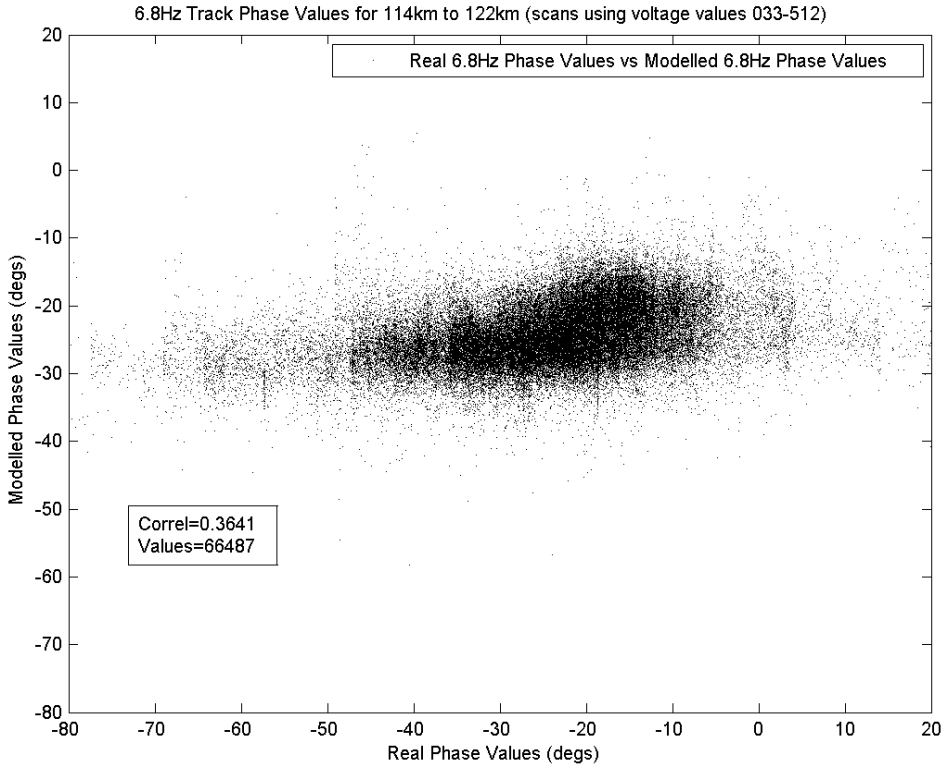
6.8Hz Track Phase Values for 114km to 122km (scans using voltage values 033-512)
Real 6.8Hz Phase Values vs Modelled 6.8Hz Phase Values
Correl=0.3641
Values=66487
Modelled Phase Values (degs)
Real Phase Values (degs)
20
10
0
-10
-20
-30
-40
-50
-60
-70
-80

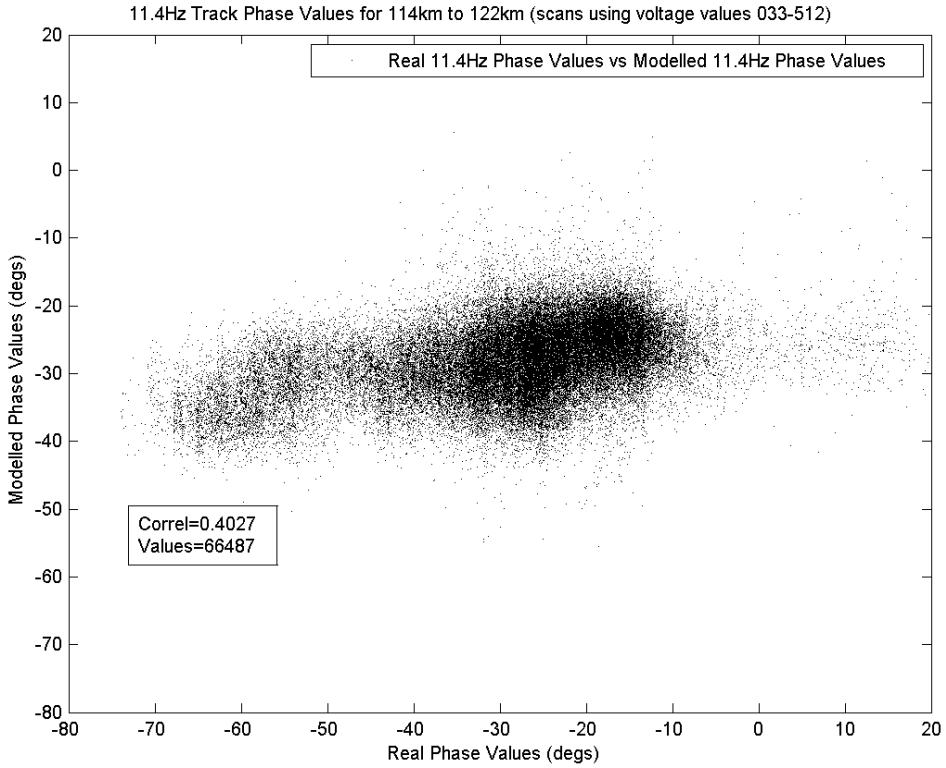
11.4Hz Track Phase Values for 114km to 122km (scans using voltage values 033-512)
Real 11.4Hz Phase Values vs Modelled 11.4Hz Phase Values
Correl=0.4027
Values=66487
Modelled Phase Values (degs)
Real Phase Values (degs)
20
10
0
-10
-20
-30
-40
-50
-60
-70
-80

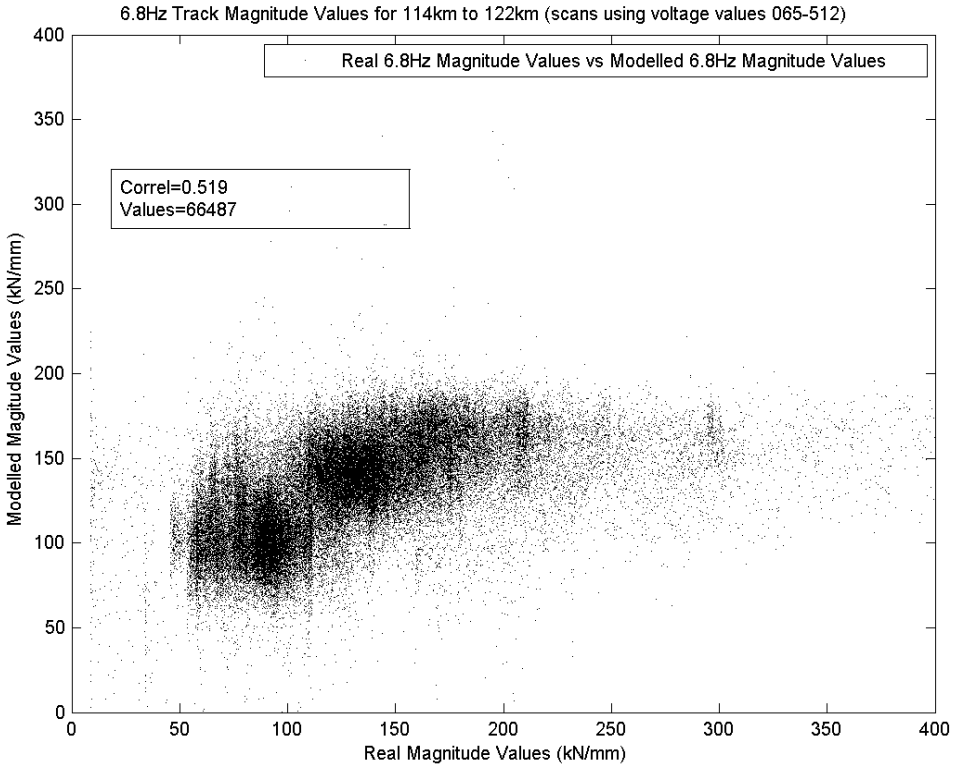
6.8Hz Track Magnitude Values for 114km to 122km (scans using voltage values 065-512)
Real 6.8Hz Magnitude Values vs Modelled 6.8Hz Magnitude Values
Correl=0.519
Values=66487
Modelled Magitude Values (kN/mm)
Real Magnitude Values (kN/mm)
0
50
100
150
200
250
300
350
400

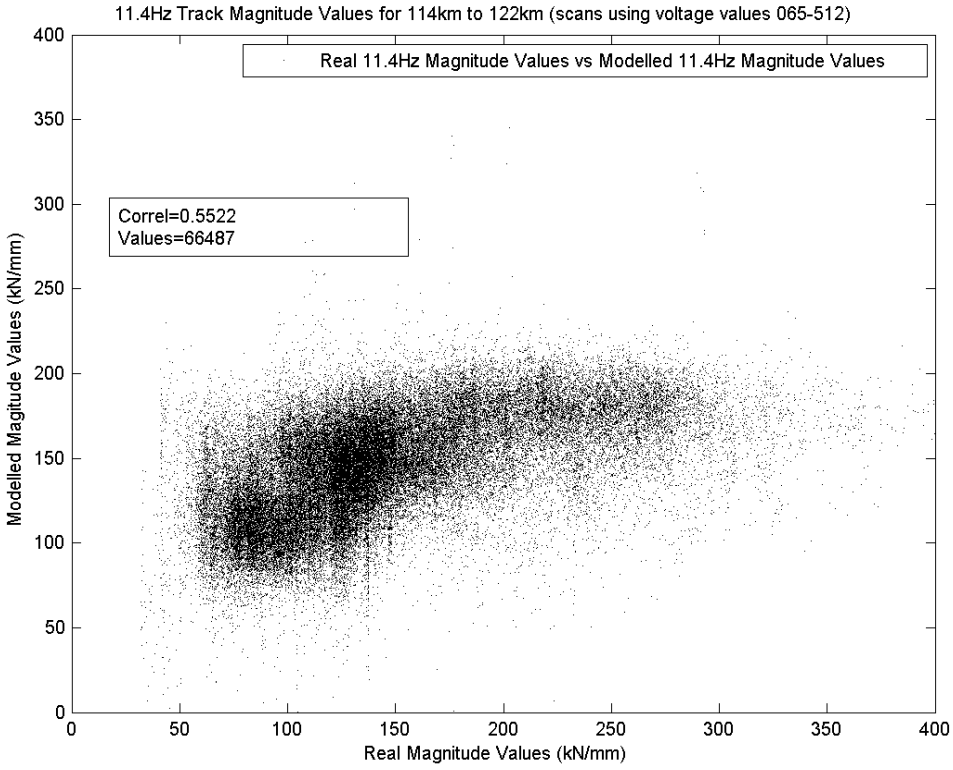
11.4Hz Track Magnitude Values for 114km to 122km (scans using voltage values 065-512)
Real 11.4Hz Magnitude Values vs Modelled 11.4Hz Magnitude Values
Correl=0.5522
Values=66487
Modelled Magitude Values (kN/mm)
Real Magnitude Values (kN/mm)
0
50
100
150
200
250
300
350
400

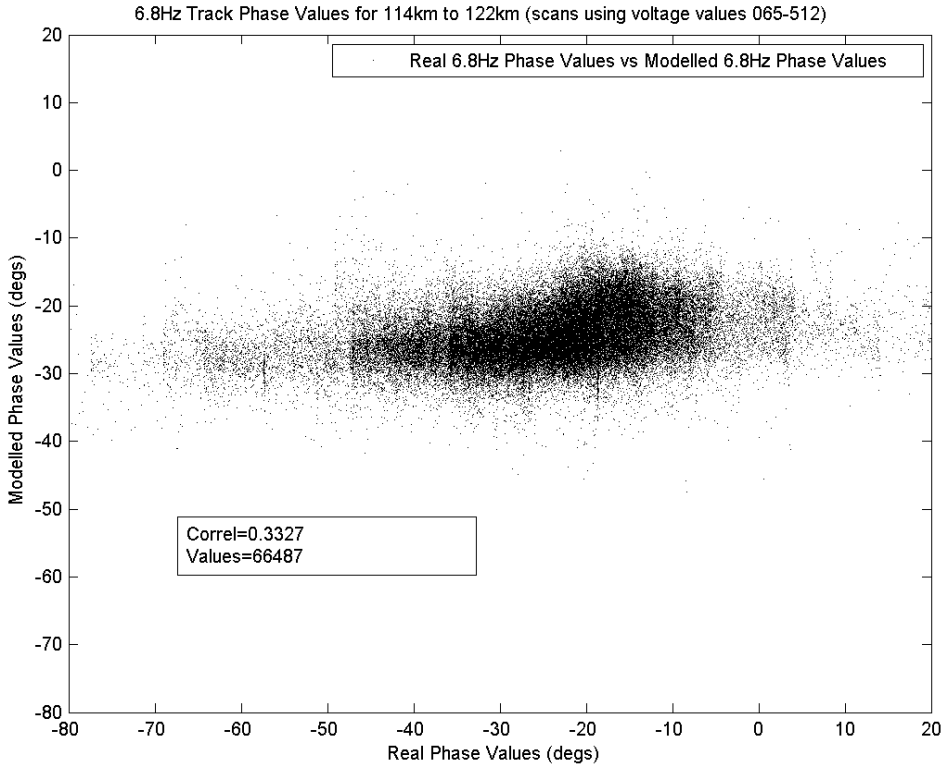
6.8Hz Track Phase Values for 114km to 122km (scans using voltage values 065-512)
Real 6.8Hz Phase Values vs Modelled 6.8Hz Phase Values
Correl=0.3327
Values=66487
Modelled Phase Values (degs)
Real Phase Values (degs)
20
10
0
-10
-20
-30
-40
-50
-60
-70
-80

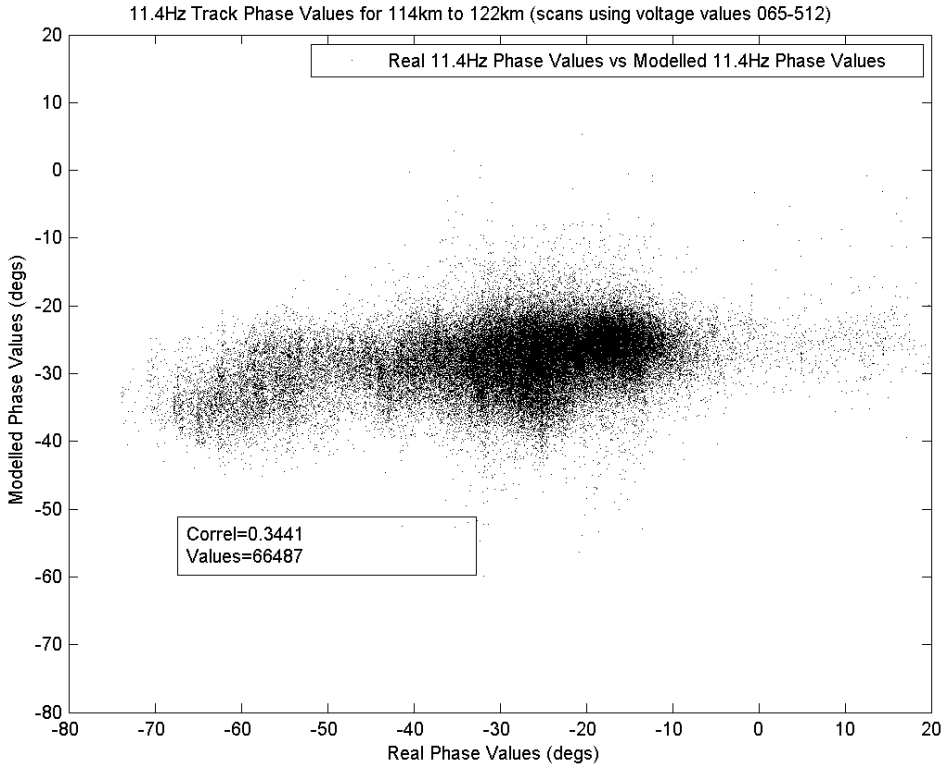
11.4Hz Track Phase Values for 114km to 122km (scans using voltage values 065-512)
Real 11.4Hz Phase Values vs Modelled 11.4Hz Phase Values
Correl=0.3441
Values=66487
Modelled Phase Values (degs)
Real Phase Values (degs)
20
10
0
-10
-20
-30
-40
-50
-60
-70
-80

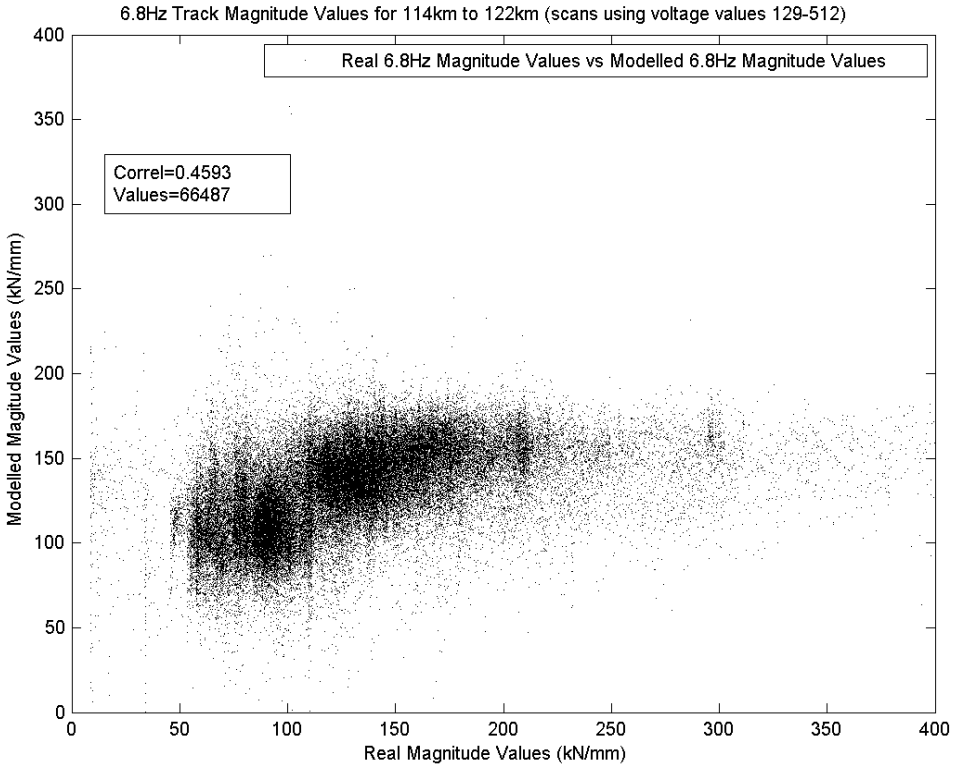
6.8Hz Track Magnitude Values for 114km to 122km (scans using voltage values 129-512)
Real 6.8Hz Magnitude Values vs Modelled 6.8Hz Magnitude Values
Correl=0.4593
Values=66487
Modelled Magitude Values (kN/mm)
Real Magnitude Values (kN/mm)
0
50
100
150
200
250
300
350
400

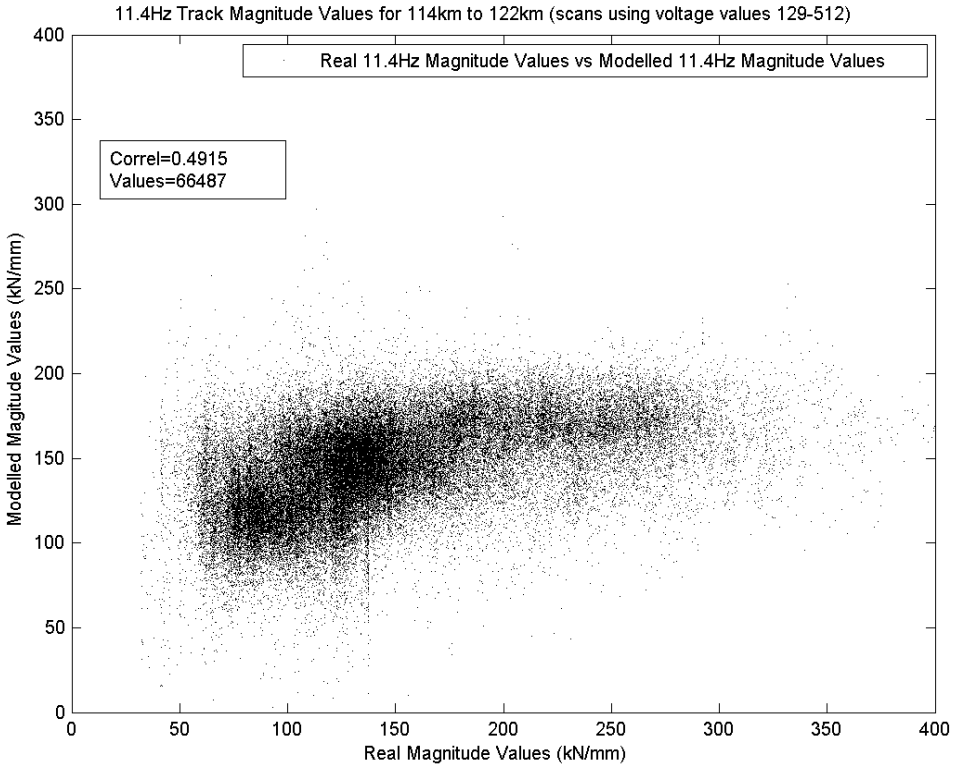
11.4Hz Track Magnitude Values for 114km to 122km (scans using voltage values 129-512)
Real 11.4Hz Magnitude Values vs Modelled 11.4Hz Magnitude Values
Correl=0.4915
Values=66487
Modelled Magitude Values (kN/mm)
Real Magnitude Values (kN/mm)
0
50
100
150
200
250
300
350
400

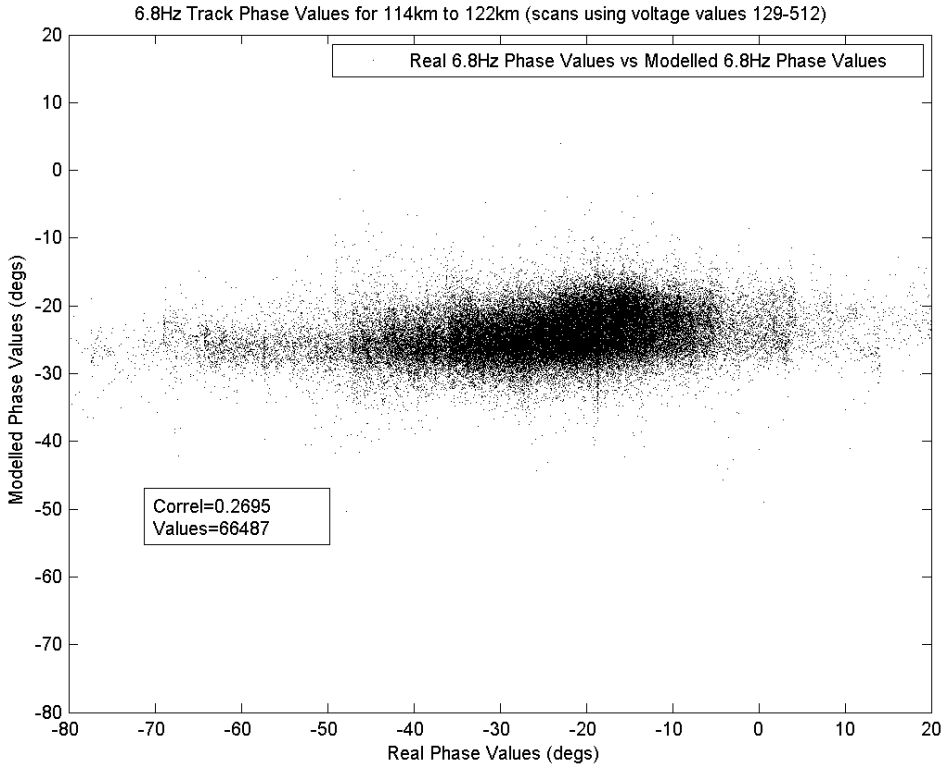
6.8Hz Track Phase Values for 114km to 122km (scans using voltage values 129-512)
Real 6.8Hz Phase Values vs Modelled 6.8Hz Phase Values
Correl=0.2695
Values=66487
Modelled Phase Values (degs)
Real Phase Values (degs)
20
10
0
-10
-20
-30
-40
-50
-60
-70
-80

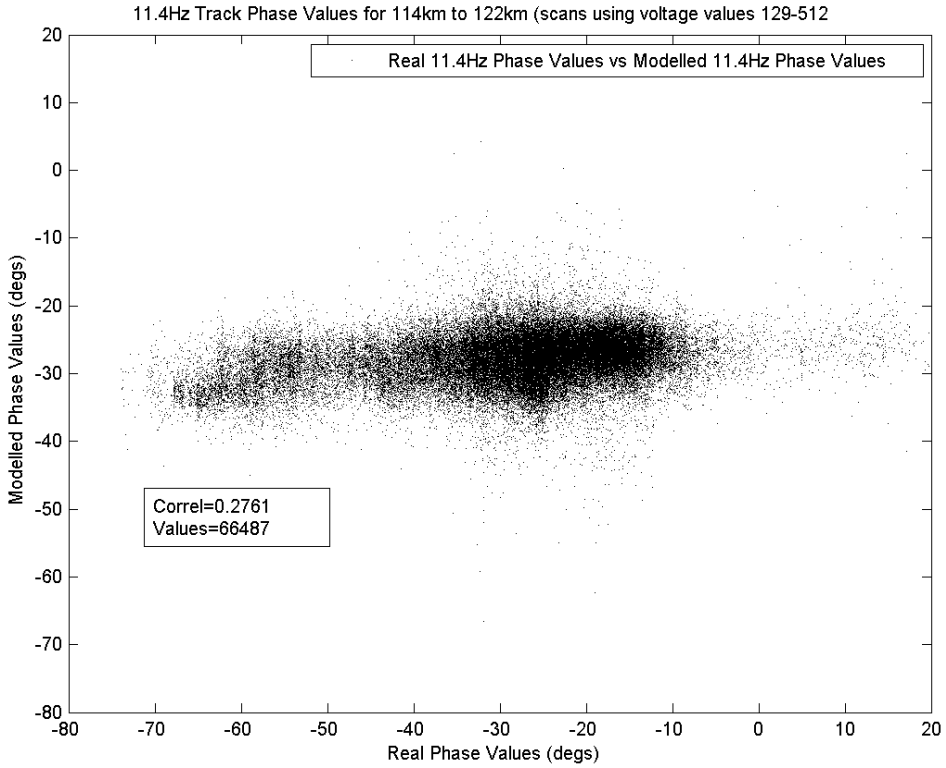
11.4Hz Track Phase Values for 114km to 122km (scans using voltage values 129-512
Real 11.4Hz Phase Values vs Modelled 11.4Hz Phase Values
Correl=0.2761
Values=66487
Modelled Phase Values (degs)
Real Phase Values (degs)
20
10
0
-10
-20
-30
-40
-50
-60
-70
-80

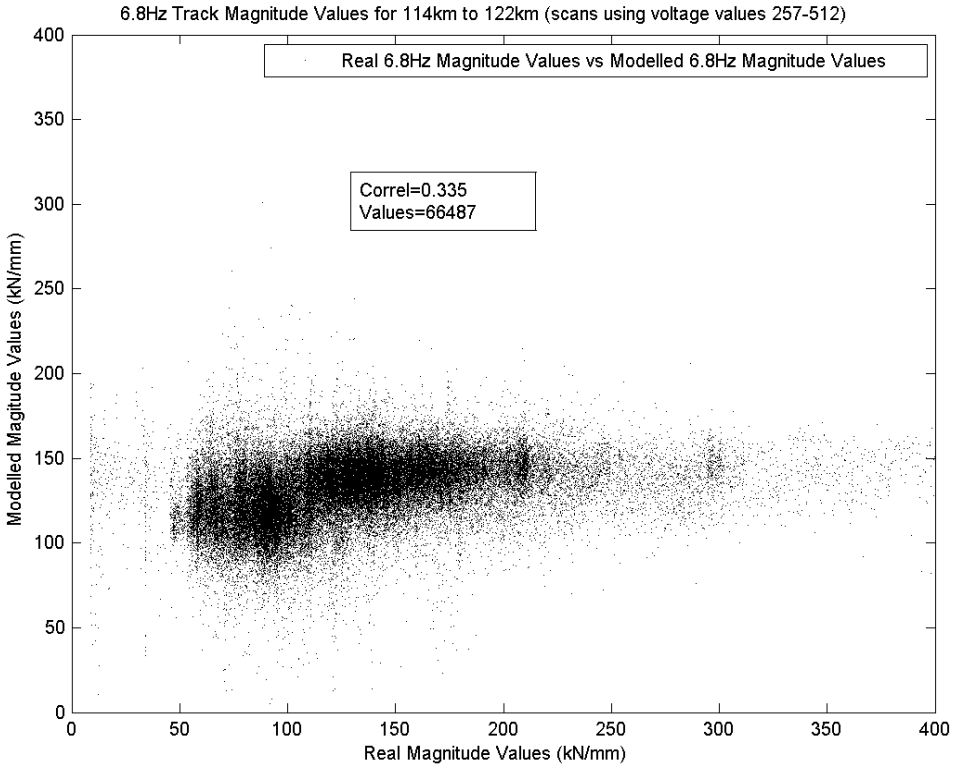
6.8Hz Track Magnitude Values for 114km to 122km (scans using voltage values 257-512)
Real 6.8Hz Magnitude Values vs Modelled 6.8Hz Magnitude Values
Correl=0.335
Values=66487
Modelled Magitude Values (kN/mm)
Real Magnitude Values (kN/mm)
0
50
100
150
200
250
300
350
400

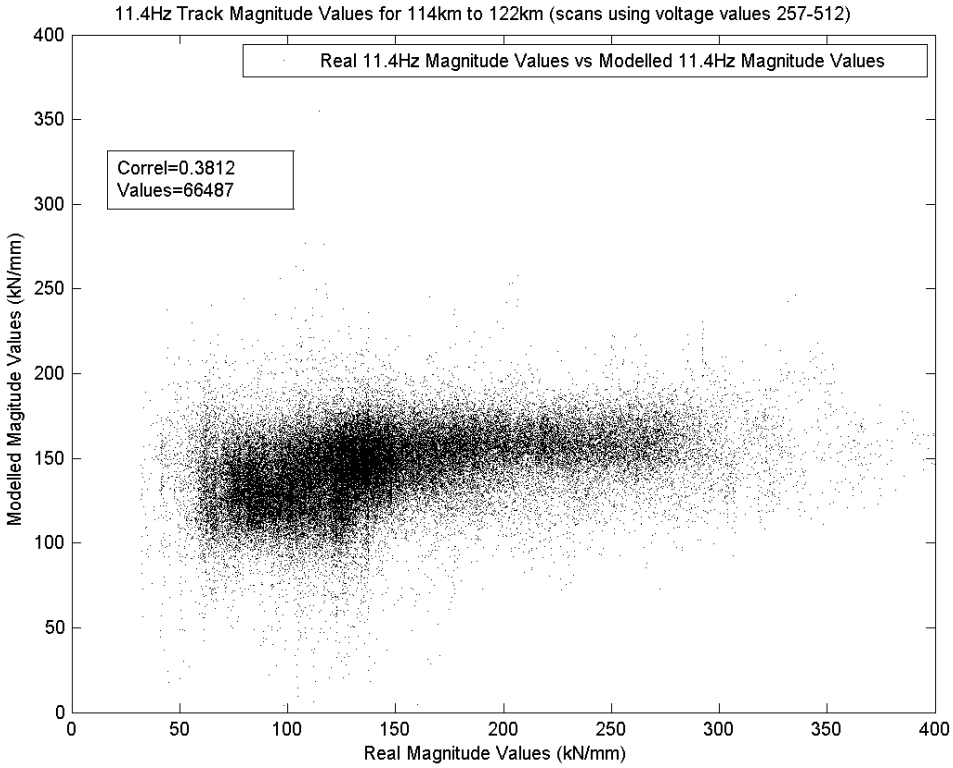
11.4Hz Track Magnitude Values for 114km to 122km (scans using voltage values 257-512)
Real 11.4Hz Magnitude Values vs Modelled 11.4Hz Magnitude Values
Correl=0.3812
Values=66487
Modelled Magitude Values (kN/mm)
Real Magnitude Values (kN/mm)
0
50
100
150
200
250
300
350
400

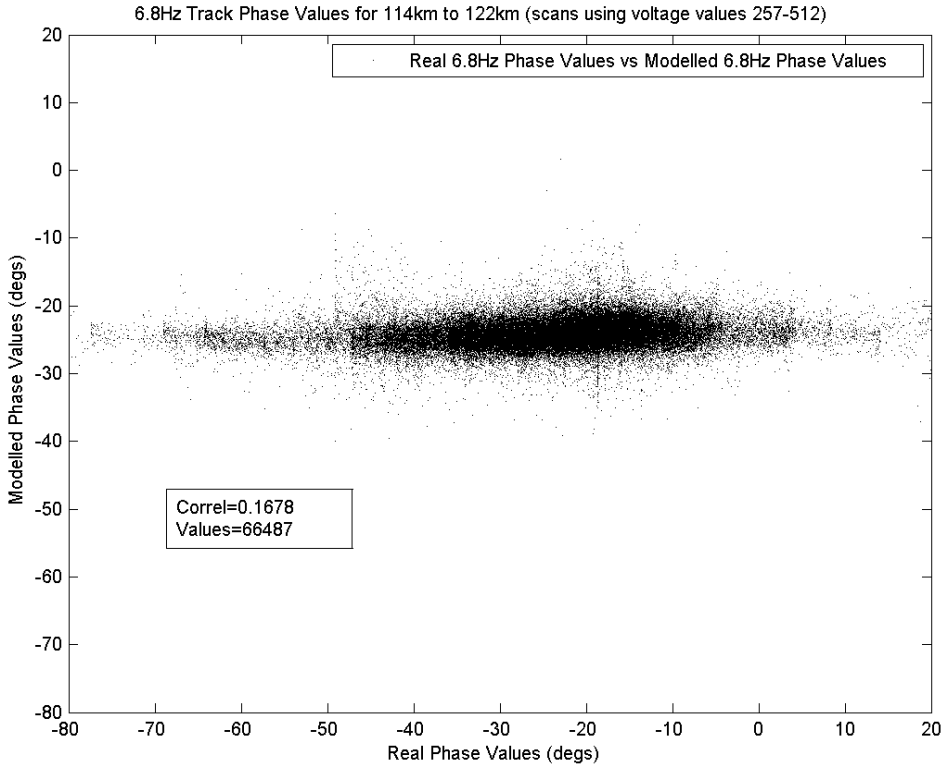
6.8Hz Track Phase Values for 114km to 122km (scans using voltage values 257-512)
Real 6.8Hz Phase Values vs Modelled 6.8Hz Phase Values
Correl=0.1678
Values=66487
Modelled Phase Values (degs)
Real Phase Values (degs)
20
10
0
-10
-20
-30
-40
-50
-60
-70
-80

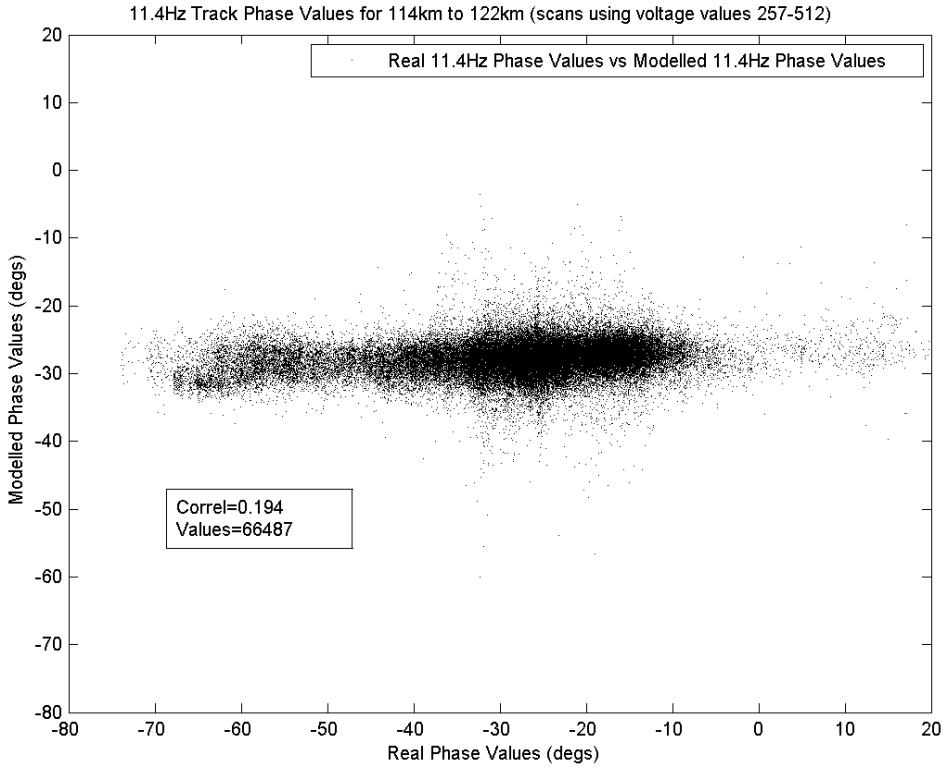
11.4Hz Track Phase Values for 114km to 122km (scans using voltage values 257-512)
Real 11.4Hz Phase Values vs Modelled 11.4Hz Phase Values
Correl=0.194
Values=66487
Modelled Phase Values (degs)
Real Phase Values (degs)
20
10
0
-10
-20
-30
-40
-50
-60
-70
-80

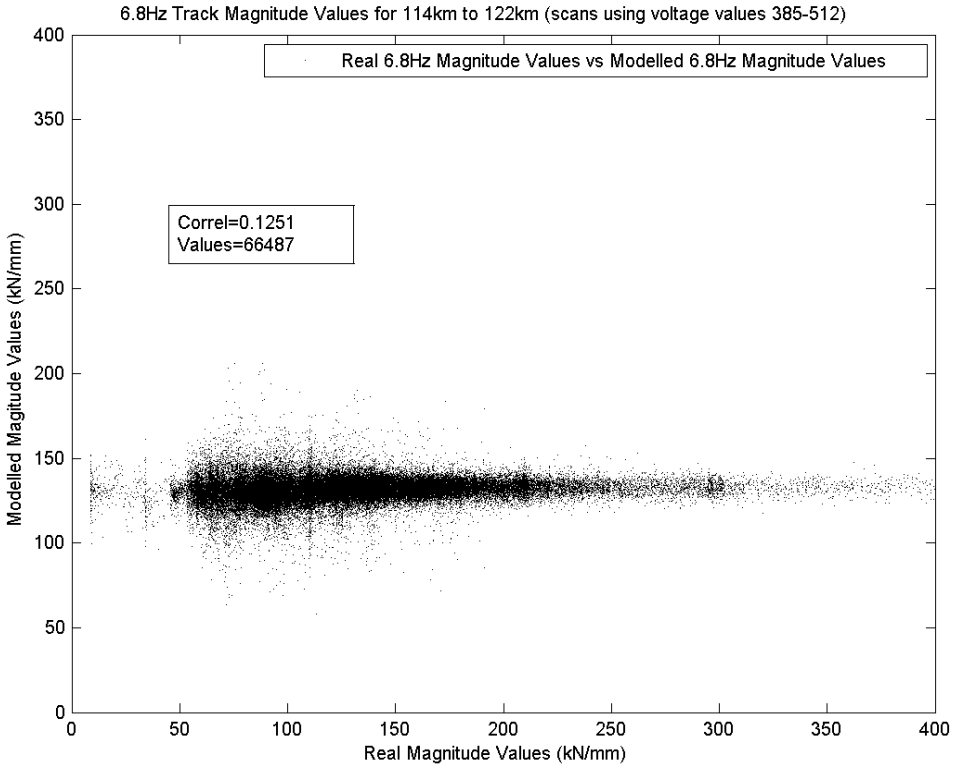
6.8Hz Track Magnitude Values for 114km to 122km (scans using voltage values 385-512)
Real 6.8Hz Magnitude Values vs Modelled 6.8Hz Magnitude Values
Correl=0.1251
Values=66487
Modelled Magitude Values (kN/mm)
Real Magnitude Values (kN/mm)
0
50
100
150
200
250
300
350
400

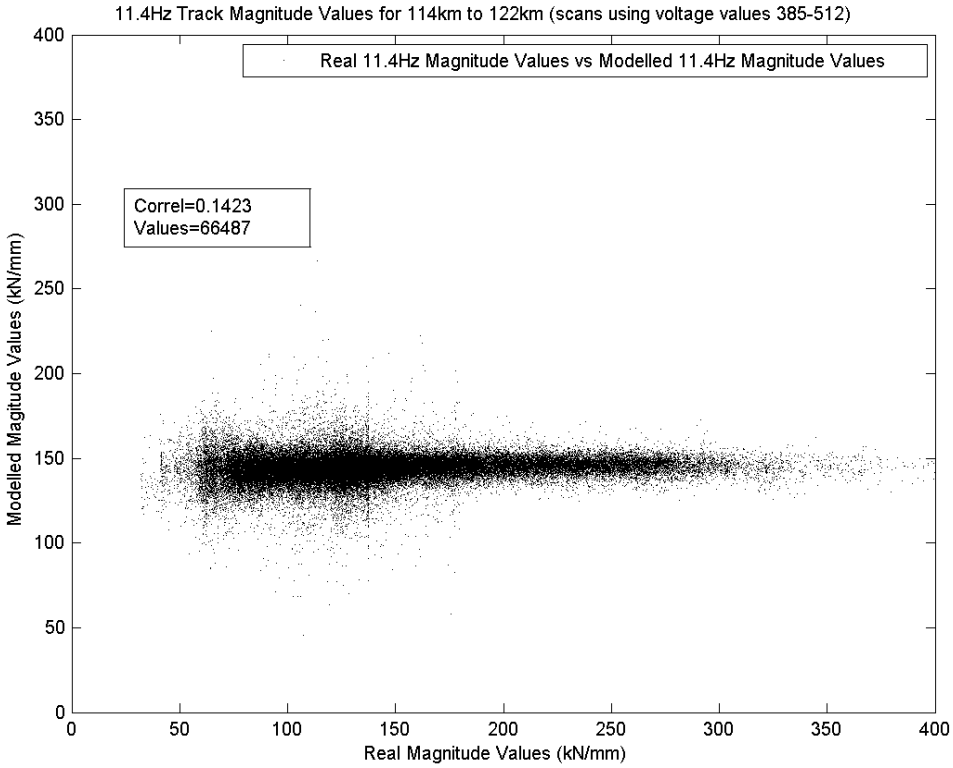
11.4Hz Track Magnitude Values for 114km to 122km (scans using voltage values 385-512)
Real 11.4Hz Magnitude Values vs Modelled 11.4Hz Magnitude Values
Correl=0.1423
Values=66487
Modelled Magitude Values (kN/mm)
Real Magnitude Values (kN/mm)
0
50
100
150
200
250
300
350
400

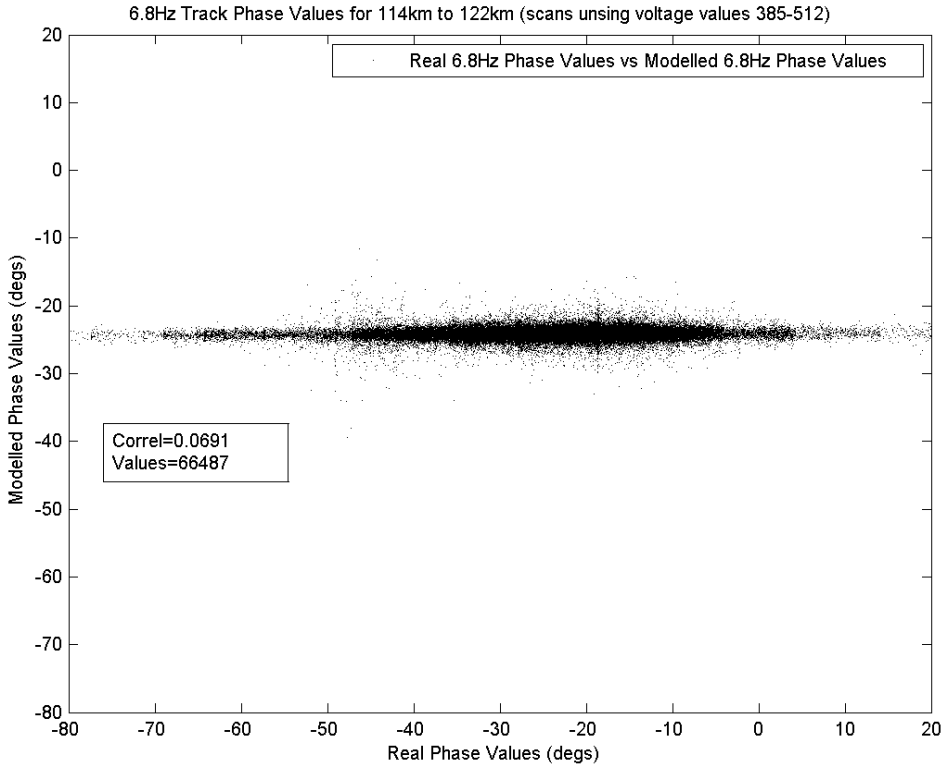
6.8Hz Track Phase Values for 114km to 122km (scans unsing voltage values 385-512)
Real 6.8Hz Phase Values vs Modelled 6.8Hz Phase Values
Correl=0.0691
Values=66487
Modelled Phase Values (degs)
Real Phase Values (degs)
20
10
0
-10
-20
-30
-40
-50
-60
-70
-80

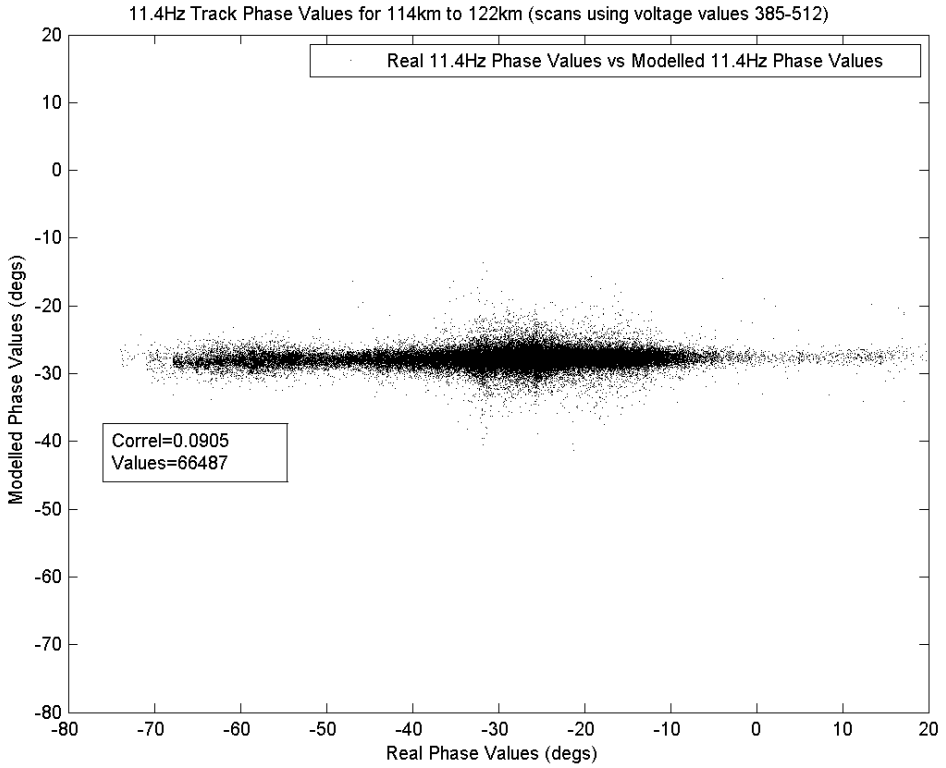
11.4Hz Track Phase Values for 114km to 122km (scans using voltage values 385-512)
Real 11.4Hz Phase Values vs Modelled 11.4Hz Phase Values
Correl=0.0905
Values=66487
Modelled Phase Values (degs)
Real Phase Values (degs)
20
10
0
-10
-20
-30
-40
-50
-60
-70
-80

APPENDIX 10 120,889M TO 121,009M MULTI-VARIATE REGRESSION (ALL SAMPLES)

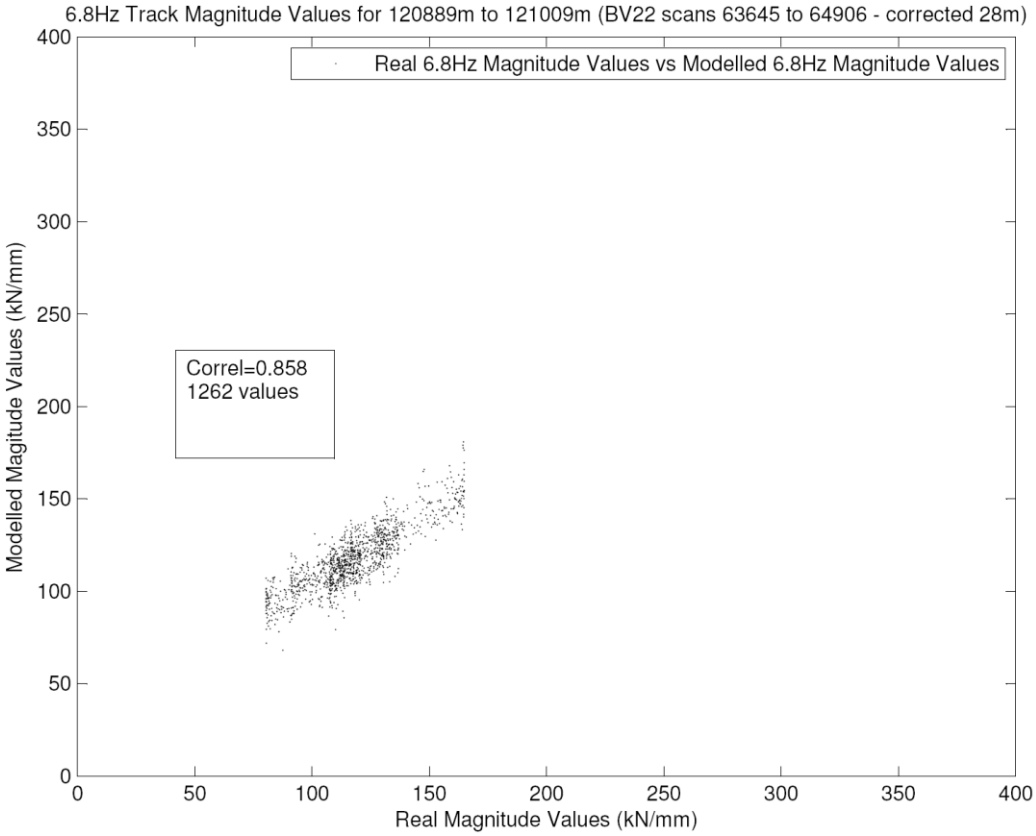
6.8Hz Track Magnitude Values for 120889m to 121009m (BV22 scans 63645 to 64906 - corrected 28m)
Real 6.8Hz Magnitude Values vs Modelled 6.8Hz Magnitude Values
Correl=0.858
1262 values
Modelled Magitude Values (kN/mm)
Real Magnitude Values (kN/mm)
0
50
100
150
200
250
300
350
400

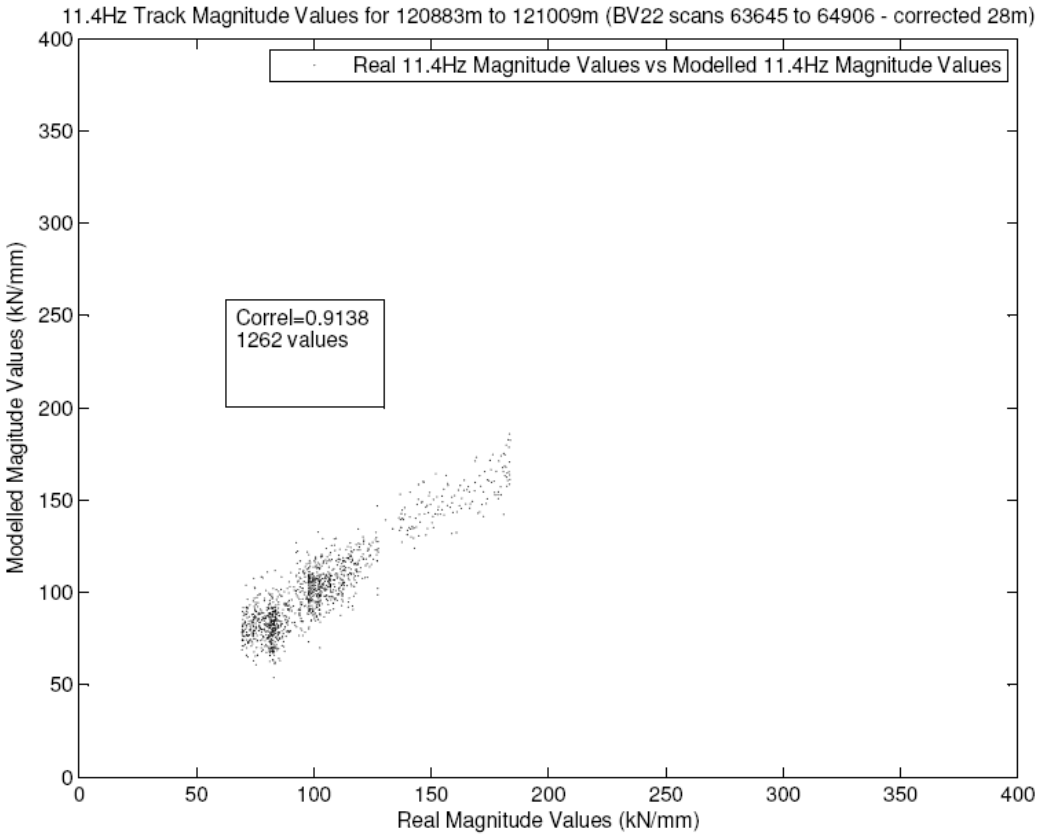
11.4Hz Track Magnitude Values for 120883m to 121009m (BV22 scans 63645 to 64906 - corrected 28m)
Real 11.4Hz Magnitude Values vs Modelled 11.4Hz Magnitude Values
Correl=0.9138
1262 values
Modelled Magitude Values (kN/mm)
Real Magnitude Values (kN/mm)
0
50
100
150
200
250
300
350
400

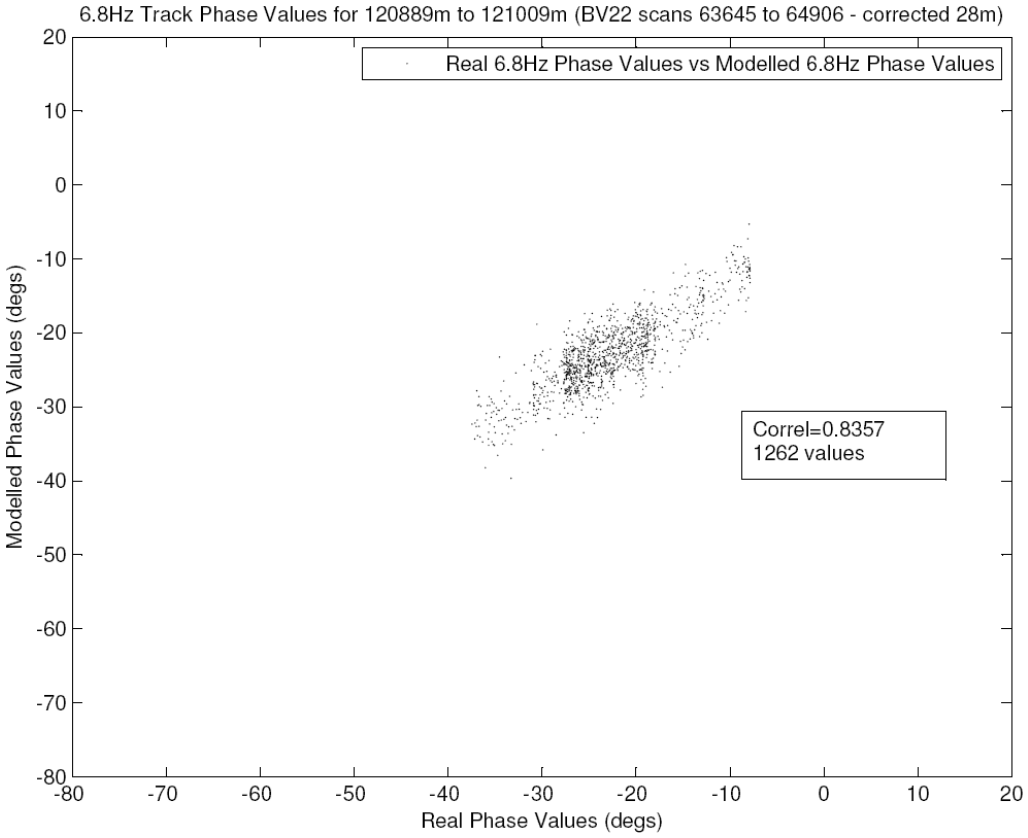
6.8Hz Track Phase Values for 120889m to 121009m (BV22 scans 63645 to 64906 - corrected 28m)
Real 6.8Hz Phase Values vs Modelled 6.8Hz Phase Values
Correl=0.8357
1262 values
Modelled Phase Values (degs)
Real Phase Values (degs)
20
10
0
-10
-20
-30
-40
-50
-60
-70
-80

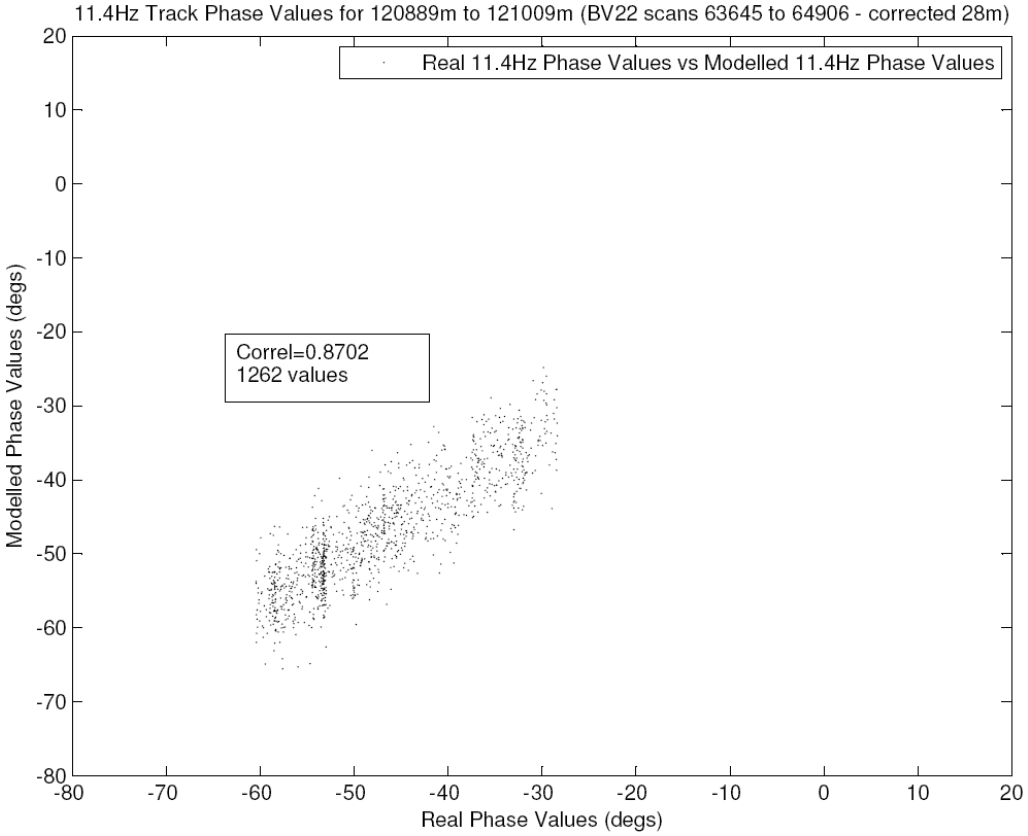
11.4Hz Track Phase Values for 120889m to 121009m (BV22 scans 63645 to 64906 - corrected 28m)
Real 11.4Hz Phase Values vs Modelled 11.4Hz Phase Values
Correl=0.8702
1262 values
Modelled Phase Values (degs)
Real Phase Values (degs)
20
10
0
-10
-20
-30
-40
-50
-60
-70
-80

APPENDIX 11 PAPERS

1. New Analysis of Ground Penetrating Radar Testing of a Mixed Railway Trackbed (De Bold et al., 2010a).

   This paper was peer-reviewed and presented as a poster for the 89th Annual Meeting of the National Academies Transportation Research Board (TRB), in Washington DC, USA, 10-14 January 2010 – paper no. 10-3142.

2. Using Frequency Response Function Testing to examine a Railway Trackbed (De Bold et al., 2010b).

   This paper was peer-reviewed and presented as a lecture for the 89th Annual Meeting of the National Academies Transportation Research Board (TRB), in Washington DC, USA, 10-14 January 2010 – paper no. 10-3033.

   A substantially revised version of this paper is currently under review and awaiting resubmission after corrections to the Journal of Nondestructive Evaluation.